PROTECT
A COVID-19 National Core Study

Understanding SARS-CoV-2 transmission: Computational fluid dynamics modelling of respiratory particles

Prepared for
The PROTECT COVID-19 National Core Study on transmission and environment

PROTECT-04 (2023)
National Core Study Report

First published 2023

The PROTECT COVID-19 National Core Study on transmission and environment is a UK-wide research programme improving our understanding of how SARS-CoV-2 (the virus that causes COVID-19) is transmitted from person to person, and how this varies in different settings and environments. This improved understanding is enabling more effective measures to reduce transmission – saving lives and getting society back towards 'normal'.

This report describes the development and use of a mathematical Computational Fluid Dynamics (CFD) model of respiratory droplet dispersion. The aim of the study was to help provide a better understanding of the physics of the transmission of the SARS-CoV-2 virus. As part of the model development, the researchers compared its predictions with experimental data. Their results demonstrated that the model is suitable for modelling real world scenarios.

The researchers' findings include the following. Firstly, screens are an effective mitigation method to reduce dispersion for short durations and prevent large droplets from reaching the other side of the screen. However, screens are not effective over longer durations as small droplets are carried by the air around the screen. Secondly, medium-sized droplets may remain suspended for longer than expected due to evaporation and could therefore be important in determining exposure risk. Thirdly, measurements of carbon dioxide in the air are only partially effective as a proxy for exposure to SARS-CoV-2.

This report and the research it describes were funded by the PROTECT COVID-19 National Core Study on transmission and environment, which is managed by the Health and Safety Executive (HSE) on behalf of HM Government. Its contents, including any opinions and/or conclusions expressed, are those of the authors alone and do not necessarily reflect UK Government or HSE policy.

Understanding SARS-CoV-2 transmission: Computational fluid dynamics modelling of respiratory particles

Simon Coldrick, Adrian Kelsey, Liam Gray, Rory Hetherington and Matthew Ivings

Health and Safety Executive
Harpur Hill
Buxton
Derbyshire
SK17 9JN

PROTECT-04 (2023)

KEY MESSAGES

The main aim of this work was to understand and characterise the behaviour of respiratory droplets emitted by a person in the environment using Computational Fluid Dynamics (CFD) modelling. The term “respiratory droplet” refers to exhaled droplets and their constituents such as respiratory viruses, including SARS-CoV-2. The work aims to improve the understanding of aerosol and droplet transport in the near field and hence improve our understanding of the transmission of SARS-CoV-2.

A CFD-based exhalation model has been developed which takes into account exhalation flows, droplet size distributions, evaporation effects, ventilation, temperature, humidity and the non-volatile components of the droplets. The model allows prediction of how droplets of different initial sizes move relative to the exhaled breath, are transported by ambient flows and whether they deposit or remain airborne.

To provide some confidence in the model, it was compared to experimental measurements of human respiratory bacteria emissions from people singing, coughing and speaking. The CFD model captured the qualitative behaviour of the droplet dispersal which was considered a good outcome given the uncertainty and variability of experiments using people.

Dispersion of exhalations is complex and depends on the exhalation type, such as speaking or coughing. Air flows, and hence the dispersion of droplets, are also complex and affected by a wide range of factors including movement of bodies and their thermal plumes, ventilation flows and natural convection. This work has clearly shown that it is not sufficient to assume that exposure risk can be based simply on a well-mixed model.

Dispersion and deposition behaviour are heavily dependent on the size distribution of the exhaled droplets. There is a continuum of droplet diameters and the distribution changes through time due to evaporation effects and deposition. This work has shown that intermediate size droplets may travel further than expected as they evaporate down to a diameter that can remain airborne. These droplets may also be carrying a relatively large amount of the virus. The distance travelled by droplets generally reduces as a function of diameter. Although there is no hard cut-off, the results from this study generally support the original 2 m distancing advice.

The CFD model was used to examine mitigation measures including screens as barriers. The results showed that screens provide a barrier against larger droplets when they are projected toward the screen but are not effective at preventing smaller droplets from reaching the far side of the screen. The screens considered in this study therefore were effective at mitigating close proximity and short duration exposure but not longer duration exposure.

Carbon dioxide concentration is often used as an indicator of ventilation effectiveness in conjunction with a well-mixed assumption and has been used as a proxy for exposure risk. While this study has shown that carbon dioxide concentration is closely aligned to the dispersion of small droplets, it has also shown that ventilation is just one factor that feeds into exposure risk and large droplets don’t correlate strongly with carbon dioxide concentration.

Significant variability has been observed in the number of droplets in exhalations generated by individuals. Uncertainty remains about the distribution of droplets in exhalations and distribution of the virus across the different sized droplets.

EXECUTIVE SUMMARY

Introduction

The SARS-CoV-2 pandemic has brought about the need to assess the risks posed by different viral and bacterial transmission routes for hazardous respiratory infections. Knowledge of the relative importance of these different routes is important in understanding the ways in which infection can be transmitted and in determining the best combination of control measures. The two main routes of infectious disease transmission are contact or airborne. Contact transmission may be by direct contact with droplets from a contaminated individual or indirect contact such as touching a contaminated surface (fomite transmission). Airborne transmission arises from pathogen laden exhaled aerosols which are inhaled.

Mathematical modelling can help provide insight into the physics of airborne transmission. Computational Fluid Dynamics (CFD) provides a means of modelling both the droplet physics and the effects of ventilation. It can also model realistic geometries and their effect on the flow. The main benefit of CFD is that it can combine models to describe the interaction of exhaled droplets with environmental flows that influence the behaviour of droplets, such as ventilation and thermal effects. CFD modelling can also be used to understand the effects of mitigation methods such as screens, more complex room geometries or the influence of additional people within the environment.

The main aim of this work is to understand and characterise respiratory droplet dispersal in the environment using CFD modelling. The work aims to improve the understanding of aerosol and droplet transport in the near field with a specific focus on the difference in behaviour of different size droplets and how they contribute to exposure risk.

This project report describes the work carried out by HSE in support of Work Package 2.2.1 during the PROTECT National Core Study. HSE collaborated extensively with Dstl and Leeds University throughout this work.

Methodology

A CFD-based exhalation model has been developed which takes into account exhalation flows, droplet size distributions, evaporation effects, ventilation, temperature, humidity and the non-volatile components of the droplets. The model allows prediction of how droplets of different initial sizes move relative to the exhaled breath, are transported by ambient flows and whether they deposit or remain airborne.

During the course of the PROTECT NCS project, an experimental dataset on droplet dispersion and deposition from human subjects at the UKHSA became available. These experiments used bacteria as a surrogate for virus and were performed in an unventilated room. Both airborne and surface samples were taken and thus provided a unique means of validating the exhalation model. A component validation approach was also taken for the CFD model, focussing on the exhalation jet, evaporation of droplets and indoor air flows. The aim was to demonstrate that the model was capable of adequately resolving the relevant flow physics and to be able to test the sensitivity of the model to different input parameters.

The CFD model developed for this study has been used to examine a number of scenarios of practical interest including a person standing in front of a screen and two people sitting

opposite each other in a work environment. Analysis of the results has helped to develop a better understanding of the efficacy of screens used to mitigate transmission risk and, more generally, the flow physics involved in transmission of the virus including the behaviour of different size droplets.

Results and discussion

The model follows the Euler-Lagrange framework of previous CFD studies and therefore would be expected to perform in a similar way to those models. In the component validation cases of droplet evaporation and an exhalation jet, the experimental data were relatively well-defined and the model results provided confidence that the relevant physics were being captured.

Despite some known uncertainties in the UKHSA experiments, the model results showed qualitative agreement with the measurements in that deposition was greater at 1 metre than at 1 to 2 metres from the person and the results from the air samplers suggested that fine particles would eventually be uniformly suspended in the room given sufficient mixing time. This suggests that a computational model based on parameters from measured aerosol and exhalation data and the physics of droplet evaporation can provide realistic representations of the fate of exhaled microbial droplets.

CFD model results from the UKHSA experiments using the Bronchial, Laryngeal, Oral (BLO) particle size distribution showed a distinct partitioning of particle diameters between the surface and air samples. This partitioning appeared to be, in part, due to the particle diameter distribution in the BLO model which has a pronounced dip in the initial diameter distribution, around 30 µm, between B and L, and O modes. These results highlight that the use of this distribution would not necessarily capture the possible behaviours of intermediate-sized particles. The particle size distribution of Pöhlker et al. (2021) did not have the same clear distinction in particle sizes.

A number of different approaches were used to model the evaporation characteristics of the exhaled particles. It was found that the most detailed method, using an artificial saliva model, was prohibitively expensive in terms of computing time. A simpler approach was therefore used in which particles were modelled as consisting of pure water with a non-volatile fraction and with no adjustment to the solution vapour pressure. This approach was demonstrated to give a reasonable approximation of the more complex artificial saliva model. The particle composition used in the current study was based on a value derived from the literature and an area for further work would be to assess the sensitivity of the results to this composition.

The validated CFD model was then applied to a number of practical scenarios to provide some insight into the effects of screens on viral exposure and the use of exhaled carbon dioxide as a proxy for exposure risk. The scenarios that have been modelled are based on relatively simple idealisations of real life including a person standing in front of a screen and two people sitting opposite each other in a work environment. These simple scenarios have allowed a better understanding to be developed of the physics involved in the transmission of the virus and the factors that contribute to variations in exposure.

Screens were widely used during the Covid-19 pandemic as a measure to control transmission. The simulations performed show that large droplets are blocked by screens and that the exhalation cloud, containing droplet nuclei, is deflected by screens. Deflecting the exhalation cloud means that, compared to the same situation without a screen, transport,

mixing and dilution would occur before the exhalation cloud reached the region where someone would be exposed to an exhalation. The effect of screen-like objects in offices, desk dividers and monitors, was also simulated. For the scenarios simulated, these modified the flow but not to the same extent as the screens.

After the initial period of the exhalation, transport and mixing of the exhalation cloud and droplet nuclei is dominated by ventilation flows. Even with the simple geometries and scenarios simulated in this study, the interaction between a person, their thermal plume, the ventilation flow and the screen were complex. In most of the simulations performed only a single person was present. In the simulations where two people were present, the additional thermal plume modified the mixing behaviour. This emphasises that understanding ventilation and its operation is important where it is used as a control measure.

The distance travelled by particles generally reduces as a function of diameter. Beyond a certain point, further reduction in initial diameter means that they evaporate and remain airborne and can therefore travel much further. This transition between ballistic and airborne is seen over a range of initial diameters between approximately 20 µm – 100 µm rather than at a single value. Results also showed that some particles with initial diameters over 100 µm can remain airborne. Very small particles, with initial diameters less than 20 µm, evaporate to aerosol sizes and typically remain airborne. They can be deposited, but their size means that they carry less virus and are not likely to contribute as much to exposure risk as larger particles.

The use of exhaled carbon dioxide as a proxy for exposure risk was also examined. Comparing predictions of carbon dioxide exposure and viral exposure from exhalations showed that for droplet nuclei small enough to behave passively, with diameters less than 5 µm, there was a strong correlation between the predicted carbon dioxide and viral exposure. However, the duration of the simulations is short compared to ventilation timescales and the discrepancy could increase at longer times. The viral exposure will also depend on the distribution of viral load amongst the droplet nuclei that remain airborne.

Conclusions

A CFD-based exhalation model has been developed which takes into account exhalation flows, droplet size distributions, evaporation effects, ventilation, temperature, humidity and the non-volatile components of the droplets. The model allows prediction of how droplets of different initial sizes move relative to the exhaled breath, are transported by ambient flows and whether they deposit or remain airborne.

The CFD model has been validated through comparison with experimental measurements of human respiratory bacteria emissions from people singing, coughing and speaking. We are not aware of other CFD models that have been validated in this way against human trials data. The CFD model captured the qualitative behaviour of the droplet dispersal which was considered a good outcome given the uncertainty and variability of experiments using people.

Dispersion of exhalations is complex and depends on the exhalation type, such as speaking or coughing. Air flows, and hence the dispersion of droplets, are also complex and affected by a wide range of factors including movement of bodies and their thermal plumes, ventilation flows and natural convection. This work has clearly shown that it is not sufficient to

assume that exposure risk, especially for short durations, can be based simply on a well-mixed model.

Dispersion and deposition behaviour are heavily dependent on the size distribution of the exhaled droplets. There is a continuum of droplet diameters and the distribution changes through time due to evaporation effects and deposition. This work has shown that intermediate size droplets may travel further than expected as they evaporate down to a diameter that can remain airborne. These droplets may also be carrying a relatively large amount of the virus. The distance travelled by droplets generally reduces as a function of diameter. Although there is no hard cut-off, the results from this study generally support the original 2 m distancing advice.

The CFD model was used to examine mitigation measures including screens as barriers. The results showed that screens provide a barrier against larger droplets when they are projected toward the screen but are not effective at preventing smaller droplets from reaching the far side of the screen. The screens considered in this study therefore were effective at mitigating close proximity and short duration exposure but not longer duration exposure.

Exhaled carbon dioxide concentration is often used as an indicator of ventilation effectiveness in conjunction with a well-mixed assumption and has been used as a proxy for exposure risk. While this study has shown that carbon dioxide concentration is closely aligned to the dispersion of small droplets, it has also shown that ventilation is just one factor that feeds into exposure risk and large droplets don’t correlate strongly with carbon dioxide concentration.

Significant variability has been observed in the number of droplets in exhalations generated by individuals. Uncertainty remains about the distribution of droplets in exhalations and distribution of the virus across the different sized droplets.

ACKNOWLEDGEMENTS

The authors would like to thank the following for their invaluable input during the course of the project: Cath Noakes and members of the University of Leeds PROTECT team; Allan Bennett, Helen Rickard and Ginny Moore at UKHSA; Tim Foat, Simon Parker, Ben Higgins, Suzie Abbs and Tom Maishman at Dstl; Gareth Evans, Delphine Bard and Alan Beswick at HSE; members of the PROTECT WP2.2.2 ventilation team and RAMP Task 7 Subgroup 2 (Aerosols).

NOTE ON TERMINOLOGY

The aim of this work was to understand and characterise respiratory droplet dispersal in the environment. Exhalations can contain droplets with a wide range of diameters. It is common to describe droplets with diameters less than 5 µm as aerosol and only those with diameters greater than 100 µm as droplets. This distinction is used in the report, but not exclusively.

Exhaled droplets are not pure water but are composed of a mixture of water, proteins and salts. Droplets from exhalations evaporate to form droplet nuclei, rather than evaporating completely. Droplets with initial diameters of 20 µm can evaporate to form droplet nuclei in the aerosol range, with diameters less than 5 µm.

The modelling described in this report does not distinguish between aerosols and droplets in terms of their diameter. The model used is the same, irrespective of the droplet diameter.

In the modelling all droplets are represented by computational particles. Each individual computational particle can represent a parcel of physical droplets. The term “particle” has often been used instead of “parcel of droplets” to aid readability.

CONTENTS

1 INTRODUCTION

The SARS-CoV-2 pandemic has brought about the need to assess the risks posed by different transmission routes for hazardous respiratory infections. Knowledge of the relative importance of these different routes is important in understanding the ways in which infection can be transmitted and in determining the best combination of control measures. The two main routes of infectious disease transmission are through surface contact or via airborne transmission. Contact transmission may be by direct contact with droplets from a contaminated individual or indirect contact such as touching a contaminated surface (fomite transmission). Airborne transmission arises from pathogen-laden exhaled aerosols which are inhaled (Stettler et al., 2022).

Mathematical modelling can help provide insight into the physics of airborne transmission. Computational Fluid Dynamics (CFD) provides a means of modelling both the droplet physics and the effects of ventilation. It can also model realistic geometries and their effect on the air flow. The main benefit of CFD is that it can combine models to describe the interaction of exhaled droplets with environmental flows, such as ventilation and thermal effects, that influence the behaviour of droplets. CFD modelling can also be used to understand the effects of mitigation methods such as screens, more complex geometries or the influence of additional people within the environment.

In early 2020, HSE conducted exploratory CFD modelling of exhalations in support of its regulatory activities. This modelling work was subsequently formalised under the National Core Study (NCS) PROTECT project[1], contributing to Work Package (WP) 2.2.1 under Theme 2, “Transmission Modelling”. The overall aims and objectives for WP2.2.1 are described below.

This is the final report describing the work carried out by HSE in support of WP2.2.1.

1.1 Aims

The main aim of the work was to understand and characterise respiratory droplet dispersal in the environment using CFD modelling. The work aimed to improve the understanding of aerosol and droplet transport in the near-field considering variability between activities and individuals. The output from the models would feed into Quantitative Microbial Risk Assessment (QMRA) models developed under WP1 of Theme 2. These could be used, together with CFD models, to study specific scenarios of interest.

1.2 Objectives

The key objective was to build computational models to quantify how respiratory droplets are emitted and dispersed into the environment, the contamination that results, and the influence of ventilation flows and layouts in buildings.

Two areas of activity were planned to meet this objective. The first of these was a review of previous modelling, to inform the approach used in the current study. The second was to

[1] PROTECT COVID-19 National Core Study | (manchester.ac.uk), accessed 13/02/2023

gain confidence in the predictions from the CFD model through comparison with measurements, examining the representation of exhalations, and model sensitivity studies.

Following the development and validation of the model, the model was applied to specific scenarios to understand: the key factors that affect the dispersal of respiratory droplets, the effectiveness of screens and screen-like mitigation strategies on reducing airborne transmission and the viability of carbon dioxide as a tracer for exhaled droplets.

1.3 Collaborations and interactions

The modelling work was carried out in collaboration with Dstl's Chemical, Biological and Radiological division and the University of Leeds. The key benefit of this collaboration was the sharing of expertise and resources and the interaction with experts in QMRA modelling at Dstl.

More informal collaboration was continued throughout the course of the project with Imperial College, London, University of Strathclyde and University of Cambridge on ventilation aspects (WP 2.2.2) and with the RAMP[2] aerosols group. Several aspects of the work were informally discussed at the RAMP aerosols group meetings, leading to the use of information in the source terms paper by Stettler et al., (2022).

1.4 Structure of the report

This report is structured as follows:

Section 2 is a review of the fluid dynamics of transmission, which was carried out in parallel to the modelling activity.

Section 3 describes the CFD modelling approach used in the current study. The approach was based on the review in Section 2 and other modelling described in the literature.

Sections 4 and 5 describe comparisons of the model with experimental data. It was recognised that an exhaustive validation campaign would be impracticable. The validation activity focussed instead on the "component" validation of relevant aspects of the model. Comparison with dispersion data from a human trials study is described in Section 5. This dataset became available during the course of the project and provided a means of validating the complete exhalation model. Additional validation of the airflow predictions in a meeting room are described by Foat et al. (2022).

Application of the exhalation model to a number of different scenarios is described in Section 6.

Conclusions and a general discussion on the results presented in this report are given in Section 7.

[2] https://royalsociety.org/topics-policy/Health%20and%20wellbeing/ramp/ (accessed 07-03-2022)

2 MODELLING THE FLUID DYNAMICS OF SARS-COV-2 TRANSMISSION

2.1 Introduction

This Section provides a narrative review of the fluid dynamics of transmission of SARS-CoV-2 (the virus that causes COVID-19) and how it can be modelled. References to the literature are used to support the review, but this is not a systematic or exhaustive review.

In October 2020, SAGE EMG and NERVTAG (2020)[3] reviewed routes and the environments where transmission occurs. They found evidence that transmission occurred by three main routes: close range respiratory droplets and aerosols, longer range respiratory aerosols, and direct contact with surfaces contaminated by the virus. Close range transmission was likely to be the most significant contributor but there was insufficient information to determine the relative risks due to contributions from the three routes, nor could the effects of variations between settings be identified.

SAGE and NERVTAG also concluded that transmission was strongly associated with proximity and duration of contact in indoor environments and that the highest risks of transmission were associated with poorly ventilated and crowded indoor settings. The likelihood of aerosol emission increased with loud speaking or singing and aerobic activity.

All the three main routes involve the transport of the virus by droplets and aerosols in exhalations as a multiphase flow.

2.2 The fluid dynamics of transmission

The transport of droplets and aerosols from exhalations containing the SARS-CoV-2 virus is a fluid dynamics problem. Bourouiba (2021) reviewed the fluid dynamics of transmission. In the process of transmission, fluid dynamics is important at scales between the microbial and cellular scale, and the population and environmental scale.

At this intermediate scale, fluid dynamics, combined with associated physiological and biophysical processes, describes the route from an infected emitter to an uninfected receptor.

Bourouiba (2021) identifies four phases to disease transmission:

1) Extraction and encapsulation
2) Emission and transport
3) Ecology and environment
4) Exposure and infection

Phase 1 describes the formation of droplets, their composition, and the distribution of droplets exhaled. The fluid dynamics of these processes are not considered in this review.

[3] The Scientific Advisory Group for Emergencies (SAGE) and New and Emerging Respiratory Virus Threats Advisory Group (NERVTAG)

Phase 2 covers the fluid dynamics in the region where the flow field is affected by exhalations. Phase 3 considers the wider environment and ventilation flows which can transport respiratory aerosols. Phases 2 and 3 provide information on exposure to pathogens, this review does not cover the fluid dynamics of the infection element of Phase 4. Phases 2 and 3 are not completely independent, there is a region where exhalation and ventilation flows interact.

2.3 Modelling the fluid dynamics of transmission

The fluid dynamics processes in the phases of transmission identified in Bourouiba (2021) show a wide range of time and length scales. Different processes have a significant influence on the flow and transmission at different scales. Addressing the full range of behaviours in a single model would be challenging and not make good use of resources. The modelling of transmission can be considered in two phases as described above: exhalations and ventilation flows. Of the three routes contributing to transmission the first two routes, close range respiratory droplets and surface transmission, can be modelled as part of the exhalation process. Longer range transmission by aerosol can be modelled as a ventilation flow.

The length and timescales of exhalations are much smaller than those of ventilation flows. However, there are intermediate length and timescales where exhalation flow interacts with ventilation flows. At the larger time and length scales, suspended droplet nuclei from exhalations behave as passive tracers carried along with the ventilation flow. The representation of exhalations in ventilation models can be simpler than in an exhalation model.

Both exhalation and ventilation flows can be modelled using a range of approaches, balancing the level of detail that is resolved and the resources needed to use and run the model.

Modelling of the respiratory tract and initial droplet break-up are not reviewed here. In the present review the inlet conditions for exhalations are assumed to be based on measurements as exhalations leave the mouth. The measurement data could be supported by modelling exhalations through the respiratory tract. Modelling inhalation flows in the respiratory tract could also support the modelling of infection, but modelling of inhalation or infection is not reviewed here.

Transmission occurs when sufficient virus to support productive infections is transported from an infected to a susceptible individual. The quantity of virus exhaled varies greatly between people and for individuals over the course of their infection. The quantity of virus carried by droplets is also affected by where within the respiratory system they are generated. Once exhaled, the viability of the virus to cause an infection is affected by evaporation of the droplets, the residence time of the droplets in the air and, if deposited, the nature of the surface. The fluid dynamics of exhalations and ventilation provides only part of the information necessary to predict transmission. Additional information about the virus (e.g. the response of the susceptible individual) is needed to determine whether infection is likely to occur.

The next two sections review the modelling of the fluid dynamics of transmission, firstly considering the regime dominated by exhalations and then by ventilation.

2.4 Modelling exhalations

Exhalations, e.g. talking or coughing, lead to multiphase clouds of warm, moist air containing droplets. Compared to the surrounding air they are warmer, have a high relative humidity and a raised carbon dioxide content. The net effect is an increase in buoyancy. The droplets in exhalations have diameters with a wide range of sizes from less than 1 µm to greater than 1000 µm.

Droplets are emitted during all exhalations: breathing, speaking, singing, coughing and sneezing. The number of droplets at a given diameter and the total number vary greatly between the activity, person and the intensity of the exhalation. Speaking or singing loudly produces a greater number of droplets than speaking or singing quietly.

Exhaled droplets are mostly water but also contain salts and proteins which affect the evaporation of the droplets (Walker et al., 2021). Droplets will evaporate in air to leave equilibrium droplet nuclei comprising the non-volatile constituents. Analysis by Wells (1934) showed that isolated droplets with initial diameters less than 100 µm, falling under the influence of gravity in a quiescent environment from a height of 2 m, would evaporate to a droplet nucleus before reaching the floor. Larger droplets, with initial diameters greater than 100 µm, would deposit on the floor before they had fully evaporated to form a droplet nucleus. The Wells' curve shows that the time taken for droplets to evaporate to droplet nuclei increases with diameter, until droplets reach the floor before reaching equilibrium diameter. On further increase in droplet diameter, the time to reach the floor decreases (because large droplets fall faster). Releasing isolated droplets in still air with an initial horizontal velocity shows that larger droplets travel further than small droplets. The smaller droplets have less momentum and are more affected by aerodynamic drag. These trends for larger droplets to travel further than smaller droplets are applicable to conditions in still air. If, however, there is a ventilation flow within the room, smaller droplets can be transported further than larger droplets (since the smaller droplets can remain airborne for longer).

Observations show that the droplets in exhalations evaporate more slowly and are transported further as part of the warm and moist cloud formed by the exhalation than they would if they were released as isolated droplets (Bourouiba, 2020). Exhalations must be modelled as a multiphase flow coupling the gas and vapour phase with the droplets to capture this behaviour.

Modelling exhalations as multiphase clouds allows the fate of the range of droplet diameters to be examined. Simulations can be used to assess which droplets are deposited and where, and which droplets remain airborne and can be transported by ventilation flows. Simulations can also account for the initial viral load of the droplets to examine where a person could potentially become infected.

Data is available to validate the individual processes of the fluid dynamics of transmission, but very little data is available to validate the complete process of exhalation, evaporation, transport, and deposition. In the work presented here, validation of individual components is shown in Section 4, while Section 5 describes comparison with dispersion data from a human trials study. This dataset became available during the course of the project and allows validation of the complete exhalation and transport model.

Studies of human subjects have shown that there is significant variability between emission rates of droplets and vapour between different people. This affects the data used to set initial

or boundary conditions in models, for example the droplet size distributions of exhalations, and any data that is available to validate models.

Different approaches that can be used to model exhalations are reviewed in the following sections.

2.4.1 Modelling exhalations using CFD

Computational Fluid Dynamics (CFD) can be used to perform transient, three-dimensional, multicomponent, multiphase simulations of exhalations from people. Simulations can take into account complex geometries, representing people within a wide range of different environments.

Choices have to be made about what physical process should be included in simulations and the approach used to model those processes. Limitations on computing resources mean that older simulations reported in the literature (e.g. Chao and Wan, 2006) often made simplifying assumptions to keep the computational requirements manageable, such as the use of representative droplet sizes rather than a distribution of sizes.

Three-dimensional fluid flow simulations of exhalations are multicomponent, meaning that additional components in addition to air need to be computed. Exhalations are formed of air that is warmer and more humid than the ambient environment. An additional transport equation needs to be solved for the water vapour component, to capture the influence of the raised humidity on exhalations and the droplets they contain. The carbon dioxide concentration in exhalations will also be higher than the ambient air. Solving a further transport equation for carbon dioxide allows the mixing of exhalations with ambient air to be compared with the movement of the droplets and droplet nuclei. Measuring carbon dioxide concentrations from exhalations is frequently used to examine ventilation performance. The gases and water vapour in the exhalation are buoyant due to their temperature relative to the surroundings. This difference in temperatures requires the solution of an energy transport equation to allow this behaviour to be captured. The flow field will also be affected by thermal plumes due to the heat given off by people and other objects.

The droplets in exhalations form a disperse phase. Multiphase simulations including heat and mass transfer are used to simulate the transport of the disperse phase droplets in the gas and vapour clouds formed by exhalations.

CFD modelling approach

Most of the reported CFD simulations of exhalations use an Eulerian-Lagrangian, discrete particle approach. In these cases the flow field of air and water vapour is calculated using an Eulerian approach and a Lagrangian approach is used to track discrete particles through the Eulerian flow field. Two-way coupling is required between the Eulerian and Lagrangian models to allow the gaseous phase to affect the dispersion of the droplets and vice versa. Steady-state simulations can be performed, but transient flows are needed to simulate exhalations. He et al. (2011) used an Eulerian-Eulerian approach, using a drift-flux model for the discrete phase, with one-way coupling from the continuous to the discrete phase. That approach was simpler than fully coupled Eulerian-Lagrangian simulations. However, a limitation of this approach is that a separate set of Eulerian equations is needed to model droplets of a given size. He et al. (2011) only modelled three particle diameters: 0.5 µm, 5 µm and 16 µm. This is not the full range of droplet diameters observed in exhalations. The initial evaporation of droplets was also not represented in the simulations. Therefore, these

particles represented the equilibrium droplets, or droplet nuclei, formed once evaporation was complete.

Tracking particles using an Eulerian-Lagrangian approach requires the coupling between the particles and the flow field to be specified and calculated. For a particle moving in air, forces due to drag from the flow field and buoyancy are usually considered. The influence of the particles on the flow field is introduced as sources when solving the flow. Heat and mass transfer of the droplets due to evaporation, and under some conditions, condensation must also be modelled.

A further consideration when simulating exhalations is that the droplets are not pure water but are actually composed of multiple components, including salts, proteins and mucins in addition to water (Walker et al., 2021). The composition of the droplets will vary depending on where they originate in the respiratory system. The presence of the other components means that when droplets evaporate a “nucleus” is left behind. The other droplet components also affect the equilibrium size and composition of the nucleus formed by modifying the vapour pressure at the surface of the droplets. These effects can be included in the simulation of droplets, but using a more detailed representation of the droplet properties will increase the computational cost of the simulations.

As exhalations are turbulent (Bourouiba, 2021), an appropriate turbulence model is needed as part of the CFD model. The most common treatment of turbulence used in simulating exhalations is the RANS (Reynolds Averaged Navier Stokes) approach. The choice of turbulence model often depends on the capabilities of the particular CFD code and the availability of computing resources. Busco et al. (2020) performed RANS simulations of sneezes using the realisable k-epsilon turbulence model and compared results to experimental measurements. Abkarian et al. (2020) used LES (Large Eddy Simulation) to simulate exhalations made during talking. Temperature and buoyancy effects were not modelled and, while Lagrangian particle tracking was used to visualise the flows, the particles were passive tracers, not droplets. Their simulations showed that as talking continued the resulting flow field behaved like a jet, rather than as individual puffs. Chong et al. (2020) simulated coughing using DNS (Direct Numerical Simulation) with a point-particle approach to examine the transport and evolution of droplets. All three approaches, RANS, LES and DNS, allow the influence of turbulence on exhalations and droplets to be examined. The treatment and information from simulations using LES and DNS provide more detail than using RANS simulations, but they usually require the use of much greater computing resources.

In all approaches, the effect of turbulence on the movement of the dispersed particles must be considered. RANS simulations predict averaged turbulence quantities. The effect of turbulent velocity fluctuations on droplet movement therefore requires an additional model. The most common approach used is the Discrete Random Walk (DRW) model. This approach assumes isotropic turbulence (i.e., equal turbulent fluctuations in each coordinate direction) and has been found to give poor predictions close to boundaries where the turbulence is anisotropic, overpredicting the rate at which small particles impact on walls. LES and DNS approaches provide more information about turbulent fluctuations, so they do not require an additional model to represent the turbulent velocity fluctuations. In principle, they are therefore able to account for the effects of anisotropic turbulence.

Many CFD studies related to virus transmission and/or aerosol transport have been reported in the literature. Zhu et al. (2006), Chen and Zhao (2010), Redrow et al. (2011) and Liu et al. (2017a) all simulated exhalations in enclosures with ventilation. However, these studies used representative droplet diameters rather than observed distributions of droplet diameters from exhalations. At the start of the pandemic CFD simulations of exhalations examining how different outdoor wind speeds might affect transmission were performed and promptly reported (Dbouk and Drikakis (2020); Feng et al. (2020); Li et al. (2020)). As the pandemic continued there was very little published evidence for longer distance (>2 m) transmission and infection occurring outside. These studies still provide useful information about approaches to capabilities and limitations of different modelling approaches. The present lack of validation data for virus transmission from exhalations means that simulations may have to be revisited when such data becomes available.

Boundary and initial conditions

Initial and boundary conditions must be described to allow simulations to be performed. The information needed will include the geometry to be simulated, the conditions of the ambient air and any ventilation flows. In addition to describing their geometry, the emitter and any receptors will provide sources of heat and will modify the ambient air flow. The thermal plume created by the presence of a person has a significant impact on air movement within an enclosure and therefore it is important to include it in a model. There are a wide range of different approaches for describing this heat flux by the boundary conditions.

Specification of exhalations requires both the carrier flow and disperse phase to be described. There is significant inter-individual variability in exhalations, they are difficult to measure, and for most measurements the volunteers have been healthy. The description of exhalations is therefore a source of significant uncertainty and variability in simulations of exhalations (see below for further details).

Carrier flow

For the exhalation carrier flow, the information required includes geometrical information, the area of the mouth, the initial inclination of the exhalation and angles describing the edges of the exhalation. The flow rate and profile, along with the composition of the flow are also required. Stettler et al. (2022) provided useful information on these model input conditions for breathing and speaking. The conditions given are a representative set of conditions that can be used to allow comparison of predictions made using different models. Additional information was provided by Gupta et al. (2009, 2010) for coughing.

Dispersed phase

The initial droplet size distribution of exhalations and the composition of droplets must be specified for each type of exhalation to be simulated. These are described in the next two Sections.

Composition

The composition of droplets in exhalations depends on their source within the respiratory system and will also depend on the health of an individual. Stettler et al. (2022) present representative droplet compositions and Walker et al. (2021) present measurements and modelling of different droplet compositions, including deep lung fluid, sodium chloride and artificial saliva. If droplets were pure water then they would evaporate completely. Since other components are present in the droplets from exhalations they evaporate to form a droplet nucleus.

Droplet size distributions of exhalations

A range of droplet sizes is generated by exhalations and there is a split between small droplets evaporating to droplet nuclei and larger droplets that deposit on a surface before complete evaporation. This was identified by Wells (1934) and means that typically more than one measurement technique is used to capture the range of droplet diameters in the distribution from an exhalation. Measurements of droplet size distribution for coughing, sneezing and speaking are reported by Duguid (1946) and for speaking, singing and coughing by Loudon and Roberts (1967a, 1968). More recent measurements of droplet distributions from speaking and coughing were used as the basis for the BLO (Bronchial, Laryngeal, Oral) model described by Johnson et al. (2011). Pöhlker et al. (2021) review respiratory aerosols and droplets in the transmission of infectious diseases, identifying datasets of droplet size distributions from exhalations.

The review by Pöhlker et al. (2021) identified fourteen papers containing measurements of droplets from breathing, ten papers containing measurements of small particles from speaking and coughs, and five papers for large particles from speaking and coughing. The references for measurements of speaking and coughing are shown in Table 1, for small particles, and Table 2, for large particles.

Table 1 Measurement data for small particles from speaking and coughs, Pöhlker et al. (2021)

Reference	**Respiratory activity**	**Measurement technique**	**Particle diameter range used in Pöhlker et al. study (µm)**
Morawska et al. (2009)	Speaking/Coughs	APS[1]	0.9 – 5
Johnson et al. (2011)	Speaking/Coughs	APS[1]	0.9 – 5
Lai et al. (2011)	Speaking	OPC[3]	0.3 – 10
Asadi et al. (2019)	Speaking	APS[1]	0.9 – 5
Lee et al. (2019)	Coughs	SMPS[4]/OPS[3]	0.01 – 0.4/0.5 – 5
Alsved et al. (2020)	Speaking/Singing	APS[1]	0.9 – 5
Hartmann et al. (2020)	Speaking/Coughs	LPC[2]	0.3 – 3
Lindsley et al. (2012)	Coughs	LPS[2]	0.35 - 10
Li et al. (2020)	Coughs	APS[1]	0.9 – 5
Gregson et al. (2020)	Speaking/Singing	APS[1]	0.9 – 5

[1]APS – Aerodynamic particle sizer

[2]LPC/LPS – Laser particle counter/spectrometer

[3]OPC/OPS – Optical particle counter/sizer

[4]SMPS – Scanning mobility particles sizer

Table 2 Data for large particles from speaking and coughs, Pöhlker et al. (2021).

Reference	Respiratory activity	Measurement technique	Sampling technique		Conversion from measurement to initial diameter	
			Airborne particles	Deposited particles	Airborne particles	Deposited particles
Duguid (1946)	Speaking/ Coughs	Dye in mouth Microscopy	Mixing and slit sampler	Impaction	Nuclei diameter × 4 With dye Diameter < 50 µm	Stain diameter × 1/2 With dye on celluloid slides Diameter > 50 µm
Loudon & Roberts (1967a)	Speaking/ Coughs	Dye in mouth Microscopy	Filter for 30 minutes after sedimentation	Sedimentation for 30 minutes	Nuclei diameter Diameter < 10 µm	Stain diameter close to Initial diameter Using regression equation[4] Diameter > 10 µm
Chao et al. (2009)	Speaking/ Coughs	Non-invasive Inteferometric Mie imaging	Measurements at 10 and 60 mm from mouth Range: 2 –2000 µm		Measurements at 10 mm assumed to be initial diameter Diameter > 2 µm	
Xie et al. (2009)	Speaking Coughs	No dye, dye, dye and sugar in mouth Image analysis No dye Image analysis	Dust monitor Readings were not consistent Not analysed or presented	Sedimentation for 2 hours		$\text{Stain diameter} \times 1/3$ Based on Duguid (1946) factor for glass slides, with additional checks Diameter > 5 µm
Johnson et al. (2011)	Speaking/ Coughs	Dye in mouth Measured		Sedimentation		$\text{Stain diameter} \times 2/3$ Compromise value for glass slides Diameter > 20 µm

[4] Loudon & Roberts (1967b)

Due to evaporation and deposition**,** the measured diameters of droplets are not usually the same as the initial diameters when exhaled. Factors are applied to convert the measured diameters to initial diameters for measurements of both evaporated and deposited droplets.

Smaller droplets from exhalations evaporate rapidly and those in the size ranges measured by aerodynamic and optical particle sizers would be expected to have evaporated to droplet nuclei before their diameters are measured. Conversion of measured diameters to initial droplet diameters, which are needed to set the initial conditions for exhalations in CFD simulations, are not usually reported. Johnson et al. (2011) discuss this in the development of the BLO (Bronchial, Laryngeal, Oral) model, describing the droplet size distributions from exhalations. Based on a review of the literature, they multiplied measurements of particle diameters made using APSs by two to give the initial diameters. The measured particle diameters were assumed to be in the range from 0.5 µm to 20 µm. In their analysis, Pöhlker et al. (2021) truncated the measurements from APSs at 5 µm due to instrument limitations of aerodynamic particle sizers. Measurements described by Duguid (1946) used dye in the mouth to identify exhaled particles for sampling. Pöhlker et al. (2021) describe all of the measurements from Duguid (1946), and other oral measurements using dye, as large particles. Duguid (1946) distinguishes between deposited droplets and airborne droplet nuclei. He multiplied the airborne, measured droplet nuclei diameters by an evaporation factor of four to convert them to droplet initial diameters. As noted previously, Johnson et al. (2011) converted airborne, measured droplet nuclei diameters, to initial diameters by multiplying by an evaporation factor of two. This means that there is a factor of two difference between the evaporation from measured to initial diameters used by Johnson et al. (2011) and by Duguid (1946). In CFD simulations, where the composition of droplets is modelled or specified (see Section 3.2.5), the relation between measured droplet nuclei diameter and initial droplet diameter can be calculated. In the work presented here, the non-volatile fraction of droplets in the CFD simulations gives a conversion factor from nuclei diameter to initial diameter of close to four which is the value used by Duguid (1946)**.**

Four of the five datasets for larger particles identified by Pöhlker et al. (2021) sampled large droplets using deposition. The remaining dataset, Chao et al. (2009), used a non-invasive approach: non-invasive interferometric Mie imaging. Chao et al. made measurements at two distances from the mouth, 10 mm and 60 mm. Based on an analysis of the results, the measurements at 10 mm were assumed to represent the initial diameter of exhaled droplets before evaporation occurs. Xie et al. (2009) analysed deposited droplets without using dye as a tracer. However, they performed additional experiments to examine the effect of using dye as a tracer, finding that it could have a significant effect on droplet numbers and their distribution. The remaining deposition analyses all used dye in the mouth to identify the droplets that had been deposited. Therefore, only oral droplets were included in the analyses. The distributions of the deposited droplets were measured by counting particles after they had been collected on a surface (Table 2).

Sampling techniques varied between studies, and further analysis was performed in each study to calculate initial droplet diameters from the size of stains formed by droplets when they deposited on surfaces. The conversion factors used in the studies are shown in Table 2. The factors used to convert from stain to initial diameters range from one third to unity. The diameter of the stain is therefore assumed to be either equal to, or larger than, the initial diameter of the droplet. The studies use values that do not change with diameter to convert

from measured to initial diameters, except for Loudon & Roberts (1967a), who use a regression equation, Loudon & Roberts (1967b)**.**

The studies identified by Pöhlker et al. (2021) show differences between data from different studies, particularly in the numbers of droplets measured. Different measurement techniques were used in different studies and for different size ranges within studies. For a distribution over the complete range of diameters of exhalation droplets, the results from the different types of measurements must be matched. In addition, conversion factors must be applied to the measured quantities, droplet nuclei diameter and droplet stain diameter, to produce a distribution of the initial diameter of droplets from exhalations. A range of values are used for these conversions, driven by the differences in approaches and conditions when the measurements were performed.

Results from the studies also show large variation between individuals within studies and between repeat measurements of individuals. Xie et al. (2009) measured droplet size distributions, without using dye, from seven people speaking and four people coughing. They observed differences in the number of droplets exhaled between individuals of up to an order of magnitude while speaking, and a factor of five from coughing. Loudon and Roberts (1967a) measured droplet size distributions from speaking and coughing for three people. For each individual both exhalations were measured twice. They observed more than an order of magnitude difference in the number of droplets between people when coughing but there was less variability between people speaking. The difference between the two measurements for individuals was also smaller speaking than coughing. One observation of coughing contributed more than half the total number of droplets observed from all three individuals when coughing.

Fitting droplet size distributions from exhalations

Pöhlker et al. (2021) fitted the data they identified following the BLO (bronchiolar, laryngeal and oral) model of Johnson et al. (2011) which is a multimodal distribution describing droplet size distributions from exhalations. In the BLO model, modes are related to where the droplets are generated in the respiratory system. A lognormal distribution describing the droplet diameter number count distribution is fitted to each mode. Johnson et al. (2011) report a multimodal fit for each type of exhalation, using data reported in Morawska et al. (2009), and Johnson et al. (2011). For each of the B, L and O modes, a lognormal distribution data was fitted to the data and these distributions are summed to give the multimodal distribution. Pöhlker et al. (2021) added two modes to improve the fit to the data. Two of the modes are described as bronchiolar (B1, B2), a single mode is used for larynx and trachea (LT), and two oral modes (O1, O2) are fitted.

Pöhlker et al. (2021) repeated the process of fitting the appropriate modes for each of the suitable data sets they identified, checking the fits were physically meaningful for both count and volume distributions. To give a single multimodal fit for each type of exhalation, the parameters describing each mode in an exhalation were calculated as the arithmetic mean of the parameter values for that mode and exhalation from all the data sets. The analysis showed small differences in the shapes of the distributions between data sets and exhalations. The same parameter values were used to describe the shape of the breathing modes, B1 and B2, in the multimodal fits for all the exhalations. The multimodal fits to speaking and coughing data used slightly different shapes for the LT, O1 and O2 modes. While the shapes of the distributions were similar across different data sets, the particle

concentrations from different data sets showed order of magnitude differences in the particle concentrations. However, only five papers were identified that contained measurements of large particles from speaking and coughing and the data describing the O1 mode is heavily influenced by one or two of those papers. The oral modes (O1, O2) were fitted to initial droplet diameters, that is measured stain diameters that had been converted to the initial droplet diameter that would create the observed stain. The bronchiolar (B1, B2) and larynx and trachear (LT) modes were fitted to measured diameters, and therefore underestimate the initial droplet diameters from exhalations.

The droplet parcels used in CFD simulations can be sampled from the distributions of droplet diameters from exhalations. There are uncertainties in measurements of droplet size distributions from exhalations and variability between individuals. The droplet size distributions of Johnson et al. (2011) and Pöhlker et al. (2021) are plotted as the number concentration, $d\,Cn\,/d\,Log\,D$, the number of particles with diameters in the interval $d\,Log\,D$ per cm^3 of exhaled breath, against the droplet diameter, D (µm), see Figure 1. The distributions represent the available information about droplet size distributions from exhalations, but do not capture the possible range of droplet counts that could be produced by individuals when exhaling. The uncertainty from measurements can be seen by comparing the two distributions. The Pöhlker et al. (2021) distribution has higher values of droplet count density at all initial droplet diameters, for both speaking and coughing exhalations. The total number of droplets introduced sampling from the Pöhlker et al. (2021) distribution will be larger than sampling from the BLO distribution. The droplet parcels tracked in CFD simulations can contain fewer than one, or more than one droplet. Analysis of how the initial droplet diameter affects the behaviour of droplets will therefore depend on how the parcels of droplets used in simulations are setup, not just on the droplet distribution. However, in the BLO droplet size distribution of Johnson et al. (2011), there is a region between the B and L modes, and the O mode with a very low droplet count density. Using the BLO model in CFD simulations means that very few droplets with initial diameters in the range 10 µm to 100 µm are tracked. The different measurement techniques used for the B and L modes, and the O mode, and conversion from measured to initial droplet diameters may all contribute to this gap. The Pöhlker et al. (2021) distribution, is a synthesis of the available measurements identified in their study. While the droplet numbers reduce between the B and LT modes, and the O modes, more droplets are predicted to be present in that region than in the BLO model. Using the Pöhlker distribution many more droplets with initial diameters in the range 10 µm to 100 µm will be tracked. Both distributions are fitted to experimental data, using the Pöhlker distribution will give more information across the full range of droplet diameters, and particularly about the possible behaviour of the droplets in the range 10 µm to 100 µm.

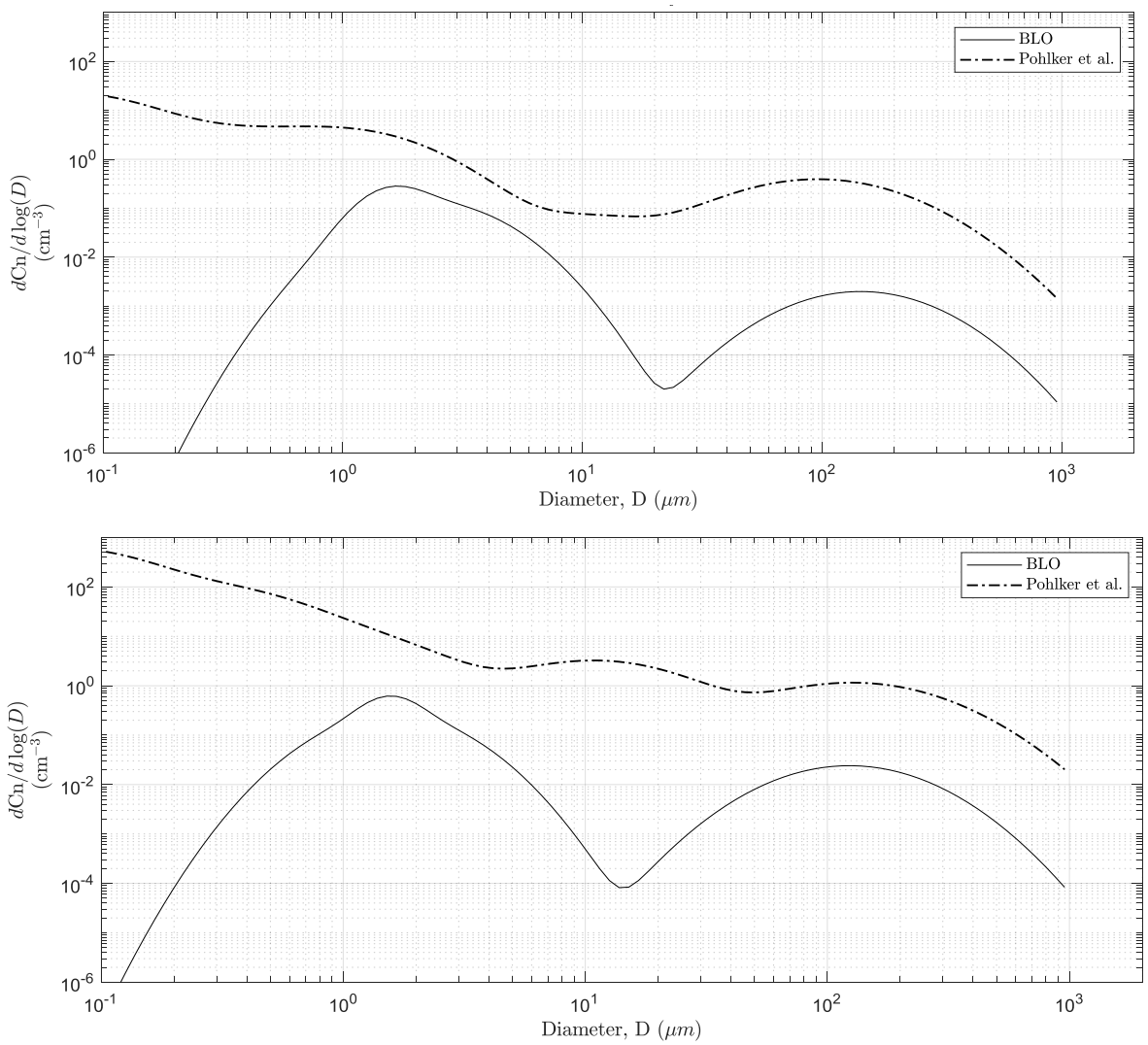

Figure 1 Comparison of count density from BLO model (Johnson et al. 2011) and Pöhlker et al. (2021). Top: speaking, Bottom: coughing.

Viral load in droplets

To predict transmission, the viral load carried by droplets must be prescribed, requiring specification of the initial viral load in droplets and whether the load changes as the droplets are transported. The viral load in droplets is not reviewed here but has been reviewed in the supplementary material in the paper by Foat et al. (2022). The viral load they used was based on a mean peak viral load for 50-year-olds from Singanayagam et al. (2022), converted to give viral load in the respiratory tract. The data in Singanayagam et al. showed that viral load changed significantly through the course of an infection and that there was also a dependency on the age of the person. Viral load may also vary with droplet size and source within the respiratory system and between different variants of SARS-CoV-2, though data is not available to vary the viral load based on these factors. The value used for the viral load, and the use of a single, constant value is an additional source of uncertainty.

Validation

There is a lack of data to validate CFD models of the whole process of exhalations and the evaporation, transport and deposition of droplets (and this was particularly the case when this work was started in 2020). Therefore, models have been validated against data for individual components of exhalation flows, e.g., the droplet evaporation data in Hamey (1982). The validation of components of CFD models for exhalations are presented in Section 4 of this report. Section 5 provides some validation of the whole CFD model by comparing predictions of patterns of microbial surface deposition and concentrations in air with experimental data. The predictions are compared with measurements from a human participant study to examine whether simulations can predict behaviour for the whole process from exhalations to deposition and airborne concentrations.

The flexibility in the scenarios that can be simulated using CFD comes at the expense of simulating a full, transient flow field. An overview of other approaches to modelling exhalations, that do not require the full three-dimensional flow field to be simulated follows.

2.5 Modelling exhalations using integral models

In CFD simulations of exhalations the flow field of the gas and vapour phase of exhalations into the environment is calculated based on initial and boundary conditions. Bourouiba (2021) notes that all exhalations can be described as starting from a turbulent point source. Jets and plumes from turbulent point sources have been studied using observations and experiments, and modelled using integral models. Integral models of jets and plumes have been used to describe the gas and vapour phases of exhalations (e.g. Liu et al, 2019; Hanna, 2022). The resources and time required to run these models are much lower than that for CFD.

Models have been developed where the gas flow field from exhalations is represented as a jet and the movement and evaporation of exhaled droplets in the exhalation is predicted using a Lagrangian approach. In this approach, the exhalations are modelled as a steady-state jet with one-way coupling between the flow field and the particles. This approach extends the isolated droplet model of Wells (1934) to include the transport and evaporation of droplets within the warm and moist cloud formed by exhalations. Droplets are transported in the exhalation cloud and their evaporation depends on the local conditions in the cloud, rather than the ambient conditions in the environment.

Xie et al. (2007) predicted the effect of droplets transported in exhalations on distance travelled and the evaporation of droplets. Liu et al. (2017b) and Wang et al. (2020) extended the predictions to include the effects of turbulence on droplet behaviour. They provided information on the distance travelled by droplets and on their evaporation to droplet nuclei. Walker et al. (2021) used the models of Xie et al. (2007) and Liu et al. (2017b) to examine the effect of droplet composition on transport and evaporation of droplets.

These models show that the behaviour of droplets, and hence their potential contribution to virus transmission, are affected by droplet composition, ambient relative humidity and turbulence.

These models are not limited to dispersion of steady state jets into quiescent ambient environments. Liu et al. (2019) extended this approach to include the interaction of the exhalation jet from breathing with mixing and displacement ventilation in a health care setting. The exposure of susceptible staff and patients to exhalations from an infected patient

are examined, but only the transport of droplet nuclei, as passive tracers, was modelled. Extensions to transient exhalations and relaxation of the assumption of one-way coupling have also been made. Bourouiba et al. (2014) developed a model of transient exhalations for violent expiratory events, i.e., coughs and sneezes. The influence of droplet fallout on the buoyancy of the cloud formed by the exhalation is also considered. Comparison with analogue experiments showed the trajectory of the exhalation was altered by the change in buoyancy as droplets left the cloud. The evaporation of droplets was not modelled. Observations (Bourouiba, 2020) showed the importance of the warm and humid clouds formed by exhalations to both the distance that droplets are transported and the evaporation of droplets.

The integral models described above were developed for violent exhalations (e.g., coughing, sneezing) except for that of Liu et al. (2019), who modelled breathing. However, all exhalations start from a turbulent point source and could therefore be represented using this integral approach (Bourouiba, 2021). Also, the work described in Abkarian et al. (2020) would support representing exhalations from speaking as a jet.

Not solving the full flow field means that integral models run more quickly than CFD simulations and can be run many times to examine the effect of varying the value of parameters. But, unlike CFD simulations, they cannot be extended to consider the interaction of exhalations with more complex ambient flows, the geometry modified to study the flow around receptors as well as emitters, or to examine the effects of introducing mitigation measures, such as screens.

2.6 Modelling ventilation flows

Bhagat et al. (2020) reviewed the fluid dynamics of different modes of ventilation and their effect on the spreading of COVID-19. In the near-field, flows due to exhalations will dominate the observed behaviour. Moving away from the source of exhalations, transmission is governed by ventilation flows. A further distinction between exhalation and ventilation behaviour is that the droplets that remain airborne will have evaporated to droplet nuclei and become passive tracers of the flow. Bhagat et al. (2020) showed that droplet nuclei whose falling speeds were smaller than the typical ventilation velocities could still transport virus. These particles can therefore remain airborne and will follow ventilation flows. Particles can still deposit, unlike a passive tracer, and therefore the possibility of infection from surfaces remain, but the main route of infection would be expected to be airborne.

Modelling transmission due to ventilation is simpler than via larger droplets as the droplet nuclei can be represented as passive tracers and therefore the flows are no longer multiphase. Droplet evaporation does not need to be modelled and neither do the transfers of momentum, heat and mass between phases. Thermal effects must also be considered, as they can have a significant effect on ventilation flows, including thermal plumes formed by the heat from people and their exhalations. The fluid dynamics of ventilation related to the transport of passive droplet nuclei and transmission are the same as those for other indoor air quality issues. Models developed to study and predict indoor air quality are therefore suitable to be used to predict ventilation flows related to SARS-CoV-2 transmission. However, ventilation is only one consideration related to indoor air quality, other factors to consider are the comfort of occupants and the energy use related to ventilation systems.

As with the modelling of exhalations, both CFD simulations and simpler models can be used to model transmission by ventilation flows. Information from detailed models of exhalation can be used to provide data to describe simplified representations of exhalations that can be used when modelling ventilation flows.

2.7 Ventilation modelling using CFD

As part of a wider study on airborne transmission of COVID-19, Vuorinen et al. (2020) used CFD simulations to study dispersion of aerosols from coughs in a supermarket environment. They modelled a geometry consisting of aisles separated by shelves, and examined the interaction of the aerosol from coughs with the ventilation flow down and between aisles. Four different CFD codes were used, enabling different aspects of the problem to be studied. In all of the simulations, turbulence was resolved using LES. This approach to turbulence modelling was chosen because ventilation flows are characterised by large scale turbulent velocity fluctuations with similar magnitude to the mean ventilation velocities. These fluctuations may have a significant effect on the dispersion of aerosols from exhalations and therefore the authors argued that the use of LES is the most appropriate approach for the simulation of aerosol dispersion. They did not present any comparison to measurements in their paper.

While Vuorinen et al. (2020) used LES in their simulations, RANS turbulence models have been widely used to simulate ventilation flows with acceptable results (Foat et al., 2017). The resources required to perform simulations using RANS are usually much less than for LES. Therefore, depending on the purpose of simulations, it may be reasonable to use a RANS approach. For both RANS and LES simulations, the predictive capability should be checked using data from suitable validation cases (i.e., experimental data).

The work by Vuorinen et al. (2020) illustrated the challenges inherent in simulating the different scales of exhalation and ventilation flows. The ventilation simulations used a domain containing shelves separating the aisles in a supermarket with length and width of around 10 m, and a height of 5 m. Resolving the details of exhalations described previously (with spatial resolutions of millimetres near the exhalation source) while simulating ventilation flows would not be an effective use of resources. A simplified representation of the exhalations was therefore used in their ventilation model, which captured the initial mass, momentum and energy of the cough. Only droplet nuclei in the airborne fraction of a cough were simulated. These were approximated as a passive scalar, which involved solving an additional transport equation using an Eulerian approach. Calculations and additional simulations were performed to check that representing the airborne fraction of droplets from coughs as a passive scalar was reasonable.

2.8 Other ventilation models

Single zone, well-mixed models have been the most widely models used to examine the influence of ventilation on airborne transmission of SARS-CoV-2. These models consider a single zone, typically a room and the well-mixed assumption implies that all changes in the concentration of the airborne fraction of droplet nuclei occur instantaneously throughout the zone. Changes in the concentration of virus occur due to people exhaling droplets, and from ventilation flows diluting the concentration of droplet nuclei and removing droplet nuclei. Additional effects on the concentration of virus can also be modelled, for example, the

influence of air cleaners as a sink of droplet nuclei. Well-mixed, single zone models provide a tool that can be used to examine how different interventions can be used to control the concentration of virus, and hence the risk of infection. However, the limitations of the well-mixed assumption would need to be taken into consideration.

In well-mixed ventilation models, exhalations are represented only as a source of infection. Other aspects that are important when modelling exhalations are not represented. The momentum of an exhalation has no effect since the flow is already assumed to be well-mixed and the mass and energy of exhalations are treated as small compared to the ventilation flows. The source of infection is treated as a passive tracer and different representations can be used. The exhalation can be modelled as a source of droplet nuclei, or of the virus carried by the droplets. These representations require additional information to calculate the risk of infection from the droplet nuclei or virus. This introduces another source of uncertainty and variability to the specification of the numbers of droplet nuclei or viral load in exhalations.

The Wells-Riley formulation (Riley et al., 1978) is an alternative to specifying the number of droplet nuclei or viral load in exhalations. In this approach the emissions from a source of infection in a well-mixed zone are measured in quanta of infection. The model can be fitted to data from outbreaks, without the need for detailed information on numbers of droplet nuclei, their viral load and the number required for infection to occur.

Miller et al. (2021) used the Wells-Riley model to determine the quanta of emission during the Skagit Valley Chorale superspreading event. Once fitted, the model could be used to examine how the number of people infected was affected by the duration of a choir practice, and by the effects of ventilation, deposition, filtration and inactivation of the virus.

Single zone, well-mixed models that can be used to examine the fate of aerosols from infected individuals and the risk of infection are available as web-based tools, for example, Airborne.cam[5]. Airborne.cam is supported by work documented by de Oliveira et al. (2021) and the exposure risk is based on viral load rather than the Wells-Riley approach. The volume and height of a room can be entered in the model and the effect of a number of parameters, such as the number of occupants, period of occupation and activity, and the ventilation, can be examined.

The well-mixed zone approach can be extended to multiple well-mixed zones. Faulkner et al. (2021) and Pease et al. (2021) use multizone modelling to examine ventilation and filtration strategies to reduce transmission in office buildings with ventilation systems. Both use the Wells-Riley approach to predict the risk of infection.

Carbon dioxide is present in exhalations at a concentration higher than in ambient air and can be modelled as a passive tracer then used as a surrogate for the presence of droplet nuclei. In spaces where exhalations from people are the only source of carbon dioxide, the change in concentration of carbon dioxide gives an indication of the ventilation effectiveness. Rudnick and Milton (2003) modified the Wells-Riley equation to use concentration of exhaled carbon dioxide in place of measuring the ventilation rate. They used data from a study of infection and predictions of carbon dioxide concentration to show that carbon dioxide concentration can be linked to the probability of infection.

[5] Airborne.cam - https://airborne.cam/ (accessed 8th March 2022)

Burridge et al. (2021) develop the approach of monitoring carbon dioxide concentrations to predict the absolute risk of infection and the number of infections from an infected individual in a space occupied by the same group of people on a regular basis. They note that when using point measurements of carbon dioxide, the well-mixed assumption within the zone, found in the Wells-Riley approach and used in Rudnick and Milton (2003), can be relaxed. However, an assumption must still be made that the exhalations from infected and susceptible individuals are well-mixed. The approach was demonstrated for a modelled open-plan office using carbon dioxide measurements from a small naturally ventilated office. The effect of different quanta of infection, due to different variants and the activity within a space, on transmission were examined. The sensitivity of transmission to different ventilation regimes and occupancy were also examined.

Models based on the well-mixed assumption are useful and widely used, allowing different strategies for control of transmission to be examined. In practice, types of ventilation other than well-mixed are used and the effects of people in a space are not all passive. Therefore an assumption of a well-mixed space will not always be appropriate. Bhagat et al. (2021) review displacement and well-mixed ventilation, and influences on ventilation such as stratification. Heat within a space, including from people, will tend to cause stratification while movement of people can reduce stratification. Bhagat et al. (2020) concludes that stratification could occur even in spaces designed for mixing ventilation. When stratification occurs, warm air, including exhalations from people, forms a layer above the height at which people inhale. This can reduce exposure, compared to a well-mixed space where contaminant is mixed throughout the space, as the contaminant is trapped above the inhalation height. The use of different ventilation strategies could provide ways to reduce the risk of infection.

2.9 Summary

The difference in scales and the processes that are important in exhalations and ventilation flows mean that modelling these flows separately makes effective use of resources.

Different modelling approaches can be used for both exhalations and ventilation flows. These different approaches provide different balances between flexibility of what is resolved and represented by models, and the resources required to perform simulations. CFD models allow a detailed representation of various fluid dynamics processes and complex geometries but at the expense of the resources needed to perform the simulations. In contrast, integral and zone models can be run many times to examine the effect of different scenarios and parameter values but are not as detailed or flexible.

Models require data both to set up the simulations and for validation to demonstrate that the results are realistic. There is significant inter- and intra-person variability in quantities related to transmission, for example, the number of droplets emitted during different activities. These quantities are difficult to measure and there is uncertainty in data in addition to variability. This should be considered when specifying models, validating models and interpreting model predictions. More data would be useful to fulfil these requirements.

3 MODELLING THE DISPERSION OF EXHALATIONS

3.1 CFD modelling approach

For the reasons outlined in the previous Section, the CFD modelling in this study used the Eulerian-Lagrangian approach, having an Eulerian fluid phase and a dispersed Lagrangian phase. This is shown schematically in Figure 2. The fluid phase was a mixture of air, water vapour and exhaled carbon dioxide and was modelled using a fixed computational mesh through which the flowfield was calculated.

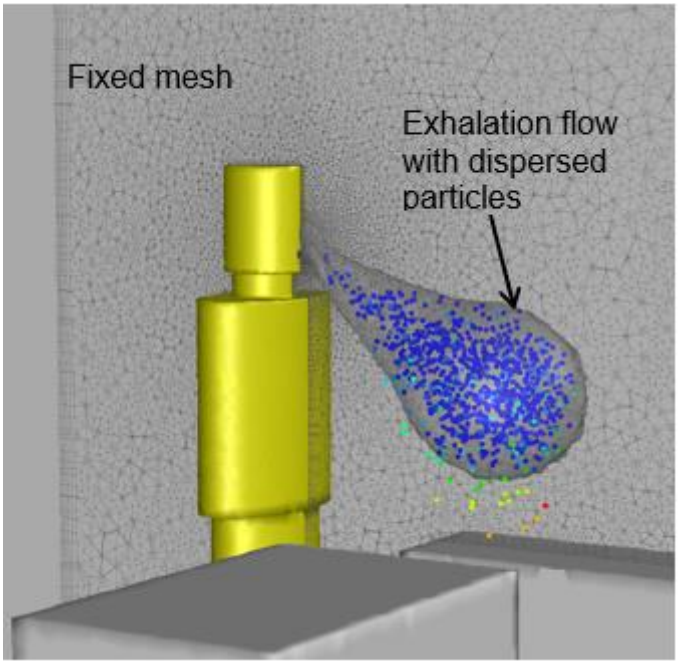

Figure 2 Schematic of the CFD modelling approach, showing the exhalation flow and dispersed particles

One of the disadvantages of the Lagrangian approach is that the computational cost of a simulation increases with the number of simulated particles. The method is often used to model applications such as sprays where it is impractical to simulate the number of droplets encountered in a real spray. For this reason, the Lagrangian approach makes use of the concept of parcels or packets of particles. Each modelled particle is treated as a parcel which contains a number of particles having average properties. This allows a more limited number of parcels to be tracked, but still ensures that factors such as droplet drag and evaporation are correctly representative of the actual particles.

The following Sections provide a description of the individual models used within the CFD simulations, which were carried out using the commercial software ANSYS Fluent 19.0 (ANSYS, 2019b). Most of the models used were those contained in the standard ANSYS Fluent installation. However, additional models and functionality were needed outside the scope of the standard installation and these are described in Appendix A.

3.2 CFD models

3.2.1 Species transport

The mixture of air, water vapour and exhaled carbon dioxide in the Eulerian phase was modelled using a species transport model. The local mass fraction of each species was solved using a convection-diffusion equation which included a source term for the transfer of water vapour from the Lagrangian droplets to the Eulerian vapour phase. In practice, this is negligible and the main effect of solving for the additional species was to account for the effects of exhaled and ambient humidity on the evaporation of particles.

3.2.2 Particle composition

Particles were modelled using either a single component model or a multicomponent model. The simpler single component model assumes that the whole particle is composed of a single material (water). The model allows for particles to have a non-volatile fraction, so that the volatile part evaporates into the Eulerian phase until the non-volatile core, or nucleus, remains. However, the density of the non-volatile core is that of the parent material. The multicomponent model allows for the non-volatile solid part and the volatile liquid part to be different materials and therefore the density of the solid part can reflect that of the salts, proteins and surfactant which are present in respiratory particles. To calculate the mass fraction of non-volatile material and for the multicomponent model its density, all of the solids were grouped into the non-volatile part. The volume-weighted density was calculated from the average of the non-volatile components (Stettler et al., 2022) as shown in Table 3. The resultant average solids density was 1830 kg/m^3, giving the particles initial mass fractions of 98.75% water and 1.25% solids. This water content was similar to the artificial saliva water content described by Walker et al. (2021), of 97.9%. Since the evaporative characteristics of respiratory particles is different to pure water, a material model was used to account for the changing vapour pressure with evaporation. This is described further in Section 3.2.5.

Table 3 Particle solids composition, taken from Stettler et al. (2022)

	Concentration (g/L)	**Density (kg/m^3)**
Salt	9	2160
Protein	3	1362
Surfactant	0.5	1082

3.2.3 Particle motion

The exchange of momentum between the Eulerian and Lagrangian phases was accounted for by equating the change of momentum of a particle to the sum of the forces acting on it

$$\frac{dp_p}{dt} = F_D + F_B + F_O \quad (1)$$

The term on the left is the change in particle momentum and the forces on the right are the drag force (F_D), buoyancy force (F_B) and other forces (F_O). Virtual mass and pressure gradient forces were not included as the density of the Eulerian phase was much lower than

the particle density (ANSYS, 2019a). The effects of Brownian motion were not modelled as it has been suggested (Ounis et al., 1991) that the effect is only significant for small particles ≤ 0.03 μm, which is considerably smaller than the particles considered in the current study.

3.2.4 Mass and energy exchange

The exchange of mass and energy between the particles and Eulerian phase is modelled in Fluent by various laws which are activated according to set criteria. For the current study, the relevant laws are inert heating/cooling and vaporisation. Particle mass transfer was modelled using the diffusion controlled model (ANSYS, 2019a), which assumes that the rate of vaporisation of component i is governed by the concentration gradient between the droplet surface and Eulerian phase

$$\frac{dm_i}{dt} = Sh\pi d_p D_i M_{w,i}\left(C_{i,s} - C_{i,\infty}\right) \tag{2}$$

where Sh is the Sherwood number, which in turn depends on the Reynolds and Schmidt numbers, D_i is the diffusion coefficient, d_p is the particle diameter, $M_{w,i}$ is the molecular weight of the component, and $C_{i,s}$ and $C_{i,\infty}$ are the concentrations at the particle surface and in the Eulerian continuum respectively.

An alternative mass transfer model is available for higher vaporisation rates when there is significant convective flow of vapour away from the droplet surface and this influences the boundary layer flow around the particle. The convection/diffusion controlled model is given by

$$\frac{dm_i}{dt} = Sh\pi d_p D_i \rho_g ln\left(1 + B_{M,i}\right) \tag{3}$$

where ρ_g is the continuum density and $B_{M,i}$ is the Spalding mass number

$$B_{M,i} = \frac{Y_{i,s} - Y_{i,\infty}}{1 - Y_{i,s}} \tag{4}$$

where Y_s and Y_∞ are the mass fractions of vapour at the droplet surface and in the Eulerian continuum respectively. The convection/diffusion model was found to have a negligible difference on vaporisation rates of water droplets at ambient conditions and therefore the diffusion controlled model was used.

For the multicomponent particles, heat transfer to the particle was modelled using the multicomponent energy equation, accounting for heat transfer by convection and vaporisation (ANSYS, 2019a)

$$m_p C_p \frac{dT_p}{dt} = hA_p\left(T_\infty - T_p\right) + \sum_i h_{fg,i} \frac{dm_i}{dt} \tag{5}$$

where m_p is the particle mass, m_i is the mass of component i, T_p is the particle temperature, T_∞ is the continuum temperature, C_p is the particle heat capacity, h is the heat transfer coefficient, A_p is the particle surface area and $h_{fg,i}$ is the latent heat of vaporisation of component i. For single component particles with a non-volatile fraction, the right hand term

in Equation 5 is replaced with the total particle mass and the latent heat is a single value for the particle material.

3.2.5 Particle material model

The surface concentration of a multicomponent particle is affected by its composition and the departure from an ideal solution becomes important, especially at high solute fractions. Drying of respiratory droplets has been extensively studied and there are numerous approaches that can be taken (de Oliviera et al., 2021; Walker et al., 2021). In the current work, the model of Walker et al. (2021) was implemented to define the particle surface vapour concentration. For a multicomponent particle, the surface concentration can be given by (ANSYS, 2019a)

$$C_{i,s} = \gamma_i x_i \varphi_i \frac{P_{sat,i}}{Z^V R T_p} \tag{6}$$

where γ_i is the activity coefficient, x_i is the component mole fraction, φ_i is the fugacity coefficient, $P_{sat,i}$ is the saturation vapour pressure at temperature T_p and Z^V is the vapour compressibility. For an ideal gas at low pressure, the fugacity coefficient and compressibility are assumed to be equal to 1. Non-ideal solution effects are accounted for through the activity, α_i, which is the product of the activity coefficient and component mole fraction (Seinfeld and Pandis, 2016)

$$\alpha_i = \gamma_i x_i = \frac{P_i}{P_{sat,i}} \tag{7}$$

where P_i is the modified vapour pressure. Walker et al. (2021) parameterised the solute mass fraction, Y_s, in terms of water activity, α_w, for deep lung fluid and artificial saliva. The parameterisation for artificial saliva was implemented in Fluent as a lookup table that returned the water activity from the solute mass fraction in the particles. Assuming the solute to be non-volatile, with water being the only vaporising component, the surface concentration was calculated by

$$C_{w,s} = \alpha_w \frac{P_{sat,w}}{R T_p}, \qquad \alpha_w = f(Y_s) \tag{8}$$

The model of Walker et al. (2021) neglects the effects of surface curvature. The effect was not implemented in the Fluent model as it has been shown to be small for particles greater than 100 nm (Mikhailov et al., 2003; Seinfeld and Pandis, 2016), which represents the majority of particles considered in this study. An additional simplifying assumption was made, based on data in Walker et al. (2021), that the models for artificial saliva and deep lung fluid were sufficiently similar that the same material model could be used for all the particles in the simulations.

The model of Walker et al. (2021) was also applied to single component water particles having a non-volatile fraction. In that case, the modification was to the water vapour pressure, of the particle, P_w

$$P_w = \alpha_w P_{sat,w}, \qquad \alpha_w = f(Y_s) \tag{9}$$

For a single component particle, the density of the non-volatile part is constrained to be the same as the volatile part and therefore the solute mass fraction, Y_s, is incorrectly specified in comparison to a multicomponent particle. However, when the solute mass fraction is small, both models should return similar particle diameters. Therefore, the model was applied to both multicomponent and single component particles as a means to check that it was implemented correctly in Fluent. Further comparisons of the evaporation model were done for pure water, artificial saliva and sodium chloride. These results are presented in Appendix A.

The multicomponent model was implemented in Fluent as a user-defined equilibrium vapour pressure model, i.e., a replacement to the default Raoult's law model, whereas the single component model was implemented as a user-defined material vapour pressure. It was found that simulations run using the multicomponent artificial saliva model required much longer to solve, in the order of five times longer. This is thought to have been due to numerical accuracy requirements in the solver. For some simulations, an alternative was used which was to model pure water droplets with a non-volatile fraction and no solution vapour pressure adjustment. This is described further in Appendix A.

3.2.6 Turbulence modelling

In the current study, the Reynolds-Averaged Navier-Stokes (RANS) approach was used where the mean flow equations were solved and the effects of the turbulent fluctuations were modelled. The RANS approach was used as it is less computationally intensive than other approaches which aim to resolve the small scale turbulent fluctuations. There are numerous turbulence models available which provide better predictions in different types of flows and therefore the result of a RANS simulation may depend on the turbulence model used. A challenge is that there is no universally applicable turbulence model which provides optimal predictions in all physical scenarios (e.g. jet flow, near wall flow etc.). Therefore, a level of compromise is often required.

3.2.7 Turbulent dispersion of particles

Turbulent dispersion is a way to introduce a random pattern to the motion of particles, to reflect the effect of small scale turbulent fluctuations that have been averaged out in the RANS approach. Without turbulent dispersion, particles injected at the same point in space and time will follow the same trajectory, because the drag force on a particle is calculated from the mean Eulerian fluid phase velocity. When turbulent dispersion is included, the motion of particles is computed from an instantaneous velocity, u, which is the sum of the mean flow velocity, $\bar{u}$, and a fluctuating component u'

$$u = \bar{u} + u' \tag{10}$$

Turbulent dispersion was modelled using the Discrete Random Walk (DRW) model (Gosman and Ioannides, 1983) where the fluctuating component is taken to be a random proportion of the local RMS (Root Mean Square) value of the velocity fluctuations, which are derived from the turbulent kinetic energy of the flow

$$u' = \zeta\sqrt{\overline{u'^2}} \tag{11}$$

$$\sqrt{\overline{u'^2}} = \sqrt{\overline{v'^2}} = \sqrt{\overline{w'^2}} = \sqrt{\frac{2k}{3}} \quad (12)$$

where ζ is a normally distributed random number and k is the turbulent kinetic energy derived from the turbulence model. The DRW model is known to give poor predictions of wall impaction rates of small particles in wall-parallel flows because of the assumption of isotropic turbulent fluctuations in the two-equation turbulence model RANS approach (Parker et al., 2008). However, for this scenario, air flows were low and deposition was likely to be dominated by sedimentation for the majority of the particle sizes. Ceiling and wall deposition rates, where sedimentation does not contribute, were expected to be very small in comparison and were not directly compared in this study.

3.3 The exhalation source term

3.3.1 Introduction

The various options available for modelling exhalation source terms were discussed in Section 2. Details of the approach taken here are described below. The source term consists of the exhalation carrier flow and a concurrent injection of particles having a defined size distribution.

3.3.2 Specification of the exhalation carrier flow

The geometry of the mouth during coughing, talking, and singing is variable and highly uncertain. Rather than attempt to capture these intricacies, exhalations were assumed to originate only from the mouth region which was defined as a circular orifice with a fixed diameter, depending on the activity. A source term was applied over this opening and consisted of a gaseous carrier flow with a specified temperature, relative humidity (RH) and transient velocity profile at a particular angle (Figure 3), along with a simultaneous injection of particles. It is known that jet dispersion results are sensitive to the inlet turbulence intensity. There is little available information on this quantity for this specific application, so the intensity and length scale were set as 10% and 0.01 m respectively.

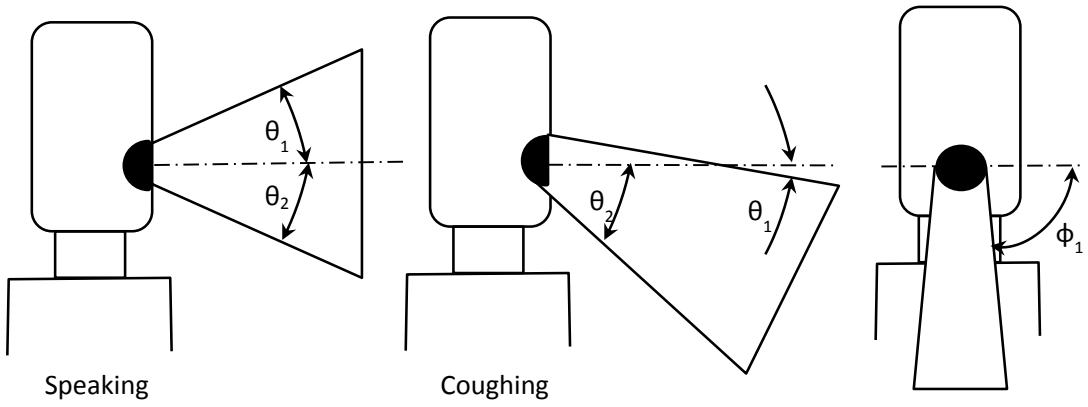

Figure 3 Initial jet expansion angles, viewed from the side and front. The front projection is the same for both speaking and coughing. The angles were fixed throughout the exhalation period

The details of the modelled carrier flow are given in Table 4. Five different carrier flows were simulated in total. Of the activities listed in the UKHSA experiments (see Section 5), only the speaking, singing and coughing activities were modelled. These activities account for the majority of the total exhalation time and have relatively well-defined sources. The carrier flow source terms for talking and singing were implemented as finite duration square waves which did not fully account for the cyclic nature of speech or breathing patterns. To examine the effect of exhalation occurring for only part of the total duration while speaking and singing, modified flows were defined which aimed to capture the maximum velocity projecting the particles, rather than an average. For modified speaking (Source 2), the duration of exhalation was halved and the average flow rate doubled. For modified singing (Source 4), the duration was halved, the average flow rate doubled and then scaled as described in the following section. Coughs are exhalations for their full duration which were approximated as a triangular wave having a duration of 0.4 seconds and a peak velocity at 0.08 seconds (Gupta et al., 2009; 2010). The carrier flow velocity was spatially varied over the mouth opening within the initial expansion angle, or half cone angle, of the jet, shown in Figure 3. These values were taken from Stettler et al. (2022) for speaking and singing and Gupta et al. (2009) for coughing.

3.3.3 Composition of the carrier flow

The carrier flow was defined as a mixture of air and water vapour. In addition to the humid air flow, an amount of 5% CO_2 (Altman and Dittmer, 1971) was included in each carrier flow source term, to explore the dispersion of the carrier flow within the room. The fractions of water vapour, X_w, air, X_a, and CO_2, X_{CO_2}, were defined as follows

$$X_w = X_{sat} \times RH, \qquad X_{CO_2} = (1 - X_w) \times 5\%, \qquad X_a = \left(1 - X_w - X_{CO_2}\right) \tag{13}$$

The mass fractions of water vapour and carbon dioxide are then

$$Y_w = \frac{X_w M_w}{\left(X_w M_w + X_a M_a + X_{CO_2} M_{CO_2}\right)} \quad (14)$$

$$Y_{CO_2} = \frac{X_{CO_2} M_{CO_2}}{\left(X_w M_w + X_a M_a + X_{CO_2} M_{CO_2}\right)} \quad (15)$$

where M_w, M_a and M_{CO_2} are the molecular weights of water, air and carbon dioxide respectively.

Table 4 Specification of the carrier flow using the speaking parameters from Stettler et al. (2022)

Source and number	**1) Speaking[1]**	**2) Modified speaking[2]**	**3) Singing[3]**	**4) Modified singing[4]**	**5) Coughing[5]**
Description	Read 1-100	Read 1-100	Happy birthday × 2	Happy birthday × 2	One cough
Diameter (m)	0.015	0.015	0.015	0.015	0.0225
Jet expansion angle θ_1 (deg)	-15	-15	-15	-15	15
Jet expansion angle θ_2 (deg)	15	15	15	15	40
Jet expansion angle φ_1 (deg)	90	90	90	90	90
Temperature (C)	34	34	34	34	34
RH (-)	100	100	100	100	100
Minute vol avg (L/min)	12	24	12	32	180
Duration (s)	50	25	30	15	0.4
Peak time (s)	Steady	Steady	Steady	Steady	0.08
Avg velocity (m/s)	1.11	2.22	1.11	2.99	7.5
Peak velocity (m/s)	1.11	2.22	1.11	2.99	15

[1]Source data taken from Stettler et al. (2022), with an assumed duration

[2]Source data taken from Stettler et al. (2022), duration halved, flow rate doubled

[3]The speaking source was used, with an assumed duration

[4]Modified singing source, based on particle count (see the following section)

[5]Approximated to a triangular waveform from Gupta et al. (2009, 2010)

3.3.4 Specification of the particle size distribution

Three different particle size distributions for exhalations have been used during this work. Initially, the modelling for the UKHSA experiments was carried out using the in-built models in Fluent and a particle size distribution given by Duguid (1946). Subsequently the BLO model (Johnson et al., 2011) and the Pöhlker distribution (Pöhlker et al., 2021) have been used in simulations, these were described in Section 2.4.1

The tracking of droplets is coupled with the gas phase and is performed as part of the simulation of exhalations, rather than as a post-processing stage. With the Pöhlker distribution there are more droplets to observe behaviour compared to using the BLO distribution. Later simulations (Section 6) used the Pöhlker distribution to improve sampling.

3.3.5 Duguid data

The standard spray model implemented in Fluent injects particles in “streams”. Each stream represents parcels of particles having a specified diameter and mass flow rate. The more streams that are modelled, the more computational parcels are tracked throughout the domain. However, the total mass of injected particles is fixed, which means that the number of particles in each parcel is proportional to the number of streams. The concept of streams means that the distribution by mass of the discrete phase parcels injected into the computational domain must be specified.

The Rosin-Rammler distribution often gives a reasonable representation of the droplet size distribution from sprays and this distribution is built in to Fluent. Rosin-Rammler distributions are described by two parameters which can be entered directly into the Fluent user interface, along with limiting maximum and minimum diameters.

A Rosin-Rammler distribution describes the mass fraction of droplets, Y_d, greater than diameter d as

$$\mathrm{Y_d} = \mathrm{e}^{-(\mathrm{d}/\bar{\mathrm{d}})^{\mathrm{n}}} \tag{16}$$

where $\bar{d}$ is the mean droplet diameter of the distribution and n is a distribution, or shape, parameter. The distribution is used to divide the total mass of droplets into the specified number of streams containing droplets with diameters between specified minimum and maximum diameters.

The total mass of droplets injected is divided into streams by splitting the linear diameter range or, as used in these simulations, the logarithm of the diameter range. The values for the mean droplet diameter range and the shape diameter were calculated from droplet count data in Duguid (1946). The droplet counts were converted into a mass or volume distribution by calculating the volume in each diameter interval as the product of the droplet count and the volume of a spherical droplet with a diameter equal to the mid-point of the diameter interval.

The approach suggested in the Fluent user manual (ANSYS, 2019b) was used to fit a Rosin-Rammler distribution to the cumulative mass fraction data in Duguid (1946). The value of the mean diameter of the distribution was found by interpolating the diameter for which the cumulative mass fraction was equal to e^{-1}. For each diameter interval a value of n was calculated from the expression

$$n = \frac{ln(-\ln Y_d)}{ln(d/\bar{d})} \tag{17}$$

The values were averaged to give a value of the shape parameter for the distribution.

The Fluent interface was used to generate lookup tables of particle diameter and mass flow for each stream. A user-defined function was used to read the lookup tables and linearly scale the mass flow of each stream according to the triangular velocity profile such that the total mass of particles was preserved over the whole injection duration. The initial velocity and direction vector of each stream was also scaled in line with the carrier flow velocity. Injection properties were set to give each stream a random starting location over the mouth area and to randomly stagger the particle tracking to avoid "clumping" of particles.

These initial simulations using the Rosin-Rammler fitted data from Duguid (1946) were used to carry out sensitivity studies for the mesh, timestep and time discretisation scheme. The results are reported in Appendix A. Following these simulations, an alternative method of particle injection was developed which allowed more flexibility and meant that other size distributions could be used. Further modelling of the UKHSA experiments was done using two different particle size distributions, described in the following Sections.

3.3.6 The BLO model

The Bronchiolar, Laryngeal and Oral "BLO" model (Johnson et al., 2011) was described in Section 2.4.1. Sampling to create droplet distributions to use in simulations of exhalations is described below. The BLO model describes the particle size distribution for complete exhalations using a tri-modal distribution fitted to experimental measurements of particles from coughing and speaking reported by Johnson and Morawska (2009) and Morawska et al. (2009)

$$\frac{d\,Cn}{d\,Log\,D} = ln(10) \times \sum_{i=1}^{3} \left(\frac{Cn_i}{\sqrt{2\pi}\ ln\ GSD_i} \right) exp\left(\frac{(ln\ D - ln\ GMD_i)^2}{2(ln\ GSD_i)^2} \right) \tag{18}$$

The number concentration, $d\ Cn$, is the number of particles with diameters in the interval $d\ Log\ D$ per cm^3 of exhaled breath, where droplet diameters, D, are measured in µm and $d\ Log\ D$ represents an interval that is constant in base 10 log space. The three modes correspond to sources of exhaled particles within the respiratory system: bronchiolar, laryngeal and oral. Each mode is fitted with a log-normal distribution. Johnson et al. (2011) provided parameterisation of the distribution with correction factors for dilution and evaporation from measurements made using Aerodynamic Particle Sizers and a spread factor for droplet diameters measured from droplet deposition. The corrected parameters used in these simulations for Geometric Mean Diameter (GMD), Geometric Standard Deviation (GSD) and Cn are shown in Table 5. These were the values suggested by Stettler et al. (2022) to describe speaking.

Table 5 Parameters of the BLO model

	Mode 1, bronchiolar	Mode 2, laryngeal	Mode 3, oral
Speaking			
GMD_i (µm)	1.61	2.40	144.7
GSD_i (-)	1.30	1.66	1.80
Cn_i (cm^{-3})	0.0540	0.0684	0.00126
Coughing			
GMD_i (µm)	1.57	1.60	123.3
GSD_i (-)	1.25	1.68	1.84
Cn_i (cm^{-3})	0.0903	0.142	0.0160

To describe the particles in an exhalation, the droplet diameter range was divided into intervals, allowing the number of particles per cm^3 of exhaled gas and vapour in each interval to be calculated. The number of particles exhaled for each interval during an exhalation is the product of the exhalation volume, derived from the parameters in Table 4, and the count density for the interval. The total number of particles was distributed throughout the duration of each exhalation and particles were introduced during each of the timesteps used to resolve the exhalation flow. It was assumed that the particle size distribution does not change during exhalations (Han et al., 2013) and that the number of particles exhaled varied only with the exhalation flow rate, effectively representing a constant concentration. It was also assumed that the particle velocity vector at the point of injection was equal to the carrier flow velocity at that point. Particles were introduced at random locations over the mouth area and at a random time fraction of each injection time step.

The number of particles emitted during each timestep was calculated as the fraction of the total volume exhaled during the duration of the timestep. Speaking and singing were described by the uniform flow rates given in Table 4 and the exhaled droplets were distributed evenly across the timesteps. For the coughing source having a triangular waveform, the number of particles introduced at each timestep was determined by the fraction of the total volume exhaled during that time interval. At each timestep, the sizes of the particles exhaled were independently sampled from the distribution for the whole of the exhalation. Over the duration of the exhalation, the sampled distribution approached the specified distribution.

The BLO model only gives particle size distributions for speaking and coughing. To reflect the fact that singing will produce a different source characteristic from speaking, a modified singing source (Source 4 in Table 4) was introduced. Gregson et al. (2020) presented measurements of speaking and singing made using an aerodynamic particle sizer. This instrument only measured particles up to a diameter of 20 µm and no corrections were made for the effect of evaporation on the droplet sizes. The measurements presented by Gregson et al. (2020) all used the same equipment and experimental approach, allowing comparison of the measurements of speaking and singing. Gregson et al. (2020) found that the shape of the droplet distribution was similar to the BLO speaking model of Johnson et al. (2011). For the modified singing source (Source 4), the speaking exhalation flow rate was doubled then scaled by the ratio of the number density of the bronchiolar modes for speaking (N = 0.74 cm^{-3}) and singing (N = 1.024 cm^{-3}) at 90-100 dB.

In a Lagrangian tracking simulation, each computational particle represents a statistical "parcel" of particles. For computational efficiency, a limited number of parcels are usually modelled and each parcel typically represents many individual particles. It is usually advantageous when simulating sprays to track a "statistically significant" number of particles (Graham and Moyeed, 2002; Wan et al., 2009). Initial simulations with the BLO model were performed with one particle per parcel (referred to as 1× oversample), so that the count of modelled particles reflected the total count expected for each activity, and each simulation effectively represented one realisation of each activity. When fitting the BLO model, the full range of exhaled droplet diameters was broken into 25 equal increments on a base 10 log scale. In some of the increments in the oral mode and between the oral mode and the smaller diameters of the bronchiolar and laryngeal modes, the total number of particles in the increments was small. Sampling from the distribution meant that some increments contained no particles or only one or two particles. To improve the representation of the distribution, simulations were performed using ten times the number of parcels of particles (referred to as 10× oversample) and the results were scaled accordingly. An additional simulation of one cough was carried out with 100× oversample, but this did not significantly change deposition patterns compared to the 10× oversample simulation. Therefore, 10× oversample counts were used for subsequent BLO model simulations. Deposition patterns for the different particle counts are shown in Appendix A and the total parcel counts are shown in Table 6.

Table 6 Total parcel counts used in the simulations with the BLO model

	Total parcel count		
	1× oversample	**10× oversample**	**100× oversample**
One cough	310	3,093	30,947
Speaking	1,211	12,130	-
Singing	726	7,278	-

3.3.7 Pöhlker et al. (2021) model

Pöhlker et al. (2021) fitted the data they identified following the model of Johnson et al. (2011) as described in Section 2.4.1. Pöhlker et al. used five modes to improve the fit to the data and the parameters describing the distribution are shown in Table 7.

Their analysis showed small differences in the shapes of the distributions between data sets and exhalations. The same parameter values were used to describe the shape of the breathing modes, B1 and B2, in the multimodal fits for all the exhalations. The multimodal fits to speaking and coughing data used slightly different shapes for the LT, O1 and O2 modes. While the shapes of the distributions were similar across different data sets, the particle concentrations from different data sets showed order of magnitude differences in the particle concentrations.

Table 7 Parameters of Pöhlker et al. distribution

	B1	B2	LT	O1	O2
Speaking					
GMD_i (µm)	0.07	0.3	1.0	10	96
GSD_i (-)	1.89	1.89	1.89	2.00	1.99
Cn_i (cm^{-3})	15.6	2.23	1.71	0.05	0.29
Coughing					
GMD_i (µm)	0.07	0.3	1.0	11	128
GSD_i (-)	1.89	1.99	2.00	1.96	2.03
Cn_i (cm^{-3})	418.0	59.0	6.95	2.36	0.89

The multimodal distribution of droplets from exhalations describes the position, *GMD*, spread, *GSD*, and particle count concentration, *Cn*, for each mode. The number of droplets in a mode for an exhalation is the product of the particle count concentration and the volume exhaled. Sampling was performed directly from the modes, rather than using the previous approach of breaking the distribution into intervals, calculating then sampling the number of droplets in each interval. The number of droplets in an exhalation is too large to track each droplet as a computational particle. The Pöhlker distribution has more droplets overall than the BLO model and many more small droplets. The droplet parcel sampling factors shown in Table 8 are used to reduce the number of computational parcels tracked in simulations. Using these factors, similar numbers of computational parcels of droplets are used to describe the droplet distribution to those in simulations using the BLO model. The factors were applied when sampling from the modes of the distribution, resulting in the total particle counts used in simulations given in Table 9.

Table 8 Sampling factors used to determine the number of computational parcels used in simulations

	B1	B2	LT	O1	O2
Speaking	0.025	0.1	0.1	1	1
Coughing	0.001	0.01	0.1	0.25	1

Table 9 Total parcel counts used in the simulations with the Pöhlker et al. (2021) model

	Total parcel count
One cough	3,566
Speaking	12,574
Singing	10,081

4 COMPONENT VALIDATION

At the time of undertaking the current study, limited validation data were available for complete simulations of exhalations. Therefore, simulations were carried out on component parts with the aim of building confidence that the physical processes in each component were being adequately modelled. These component simulations were also used to guide the selection of appropriate models and meshing parameters for use in the exhalation simulations. An area for future work would be to extend the validation to datasets such as Chao and Wan (2006), which looked at an experimentally simulated cough in a ventilated chamber.

4.1 Decay of a turbulent jet

Simulations were undertaken of an isolated, axisymmetric turbulent jet, to inform the meshing and turbulence model selection in the case of modelling a cough jet. Numerous experimental datasets for isolated jets are available in the literature. The data from Hussein et al. (1994) is at a similar scale and the inlet conditions are fully defined. However, their experimental apparatus included flow conditioning to achieve a top-hat profile and the initial turbulence intensity is somewhat lower than could be expected for a jet resulting from a cough. A comparison of the jet parameters is given in Table 10, where the cough jet parameters are given fully in Section3.3.2.

Table 10 Comparison of modelled cough jet parameters with jet data from Hussein et al. (1994)

	Hussein et al. (1994)	**Modelled cough jet**
Diameter (mm)	25.4	22.5
Peak velocity (m/s)	56.2	15
Turbulence intensity (%)	0.58	10
Reynolds number (-)	9.55×10^4	2.26×10^4

The jet was modelled using a cylindrical domain with a circular inlet on one end. The sides of the cylinder and the end faces were set as pressure boundaries. The jet inlet was set as a pressure inlet, with the pressure specified to give the correct jet centreline velocity. Turbulence intensity was initially specified according to the experiments at 0.58%, though additional runs were carried out with the intensity set to 10%. A number of meshes were made, all using unstructured tetrahedral cells and with varying levels of mesh refinement, both on the jet inlet face and also in the volumetric jet region. Turbulence was modelled with the k-ε (Launder and Spalding, 1972), k-ω SST (Mentor, 1994) and k-ε RNG (Orszag et al., 1993) models.

Solutions were obtained using the coupled pressure based solver with second order differencing for all equations and the PRESTO! pressure interpolation scheme (ANSYS 2019b). Steady state results were obtained using the pseudo-transient method in which the solution is advanced using a virtual time step.

4.1.1 Results

The results of the simulations are presented as the normalised jet velocity with distance from the orifice, where U_o is the jet exit velocity and U_m is the centreline velocity. The results of Hussein et al. (1994) are also plotted alongside their fitted line having a virtual origin, x_o/d = 4, and slope, B = 5.8. The vertical axis is plotted as U_o/ U_m because the decay is expected to be proportional to 1/x. Results for the three meshes all using the k-ω SST turbulence model are shown in Figure 4. The medium and fine meshes slightly overpredicted the virtual origin distance compared to the fitted value, while the coarsest mesh underpredicted it. All three meshes gave broadly similar results in the far-field. In all cases, the jet decay was overpredicted.

Turbulence model sensitivity is shown in Figure 5. All results were obtained on the coarse mesh (mesh 3). Both the k-ε and k-ω SST models gave comparable results in the far-field with the k-ε overpredicting the decay rate in the near field. Relatively poor results were obtained for the k-ε RNG model, though the reason for this is not clear. To assess the effect of the inlet turbulence intensity, simulations were run on both the coarsest and finest meshes, with the k-ω SST model with two different levels of inlet turbulence intensity. Results are shown in Figure 6. For the lower level of intensity of 0.58%, corresponding to the measured value, the distance to the virtual origin was slightly over-predicted on the finest mesh and underpredicted on the coarsest mesh. For comparison, at a high level of 10%, the jet began to decay sooner and the result is less sensitive to the level of mesh refinement. At the higher level of intensity, the rate of decay predicted by the model had a better fit to the data.

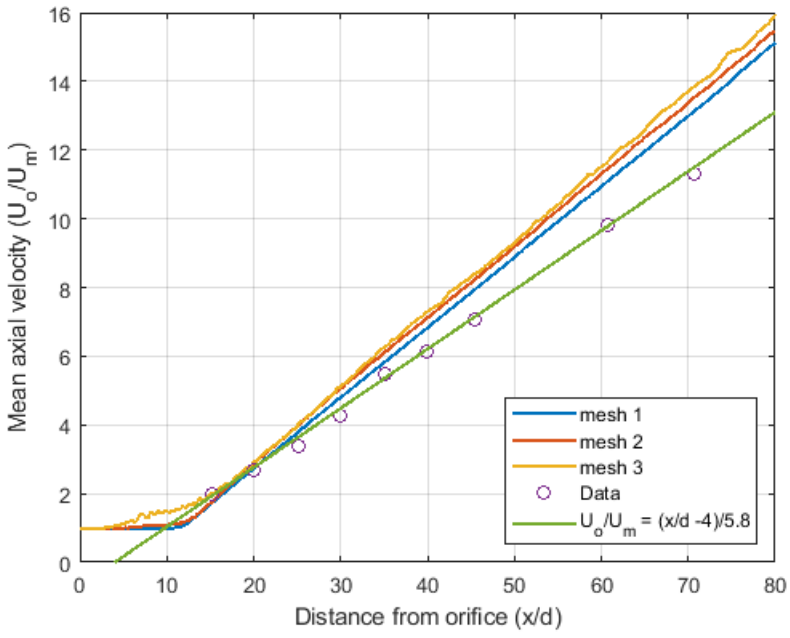

Figure 4 Axisymmetric jet velocity predictions, mesh refinement

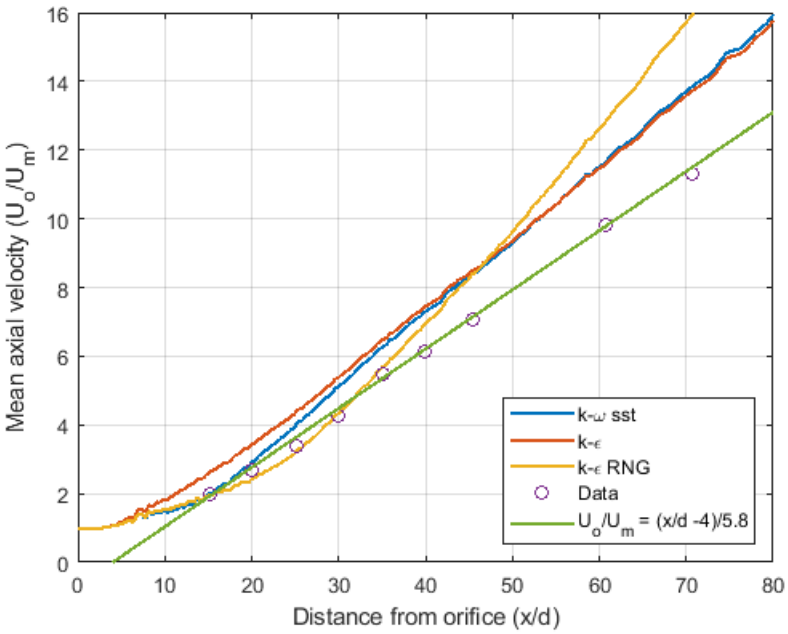

Figure 5 Axisymmetric jet velocity predictions, turbulence model comparison

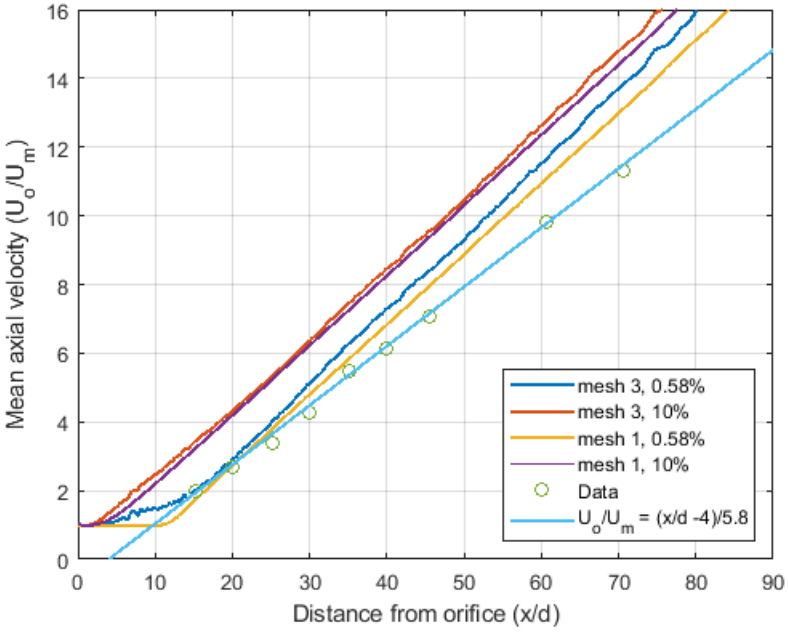

Figure 6 Axisymmetric jet velocity predictions, inlet turbulence intensity

4.2 Evaporation of a falling droplet

Hamey (1982) carried out experiments measuring the diameter of free-falling water droplets in ambient air. Droplets were introduced into still air with a relative humidity of 70% and a temperature of 20 °C. The experiments were modelled in Fluent using a cylindrical domain 2 m high and 0.5 m diameter. The domain was filled with a mixture of air and water vapour, where the initial mass fraction of water vapour was determined from the Antoine equation

$$P_{sat} = exp\left(A - \frac{B}{T + C}\right) \tag{19}$$

where P_{sat} is the saturation vapour pressure (kPa) at temperature, T (K) and A, B and C are model constants, given in this case by Hinds (1999) as 16.7, 4060 and -37 respectively. The saturation mole fraction is the ratio of the saturation pressure to the total pressure, in this case the ambient atmospheric pressure, P_{amb}

$$X_{sat} = \frac{P_{sat}}{P_{amb}} \tag{20}$$

The final mole fractions of water vapour, X_w, and air, X_a depend on the relative humidity, RH

$$X_w = X_{sat} \times RH, \qquad X_a = 1 - X_w \tag{21}$$

The mass fraction of water vapour is then

$$Y_w = \frac{X_w M_w}{(X_w M_w + X_a M_a)} \tag{22}$$

where M_w and M_a are the molecular weights of water and air respectively.

Figure 7 shows the result of the falling droplet calculation for the two different droplet evaporation models, the diffusion controlled model (Equation 2) and the convection-diffusion controlled model (Equation 3). Generally, there was good agreement with the experiments, though the final data point for the 110 µm droplet was underpredicted. There was relatively little difference between the two evaporation models, indicating that the simple diffusion controlled model would be sufficiently accurate for the current application. Figure 8 shows the result of the same calculation, but with the droplet having a non-volatile fraction of 1.8% by mass. In this case there was no difference in results. Further runs of this model to test its sensitivity to mesh and timestep are described in Appendix A.

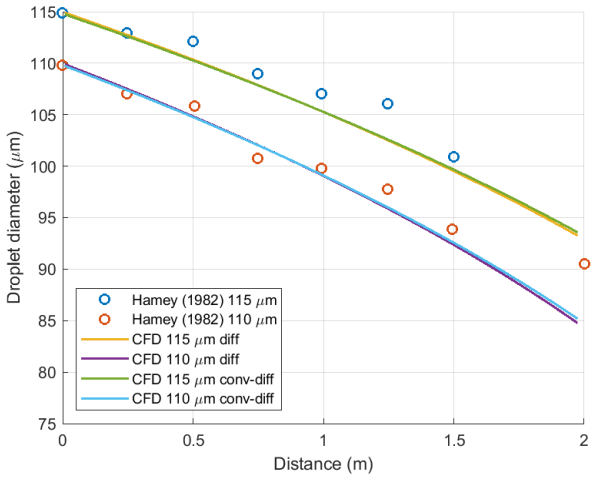

Figure 7 Comparison of diffusion controlled (diff) and convection-diffusion controlled (conv-diff) evaporation models

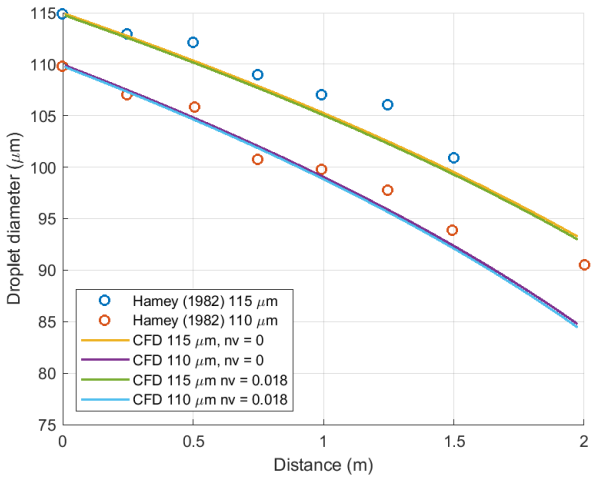

Figure 8 Comparison of droplet evaporation, with different non-volatile (nv) initial fractions. The model results are overlaid

4.3 Ventilated room

The heat released by a person can induce air flows which are sufficient to alter the distribution of a contaminant around that person. Experimental investigations of the airflow around a person in a ventilated room were carried out at the University of Tokyo (Nielsen et al., 2003). These experiments were designed as a benchmark test case for CFD modelling and therefore have been the subject of numerous modelling studies, e.g. Deevy and Gobeau (2006), Srebric et al. (2008).

The test case was a simple cuboidal room having displacement ventilation and a mannequin placed in the centre, shown schematically in Figure 9. Air velocity and temperature were measured on an array of vertical lines on the central plane of the room (Figure 10). Boundary conditions for the CFD simulations are given in Table 11.

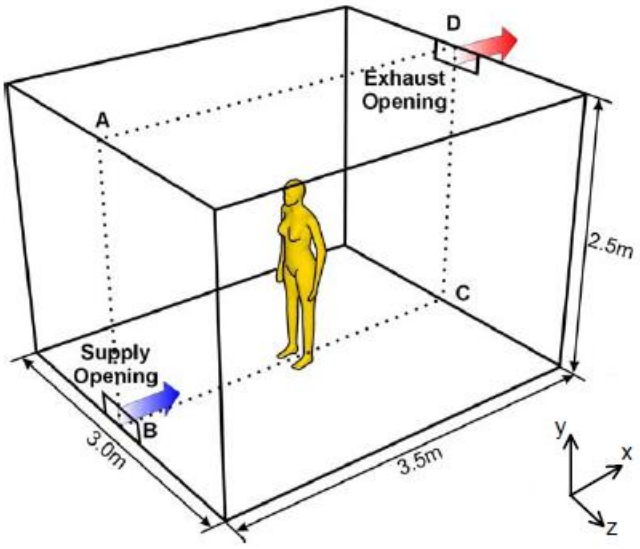

Figure 9 Schematic of the displacement ventilated room set up

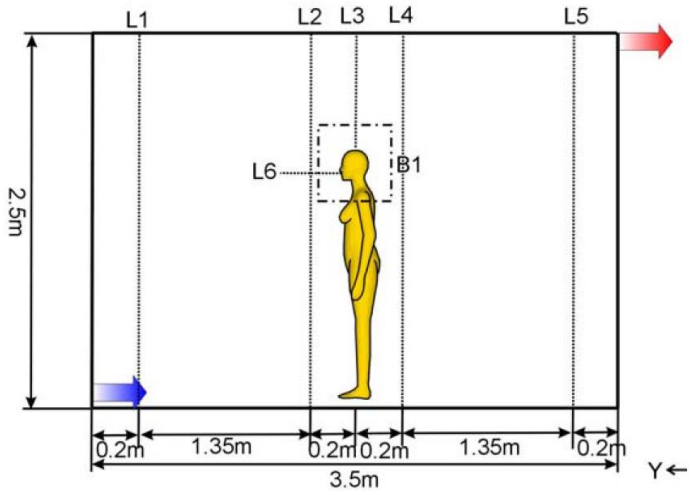

Figure 10 Schematic of the displacement ventilated room set up, showing measurement lines L1-L5

Table 11 CFD model boundary conditions

Parameter	Value
Inlet velocity (m/s)	2
Inlet temperature (°C)	22
Inlet turbulence intensity (%)	30
Inlet turbulent length scale (m)	0.1
Heat flux from mannequin (W)	38 without radiation, 76 with

The case was modelled in Fluent using a simplified geometry for the mannequin, based on overall size data for an American female (NASA, 1995). The simplified mannequin was used to avoid potential meshing issues as the effect of the geometry was found to have only a

small effect on predicted contaminant distribution in a room (Deevy and Gobeau, 2006). The modelled geometry is shown in Figure 11.

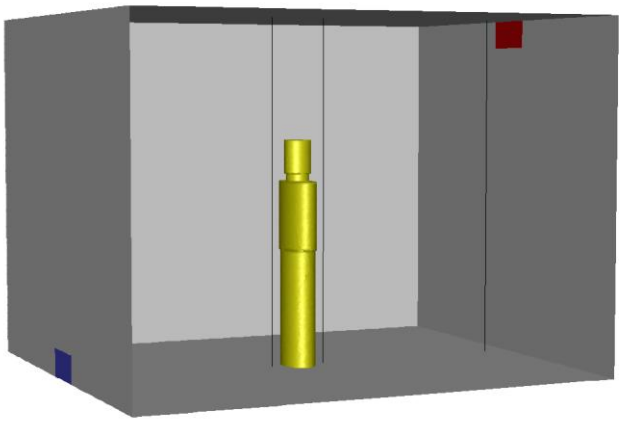

Figure 11 Computational domain showing ventilation openings and measurement lines

The geometry was meshed with unstructured tetrahedral meshes having prismatic inflation layers adjacent to the solid surfaces. Three mesh sizes were run, with node counts between 393000 and 656000. Similar results were obtained across all the meshes, so the following results are presented on the coarsest mesh. The coarsest mesh roughly corresponds to the finest mesh used by Deevy and Gobeau (2006) and reasonable run times were obtained on that mesh. Simulations were carried out with both the k-ε and k-ω SST turbulence models. Neither model was clearly superior to the other in terms of velocity prediction and both gave similar predictions of temperature distribution. In view of this, and the conclusions of Deevy and Gobeau (2006), the k-ω SST model was used for all subsequent runs. The walls were set either at a fixed temperature equal to the inlet temperature, or set as adiabatic when the radiation model was used. The total heat flux from the mannequin was 76 W (Nielsen et al. 2003) of which 38 W was assumed to be a convective heat flux, giving a convective to radiative ratio (CR ratio) of 50:50. In simulations run without the radiation model, the surfaces of the mannequin were set to a heat flux of 25 W/m^2 which corresponded to the heat output of 38 W. A heat flux of 50 W/m^2 was therefore used when the radiation model was used. The choice of CR ratio is somewhat uncertain and it has been suggested that values may range from 70:30 to 30:70 (Srebric et al., 2008). Radiation was modelled using the P1 model (ANSYS, 2019a), along with an absorption coefficient of 0.01 (Deevy and Gobeau, 2006). The choice of the absorption coefficient is also subject to some uncertainty as pure air is optically thin and does not respond to radiation. However, Deevy and Gobeau (2006) suggested that the absorption coefficient is closer to 0.17 for air with a relative humidity of 50%.

The simulations were run using the pseudo-transient solver and the average temperature of the outlet vent was monitored. Although the level of the residuals indicated that the solutions were converged, it was necessary to run the simulations beyond this point until a steady outlet temperature value had been reached. It was also observed that the geometry of the mannequin coupled with the ventilation flow jet along the floor introduced an inherent unsteadiness to the flow. The thermal plume from the mannequin was also not completely steady. A single transient simulation was run for a time period of one hour, which showed

some time dependence on the velocity field near the mannequin (on the measurement line L4 – see Figure 8) but there was little effect on the temperature field.

Srebric et al. (2008) suggested that there is some uncertainty in the thermal boundary conditions due to small heat fluxes through the insulation and therefore the assumption of adiabatic walls may not be entirely correct. They attempted to account for this discrepancy by introducing a further 10 W heat flux over the floor area which resulted in better agreement with the measured values. An additional run was carried out using the radiation model and this additional heat flux applied to the floor.

Velocity predictions for the different thermal boundary conditions are shown in Figure 12. The series marked as “fixed temperature” and “adiabatic” refer to the wall boundary treatment for the lower mannequin heat flux of 25 W/m^2. The velocities along measurement lines L1 and L2 in front of the mannequin were reasonably well predicted in all the cases, with the floor jet from the vent inlet being slightly overpredicted. Velocities along L4 immediately behind the mannequin were significantly overpredicted by the models with the lower 25 W/m^2 heat flux which did not include radiation.

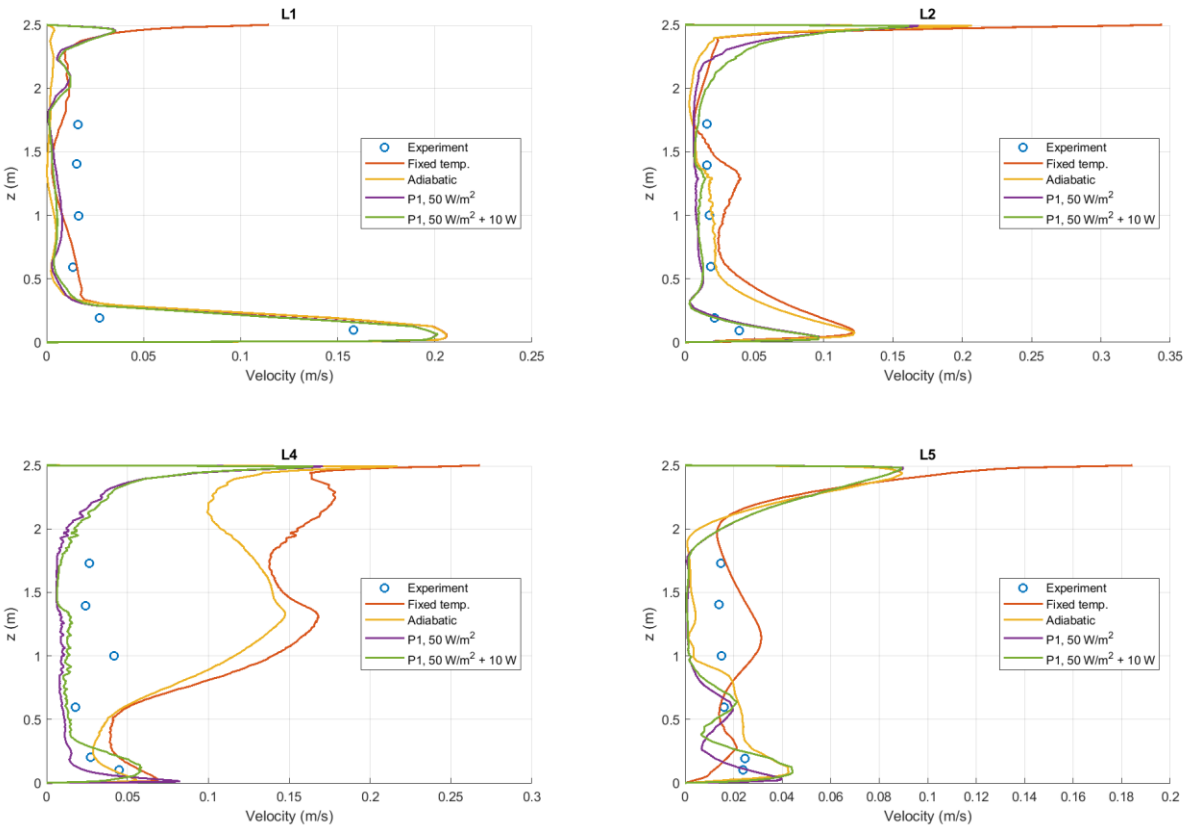

Figure 12 Velocity predictions for the displacement ventilation case. “Fixed temp” and “Adiabatic” refer to simulations with the lower mannequin heat flux of 25 W/m^2. P1 refers to the runs using the radiation model

Temperature predictions are shown in Figure 13. In the cases which did not include radiation, the predicted temperatures were significantly lower than the measured values at all the

measuring locations. Relatively good agreement was obtained with the higher mannequin heat flux and radiation model. The average temperature rise of the ventilation flow of air with a 76 W heat input was roughly 3.8 K, which corresponds roughly to the maximum value seen at measurement line L5. However, the predicted values at all locations were somewhat lower than the observed ones. A simulation was also carried out with an absorption coefficient of 0.17. This did not alter the velocity predictions significantly, but did slightly increase the temperature in the lower half of the room. It is not clear whether the additional 10 W heat flux applied over the floor area was the cause of the differences between measurements and predictions, but its inclusion resulted in a better match of temperature gradients over the height of the room and had a more significant impact than changing the absorption coefficient.

In general, good agreement was obtained with the displacement ventilation chamber experiments, but the simulations showed that the thermal treatment of the boundaries has a considerable effect on results, particularly in this stationary environment with quiescent flows.

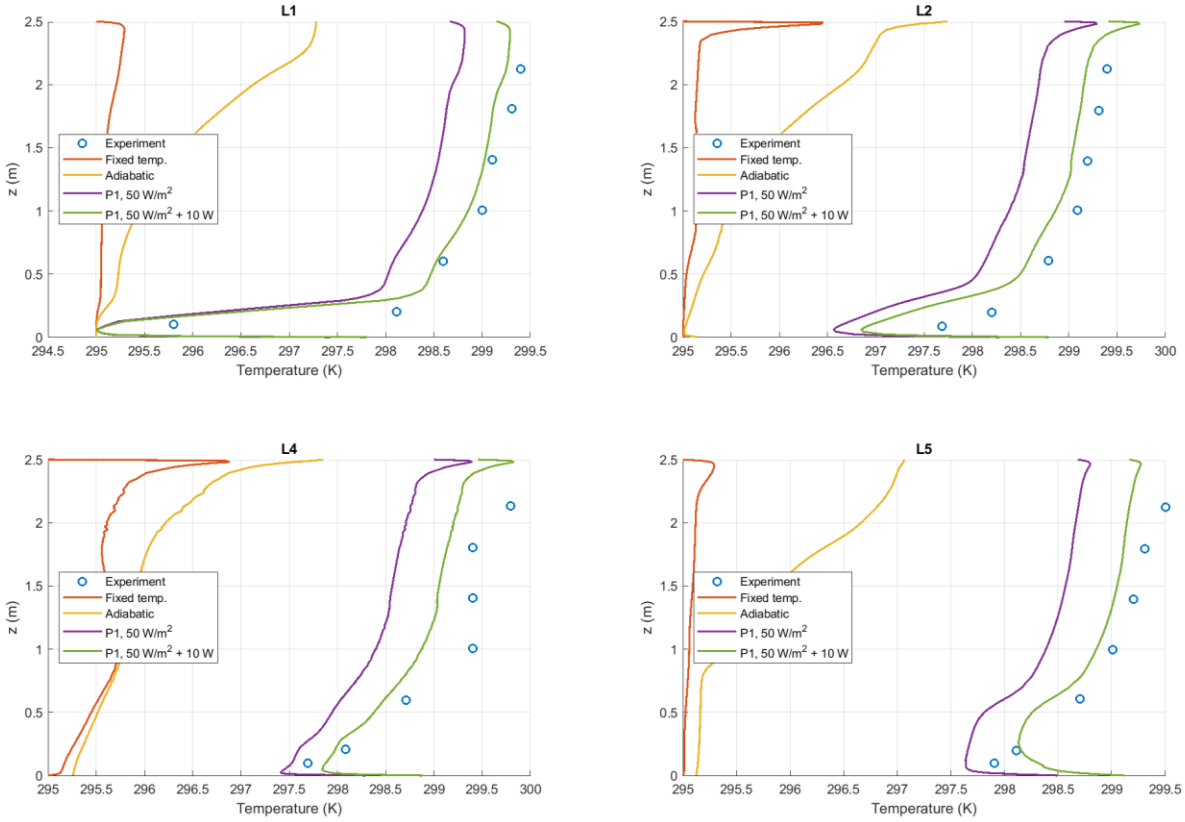

Figure 13 Temperature predictions for the displacement ventilation case

5 UKHSA EXPERIMENTS

5.1 Experimental description

Experiments were carried out by the United Kingdom Health Security Agency (UKHSA) to investigate the behaviour of exhaled aerosol and droplet particles. The study measured respiratory bacteria as a means of assessing the dispersion characteristics of aerosols and droplets in a 4 m x 2.3 m x 2.3 m (Length × Width × Height) environmental chamber, shown in Figure 14(a). The chamber was unventilated during experiments, with the only flow provided by air samplers operated during the study.

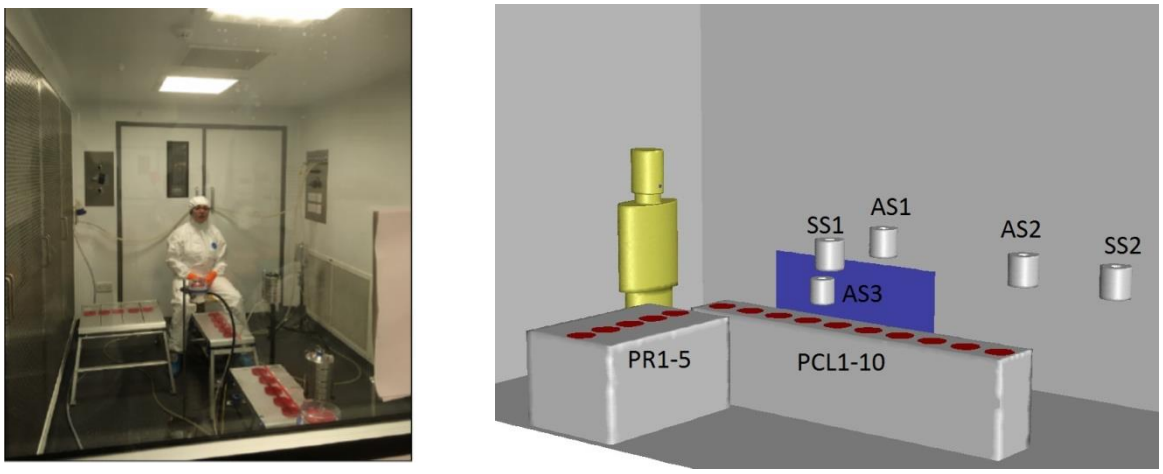

a b

Figure 14 Experimental set up in the environmental chamber and modelled geometry (b). The modelled geometry shows the sampler locations with the naming convention used to present the results

Ten laboratory workers were recruited to carry out the study, with an age range of 21-59 years and gender balance of 50% female and 50% male. Ethical approval for the study was given by the UKHSA Research Ethics and Governance of Public Health Practice Group (UKHSA REGG). The participants wore hooded Tyvek suits, shoe coverings and gloves to reduce shedding of non-oral micro-organisms and remained seated facing forwards during the study. Participants provided a spit sample into a universal container before each experiment, primarily to assess bacterial load. Participants were seated at one end of the chamber and were required to perform a sequential set of activities as follows: cough three times; read out loud the numbers from 1 to 100; inhale and exhale 3 times; sing happy birthday twice loudly; inhale and snort 3 times; read out loud the numbers from 1-100; and cough three times.

Samples were collected by air samplers (Andersen 6 stage and Slit samplers) and on 15 Columbia Blood Agar (CBA) settle plates placed at 20 cm intervals directly in front of and to the side of the subject. The Andersen samplers operated at 28.3 L/min and collected particles onto six CBA plates fractionated by particle diameter, though the breakdown by diameter was not included in the results. The slit samplers sampled onto a rotating CBA plate at the same flow rate. Both samplers were operated for a period of ten minutes. Sampler positions are described in the CFD modelling section below. Immediately before the start of the experiment, the settle plates had their lids removed, the air samplers were switched on

automatically and the ventilation was turned off remotely. At the end of each ten minute period, the samples were collected and incubated for analysis and the room was ventilated with filtered air for at least ten minutes at 180 air changes per hour before the next study.

The number of colony forming units (CFUs) collected and cultured on each plate were used to define the bacterial deposition onto the surface or the total sampled from the air over the ten minute experimental period. The type of bacteria and their origin (e.g., organisms from the respiratory tract) that formed the colonies in these assays has not yet been determined. Consequently, a proportion of the colonies detected may have come from other sources.

5.2 Geometry and meshing

The modelled geometry is shown in Figure 14 b. The tables holding the settle plates were 0.5 m high and approximated by cuboidal volumes, with the centreline settle plates labelled PCL1-PCL10 and the right hand side settle plates labelled PR1-PR5, with PCL1 and PR1 being closest to the subject. The centreline plates were set out to a distance of 2 m from the subject's assumed knee position and the right hand plates were set out to 1 m from the subject's assumed knee position. The air samplers, at 1 m height, were represented by floating cylindrical volumes, labelled Andersen "AS" and slit "SS". AS1 and SS1 were located at 1 m, AS2 and SS2 at 2 m and 2.5 m respectively and AS3 at 1 m to the left of the participant. The subject was approximated by a simplified geometry (NASA, 1995), having a mouth defined by a circular opening set at a height to match a sitting position. In the experiments, there will have been some variability of the subject's dimensions, along with the distance from the subject's face to the first settle plate.

The chamber was meshed using unstructured tetrahedral cells, with prismatic inflation layers adjacent to the solid surfaces. In the region where the thermal plume from the person impinged on the ceiling, wall y^+ values were approximately 11.5, with an average of 2.5 on the body surface. Mesh refinement was applied in the region of the mouth and the exhaled jet, based on isolated jet simulations. Cell sizes varied from approximately 3 mm at the mouth, to approximately 75 mm in the room, away from walls or openings. The results reported here were obtained on meshes of approximately 655,000 nodes, which provided reasonable run times. A mesh sensitivity study was carried out, which showed that particle sample results were insensitive to further mesh refinement. An explanation for this behaviour is that the sampled results are driven by ballistic deposition or sedimentation, rather than wall parallel flow, where mesh effects can be important. Increasing the overall mesh density to 2.3 million nodes did not appreciably change the diameter ranges or quantity of particles collected by the settle plates or air samplers. The air samplers mainly collected small particles, which are influenced by the room air flow.

5.3 Boundary conditions

The experiments were carried out at an ambient temperature of 22 °C and a relative humidity (RH) of between 44% and 50%. All solid walls were set to the ambient temperature value and the solution initialised with a RH of 50%. As the people in the experiments were fully clothed apart from their face, only the convective heat flux from the subject was modelled, which was applied as a surface heat flux of 25 W/m^2. This value is similar to that measured by Zhu et al. (2006) for a resting subject. The inlet of each air sampler was a circular region, set as an outflow through which air was drawn at a constant volume flow rate, equal to the

experimental flow rate. The room was specified as being unventilated during the trials, but there was likely to be a small air exchange through the door seal and ventilation system. A pressure boundary matching the position of the ventilation inlet in the chamber was defined (shown in blue in Figure 11b) to balance the outflow of air through the samplers. This was specified as a relative pressure of zero and backflow temperature equal to the room temperature. In practice, the leakage flows are unknown. However, the air velocity through this balancing opening was very small, and did not influence the flows in the room.

5.4 Simulation strategy

Simulating all the activities sequentially (i.e., coughing, speaking, singing) in a single simulation would result in having to track a large number of particles and would also incur a substantial computational overhead from having to resolve in time each activity in the sequence. For practical purposes, the simulations were carried out individually, where single simulations of one activity (coughing, talking or singing) were run with subsequent output of particle fates over a ten minute period, corresponding to the experiment, and the particle data were concatenated in post-processing as shown in Table 12. One drawback with this method of simulation is that potential additional dispersive effects of subsequent activities were not accounted for. To further reduce the computing overhead, each ten minute simulation period was divided into three phases; a 30 second initialisation phase with a one second time step, the activity phase with a finer time resolution of 0.01 s (coughing) or 0.1 s (speaking/singing), and a settling phase lasting the remainder of the duration again having a one second time step. These were based on an assessment of the sensitivity of the results to the time step length. In the settling period, the effects of subsequent activities and breathing were ignored.

Table 12 Method for concatenating the particle data

Name	Speaking	Singing	Coughing
Standard source	2 × source 1	1 × source 3	6 × source 5
Modified source	2 × source 2	1 × source 4	6 × source 5

5.5 Modelling the bacterial load

The experimental data were presented as the mean number of bacterial colony forming units (CFUs) recovered from each sample plate and aerosol sampler, with error bars to represent one standard deviation. This was considered an appropriate measure for comparison against computational results. It should be noted that the generation of bacteria was variable by person; one participant generated 39% of all deposited bacteria and 29% of airborne particles, and 50% of participants generated 80% of deposited and airborne bacteria.

In comparing the computational results to experimental data, it was assumed that the collection efficiency of the aerosol samplers was 100% for all sizes. Sample results were compared with the predicted concatenated cumulative particle dataset, where for the idealised case it is assumed that each sampled computational particle results in a bacterial colony and the number of sampled computational particles can be directly compared to the experimental data. For the k^{th} sample location, the total number of particles, N_k, can be defined as follows

$$N_k = N_{parcels,k} \times N_p \tag{23}$$

where $N_{parcels,k}$ is the number of sampled parcels and N_p is the number of particles per parcel. An alternative measure is to compute relative counts which can be used to assess the level of dispersion among the sample locations. The first centreline settle plate (PCL1) was chosen to normalise the results, to give a normalised count, $N_{norm,k}$, as follows

$$N_{norm,k} = \frac{N_{parcels,k}}{N_{parcels,PCL1}} \tag{24}$$

Results from the experiment were normalised in the same way, using the count on the first settle plate. The viability of airborne bioaerosols is influenced by a number of factors (Fernandez et al., 2019) so the count of modelled particles may tend to overestimate the number of viable particles emitted. In this case, viable refers to the initial probability of a particle containing viable material; it does not account for further effects such as viability in cell culture, damage due to drying, or the possibility that the final dried particle diameter might be smaller than the dimension of a bacteria. The mean number of colony forming units in a particle of initial diameter, d_0, can be expressed by (Anand and Mayya, 2020)

$$\mu = \frac{\pi}{6} d_0^3 C_b \tag{25}$$

where C_b is the mean number of aerobic bacteria cultured and was estimated from the UKHSA experiments to be 7.37×10^7 CFU/mL (SD ± 6.43×10^7, range 1.5×10^7 CFU/mL to 2.37×10^8 CFU/mL). Assuming a Poisson distribution, the probability that a particle will contain at least one CFU is given by (Anand and Mayya, 2020)

$$P = 1 - e^{-\mu} \tag{26}$$

Figure 15 shows the variation of P with particle diameter for the range of C_b given above. The number of viable particles, $N_{viable,k}$, at the k^{th} sample location was calculated by:

$$N_{viable,k} = N_p \sum_k P \tag{27}$$

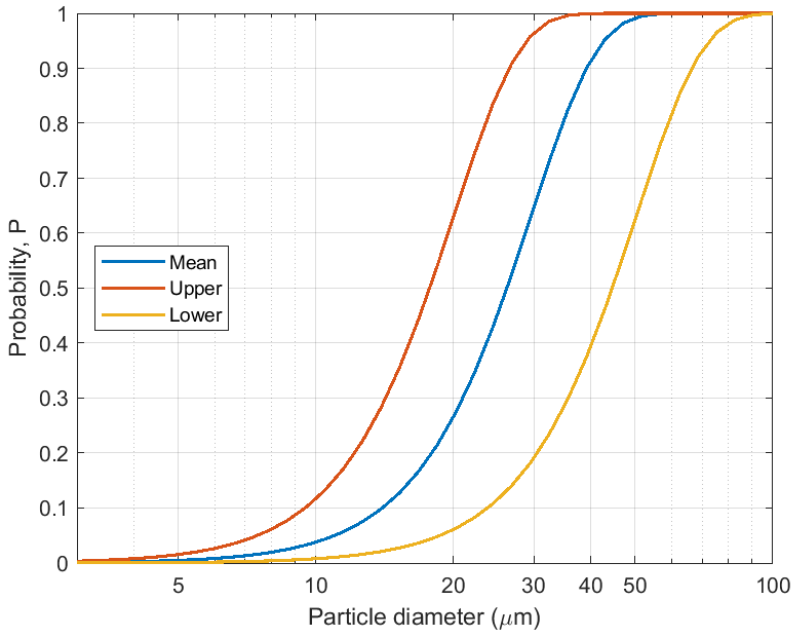

Figure 15 Variation of the probability, P, that a particle will contain at least one CFU with particle diameter

5.6 Results – BLO model

5.6.1 Comparisons in air and on surfaces

Comparisons between the measured experimental microbial data and simulated particle counts in air and on surfaces are shown in Figure 16. Both experimental and computational results show the same trends, with greater deposition onto surfaces closer to the source than at a further distance. Experimental results also clearly show that exhaled bacteria were present in the air and on surfaces at 2 m from the source. The number of bacteria that deposited at 2 m is around a quarter of the number at 0.2 m, but the particle count extracted from the air in this small unventilated chamber was actually greater at 2 m than at 1 m, and greater than that deposited onto surfaces.

Results for the centreline settle plates are shown in Figure 16 a, using the idealised particle count given by Equation 23. Particle count on the closer plates was overpredicted with those on the first plate overpredicted by a factor of five. One reason for this overprediction is that every particle that landed on a plate is counted in the simulation, whereas in the experiment, only those that formed a culture were recorded. The modified source terms for speaking and singing resulted in slightly increased deposition on the nearest plates, due to the increased particle input velocity. However, most of the particles deposited on all the plates were from the coughing activity and the contribution of speaking and singing to the total count on the plates remained small. Figure 16 b shows a comparison of the viable particles for the centreline plates, using Equation 27. The results are the same as the idealised case for the first two plates where the rapid deposition of larger particles dominated. Further away, the predicted viable count decreased compared to the idealised case. The results with the normalised particle count using Equation 24 shown in Figure 16 c show that the predicted rate of decay with distance was steeper than seen in the experiments with a greater number of bacteria collected on the more distant plates than predicted by the model. This was likely

to be a result of the variability within the experiments, including individual differences in exhalation velocities and particle size ranges which were not fully replicated in the model. The simulated input carrier flow was fixed in each case such that variability was only included in the particle oversampling, which only accounted for part of the overall variability. The order of magnitude difference in counts on the plates observed between individuals was not represented in the model. In the model, no particles were predicted on the off-axis plates to the right of the subject. However, a small number of particles were collected on these plates in the experiment.

Results for the Andersen air samplers are shown in Figure 16 d to f. The model overpredicted absolute counts at the inline samplers (AS1, AS2), see Figure 16 d, while no particles were predicted to be collected by the off-axis sampler to the left of the person (AS3) although samples were collected in the experiments. Figure 16 e shows the adjusted results for the Andersen air samplers, accounting for the viability of the particles. These results are significantly different. In the model, these samplers collected only the smallest particles (<10 µm), which have a lower probability of containing viable bacteria (Figure 15). It is likely that these results are heavily influenced by the initial droplet size distribution. Figure 16 f shows that relative collection was around three times higher at the 1 m sampler in the simulation, whereas at 2 m the experimental and computational results are similar. Further analysis of the model results showed that a chamber length recirculation, driven by the subject's thermal plume, was transporting particles from the ceiling towards the end of the room and down the end wall. This may explain why the second Andersen sampler (AS2) in the experiment collected a relatively large number of particles.

In the model, this recirculation also resulted in an increased predicted particle count in the slit sampler adjacent to the end wall. The air sampler results suggest that the dispersion off the centreline axis is being underpredicted. There are several reasons why this may have occurred. Firstly, it is likely that there were small but finite ventilation flows in the experimental chamber that were not captured by the model, such as leaks through the door or ventilation panels, air movements due to the movement of the subjects, residual air movements from setting up the experiments or residual air movements from ventilation. Secondly, in the experiments, each activity was carried out in succession and this would have had a mixing effect on the particles exhaled from the previous activities. This effect would not have been captured in the simulations, where each activity was carried out in isolation. Finally, the intra-person variability would have resulted in a wider spread of data, while parameters such as the carrier flow and projection angles were fixed in the simulations.

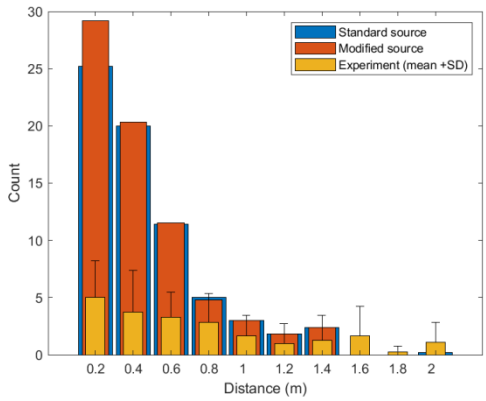

a: Cumulative results, centreline (count)

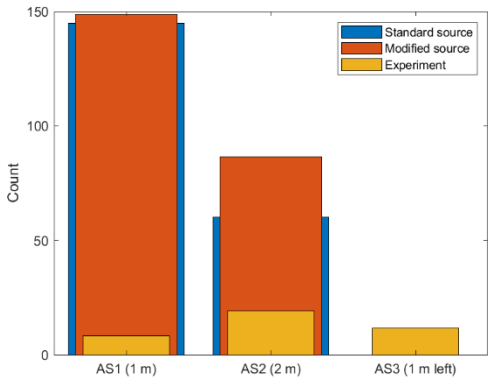

d: Cumulative results, Andersen (count)

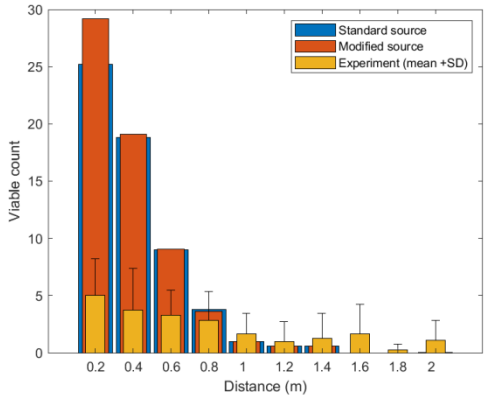

b: Cumulative results, centreline (viable count)

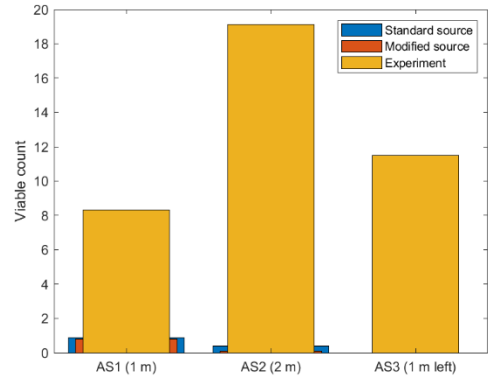

e: Cumulative results, Andersen (viable count)

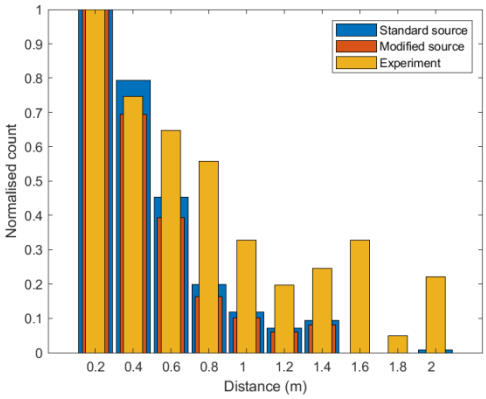

c: Cumulative results, centreline (normalised count)

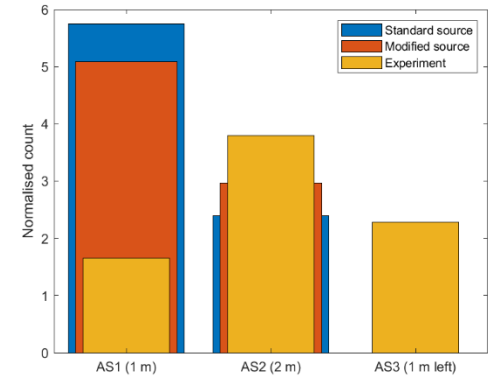

f: Cumulative results, Andersen (normalised count)

Figure 16 Comparison of measured (mean+SD) microbial counts (yellow) with simulated predicted counts at the sample locations using different metrics and the standard source (blue) and modified source (orange). Cumulative counts were obtained from the concatenated datasets for each activity at each location. a) and d) show actual simulated number of particles, (Equation 23). b) and e) show predicted number of viable particles, (Equation 27), c) and f) show normalised count (Equation 24)

5.6.2 Analysis of particle sizes

Figure 17 shows the partitioning of sampled particle sizes from the CFD simulations on the surfaces and collected in the air samples, for each individual activity. In each case, the count refers to the number of parcels sampled at each location and these are compared with the input number of parcels shown in blue. The diameters in Figure 6 are the initial diameters of the particles at their time of injection, for both input and sampled particles; although the diameter change due to evaporation is modelled, the comparison is made using the initial diameters to illustrate the ultimate fate of different sizes of exhaled particles. For clarity, the surface samples were grouped together into “Centreline dishes” (orange), “Centreline tables” (yellow), “Right table” (purple) and “Floor” (green). The right hand plates are not included in these plots, because no particles were predicted to deposit there. The air samples are recorded at “AS1” (orange), “AS2” (yellow), “SS1” (purple) and “SS2” (green), see Figure 14 b. The general trend is that the larger particles, representing the oral mode of production, were deposited on surfaces. The predicted air samples were generated entirely by the bronchiolar and laryngeal modes from the input BLO particle distribution. The exception was the cough, in which most of the full range of sizes was projected on to the surfaces. This partitioning of diameters between surfaces and air samples appears to be, in part, due to the droplet diameter distribution in the BLO model which has a pronounced dip in the initial diameter distribution, around 30 μm, between B and L, and O modes.

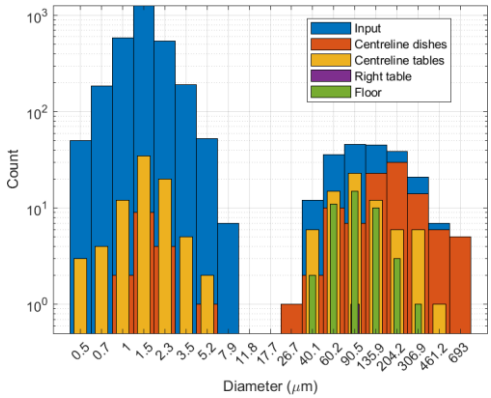

a: surface sample count, one cough

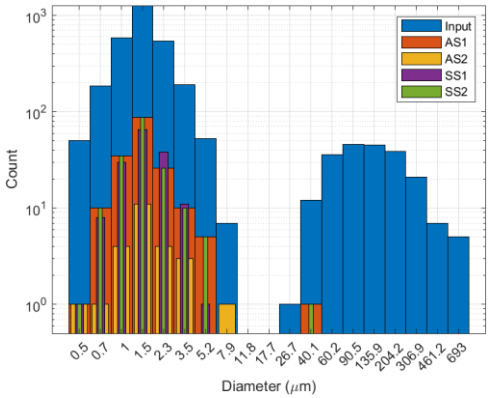

d: air sample count, one cough

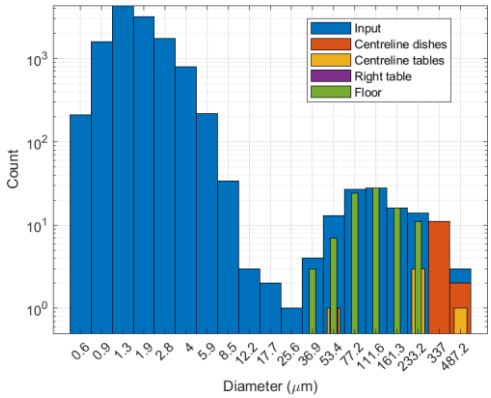

b: surface sample count, speaking

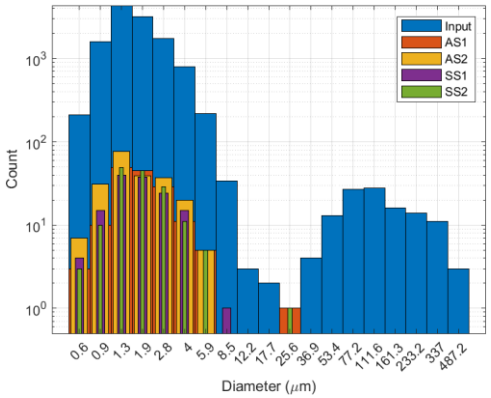

e: air sample count, speaking

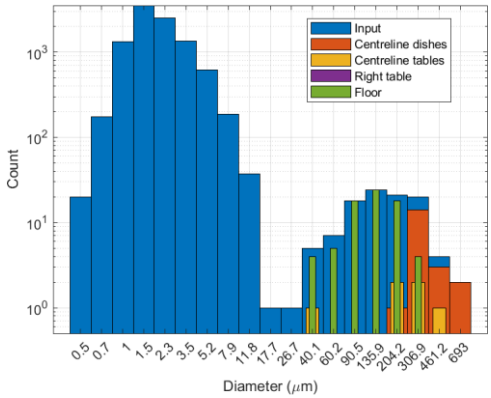

c: surface sample count, singing

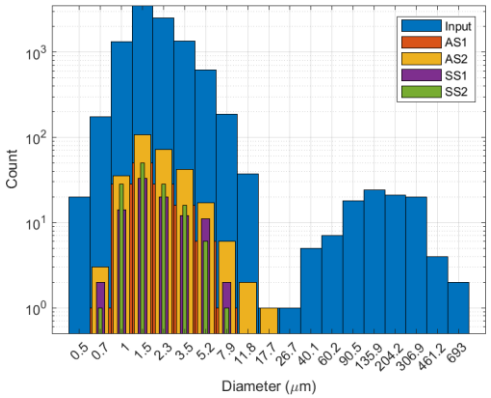

f: air sample count, singing

Figure 17 Comparison of sampled particle diameters with the input diameters for the BLO model. On the left (a, b, c) are all of the surface samples for coughing, talking and singing respectively and on the right (d, e, f) are the corresponding air samples. In each case, the diameter is the initial diameter of the particles at their time of injection, irrespective of their diameter at the point of sampling

5.6.3 Influence of evaporation

Figure 18 shows the change in particle diameters from the original to the diameter at the point of sampling for the three activities. Sampled particles are those collected on a surface, extracted by the air samplers or those remaining suspended at the end of the simulation period. The results suggest that the division between the B/L and O modes remains pronounced at the point that particles are sampled. Small particles have relatively fast

evaporation timescales but longer persistence in the air. Larger particles have slower evaporation timescales but deposit relatively quickly on surfaces.

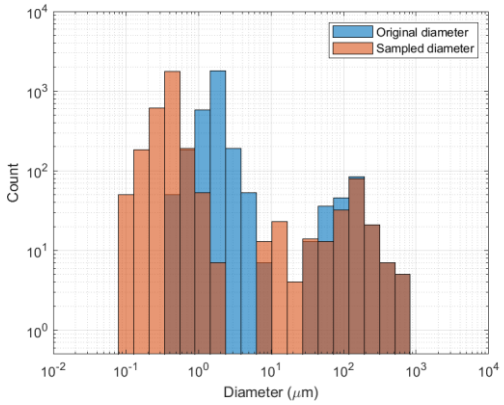

a: one cough

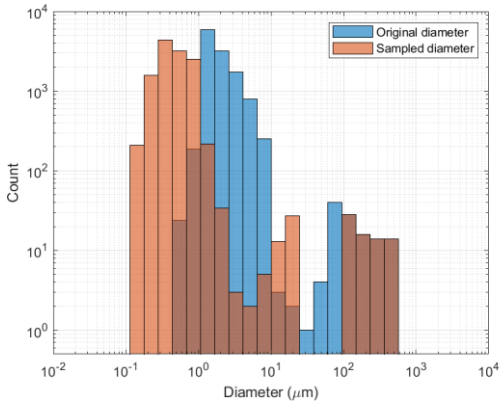

b: speaking

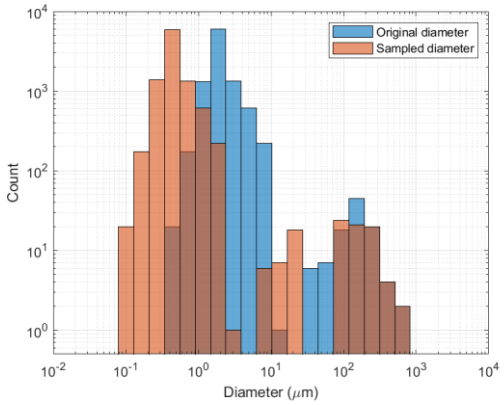

c: singing

Figure 18 Comparison of model particle counts for the initial (blue) and sampled (orange) diameters for the BLO model. In addition to deposited and extracted particles, any suspended particles at the end of the simulations were counted as sampled. The darker shaded bars are where both input and samples overlap

5.7 Results – Pöhlker et al. (2021)

5.7.1 Comparisons in air and on surfaces

Simulations using the distribution described by Pöhlker et al. (2021) were run for the modified sources only (Sources 2, 4 and 5 in Table 4). Deposition results for the distribution are shown in Figure 19 a to c. It is clear that this distribution contains many more particles than the BLO model and therefore deposition is significantly overpredicted using the idealised count given by Equation 23. Similar results were obtained taking into account viability given by Equation 27, suggesting that particles sufficiently large (according to Equation 26) to contain one bacterium were being deposited. Comparison of the normalised count (Figure 19 c) showed that the decay rate was relatively well predicted using the Pöhlker et al. (2021) distribution.

Results for the Andersen air samplers are shown in Figure 19 d to f. As for the centreline settle plates, the absolute counts are again significantly overpredicted, as this distribution produces much more airborne material. However, it is noteworthy that relatively few particles were captured by the off-axis sampler AS3.

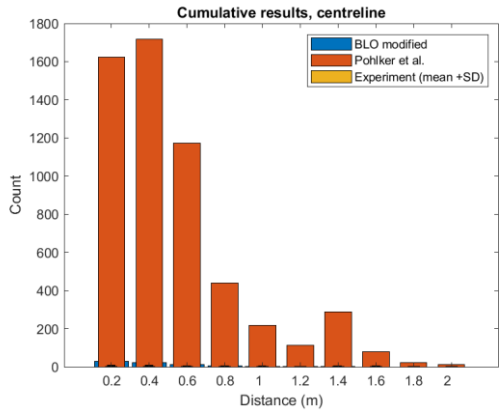

a: Cumulative results, centreline (count)

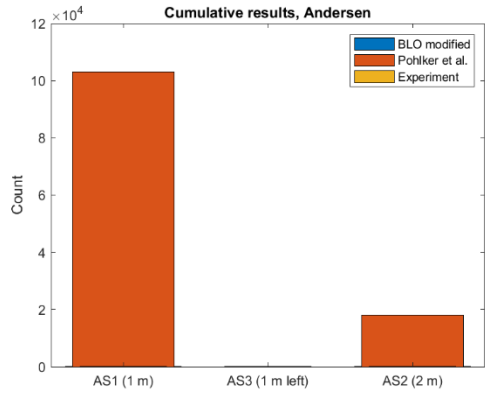

d: Cumulative results, Andersen (count)

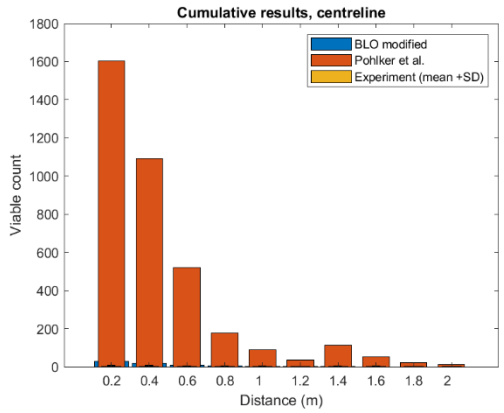

b: Cumulative results, centreline (viable count)

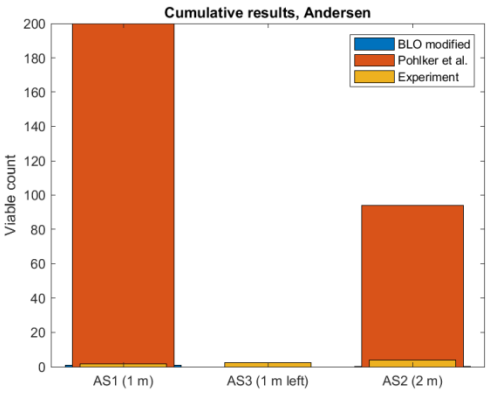

e: Cumulative results, Andersen (viable count)

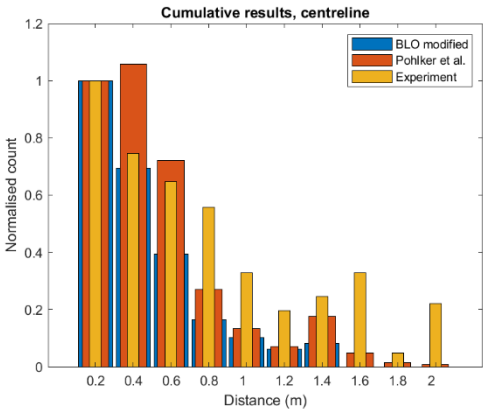

c: Cumulative results, centreline (normalised count)

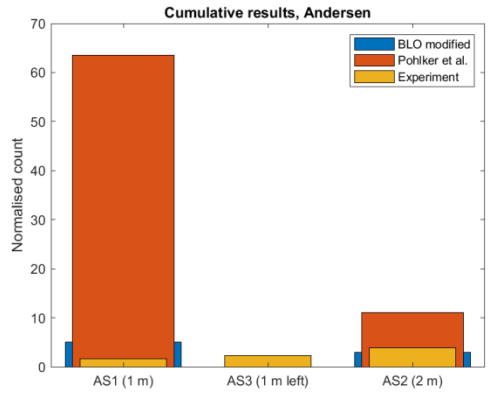

f: Cumulative results, Andersen (normalised count)

Figure 19 Comparison of measured (mean+SD) microbial counts (yellow) with simulated predicted counts at the sample locations using different metrics with the BLO model (blue) and Pöhlker et al., (2021) (orange). Cumulative counts were obtained from the concatenated datasets for each activity at each location. a) and d) show actual simulated number of particles, (Equation 23). b) and e) show predicted number of viable particles, (Equation 27), c) and f) show normalised count (Equation 24)

5.7.2 Analysis of particle sizes

Figure 20 shows the partitioning of sample sizes for the Pöhlker et al. (2021) distribution. The surface samples are shown in Figure 20 a to c. As with the BLO model, the cough activity projected the full range of particle diameters onto the surfaces. The speaking and singing activities projected the largest particles on to the centreline tables and dishes. These

activities also resulted in a small number of particles (around 20 µm) depositing on surfaces. However, the timescales associated with the deposition of these small particles was relatively long, suggesting that they are being transported by the room air flow. The air samples are shown in Figure 20 d to f. For all the activities, there is a relatively clear cut-off of particles that remained airborne. Some relatively large particles (around 90 µm) were captured by the air samplers. This behaviour was not seen with the BLO model where relatively few of these mid-range particles were simulated.

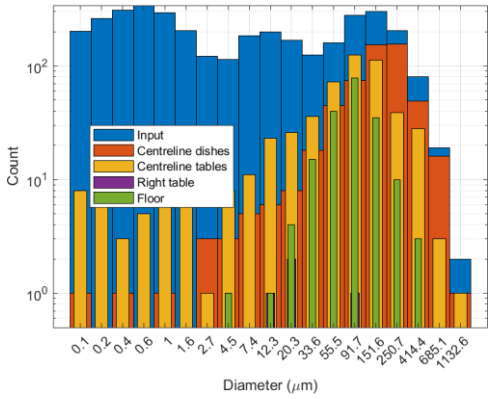

a: surface sample count, one cough

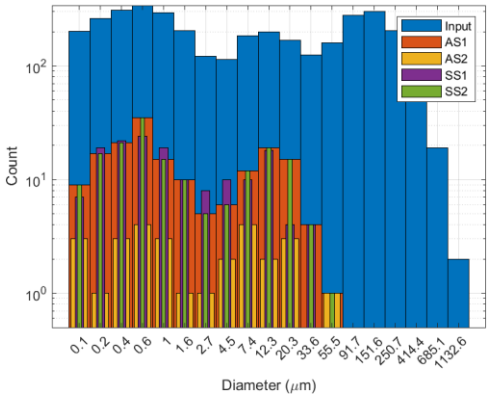

d: air sample count, one cough

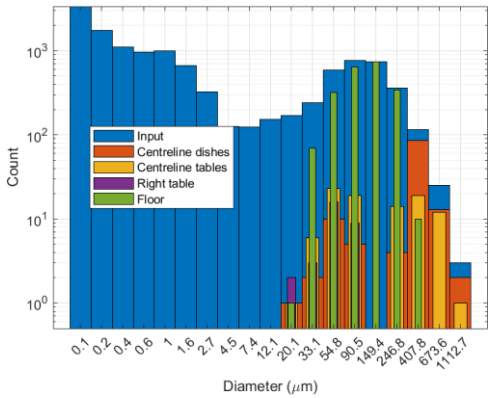

b: surface sample count, speaking

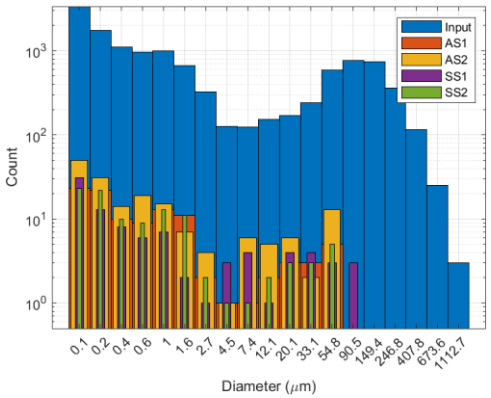

e: air sample count, speaking

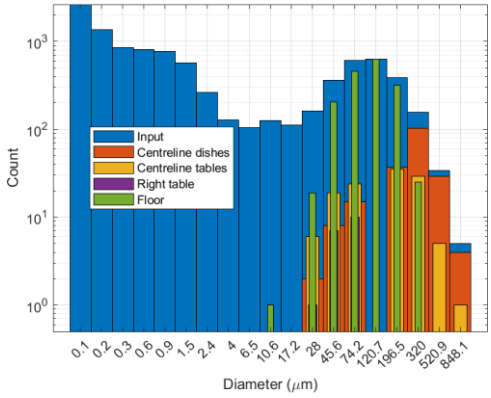

c: surface sample count, singing

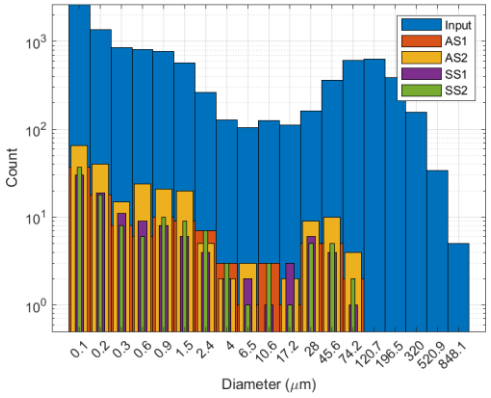

f: air sample count, singing

Figure 20 Comparison of sampled particle diameters with the input diameters for the Pöhlker et al., (2021) model. On the left (a, b, c) are all of the surface samples for coughing, talking and singing respectively and on the right (d, e, f) are the corresponding air samples. In each case, the diameter is the initial diameter of the particles at their time of injection, irrespective of their diameter at the point of sampling

5.7.3 Influence of evaporation

Figure 21 shows the change in particle diameters from the original to the diameter at the point of sampling for the three activities. As with the BLO model, the smallest diameter particles evaporate to their minimum diameter, whereas the largest particles were sampled before significant evaporation occurred. Unlike the BLO model, the full range of particle diameters were sampled.

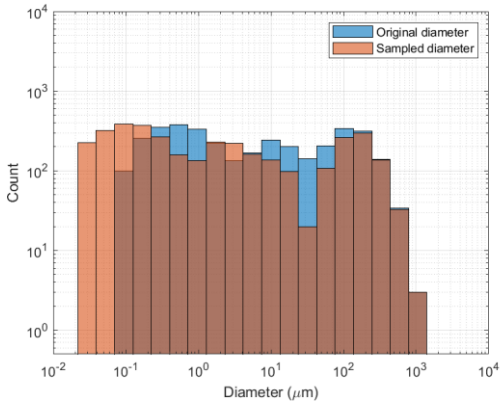

a: one cough

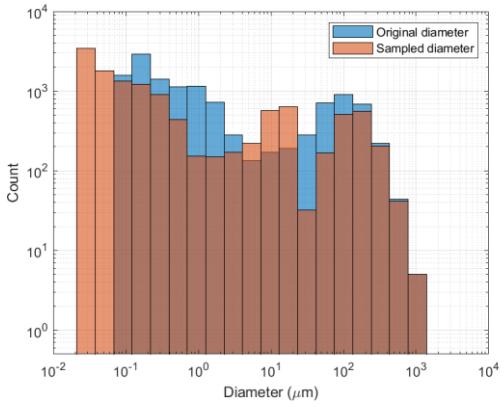

b: speaking

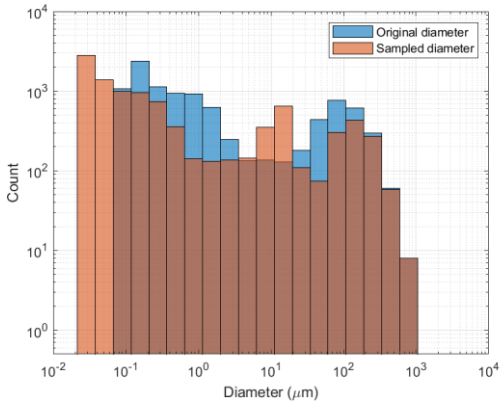

c: singing

Figure 21 Comparison of model particle counts for the initial (blue) and sampled (orange) diameters for the Pöhlker et al., (2021) model. In addition to deposited and extracted particles, any suspended particles at the end of the simulations were counted as sampled. The darker shaded bars are where both input and samples overlap

5.8 UKHSA modelling conclusions

Comparisons with the UKHSA human participant study showed that the model was able to produce realistic patterns of microbial surface deposition and concentrations in air, although it slightly underpredicted the distance travelled by both aerosols and droplets. Given the uncertainties involved in simulating these experiments, the computational results obtained on the centreline were particularly encouraging. The discrepancies seen off-axis require further investigation to understand the variability in the experimental study deposition results. The simulations are based on a mostly uniform set of conditions and therefore will not capture much of the intra- and inter-person variability seen in the volunteer experiments. In a modelling study, the effects of this variability can be further understood through a sensitivity analysis of the type reported by Ho (2021). However, this would be a significant computational undertaking without making numerous simplifying assumptions.

The approach taken in the current modelling study was to implement a practicable estimate for a source term for different exhalation activities, and to simulate activities separately and sum the effects rather than simulate sequentially. In the case of the BLO model, some variability has been included through the use of ten-times oversampled particles, giving a greater spread of particle injection times and velocities. However, the off-axis samples are likely to be influenced by aspects of the ventilation flow that were not accounted for in the simulations, where it was assumed that the flow of air drawn by the samplers was balanced by that through a single vent panel. In practice, there will have been small but finite air flows through the doors and other ventilation controls which may have increased mixing within the chamber. In addition, the sequence of vocal activities in the experiment would contribute to the overall mixing in the room.

The thermal conditions in the room and the heat output from the person will have affected the air flows within the room. The thermal conditions in the experiment may have differed from the idealised case simulated and it is not possible to replicate these in the model without detailed experimental measurements. This may be significant in terms of the heat input from the person, where existing experiments (e.g. Nielsen et al., 2003) assumed an unclothed subject. The validation study described in Section 4.3 showed that air velocities and temperatures are sensitive to small changes in surface heat fluxes and thermal radiation.

The model results depend on a number of assumptions and input models, including the need to specify emission rates of respiratory droplets and aerosols and exhalation parameters such as velocity and angle of the jet. The BLO model (Johnson et al., 2011) resulted in a fairly clear distinction between particles that would remain airborne and those which deposit relatively quickly, however it is noted that the bimodal distribution is not seen in other measured data (Duguid, 1946; Pöhlker et al. 2021) and may be related to how the different size categories of respiratory particles are measured and sampled. The BLO model is based on data collected over multiple studies, with multiple volunteers and using different measuring techniques. It is representative across the range of measured particle sizes. However, it is recognised that there is an inherent variability in such measurements.

The particle size distribution of Pöhlker et al. (2021) did not have a clear distinction in particle sizes and also contained many more particles than the BLO model. The surface and air samples showed that there was an overlap between the diameter range that remained airborne and those that deposited on surfaces.

The CFD model also assumed that microorganisms were uniformly distributed by volume, which may not be the case if there is preferential aerosolisation into smaller or larger sizes due to hydrophobicity effects, or clumping of bacteria.

Despite these uncertainties, the model results showed similar behaviour to the experiments in that deposition was greater within 1 m than at 1 to 2 m from source and the results from the air samplers suggested that fine (approx. 0.1 µm to 90 µm for the Pöhlker et al., (2021) distribution) particles would eventually be uniformly suspended in the room given sufficient mixing time. This suggests that a computational model based on parameters from measured aerosol and exhalation data and the physics of droplet evaporation can provide realistic representations of the fate of exhaled microbial particles.

6 APPLICATION OF THE MODEL

6.1 Scenarios with screens and ventilation

As a result of interest in different mitigation measures, such as screens and screen-like mitigations, a number of scenarios were modelled with the aim of improving the understanding of the physics of droplet behaviour in response to these mitigation measures. For these cases, a representative screen was used as a physical barrier to reduce the transmission of large exhaled droplets when individuals come into close proximity. The range of scenarios modelled was not exhaustive, but was selected to be representative of some generic geometrical and ventilation configurations. The aim wasn't to provide specific advice on mitigation measures or their efficacy, but, through providing a better understanding of the fluid dynamics of virus transmission, to provide an improved understanding of where and how different mitigation measures could be used most effectively.

6.1.1 Geometry and mesh

The simulations were based around a room having the same geometry as the ventilated chamber described in Section 4.3, which has dimensions of 3.5 m x 3.0 m x 2.5 m (L x W x H). These dimensions are representative of a small meeting room, though the ceiling height is somewhat lower than a standard room height. The geometry was created with openings for displacement ventilation, as modelled in Section 4.3, as well as mixing ventilation diffusers in the ceiling. A limited number of model runs were carried out with the displacement ventilation, but full analysis of the results were not carried out as mixing ventilation is more common in practice. The modelled geometry is shown in Figure 22.

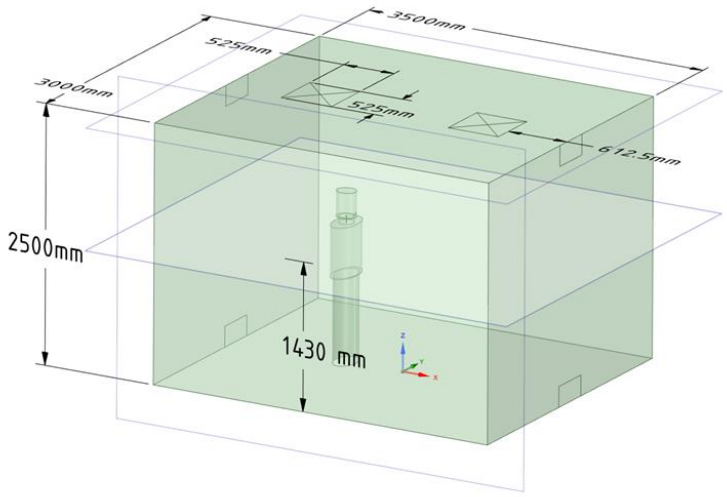

Figure 22 Modelled geometry showing overall dimensions. The plane at 1430 mm from the floor is the mouth height. The screen, if used, was set in the middle of the room

In all simulations with screens, the screen was placed centrally in the room and the distance from the person to the screen was varied by moving the person.

Different configurations of the mixing ventilation opening, screen and person were modelled, these are shown in plan view in Figure 23. The meshing strategy was the same as was used for the UKHSA experiments in Section 5 and the ventilated room described in Section 4.3. Meshes were composed of tetrahedral cells with prismatic inflation layers adjacent to the solid surfaces and having a volumetric refinement region in the vicinity of the mouth to capture the jet. The list of scenarios modelled is shown in Table 13. Note that the first row in the table represents four simulations, i.e. where a screen is either present or not and the distribution used was either the BLO distribution, Johnson et al. (2011) or the Pöhlker distribution, Pöhlker et al. (2021). The direction of the ventilation flow is determined by assignment of each vent as either an inlet or an outlet which is also given in Table 13.

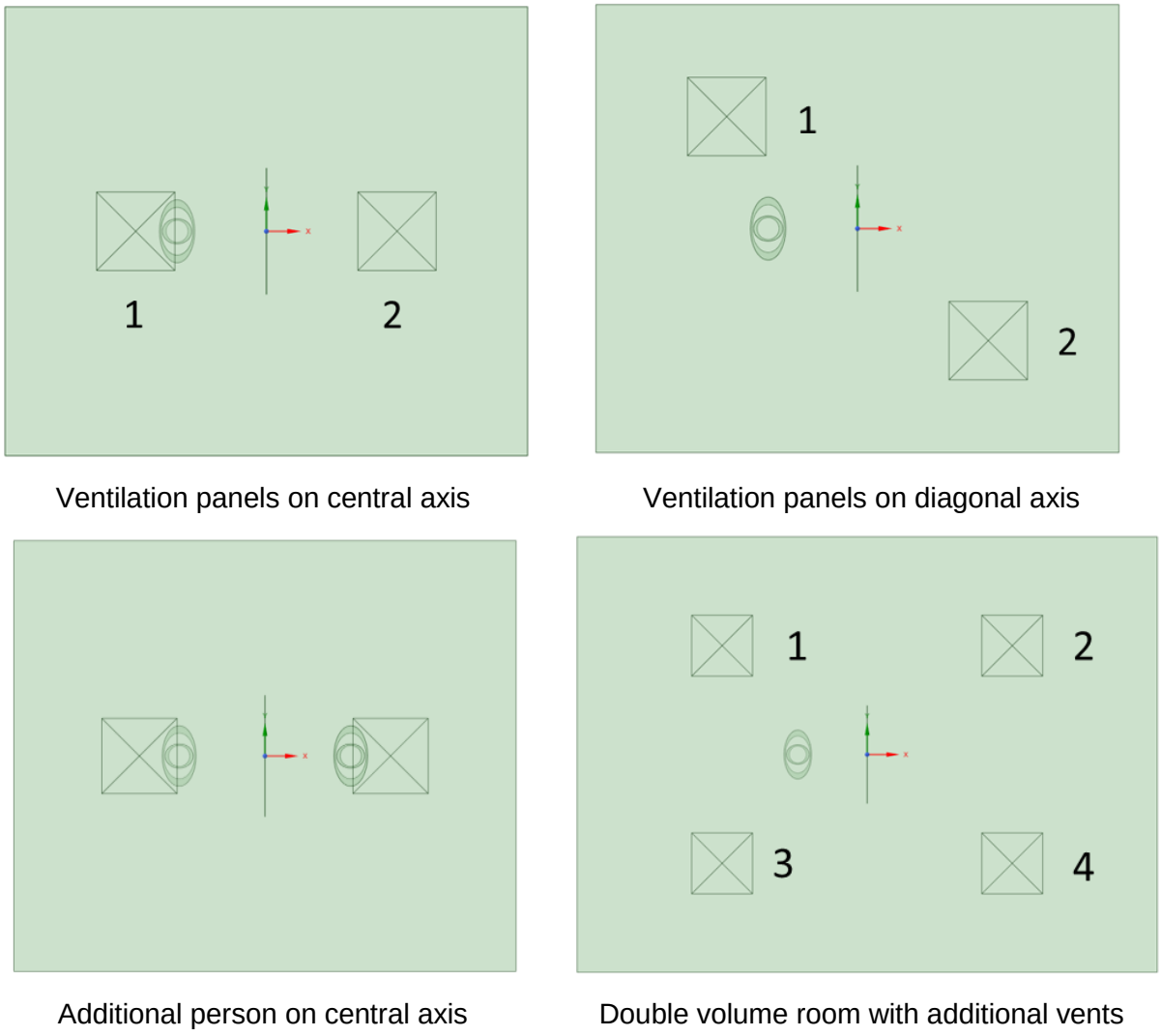

Ventilation panels on central axis

Ventilation panels on diagonal axis

Additional person on central axis

Double volume room with additional vents

Figure 23 Plan view of the different mixing ventilation configurations

6.1.2 Boundary conditions and source term

The four-way diffusers positioned in the ceiling were set as velocity inlets with corresponding pressure outlets. In each case, the diffuser areas were split into quadrants with the inlet and extract flows 30° to horizontal (Foat et al., 2022). The total flow was specified to give an air

change rate of 5 air changes per hour (ACH). For the double volume room, this was achieved by doubling the number of inlets, but keeping the ventilation velocity the same. The vent inlets had a turbulence intensity of 5%, a length scale of 0.01 m and a temperature of 22 °C. For the mixing ventilation simulations the displacement vent openings on the room ends were not used and were set as wall boundaries. All walls were set as a fixed temperature of 22 °C and the heat flux from the person fixed at 25 W/m^2.

Two source terms were modelled, these were the speaking and coughing sources (sources 2 and 5 in Table 4, Section 3.3.3). The particle sizes were defined using both the BLO distribution, Johnson et al. (2011), and distribution of Pöhlker et al. (2021) which are detailed in Section 3.3. As with the UKHSA simulations, the total simulation time was split into three parts. The first part was a flow initialisation period of 10 minutes. This was followed by either 25 seconds of speaking, or a single cough. The speaking or cough were followed by a final mixing period of 5 minutes.

Droplets within the simulations using the BLO distribution were modelled using the multicomponent artificial saliva model detailed in section 3.2.5. In view of the relatively large number of additional simulations required and the computing overhead, simulations with the Pöhlker distribution were modelled using pure water with a non-volatile fraction, rather than the multicomponent artificial saliva model. This simplification was justified on the basis of the similarity of deposition patterns between the two material models as detailed in Section A.4.

Table 13 Scenario list. Screen thickness was 5 mm with a width of 842 mm for all cases, the default height was 1861 mm. By default there was one person performing the exhalations.

Screen	Distance from Screen (mm)	Ventilation	Distribution	Exhalation
None/1	500	1 in, 2 out	BLO/Pöhlker	Speaking
1	750	1 in, 2 out	Pöhlker	Speaking
1	250	1 in, 2 out	Pöhlker	Speaking
None/1	500	1 in, 2 out	Pöhlker	One cough
1	500[1]	1 in, 2 out	Pöhlker	Speaking
None/1	500	1 in, 2 out; Diag	Pöhlker	Speaking
None/1	500	2 in, 1 out	Pöhlker	Speaking
1	500	1, 4 in, 2, 3 out	Pöhlker	Speaking
1	500	1 in, 2 out; 0.5 or 2.5 ACH	Pöhlker	Speaking

[1]Additional person on non-emitter side of the screen

6.1.3 Output locations

For each simulation, the particle data were extracted for the entire room volume and a number of the surfaces. In addition, two sub-volumes were defined ‘emitter’ and ‘non-emitter’ either side of the screen as shown in Figure 24. The sub-volumes intend to represent approximate “breathing zones” for calculation of viral exposures as defined in section 6.1.4. The zones were defined from 1 m – 2 m height, extending the full width of the screen and projecting 1 m away from the screen. Samples were also extracted at these volumes in the cases without a screen. The sample locations are shown schematically in Figure 24.

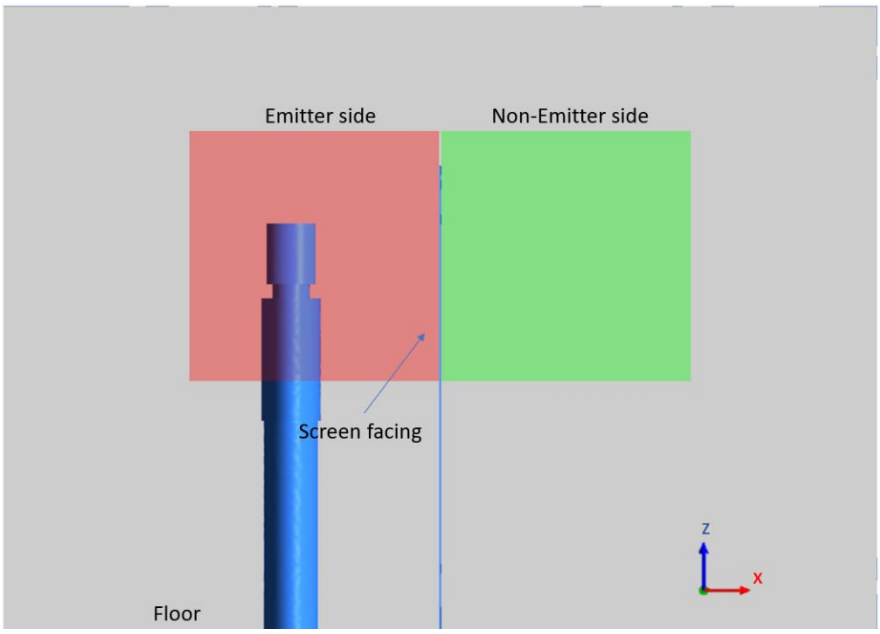

Figure 24 Schematic of the locations for output of the results. The left red volume and right green volume represent volumes in which particle data was sampled.

6.1.4 Calculating viral exposure

The potential viral exposure gives a metric of determining how exhaled aerosols contribute to a potential risk of infection within different areas of the CFD domain. Assuming a uniform viral load in the droplets ($c_v = 2.76 \times 10^{15}\ copies \cdot m^{-3}$) following the approach of Foat et al. (2022), the number of viral copies for a given droplet of diameter d_k can be calculated as,

$$\mu_k = c_v \frac{\pi}{6} d_k^3 \tag{28}$$

Note that Equation 28 is the same as Equation 25, except for the use of the viral load, c_v.

Within a sample volume V, occupied by N droplets, the viral exposure ($copies.s.m^{-3}$) is defined as:

$$E = \frac{\sum_{k=1}^{N} \mu_k t_k}{V} \tag{29}$$

with t_k the residence time of droplet k within the sample volume.

The work of Dargaville et al. (2021) has a viral half-life of approximately 33 minutes for similar ambient conditions. Viral decay was not included within the current modelling approach as the presented simulations span 5 minutes from the start of exhalation to the end

of the ventilation phase and therefore viral decay was deemed not to be significant in the time scales simulated.

6.2 Screen and ventilation results

The different scenarios simulated in Table 13 allow a comparison to be made to determine how differences in geometry and boundary conditions may influence the exhalation, transport of exhaled droplets and the potential viral exposure. The top row of Table 13 provides the base case against which other simulations are compared. Results for the base case are presented from simulations made using both the BLO distribution and Pöhlker et al. (2021) distribution. All the other results presented are from simulations made using the Pöhlker distribution. It can be assumed that, unless stated otherwise, the results presented used the Pöhlker distribution. The key aspects investigated through these results are the effectiveness of screens at limiting droplet transport and the influence of geometry specific ventilation on these results. The effect on the physical behaviour of droplets, categorised as small ($d_0 < 20$ µm), medium (20 µm $< d_0 < 100$ µm) and large ($d_0 > 100$ µm, based on their initial diameter, and the effect on viral exposure are both described.

6.2.1 Effectiveness of screens

During the exhalation period, droplets are injected into the domain with sizes sampled from the speaking distributions detailed in Section 3.3. The position of these droplets at 10 second intervals, starting four seconds into the exhalation, and continuing through the first 35 seconds can be seen in Figure 25, for the base cases with and without a screen. The trajectories show that during the exhalation period the smaller droplets are transported by the exhaled carrier flow. The exhalation travels axially and begins to rise due to buoyancy. This is because the exhaled air is warmer and therefore less dense than the cooler ambient air. The larger droplets behave ballistically, and have trajectories reflecting this, being dominated by their initial velocity and depositing under the influence of gravity. The medium size droplets exhibit behaviour that overlaps with the behaviour of the small and large droplets.

When no screen is present the exhalation travels to the non-emitter side without obstruction. At 14 seconds into the speaking activity the aerosol cloud generated is well within the non-emitter side sample volume. Contrasting this with the screen case, the aerosol cloud moves radially to the edge of the screen before then being transported by the ventilation flow.

The screen influences the direction of the carrier flow resulting in flow curvature due to its presence. This in turn affects the trajectories of the droplets. The large droplets which would have continued along ballistic trajectories impinge onto the screen.

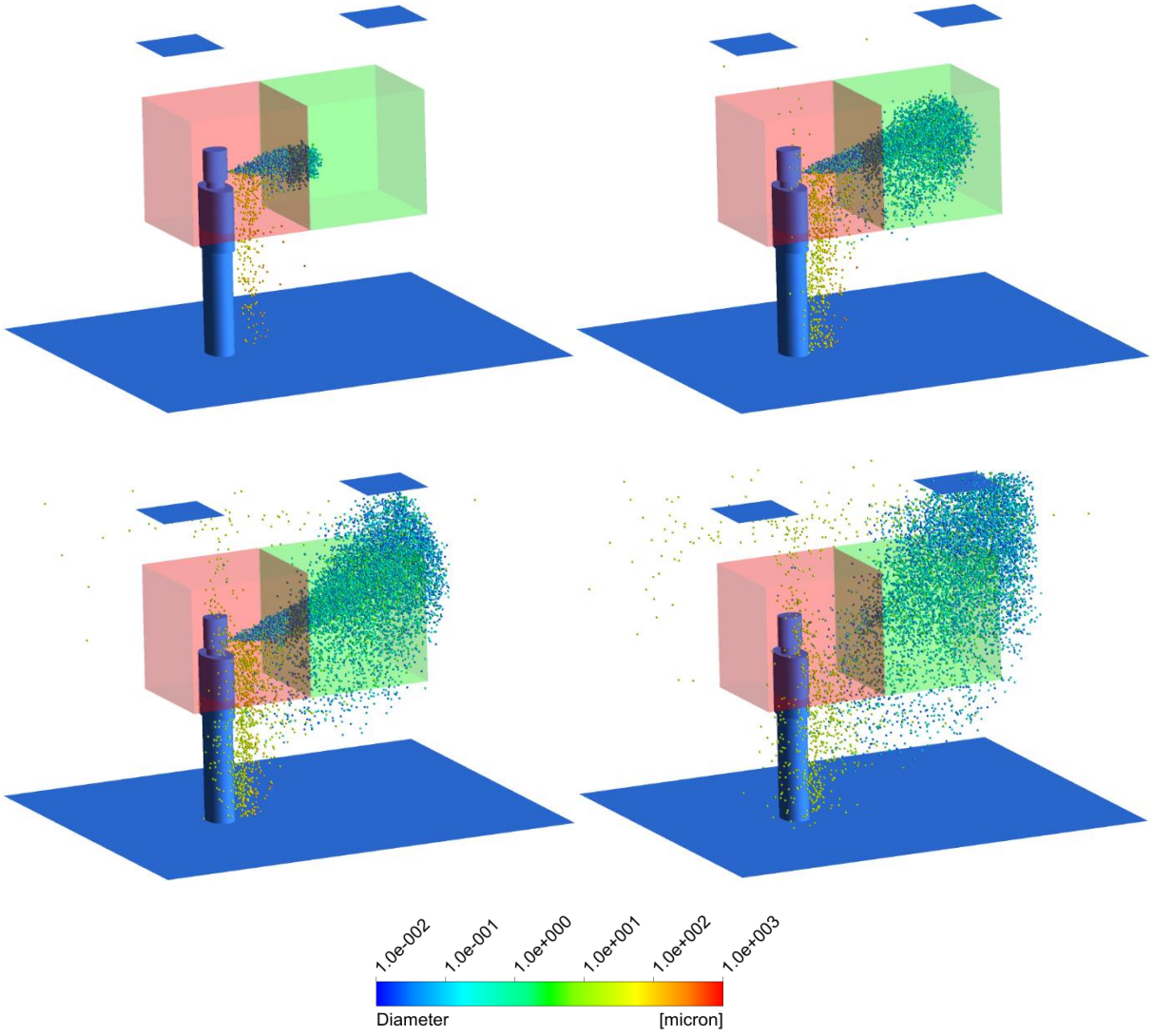
1.0e-002
1.0e-001
1.0e+000
1.0e+001
1.0e+002
1.0e+003
Diameter
[micron]

(a)

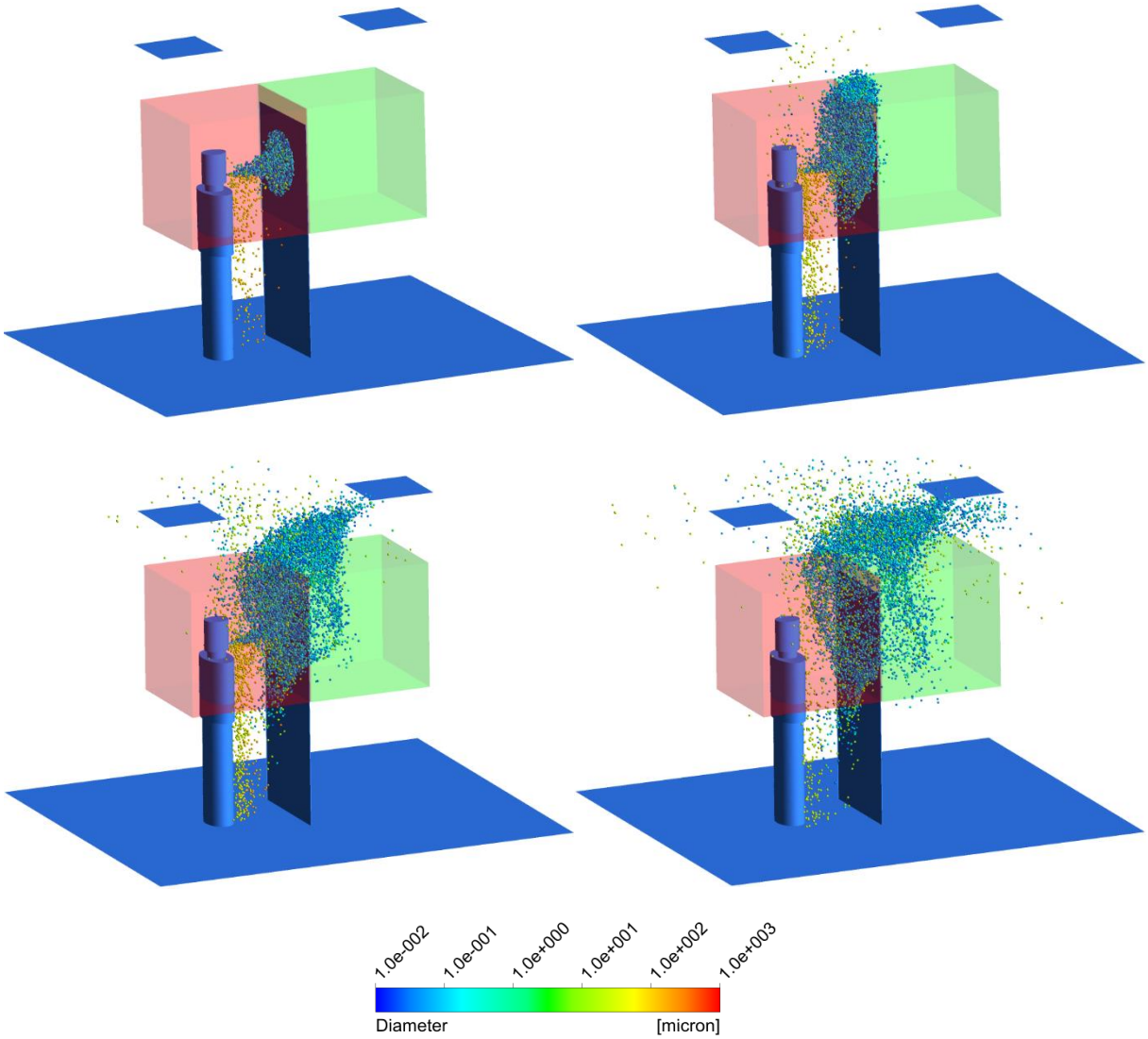

(b)

Figure 25 Droplet positions top to bottom at: 4 s, 14 s, 24 s and 34 s for the base case (a): without a screen and (b): with a screen. The vent above the person is an inlet, the other vent is an outlet. The sample volumes on the emitter side and non-emitter side are coloured and shown as red and green volumes respectively.

The medium sized particles which are carried with the exhalation reach the screen, but some are too large to follow the curvature of the flow and deposit onto the screen. Other medium sized particles evaporate down to a size small enough to be suspended by the body's thermal plume. The small droplets can follow the flow curvature and continue to be transported with the carrier flow. With increasing time, the transport of the particles transitions from being dominated by the initial exhalation flow to being dominated by the ventilation flow. Extraction of particles from the room, due to the flow through the ventilation outlet, and increased dispersion of the aerosols can be observed in Figure 25 at 24 and 34 seconds.

Plotting the times taken and distances travelled for droplets to either evaporate to a non-volatile core or to be deposited provides additional information on the behaviour of droplets in the different size ranges. Box plots of the time it takes for the droplets to evaporate down to their droplet nuclei size or deposit onto a surface (whichever occurs first) are shown in Figure 26. To draw the box plots, the logarithm of the full range of initial droplet diameters was partitioned into intervals of equal logarithmic width. The droplets with initial diameters in each interval were separated into those that deposit and those that evaporate. Box plots of times to deposition and evaporation were then drawn for each interval. The plot shows that the small droplets, with initial diameters less than 20 µm, evaporate rapidly to a non-volatile core in the aerosol size range, with diameters less than 5 µm. Larger droplets, with initial droplet diameters above approximately 100 µm, deposit before they have completely evaporated, and the time they take to deposit is also small. The medium range droplets exhibit behaviour from both groups. Droplets which initially fall under the influence of gravity may evaporate to a diameter that can be suspended by the thermal plume from the body before they deposit. Droplets which evaporate to nuclei with diameters in the range 5 µm to 25 µm, though larger than the aerosol size range, can remain airborne for some time. Assuming that viral load is uniformly distributed by the initial volume of droplets, then, due to their greater initial volume, these medium sized particles may be carrying a larger viral count than those that evaporate to aerosol particle sizes. The form of the box plot captures the trend seen in the classic Wells Curve (Wells,1934) with increasing evaporation time for increasing diameter up until some diameter where deposition dominates and then the time until deposition decreases as diameter increases. The box plots also show that there are wider ranges of time to evaporation or deposition for the medium droplets than small and large droplets which either all evaporate or all deposit.

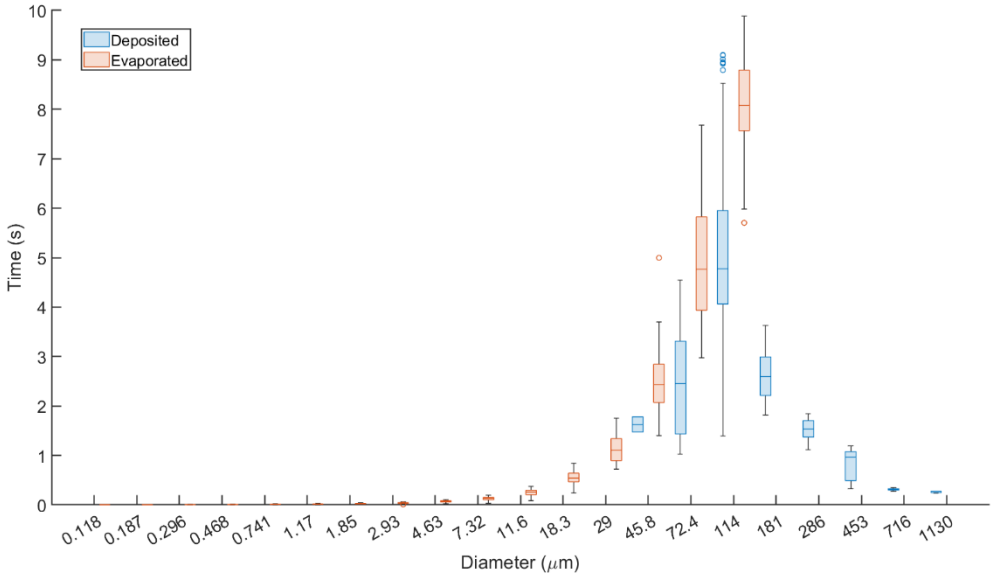

Figure 26 Box plots of evaporation (orange) and deposition (blue) time for the base case with a screen with injected droplet sizes from the Pöhlker distribution. Box plots are offset from the diameter they correspond to, deposition to the left and evaporation to the right.

The distance travelled by the droplets before they evaporate or deposit is calculated by integrating over the droplet trajectory and also by measuring the straight line distance between their final location and injection location. Both these distances, plotted against initial

droplet diameters, are shown for the case with a screen in the top two images in Figure 27**.** The small aerosols evaporate quickly, only travelling a small distance from the mouth before reaching their droplet nuclei size. The largest droplets behave ballistically and impinge onto the screen 0.5 m away. Transitioning from the large to the medium range, droplets with larger initial diameters, within the range, impinge on the screen. As the initial diameter decreases further, the droplets do not travel as far as the screen, but deposit on the floor, with the distance travelled approximately equal to the height of the mouth from the floor (approximately 1.5 m).

For droplets with diameters in the interval linearly centred on 114 µm diameter there are observable differences between the integrated path and straight line distances for the evaporated droplets. The straight line distance shows, that for a number of droplets, they are within 0.2 m of the mouth with the integrated path distance showing they have travelled at least 0.7 m. This is because these evaporating droplets begin to settle close to the body and reach a size where the flow induced by the buoyancy of the thermal plume is sufficient to transport the droplets back up into the ventilation flow and in doing so pass close to the mouth when they reach their droplet nuclei size. The deposited droplets which have a straight line distance less than 0.5 m have deposited onto the body as this is the only surface within that distance.

When no screen is present the results in the lower two images in Figure 27 show that the large droplets are unimpeded and they travel past where the screen is located up to a distance of close to 2 m for the largest droplets.

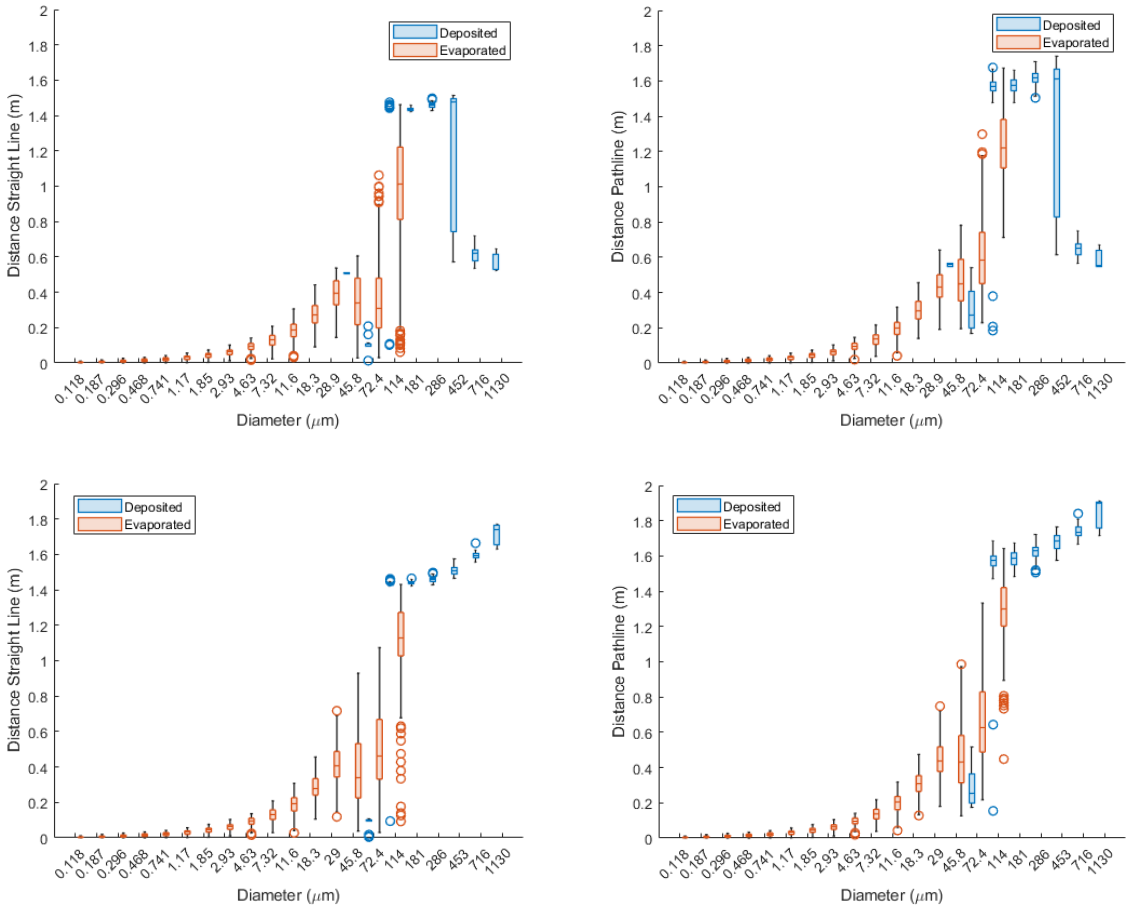

Figure 27 Base case speaking with screen (top) and no screen (bottom) with the Pöhlker distribution. Box plots of distance travelled to the point of evaporating down to their droplet nuclei size (orange) or depositing (blue), calculated by Left: straight line between initial and end point or Right: integrating over the particle trajectory. Box plots are offset from the diameter they correspond to, deposition to the left and evaporation to the right.

Influence of Evaporation

The particle size distribution measured in the non-emitter side sample volume is plotted against the initial droplet diameter distribution in Figure 28**.** This Figure shows the effect of evaporation on the number of droplets within each size range. As the droplets evaporate and become smaller, they can move to a smaller size range and hence move to the left in the Figure.

The smallest droplets all quickly evaporate to their droplet nuclei size and this can be seen clearly in the Figure where the sampled count distribution moves to the left. The large range do not have sufficient time to evaporate and for some of the large exhaled droplets they pass through the sample volume along their ballistic trajectory and when doing so are still of a similar size to that of when they were injected. Large droplets, with initial diameters greater than 300 µm, have enough momentum to travel into the exposure sample volume. Droplets around 100 µm though, have less momentum and therefore don't travel as far before depositing, resulting in a gap in the sampled distribution. For the middle size range, some of these droplets will deposit and not be sampled whereas others can evaporate down to a smaller size and contribute to the particle count of intervals containing droplets with smaller diameters.

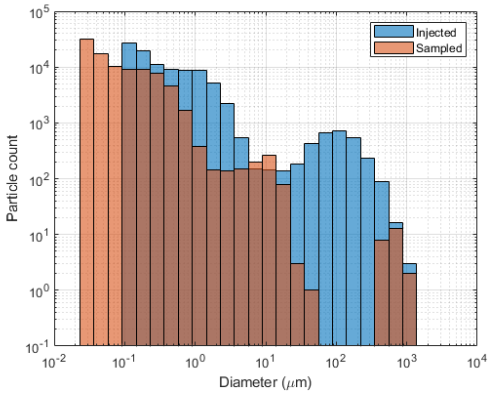

Figure 28 Initial droplet diameter distribution by particle count and sampled size distribution by particle count of particles sampled from the non-emitter side sample volume, partitioned and counted in intervals of droplet diameter, by their final sampled diameter, for the base case without a screen.

Figure 29 shows the time evolution of particle counts in the non-emitter side sample volume. The particle counts over 10 second intervals are partitioned into intervals of droplet diameter by injected diameter in the image on the left and their current diameter on the right**.** The largest droplets sampled in the non-emitter sample volume are sampled within seconds of exhalation and their diameter remains close to their initial diameter. The smallest droplets though have evaporated down to their droplet nuclei size before reaching the non-emitter sample volume as shown by the distribution moving to the left in Figure 29. The faster evaporation rates for smaller droplets are expected due to the rate of change of droplet diameter scaling as the inverse square of diameter (Equation 2).

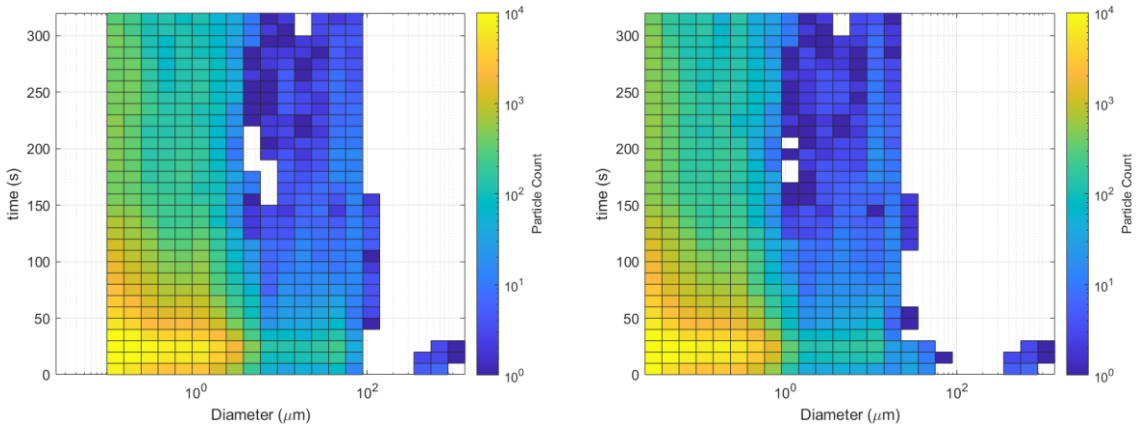

Figure 29 Particle count as a function of time in the non-emitter side sample volume without a screen. Each rectangle is coloured by sample count in a 10 second intervals. Left: Particle count by initial droplet diameter and Right: Particle count by final sampled droplet diameter. Particles partitioned in intervals of droplet diameter to give sample count.

Some of the droplets within the middle size range initially pass through the non-emitter sample volume while still evaporating and have not reached their droplet nuclei size. These droplets may then be mixed by the ventilation flow and re-enter the sample volume, being resampled at a later time with a smaller droplet diameter. Figure 26 shows that for the conditions simulated, the maximum time before a droplet evaporates to its nuclei size is approximately 10 seconds. After a simulation time of 35 s (25 s of breathing + 10 s maximum evaporation) any droplets sampled will be at their droplet nuclei size.

The temporal evolution by initial diameter shows that droplets that are initially on the boundary of the medium to large diameter ranges, at 100 µm, can remain airborne and be sampled on the non-emitter side up to 2 minutes after the exhalation has finished. Droplets within the medium diameter range ($20\ \mu m < d_0 < 100\ \mu m$) can be suspended by the flow and be sampled within the non-emitter side sample volume throughout the entire 5 minute ventilation phase. The temporal evolution of the sampled diameters shows that they have evaporated to droplet nuclei and these are sufficiently small to remain airborne.

Plots are presented in subsequent sections of this report in which the droplets are partitioned and counted in intervals of droplet diameter by their initial injected droplet size. This is to allow a distinction between small ($d_0 <$ 20 µm), medium ($20\ \mu m < d_0 < 100\ \mu m$) and large ($d_0 > 100\ \mu m$) droplets, defined by the given size ranges of their initial diameter. Using a sampled droplet size results in difficulty in determining which of the exhaled droplets are contributing to the counts as they can change size and move between droplet diameter intervals due to evaporation.

Viral exposure

Analysis of the time evolution of viral exposure throughout the particle size distribution provides insight into how different size droplets contribute to the total viral exposure within the sample volumes through time. Viral decay is not modelled and the viral count in droplets is assumed to not change with time. Therefore, predicted changes in exposure are due to the physical effects of mixing and transport. Figure 30 shows the time evolution, in 10 s intervals, of the total particle count and viral exposure distributions for the base case of no screen using the Pöhlker distribution for speaking, partitioned and counted in intervals by initial droplet diameter (note Figure 29 was for the non-emitter side sample volume). The bottom three rows capture the 25 s exhalation period, after which there is a significant drop due to those droplets leaving the sampling volume. The droplets which are measured within the sample volume are due to mixing within the room and re-entering the sampling volume.

The particle count evolution shows that during the initial exhalation period of 25 s that the number of smaller droplets ($d_0 < 20\ \mu m$) exhaled far exceeds the larger droplets ($d_0 > 100\ \mu m$) with particle counts within the middle range ($20\ \mu m < d_0 < 100\ \mu m$) somewhere in-between. Contrasting this with the viral exposure evolution shows that due to the scaling of viral copies with d^3 (Equation 28) that the total viral exposure is heavily weighted for the larger droplets. Also note that at longer times, the medium sized droplets are contributing the most to the viral exposure. This is something to keep in mind when looking at viral exposure, droplet size and their overall contribution.

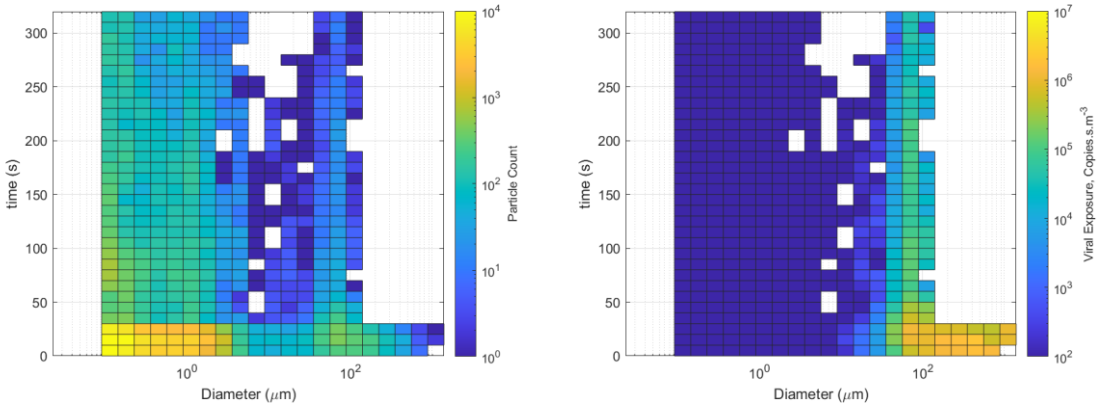

Figure 30 Time evolution in the emitter side sample volume within 10 second intervals for the no-screen, Pöhlker speaking simulation. Left: particle count distribution, Right: viral exposure distribution.

A simple representation of the total viral exposure from the entire size distribution for the initial 25 s during exhalation and final 25 s of the simulation can be seen in Figure 31. For short times the viral exposure on the emitter side has a contribution from every particle exhaled during the activity, resulting in the greatest viral concentration observed. On the non-emitter side the viral exposure decreases as fewer droplets reach the sample volume. The influence of the screen for this initial 25 s period is clear, with a reduction of viral exposure by nearly two orders of magnitude.

At a later time after the speaking activity, the viral exposure measured on the emitter side of the screen is significantly less whereas on the non-emitter side there remains a similar order of viral exposure. This trend is seen whether a screen is present or not, showing that the screen is more effective for time periods during the speaking activity rather than over longer periods.

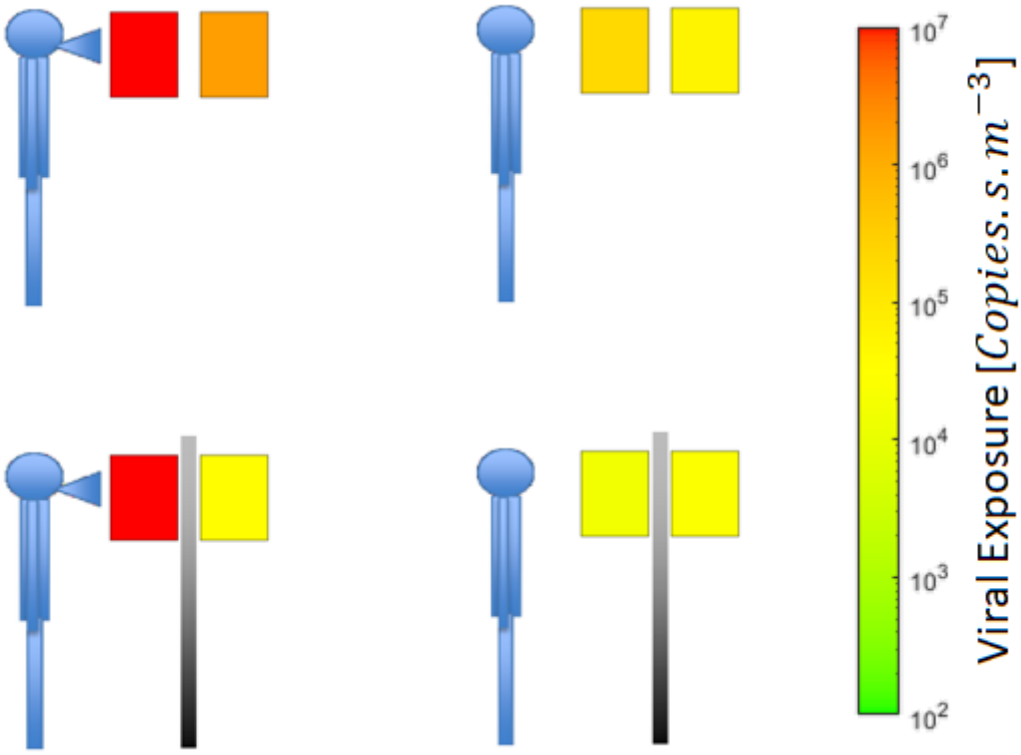

Figure 31 Initial and final exposure plots of viral exposure for the two base cases. Top: no screen, Bottom: screen, Left: $0 - 25\ s$, Right: $300 - 325\ s$ for the speaking, Pöhlker distribution simulation.

Figure 32 shows the viral exposure evolution in 10 second intervals over the full duration of the simulation and provides a more detailed breakdown of the data that is used to feed into Figure 31. The distributions provide insight into the viral exposure contributions from the different particle sizes to the total viral exposure observed. On the emitter side of the screen the viral exposure due to the small size range shows some influence due to the presence of the screen during the initial 25 s. The buoyant exhaled carrier flow which transports these particles is impeded by the screen resulting in the jet spreading radially. This results in these small particles spending longer within the sample volume and therefore the viral exposure remains high.

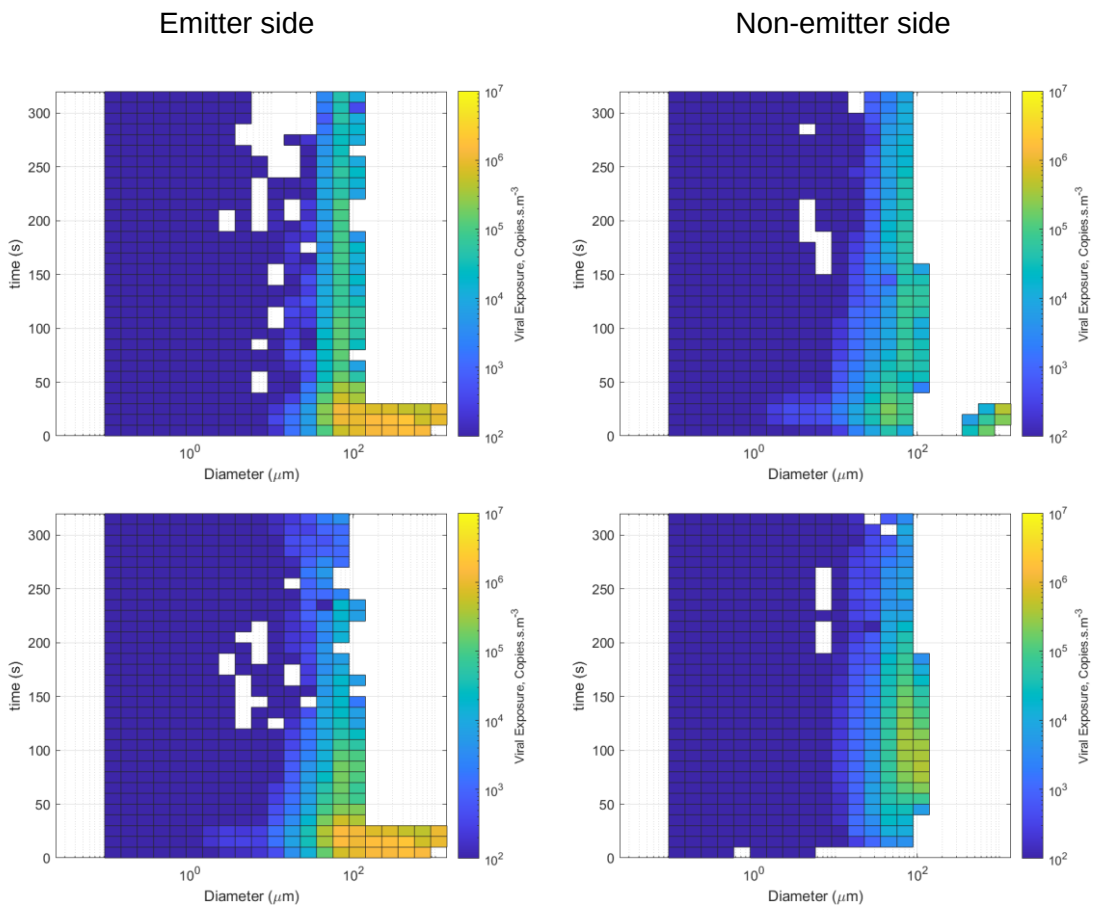

Figure 32 Viral exposure as a function of time and initial droplet diameter. Bottom: screen and Top: no screen.

When no screen is present some of the largest droplets exhaled are sampled on the non-emitter side of the screen due to their ballistic behaviour. A gap between the large range to mid-range is observed due to those particle sizes settling out onto the floor before having sufficient time to evaporate and become suspended to reach that sample volume. When a screen is present the large droplets are not observed on the non-emitter side of the screen because they impinge on the screen surface.

During the exhalation the larger droplets behave ballistically, therefore their trajectories are determined by the initial conditions imposed, whereas the small particles behave like tracer particles of the flow and follow the carrier flow. Smaller particles within the mid-range are able to follow the carrier flow whereas the larger particles within this range leave the carrier flow and begin to settle out. In the evolution of viral exposure, it can be observed that some of the exhaled particles at the larger end of the mid-range initially started to settle out, but during this settling, have time to evaporate down to a size that is able to be suspended by the body's thermal plume and mixed to the non-emitter side by the ventilation flow. This is observed whether a screen is present or not.

The larger end of the mid-range contributes the largest proportion to the viral exposure for long times and are the most interesting cases. Due to the assumption of uniform viral load these droplets hold a large number of viral copies but once they have evaporated they are small enough to remain airborne. Figure 32 shows that these droplets are still present on the

non-emitter side up to the end of the simulation, 5 minutes after exhalation, continuing to contribute to potential viral exposure.

Further examination of Figure 32 shows that with the presence of the screen the particles from the exhalation have a delay in reaching the sample volume on the non-emitter side of the screen. This delayed viral exposure at 100 s is of the same order of magnitude as the viral exposure from the initial 25 s exhalation period when no screen is present. As viral exposure is a product of concentration and residence time the potential exposure does not fully capture the number of viral copies that a person would come into contact with from deposition of a ballistic droplet onto a mucus membrane. The impact of the very specific geometry setup is believed to also affect the results here.

Person to screen position

The distance between the emitter and the screen was varied from 25 cm, 50 cm (the base case) and 75 cm to investigate the screen effectiveness at different distances. Figure 33 shows the deposition of particles onto the screen for the different distances simulated. In the simulations the distance is varied by moving the person, rather than the screen, so the change in results is also affected by the person's location with respect to the vents and ventilation flow. In the base case, where the person to screen distance is 50 cm, the person is positioned below a vent. The influence of the ventilation setup is covered in a later section.

Horizontally, the initial condition applied to the droplets has a zero cross-stream velocity, following the source condition of Stettler et al. (2022)**.** This results in the vertical straight line deposition pattern observed on the screen shown in Figure 33. The droplets depositing on the screen are larger droplets, following a ballistic trajectory, rather than carried by the exhalation flow. As the distance travelled increases as the person moves further from the screen, the droplets drop further and therefore deposit further down the screen. For the case at 0.75 m, there is a reduction in the number of the larger droplets which have deposited on the screen. The larger droplets which do not deposit on the screen with this separation are likely to deposit onto the floor between the person and the screen, and not have sufficient time to evaporate and stay suspended.

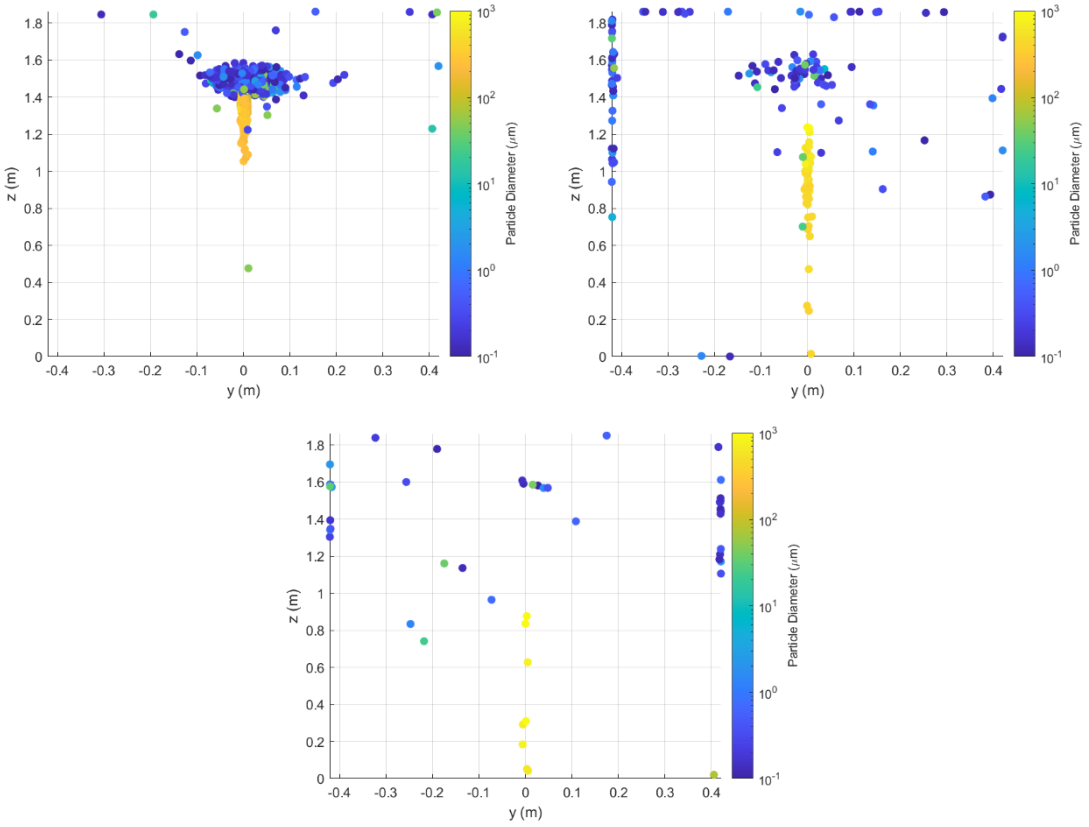

Figure 33 Particle deposition onto the screen, coloured by initial droplet diameter, for varying distances away from the screen. Top to bottom, left to right: 0.25 m, 0.5 m, 0.75 m.

For shorter person to screen distances, the deposition of the large droplets still fall along a vertical straight line on the screen and the droplets generally deposit higher up the screen and in greater numbers. Also, smaller droplets (within the middle range) deposit onto the screen as the person is sufficiently close for the droplets to have neither deposited on the floor nor finished evaporating. Some droplets in the small range also deposit on the screen, but do not follow the same straight-line pattern and are spread radially across the screen. The flow from the exhalation spreads radially due to the interaction of the exhalation jet with the screen. The increase in small droplet deposition could be because of higher axial velocities, due to less jet momentum decay in the short distance from person to screen, increasing the particle Stokes number (ratio of particle time scale to flow time scale). Particles start by following the flow but then detach from the curved streamlines of the flow and impinge on the screen. It could also be a result of numerical issues with the simulation.

There is some uncertainty in the model predictions of particle deposition. There are known deficiencies in the DRW turbulence model as it assumes an isotropic turbulent velocity which could artificially increase the chance of deposition. Also, the boundary layer over the screen may not be sufficiently resolved. The detailed interaction and deposition of small particles on surfaces was not the main purpose of this work and was therefore not investigated further.

Figure 34 shows the viral exposure with time in the non-emitter side sample volume for the three cases of different person to screen distances. The relative location of the vents and hence the ventilation flow influence the lower end of the middle range of droplets where zero viral exposure is predicted for both the shortest and longest person to screen distances. This is because the flow is sensitive to the position of the person relative to the screen and this

highlights the complexities in resolving such ventilation flows. There is, however, an order of magnitude reduction in viral exposure for the large end of the middle range for the shortest person to screen distance. This is because of the increased deposition of that size onto the screen.

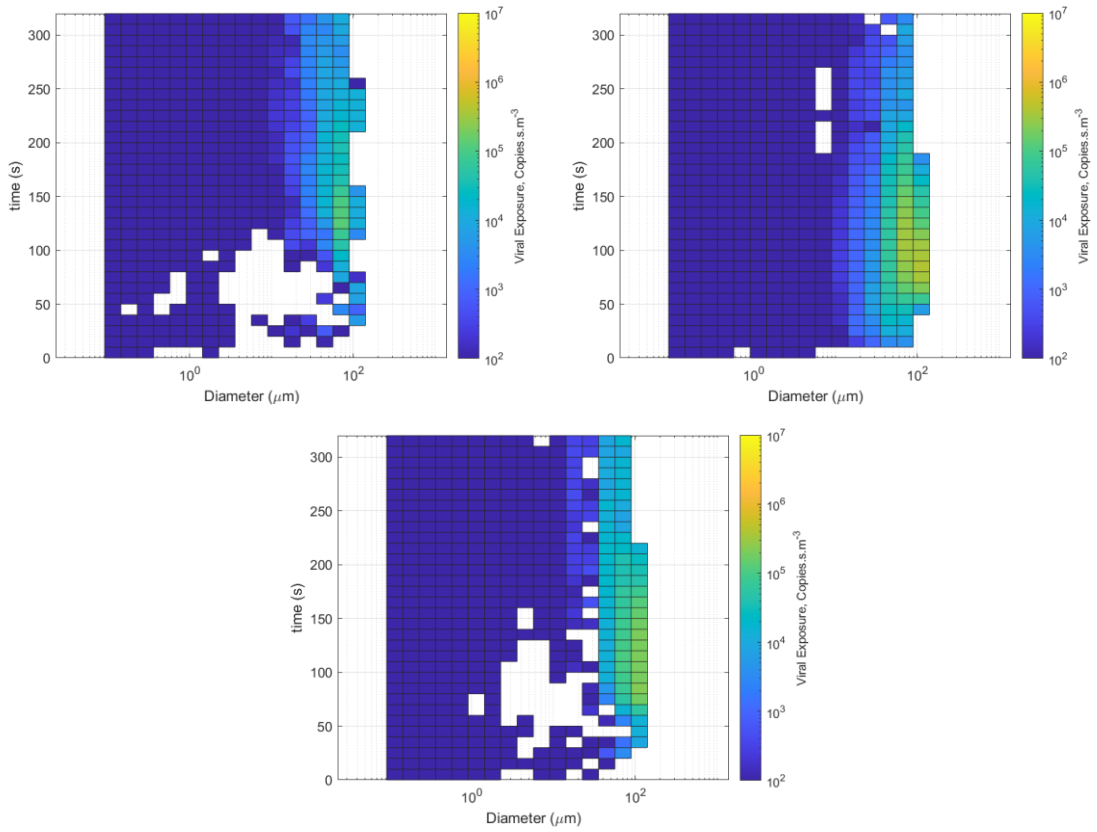

Figure 34 Viral exposure as a function of time and initial droplet diameter for different person to screen distances. Top to bottom left to right: 0.25 m, 0.5 m and 0.75 m.

The total viral exposure in the non-emitter side sample volume from all particle sizes through time is plotted in Figure 35 for the different person to screen distances. The exposure is calculated every 10 seconds and also cumulatively over the whole duration of the simulation. The exposure for each 10 second interval is the sum of the viral exposure rows from all particle diameters shown in Figure 34. A peak in exposure can be seen in the range 75 – 140 s and is dependent on person-screen distance. There is not a clear trend for when the peak exposure is observed. The distance of the person from the screen also changes the location of the body's thermal plume and location with respect to the ventilation vents. This confounds the effects of the mixing flow (plume and ventilation) and jet-screen interaction showing how complicated and sensitive these flows are to small differences in the geometry.

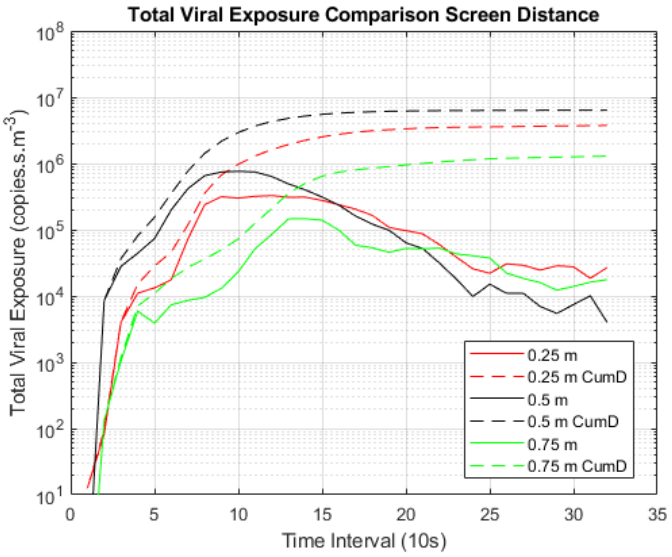

Figure 35 Plot of total viral exposure in the non-emitter side sample volume for speaking with a screen, sampled every 10 seconds (solid line) and cumulatively (CumD, dashed line) through the entire time for varied person to screen distances. Red: 0.25 m, black: 0.5 m and green 0.75 m.

Source terms

The two activities simulated were speaking and coughing, which have different source terms as defined in Section 3.3**.** The difference in deposition pattern on the screen between the two activities is shown in Figure 36. Even though the person is located at the same distance away from the screen, and the cough is directed downwards, the greater initial velocity of the droplets associated with coughing results in most deposition of droplets in the large range occurring further up the screen and increased deposition for droplets within the middle range. There is also a wider radial spread for the cough compared to speaking, where the higher velocity of droplets from a cough means that they deposit, rather than follow the flow around the screen.

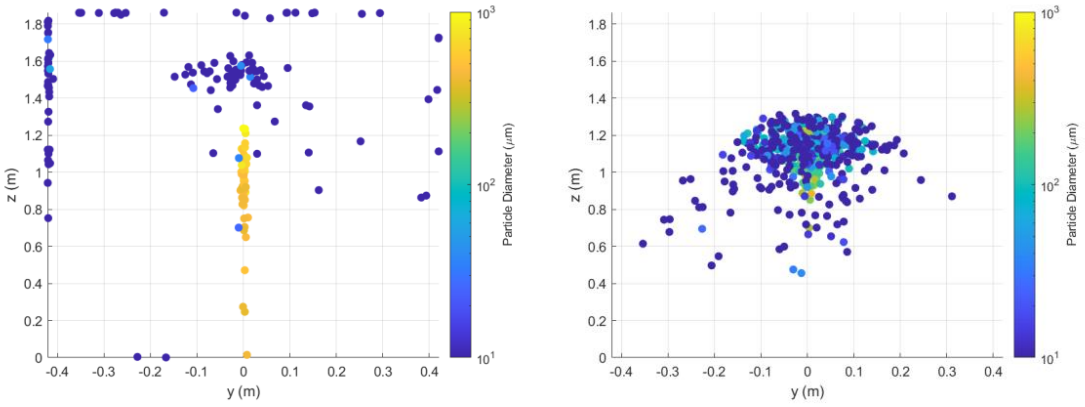

Figure 36 Screen deposition pattern coloured by particle diameter. Left: 25 s of speaking. Right: one cough.

For coughing Figure 37 shows the total viral exposure for the entire size distribution for the initial 25 s from the exhalation, coughing for 0.4 s followed by mixing flow until 25 s is reached, and final 25 s of the simulation. The effectiveness of the screens for short times is clear, with a reduction of viral exposure on the non-emitter side. The reason for this is the

same as for speaking, with larger droplets depositing on the screen as well as deflection of the jet by the presence of the screen. Over long times the viral exposure on the non-emitter side of the plot is of the same order of magnitude whether a screen is present or not and therefore shows that the screen is not effective at reducing exposure to the smaller particles over longer periods.

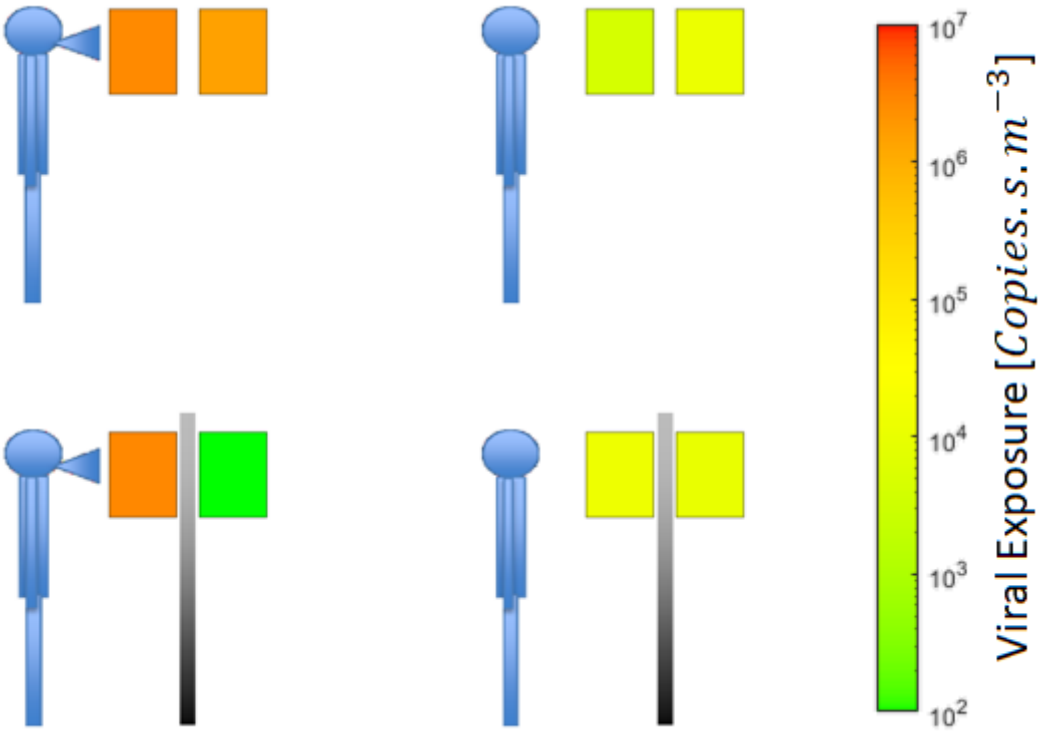

Figure 37 Initial and final exposure plots of viral exposure for the Pöhlker coughing source term. Top: no screen, Bottom: screen, Left: $0 - 25$ s, Right: $300 - 325$ s.

By contrasting the coughing results (Figure 37) with those of speaking (Figure 31) the viral exposure for the initial 25 s on the non-emitter side is of the same order when no screen is present. For the final 25 s the viral exposure is comparable in the non-emitter side sample volume with and without a screen in the coughing case as it is for speaking. With the source terms used, the influence of one cough, which lasts less than 1 second, gives comparable levels of viral exposure to 25 s of speaking loudly on the non-emitter side when no screen is present. When a screen is present the viral exposure is greatly reduced for the coughing activity and also reduced for the speaking activity, when measured within the first 25 s.

The viral exposure contribution from the different size droplets generated during a coughing event is shown in Figure 38 with and without a screen. When no screen is present some of the droplets generated from coughing are sampled within the non-emitter side control volume in the first 10 second sample interval. This includes the contribution from the large droplets that pass straight through the sample volume. The cough source is projected downwards and as a result there is a significant amount of time between the coughing event and the bulk of the aerosol cloud reaching the sample volume both with and without a screen.

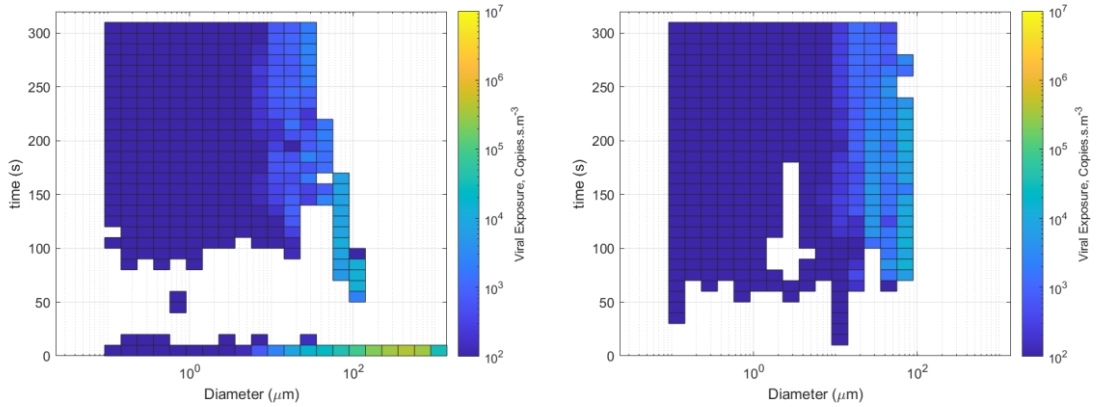

Figure 38 Viral exposure as a function of time and initial droplet diameter for a coughing event in the non-emitter side sampling volume. Left: No screen, Right: Screen.

Two different exhalation droplet size distributions have been used in the simulations. These are the BLO model (Johnson et al., 2011) and the Pöhlker distribution (Pöhlker et al., 2021). All the results of simulations reported in this section so far have used the Pöhlker distribution. The droplet counts using the two distributions on the non-emitter side are compared in Figure 39. This shows that there is a smaller number of droplets at all droplet diameters and a wider gap between small and large droplets for the BLO model than with the Pöhlker distribution. The BLO model has few droplets in the range 20 µm to 100 µm, while many more are present sampling from the Pöhlker distribution. These simulations do not include a screen and there are fewer large droplets in the BLO model. The effect of this can be seen in the number of droplets reaching the non-emitter side compared to the Pöhlker distribution. The smaller number of droplets, the gap between small and large droplets and the difference in the number of large droplets would be expected from the BLO model compared to the Pöhlker distribution. There are more droplets when sampling the flow using the Pöhlker distribution so more can be learnt about the behaviour of different sized droplets given the known uncertainty and variability in the initial droplet diameter distribution.

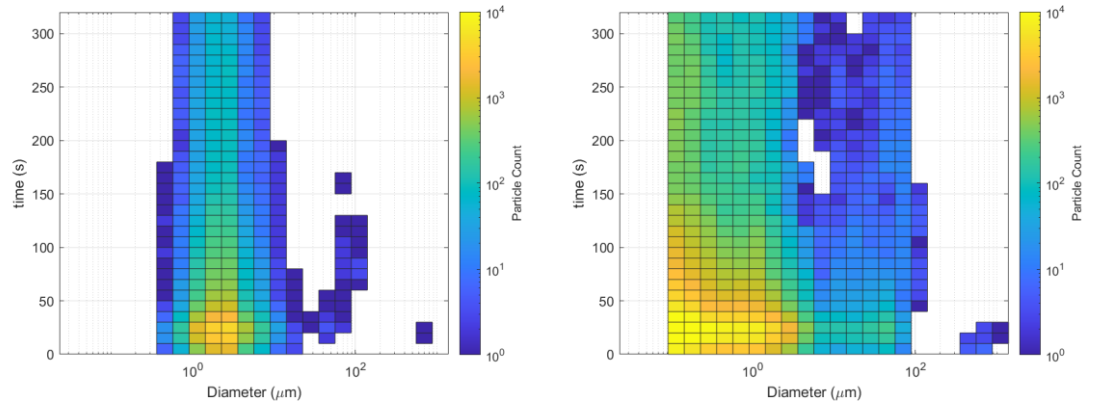

Figure 39 Particle count as a function of time and initial droplet diameter for speaking in the non-emitter side sample volume without a screen. Left: BLO model, Right: Pöhlker distribution

The viral exposure from the two distributions, based on the count data shown in Figure 39, are compared in Figure 40. The calculated viral exposure using the BLO model shows the effect of both the overall number of droplets, the wider gap between small and large droplets and the smaller number of large droplets. The viral exposure predicted using both

distributions is concentrated in droplets with initial diameters between 20 µm and 100 µm. The assumption that viral copies are distributed uniformly by volume means that the largest droplets that remain airborne contain the most virus. The greater number of droplets in this diameter range using the Pöhlker distribution emphasises how viral exposure is distributed according to the droplet diameter distribution.

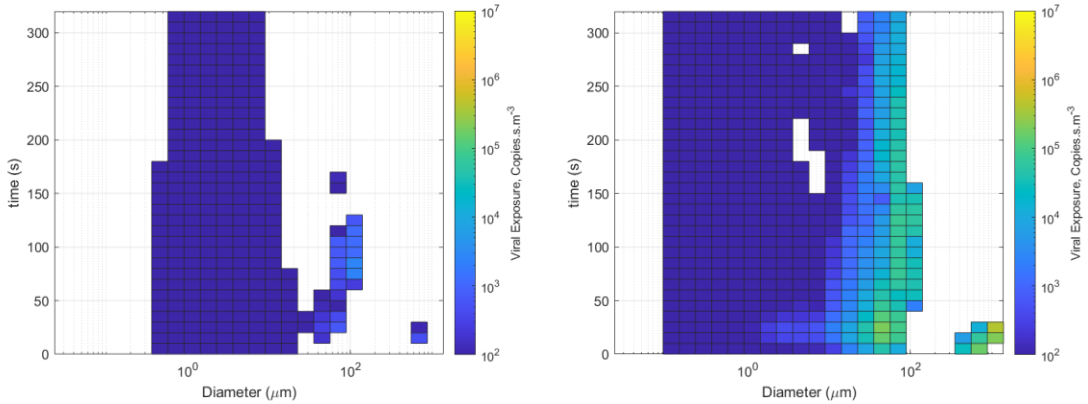

Figure 40 Viral exposure as a function of time and initial droplet diameter for speaking on the non-emitter side without a screen. Left: BLO model, Right: Pöhlker distribution

One person versus two people

Figure 41 shows the viral exposure distribution on the non-emitter side of the screen when an additional person is included on the non-emitter side of the screen. Including a person on the non-emitter side of the screen introduces not only an additional geometry that the ventilation flow has to navigate, but also an extra source of heat and therefore a thermal plume. Particle entrainment into the thermal plume of the additional person leads to particles becoming suspended on the non-emitter side of the screen.

Figure 42 compares the total viral exposure measured in the sample volume on the non-emitter side of the screen for the one person and two people simulations. When a person is present on the non-emitter side of the screen the decay rate of the total viral exposure is less than when a person isn't present. This is due to the strong influence of the thermal plume resulting in droplets which would have settled out remaining suspended. The highest exposure with one person, at around 100 s, is also decreased due to the enhanced mixing due to the thermal plume.

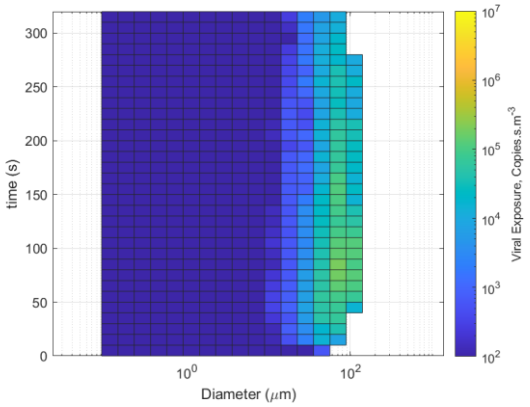

Figure 41 Viral exposure as a function of time and initial droplet diameter on the non-emitter side for speaking with a second person in the room.

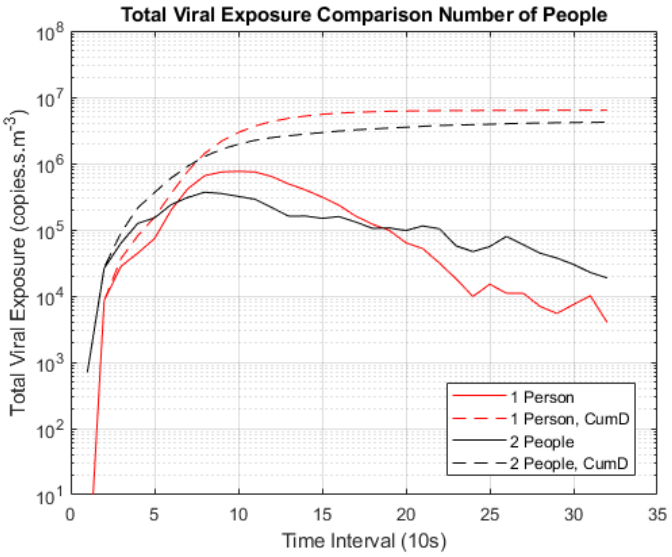

Figure 42 Plot of total viral exposure in the non-emitter side sample volume for speaking with a screen, sampled every 10 seconds (solid line) and cumulatively (CumD, dashed line) through the entire time for: red: 1 person, black: 2 people.

6.2.2 Influence of ventilation setup

The previous section looked at the effect of geometry on exposure, this section examines the effect of different ventilation configurations and rates on exposure.

The ventilation flow drives the mixing of the particles within the room after the exhalation. The different ventilation positions as well as the direction of flow are investigated by switching the inlet and outlet, and by moving the vents off the centre axis.

Diagonal ventilation

In the base case the person is positioned immediately below the inlet, by moving the ventilation from the centreline of the room the results can provide insight into whether the results are specific to the geometry of the base case. Figure 43 shows the initial and final exposure plot of viral exposure where the vents are positioned diagonally for the cases of a screen and no screen. The impact of having diagonal vents when no screen is present

shows little difference in total viral exposure. However, when a screen is present there is a greater reduction in viral exposure on the non-emitter side within the initial 25 s. The different interaction of the screen and ventilation flow is the only driving factor for this reduction. This is a geometry specific effect which makes it difficult to draw general conclusions. What is clear, however, is that after the initial exhalation the dispersion of the exhaled droplets is driven by the ventilation flow. Therefore, for specific scenarios it may be possible to develop ideal ventilation flows which improve control of aerosol dispersion.

The viral exposure at long times shows some change when a screen is present which is again due to the different interactions with the ventilation flow and the presence of the screen, however, the differences are not significant. When no screen is present the viral exposure is of the same order of magnitude to that of the central ventilation configuration as seen in Figure 31.

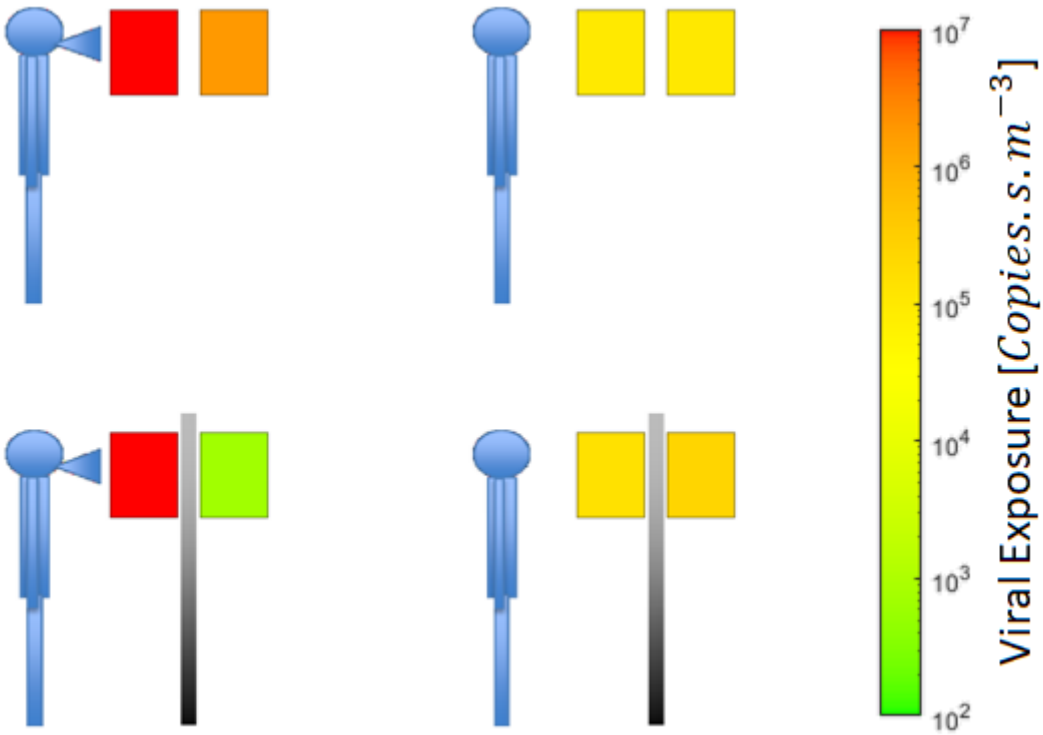

Figure 43 Initial and final exposure plots of viral exposure for, top: screen, bottom: no screen, left: $0 - 25$ s, right: $300 - 325$ s for the speaking Pöhlker distribution and diagonal vents.

The viral exposure evolution on the non-emitter side for the diagonal vents case is shown in Figure 44. The differences within the exhalation period are the same as discussed for the base case (Figure 32). The impact of ventilation isn't realised until the momentum of the jet dissipates, and the ventilation flow begins to dominate. Comparing with the evolution of the base case (Figure 32) there is a decrease in exposure during the period (75 – 150 s) where the largest viral exposure contribution is measured in the non-emitter side control volume.

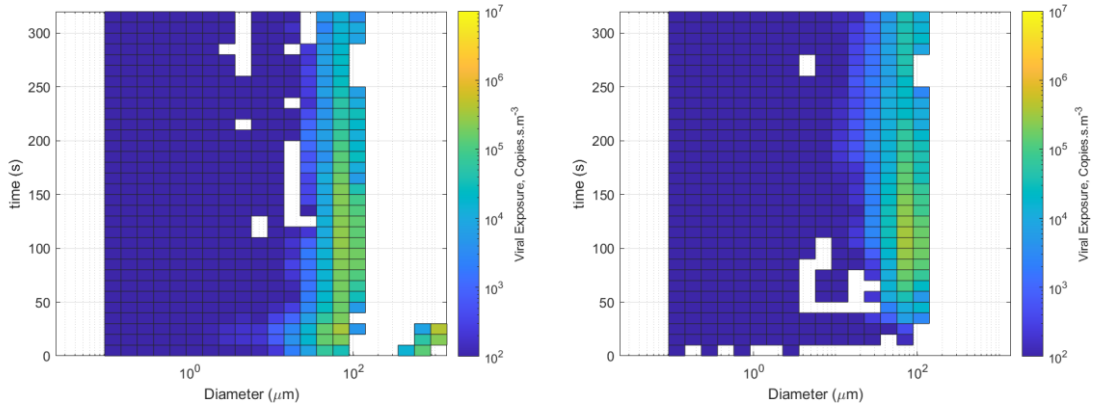

Figure 44 Viral exposure as a function of time and initial droplet diameter on the non-emitter side for speaking and diagonal vents, Left: No screen, Right: Screen.

Figure 45 shows the total viral exposure evolution measured on the non-emitter side within the 10 s intervals for the central vents and the diagonal vents speaking case. The particular setup, top right in Figure 23, shows that having diagonal vents influences when the aerosols are sampled in the control volume on the non-emitter side. A delay is seen for the diagonal vents due to flows directed off the central axis of the domain. The cumulative plots show that the total viral exposure measured throughout the entire simulation is of the same order of magnitude. As in previous simulations, the mixing period is simulated for 5 minutes, due to the availability of computational resources. As the ventilation flow rate is set to result in an air change rate of 5 ACH the impact of extraction due to the ventilation is not fully captured. The dip in total viral exposure is most likely due to uneven mixing within the domain.

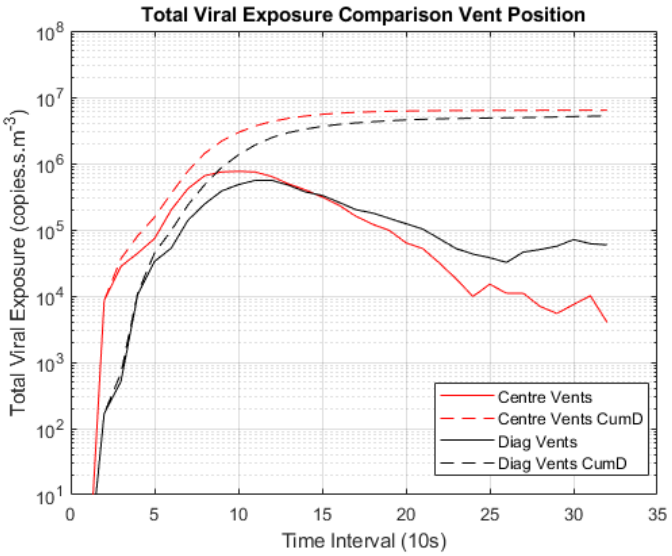

Figure 45 Plot of total viral exposure in the non-emitter side sample volume for speaking with a screen, sampled every 10 seconds (solid line) and cumulatively (CumD, dashed line) through the entire time for varied ventilation positions, red: centre vents and black: diagonal vents.

Reverse ventilation direction

Another variation in ventilation flow considered is the direction in which the ventilation is flowing. This is done by switching the inlet and outlet boundary condition of the vents in the base case. Figure 46 shows the viral exposure measured within the initial 25 s and final 25 s for the speaking case where the ventilation direction is opposing the direction of speaking. The viral exposure for the final 25 s is slightly larger than that when the ventilation direction is the same direction as speaking (Figure 31), irrespective of whether a screen is present or not. For the initial 25 s the results are not significantly affected by the ventilation direction. Although the results are very similar, the flow that led to them is different. To fully understands the reasons for the computed exposure levels requires a more detailed analysis that the exposure plots alone cannot provide.

Figure 47 compares the total viral exposure on the non-emitter side between the base cases, where the ventilation direction is in the same direction as the carrier flow (1 in 2 out) and when the ventilation direction opposes the carrier flow (2 in 1 out). During the exhalation dominated time (the first three 10 s sample periods) the exposures look very similar. When no screen is present the largest viral exposure is predicted just after the activity period which then sharply decreases as the large droplets settle to the ground and the carrier flow lifts up into the ventilation flow. When the ventilation flow opposes the direction of carrier flow, the decrease in viral exposure is larger than when the ventilation is with the carrier flow, as the ventilation flow transports aerosols back onto the emitter side of the room. The ventilation flow then mixes the room further and an increase of viral exposure is observed. The decrease followed by an increase in exposure is not seen when the ventilation is in the same direction as the carrier flow.

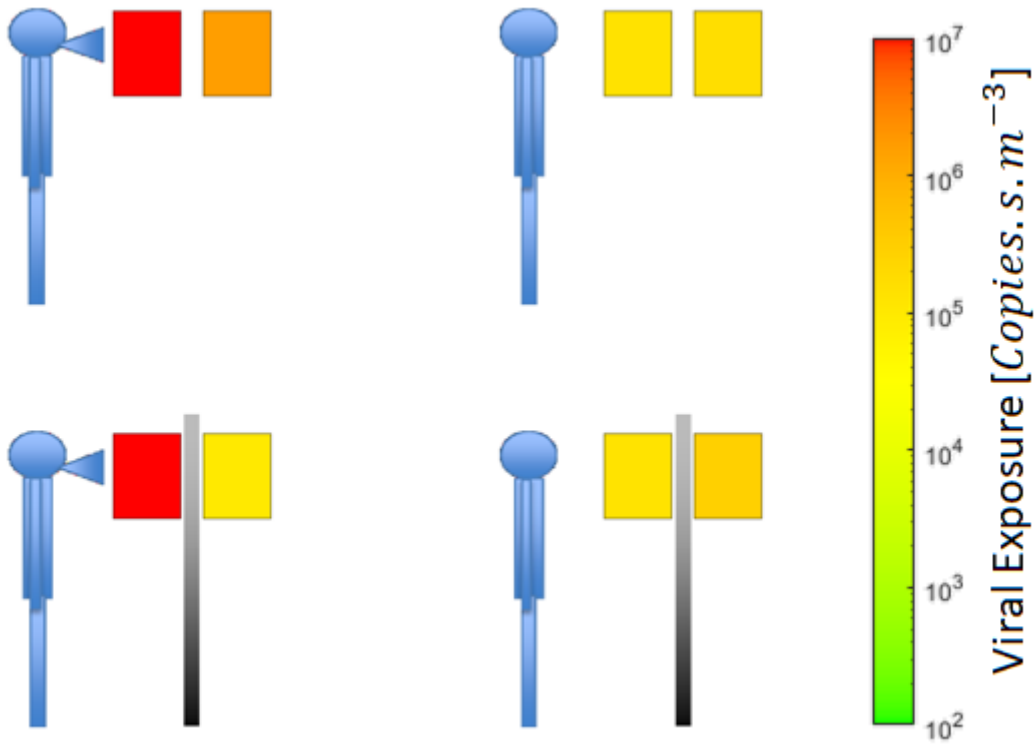

Figure 46 Initial and final exposure plot of viral exposure for the ventilation direction 2 in 1 out. Top: screen, Bottom: no screen, Left: $0 - 25$ s, Right: $300 - 325$ s for the speaking Pöhlker distribution.

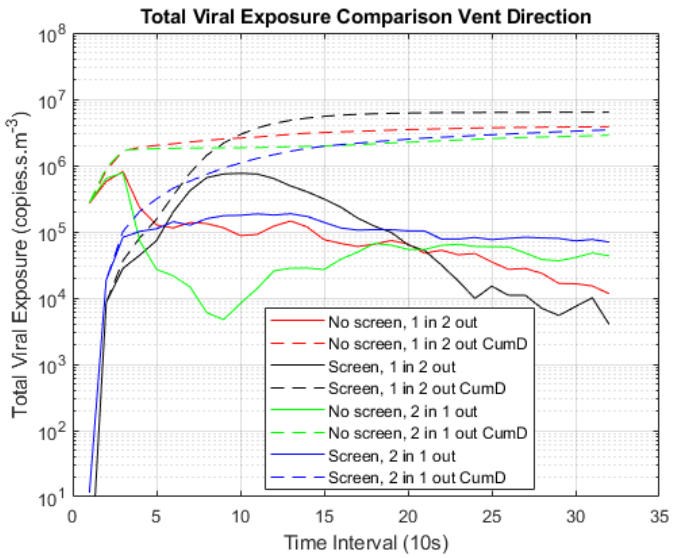

Figure 47 Plot of total viral exposure in the non-emitter side sample volume for speaking, sampled every 10 seconds (solid line) and cumulatively (CumD, dashed line) through the entire time for varied ventilation direction. Red: no screen and 1 in 2 out, black: screen and 1 in 2 out, green: no screen and 2 in 1 out, blue: screen and 2 in 1 out. Ventilation flow: 1 in 2 out, coflow, 2 in 1 out, opposed flow (see Figure 23).

For the case with a screen where the direction of ventilation is with the carrier flow, once the jet rises above the screen the ventilation flow transports the aerosols to the non-emitter side. This can be seen in Figure 47, where the peak of viral exposure is measured when the bulk of the carrier flow reaches the sample volume. When the ventilation flow opposes the carrier flow there is an increased separation and breakup of the exhaled aerosol cloud which results in enhanced mixing of the aerosols within the room. Figure 47 shows this, where the viral exposure is consistent relative to the other cases, with a gradual decrease from extraction of aerosols through the ventilation outlet and droplets within the middle range settling out.

Effect of a larger room

So far the results presented have been for a room of size 3.5 m x 3.0 m x 2.5 m (L x W x H) which is representative of the chamber described in Section 4.3. A room geometry of double the volume has been simulated with length and width scaled by $\sqrt{2}$ while keeping the height the same. The geometry comparison can be seen in Figure 23. Figure 48 shows the predicted viral exposures in the two sample volumes in the first and final 25 s of the simulation.

There is a significant reduction in total viral exposure within the initial 25 seconds on the non-emitter side of the screen relative to the base case (Figure 31) whereas at longer times there is an increase in total viral exposure on both sides. The viral exposure due to different sized particles presented in Figure 48 shows that there are considerably fewer droplets being sampled in the non-emitter side sample volume. As the room volume is greater and therefore more space for mixing, there is less chance of the particles passing through the sample volume. In the larger room the flow and particles are not as constrained by the walls as they pass the screen, and they can mix into the larger space available, thereby reducing the concentration in the sampling volume on the non-emitter side of the screen.

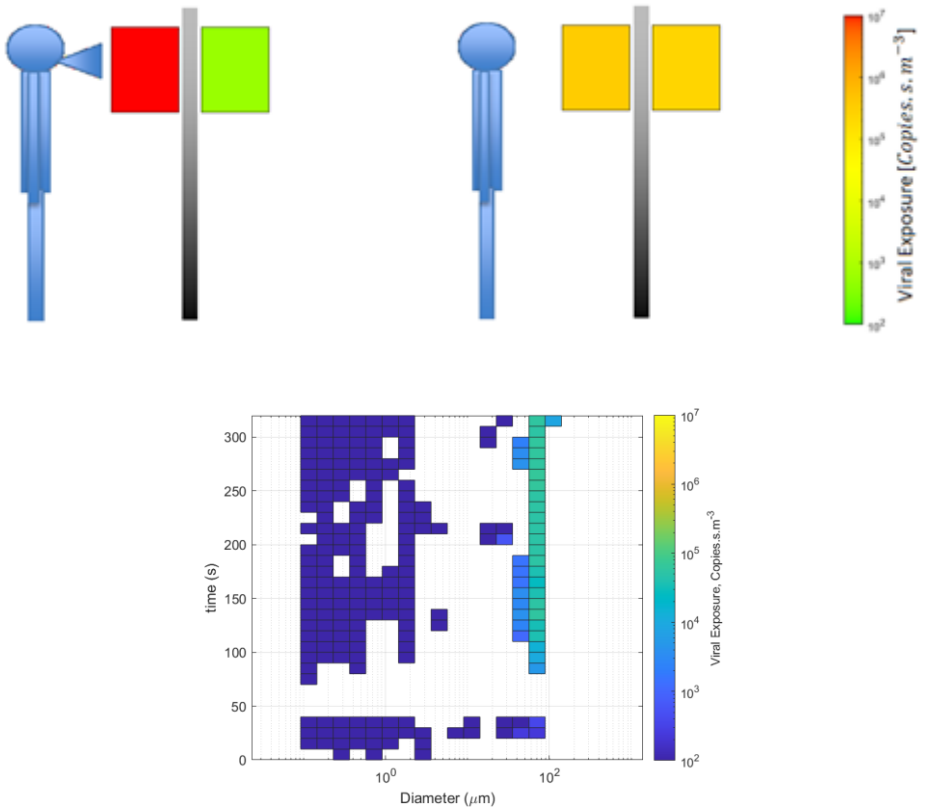

Figure 48 Top: Initial and final exposure plots of viral exposure for a large room. Left: $0 - 25\ s$, right: $300 - 325\ s$. Bottom: Viral exposure as a function of time and initial droplet diameter on the non-emitter side for speaking.

The total viral exposure is compared for the base case with screen and the large room case and is shown in Figure 49. The results show that in the large room the exhaled aerosol cloud, once it has interacted with the screen, takes a significant time before reaching the non-emitter side sample volume compared to in the small room. Within the initial 50 s the exposure is only contributed to by a small number of stray droplets. After this initial period, as mixing continues, the cumulative exposure begins to rise, and the exposure remains at a constant level. In comparison, the exposure in the small room rises more quickly to a higher level, but also drops more rapidly, falling below the exposure in the large room after 200 s.

The difference between the measured exposures in the two rooms shows the inherent dependency of ventilation flows on room geometry and that it is difficult to draw general conclusions on how geometric variations will impact longer term exposure.

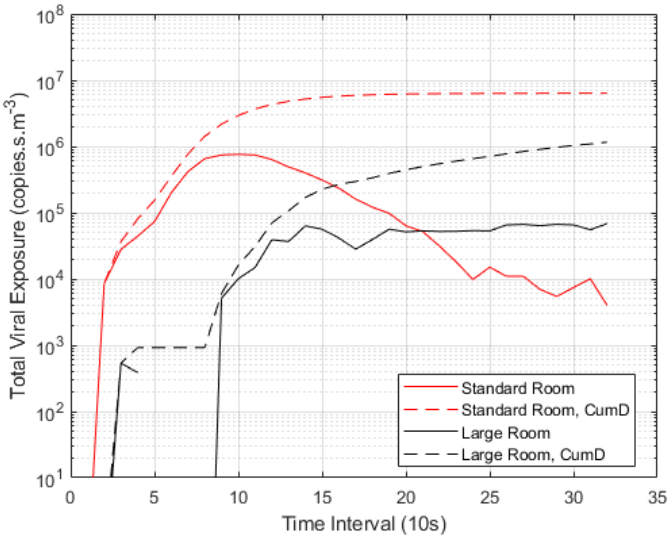

.

Figure 49 Plot of total viral exposure in the non-emitter side sample volume, sampled every 10 seconds (solid line) and cumulatively (CumD, dashed line) through the entire time. Red: base case room, black: large room.

Influence of air change rate

The ventilation flow plays a key role in the mixing of exhaled aerosols through the domain after the exhalation period. Changing the ventilation rate (specified as air changes per hour, ACH) has a significant impact on the flow field within the domain. Here air change rates of 5 ACH (the base case), 2.5 ACH and 0.5 ACH are simulated for the base case geometry with a screen. For the 5 minutes simulated, these air change rates correspond to 0.42, 0.2 and 0.042 of the volume of the room respectively. A full air change would need the simulations to be run for 12, 24 and 120 minutes respectively. With the available computational resources this was not feasible.

The path of the carrier flow, shown in Figure 50, at the end of the exhalation is greatly impacted by the air change rate for the geometry and configuration modelled. At the lowest ventilation rate, 0.5 ACH, the flow is dominated by buoyant flows, with the thermal plume from the person drawing in the exhalation as it rises above the screen. At the highest ventilation rate, 5 ACH, the ventilation flow dominates, pushing the exhalation over and around the screen. At the middle ACH there are competing factors from the buoyancy effects and the ventilation flow, resulting in the exhalation rising straight up off the screen.

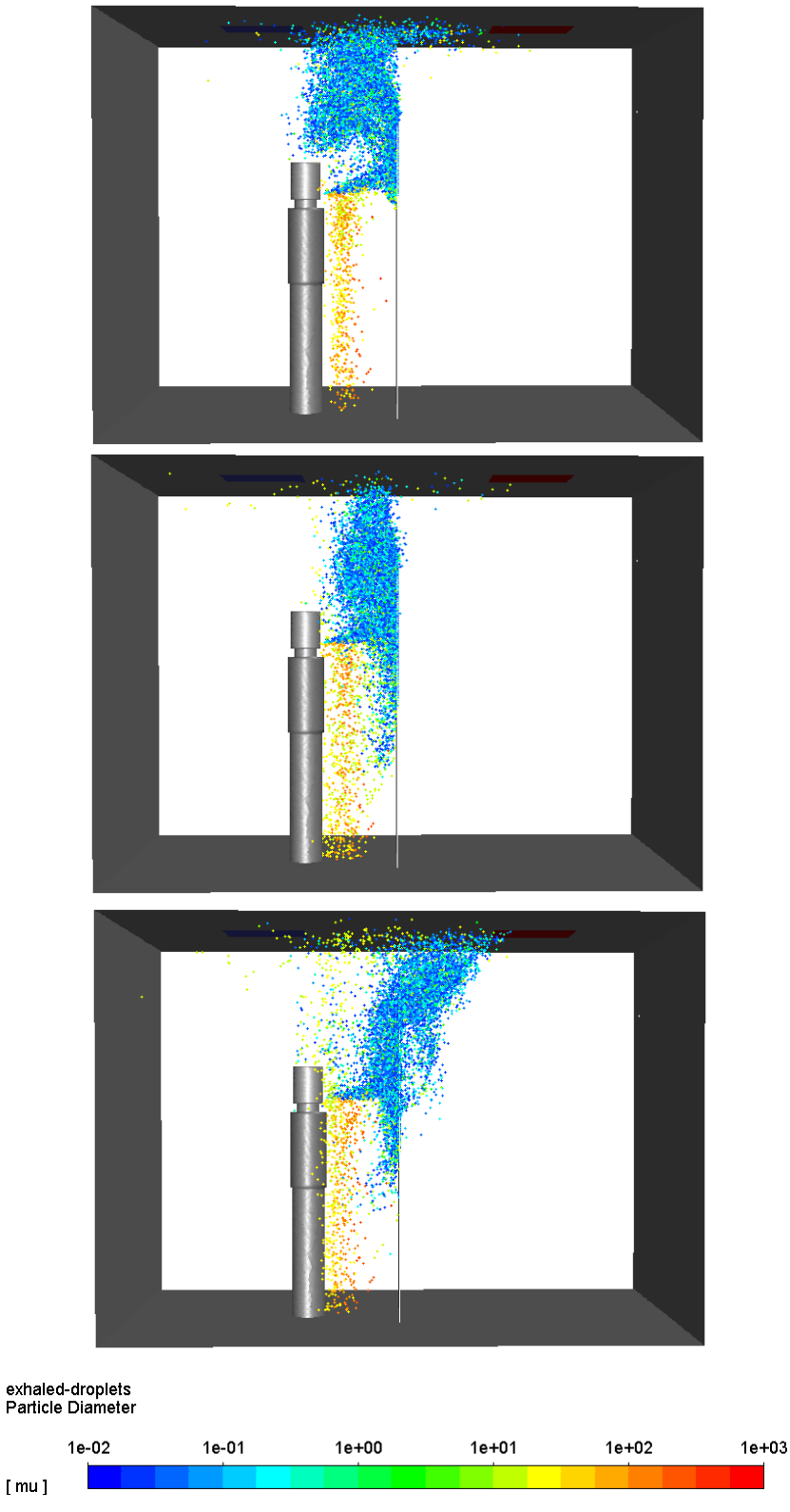

Figure 50 Particle position at the end of the exhalation (25 s) for air change rates of, top to bottom: 0.5 ACH, 2.5 ACH and 5 ACH.

Figure 51 shows velocity contours on a log scale, streamlines and vectors along two vertical planes for the different ventilation rates. Both vertical planes run through the centre of the inlet vent, with one in line with the direction of the exhalation and ventilation, and the other perpendicular to it. The figure shows the flow fields at the end of the simulations. The main flow features are mixing by the ventilation flow and the thermal plume from the body.

At the lowest air change rate the velocity contours show a separation between an upper region of higher velocities and a region below this where the velocities are lower. This results in an environment where exhaled particles will tend to be more stratified and not mixed throughout the room. As the air change rate increases the higher velocities continue further down the walls and reach the bottom of the room, which results in increased mixing throughout the room.

Two-dimensional streamlines are plotted on the plane perpendicular to the direction of the exhalation, showing the size of the vortex structures, generated due to the interaction of the ventilation flow and the walls. At the lowest air change rate the vortex structures are significantly smaller than those observed at higher air change rates. At the highest air change rate the wall vortex reaches further down within the domain before separating from the wall. This bigger structure aids in breaking down the stratification observed at the lowest air change rate and improves the mixing.

Velocity vectors plotted on the two planes show the influence of the thermal plume. Most of the flow is drawn towards it, even at the highest rate of ventilation. A short-circuiting effect can also be seen, with flow going directly from the inlet vent to the outlet vent along the top of the domain.

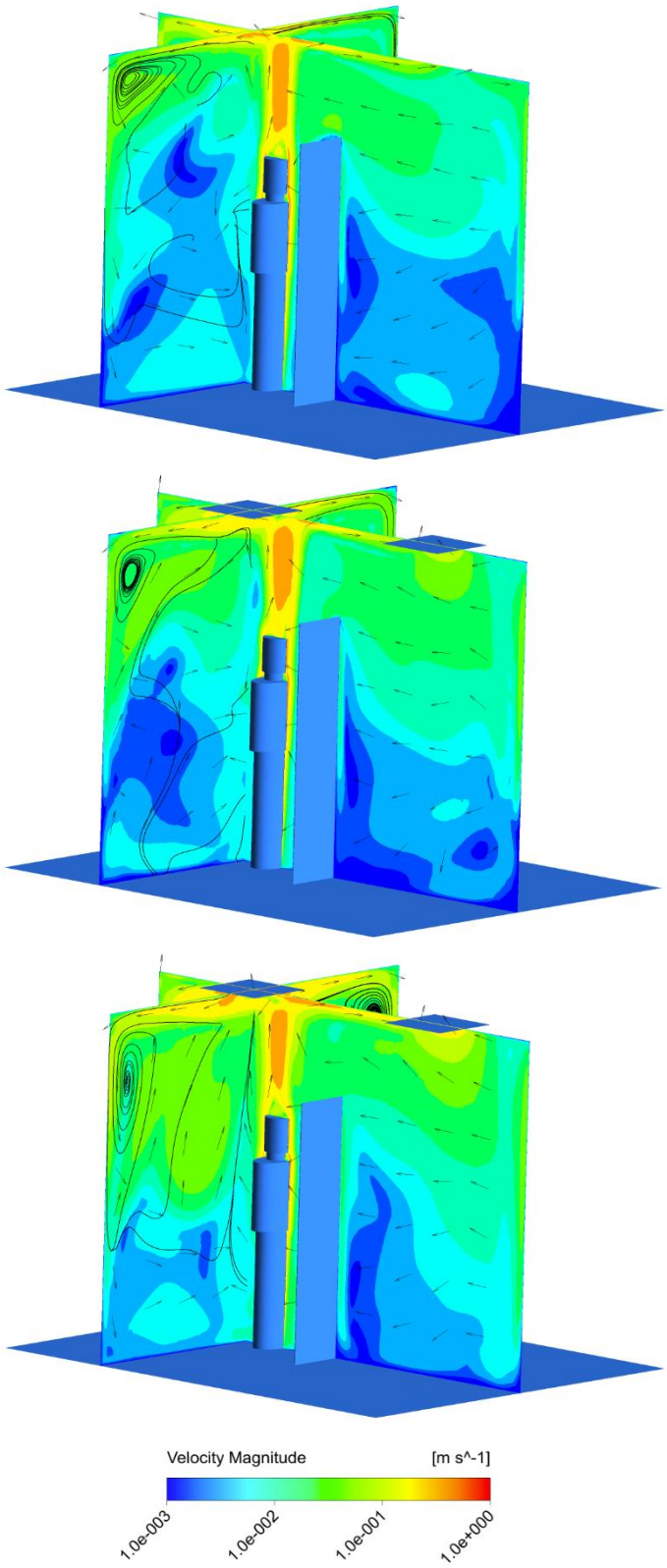

Figure 51 Log-scaled velocity contours, streamlines and vectors, at the end of the simulations, on vertical planes through the centres of the vents, for air change rates of top to bottom: 0.5 ACH, 2.5 ACH and 5 ACH.

The injected particle count distribution is plotted in Figure 52 for the different ventilation rates, along with the count distributions for those particles that deposit, get extracted by the ventilation, and remain airborne at the end of the simulation. Independent of the air change rate the largest droplets all deposit, as they behave ballistically and their movement is dominated by the initial conditions with the ventilation flow having little to no effect. The mid-range droplet size results show that the deposition is higher at the fastest air change rate and for the small droplet sizes deposition is higher at the lowest air change rate. This is most likely to be due to the higher air change rate resulting in higher ambient flow velocities and as a result the mid-sized droplets are impacting the wall more, whereas for the lower ventilation rate, the small particles are approaching the walls and depositing due to the applied turbulent velocities.

The particles that are extracted, not surprisingly, show a clear trend that the higher the ventilation rate the more particles are extracted. With an increased air change rate, larger particles are also able to be extracted compared to lower air change rates, this is because the higher ventilation velocities within the room are able to keep them airborne. The count of droplets which remain airborne is calculated as the number injected minus the number deposited and extracted and is shown in Figure 52. Compared to the trend for extraction, the opposite trend is observed. For a lower air change rate the number of particles airborne is higher.

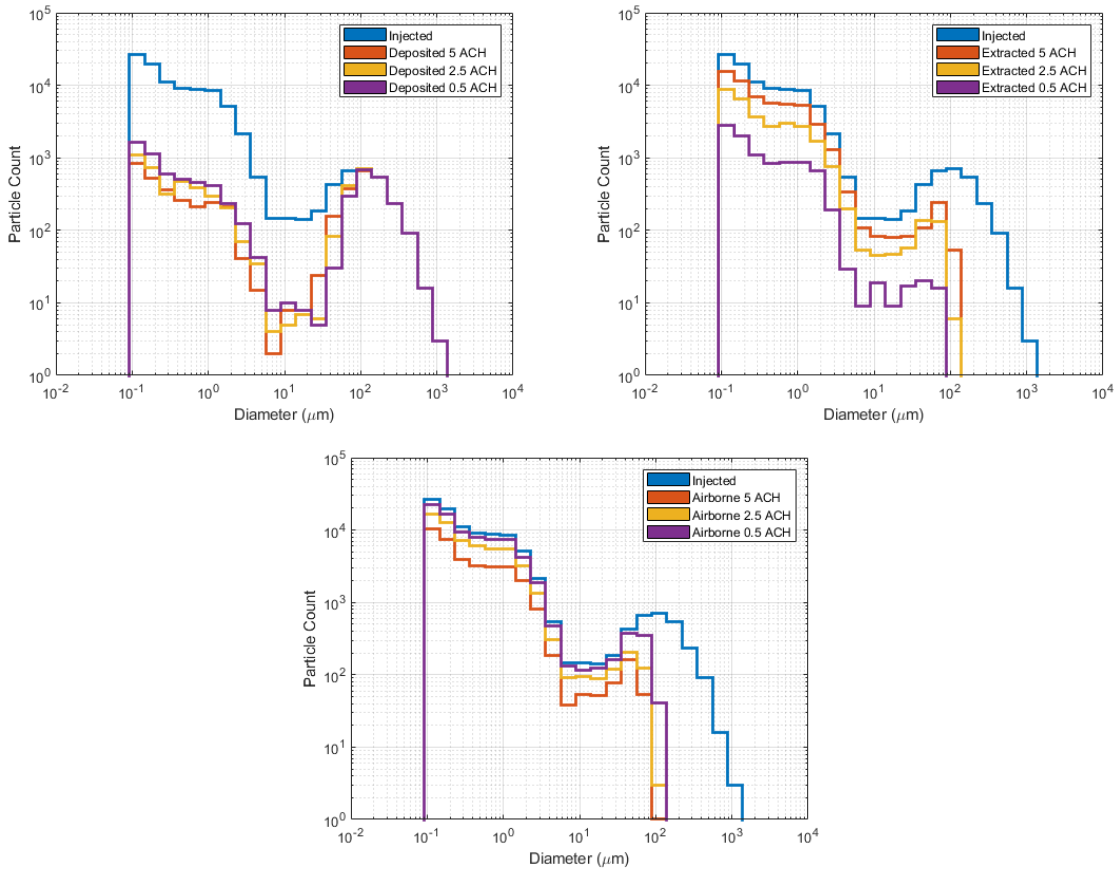

Figure 52 Particle count distribution at 5 minutes for varied air change rates of, top to bottom, left to right: Deposited particles, extracted particles and particles that remain airborne.

The viral exposure was calculated within the sample volumes on the emitter side and non-emitter side of the screen. The resultant initial and final exposure plots are shown in Figure 53. For short times the viral exposure on the emitter side of the screen remains high as this is dominated directly by the exhalation. On the non-emitter side of the screen the greatest viral exposure in the initial 25 s is predicted at the highest air change rate, due to the increased mixing and resulting number of particles which are able reach the non-emitter side. There is no clear trend in viral exposure with air change rate for the non-emitter side in the initial 25 s. This is most likely due to the flow field changes within the room from the changes in the air change rate, and the interaction with geometry, exhalation and the thermal plume.

At the end of the simulations the viral exposure on the non-emitter side of the screen is lower by an order of magnitude at the highest air change rate compared to the lower air change rates. This is due to the higher air change rate extracting more particles during the simulation, leaving fewer particles in the domain, and increased mixing and dilution throughout the domain. At an air change rate of 2.5 ACH, fewer of the particles are extracted but there is still significant mixing throughout the domain, giving equal exposure on the emitter and non-emitter side. As a result, there is a greater viral exposure on the non-emitter side compared to the higher air change rate. For the lowest air change rate there is still a difference between the viral exposure on the emitter and non-emitter side, due to reduced mixing of the aerosols. This results in most of the exhaled aerosols remaining on the emitter side of the domain and results in an increased contribution to the viral exposure on the emitter side compared to the non-emitter side.

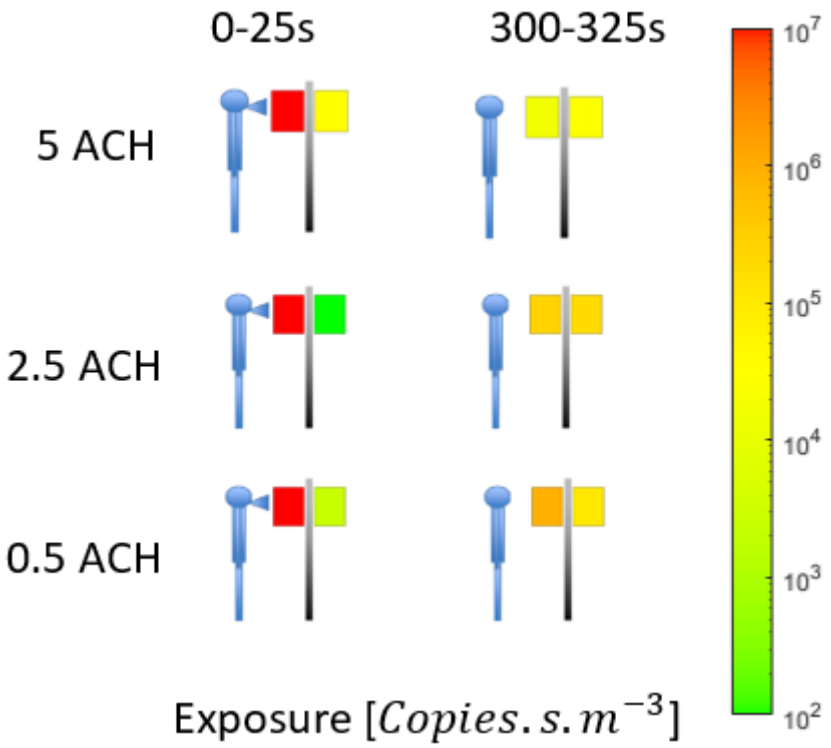

Figure 53 Initial and final exposure plots of viral exposure at the different air change rates, top to bottom: 5 ACH, 2.5 ACH and 0.5 ACH, left: $0 - 25$ s, right: $300 - 325$ s.

The viral exposure and cumulative total viral exposure on the non-emitter side are plotted in Figure 54 for the three different air change rates simulated. The highest total viral exposure at an air change rate of 5 ACH is reached after 80 s and then decays more rapidly than for the lower air change rate cases. The lower air change rates do not show a clear trend. At the lowest air change rate the exposure increases by two orders more quickly than for the middle air change rate case. This is likely to be due to particles overtopping the screen and being sampled within the non-emitter sample volume. The two lower air change rates reach a similar peak in viral exposure at 110 s, which is later than the peak for the highest air change rate, and the viral exposure for both decay at a similar rate, which is slower than the high air change rate case.

The cumulative viral exposure at an air change rate of 5 ACH is considerably higher than for the other air change rates simulated. This is largely due to the initial mixing of the exhalation onto the non-emitter side and the peak observed when the exhalation moves through the non-emitter sample volume. At the lower air change rates, the exhalation mixes more slowly within the domain and the resultant exposure appears more constant. At the end of the simulations the viral exposure contribution to the cumulative viral exposure for the lower air change rates is still steadily increasing, the total viral exposure at the highest air change rates falls below that of the lower air change rates half way through the simulation, so the increase in cumulative viral exposure becomes slower.

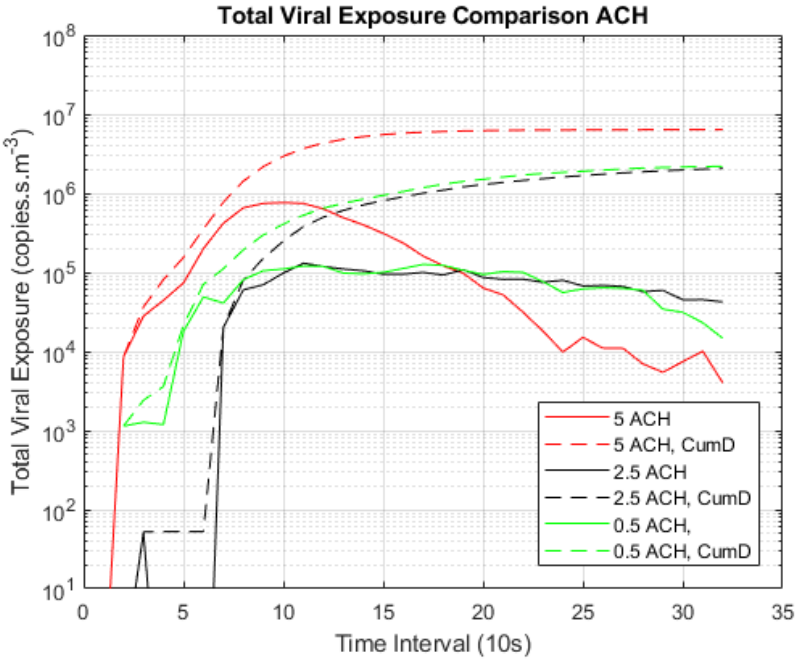

Figure 54 Plot of total viral exposure in the non-emitter side sample volume for speaking with a screen, sampled every 10 seconds (solid line) and cumulatively (CumD, dashed line) for air change rates of 5 ACH (red), 2.5 ACH (black) and 0.5 ACH (green).

6.2.3 The analogy between exhaled breath carbon dioxide and particles

The use of exhaled carbon dioxide as an indicator of ventilation effectiveness was discussed in Section 2. CFD modelling carried out under the PROTECT NCS project (Dargaville et al., 2021) used exhaled carbon dioxide concentration as an indicator of exposure risk. The CFD modelling does not rely on a well-mixed assumption, but assumes that the region of interest is still in the “far-field”, i.e. within the region in which particles behave passively. Preliminary analysis of predicted carbon dioxide concentration compared to particle concentration is reported in the Indoor Air paper by Coldrick et al. (2022). Although exhaled carbon dioxide concentration was not measured in the UKHSA experiments (see Section 5), it is possible to determine it from the CFD model. Coldrick et al. conclude that there is an analogy between the exhaled carbon dioxide concentration and particle concentration (for airborne particles).

As stated in Section 3.1, the Eulerian-Lagrangian method used in the current study has the advantage that it allows distributions of particles sizes to be modelled and allows for detailed analysis of particle tracks and deposition. However, this fundamental division of the physics into the continuous and discrete phases means that care is needed in comparing discrete phase particle quantities with continuous phase carbon dioxide concentration. The notion of a particle ‘concentration’ in a CFD computational cell volume becomes dependent on the local cell volume and the number of particles simulated. This gives rise to a different level of mesh dependency than is used to assess particle tracks and deposition, which have so far been the quantities of interest in the current study.

The work in this section further investigates the link between exhaled carbon dioxide and particles by separating the droplet sizes into three size ranges. The approach for calculating the viral exposure is explained in Section 6.1.4, although here the control volumes are now

the computational cells of the domain. To calculate the carbon dioxide exposure (with units of $kg.s.m^{-3}$) first the concentration of carbon dioxide within the cell is calculated by taking the product of the mass fraction of carbon dioxide in the cell and the density of the mixture within the cell,

$$C_{CO_2} = Y_{CO_2}\rho. \tag{30}$$

The carbon dioxide exposure is then calculated as the product of concentration within the cell multiplied by the simulation timestep (Δt),

$$E_{CO_2} = C_{CO_2}\Delta t. \tag{31}$$

Calculating the ratio of viral (droplet) exposure to carbon dioxide exposure provides a metric which aims to eliminate the influence of cell volume dependency. This metric also allows an assessment to be made of the effectiveness of using carbon dioxide concentration as a tracer for exposure risk from particles. The size distribution is separated into three size ranges or 'bins', following Foat et al. (2022): small ($b_1;\ d_0 < 20$ µm), medium ($b_2;\ 20 < d_0 < 100$ µm) and large ($b_3;\ d_0 > 100$ µm. This allows an investigation of the effectiveness of carbon dioxide as a tracer for these size ranges. The exposure ratio (E_{r_i}) for size bin b_i is defined as

$$E_{r_i} = \frac{E_{b_i}}{E_{CO_2}}, \tag{32}$$

where E_{b_i} is the viral exposure from size bin b_i and E_{CO_2} the carbon dioxide exposure.

The exposure ratio was calculated at each time step throughout the simulation. The viral concentration from size bin b_i is calculated by taking the sum of viral exposures from the contributing droplets within the cell,

$$E_{b_i} = \frac{\sum_{k=1}^{N} \mu_k\, t_k}{V} = \frac{\sum_{k=1}^{N} \left(\frac{\pi}{6} d_k^3 c_v\right) t_k}{V} \tag{33}$$

Here μ_k is the number of viral copies within the droplet and c_v is the viral load. In this work the viral load is assumed to be distributed uniformly by volume throughout the droplet size distribution taking the value of $c_v = 2.76 \times 10^{15}$ copies$\cdot m^{-3}$ from Foat et al. (2022). The work of Coleman et al. (2021) suggests the viral distribution has an increased weighting towards the smaller end of the distribution. Due to the lack of detail on droplet size dependant viral loads, the uniform assumption is deemed appropriate here.

The carbon dioxide exposure, viral exposure for each size bin and the ratio of these quantities have all been calculated for the base case simulation with a screen. The exposure ratio aims to eliminate dependency on cell volume as both exposures have units including volume.

The jet region and droplet locations are first visualised at 4 s after the start of the breathing period to understand how the different size droplets follow the exhalation. Figure 55 shows:

a) iso-volume of carbon dioxide mass fraction greater than or equal to 0.001 kg/kg

b) the position of exhaled droplets with sizes corresponding to the three size bins, and

After 4 s the droplets will not all have evaporated down to droplet nuclei. Therefore, some of the droplets change size range between the initial and evaporated diameter plots. As the only source of carbon dioxide in the domain is through the mouth, this iso-volume method allows us to distinguish the carrier flow region relative to the ambient. The exhaled jet region can be seen as well as the spreading of the exhalation after impingement onto the screen.

The droplets in the smallest size range can be seen to closely follow the carrier flow region during the initial 4 s of exhalation and are mixed throughout the carrier flow and impingement region. Some of the droplets begin to leave the iso-volume after the jet impinges the screen, this is most likely due to the choice of cut-off used for the iso-volume where lower values would still be representative of the carrier flow region. The droplets which have left the iso-volume between the mouth and screen are due to the random turbulent fluctuations, perturbing the droplet enough to leave the jet region.

Droplets with initial diameters in the middle size range are not present in the upper half of the jet and can be seen to settle out of the carrier flow at a small distance away from the mouth. Almost all the droplets in the largest size range have dropped out of the carrier flow region, any remaining in the region are close to its bottom edge. The larger droplets travel further than the medium droplets before dropping out of the carrier flow, this is due to their ballistic nature.

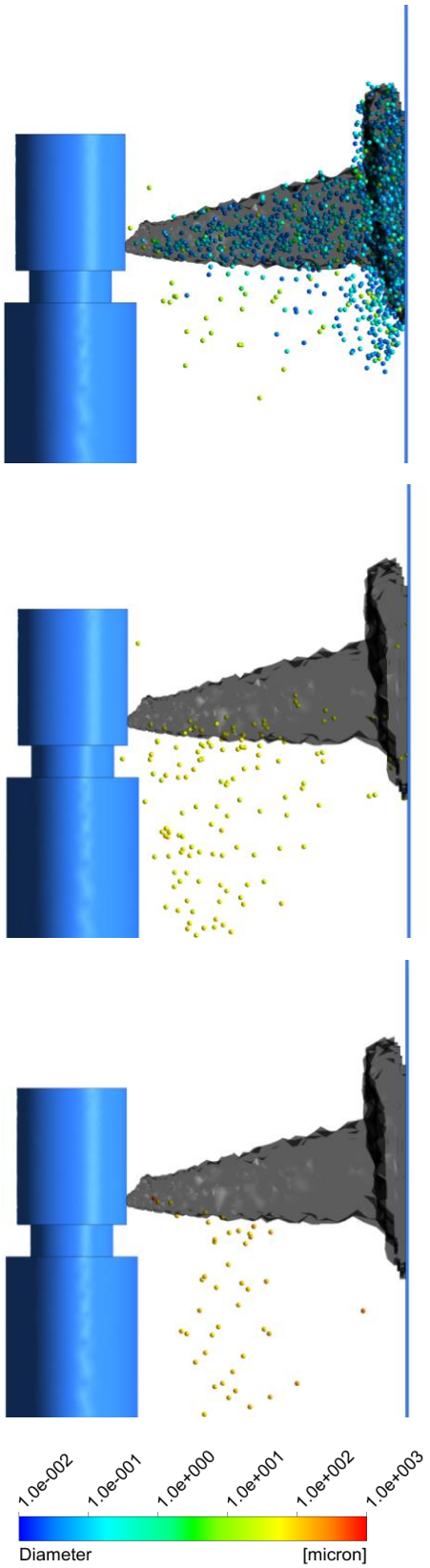

Figure 55 Simulation of base case of talking with a screen at 4 s. The grey region is an iso-volume of carbon dioxide mass fraction greater than or equal to 0.001. Images top to bottom show the particle positions, coloured by droplet size, for the three different size bins: $d < 20$ µm, 20 µm $< d < 100$ µm and 100 µm $< d$.

During the initial 4s of exhalation, the droplets in the smallest size range closely follow the exhaled carbon dioxide, the large size range droplets quickly stop following the exhaled carbon dioxide, while the medium size range exhibits behaviour of both, where some of the droplets settle out and others follow the exhalation. Within this time the carbon dioxide acts well as a tracer for the small and some of the medium range droplets, further analysis examines whether this tracing behaviour continues through time.

To investigate carbon dioxide tracer viability for longer times, contours of carbon dioxide exposure and viral exposure for the three different size ranges are plotted across a central vertical slice through the domain for times of 4 s, 25 s, 150 s and 300 s after the start of the exhalation, these can be seen in Figures 56 to 59**.** Note that these results are sensitive to the distribution of virus through the particle size distribution as well as the particle size distribution used.

Figure 56 shows the same trends that were observed in Figure 55. From the carbon dioxide exposure plot the influence from the thermal plume during the exhalation is also seen with an increase in carbon dioxide exposure above the manikin. The carbon dioxide tracing of the particles during this initial point of the exhalation has already been discussed.

At the end of the exhalation, after 25 s, the carbon dioxide still acts well as a tracer for the droplets in the small size range, see Figure 57. The medium size range shows behaviours of both types, with some droplets following the exhalation and others having deposited. Suspension of evaporated droplets in the mid-range, due to the body's thermal plume, is clearly seen in the mid-range viral exposure plot. The thermal plume also introduces further deviation of the carbon dioxide from the position of the mid-range droplets. This effect is enhanced due to the location of the inlet vents being positioned directly above the body. The effect is seen because droplets which have left the carrier flow start to settle and during this period are evaporating down to a size that can be suspended by the thermal plume. Once in the thermal plume, they are transported to the ceiling of the room. Those droplets are no longer following the exhalation and therefore no longer being traced by the carbon dioxide. The large droplet behaviour remains the same, having left the carrier flow they are deposited, either on the screen or the floor. On the emitter side of the screen the potential viral exposure from these droplets can be seen to increase to the highest levels predicted. On the boundary of the size range, close to 100 μm initial droplet diameter, some droplets that are in the large size range evaporate to a size that can be lifted by the thermal plume, the same behaviour observed for droplets in the medium size range.

Figure 58 shows the carbon dioxide and viral exposures from the different size ranges approximately half-way through the ventilation phase of the simulation (150 s after the start of exhalation). Looking at these exposure contours, droplets in the small range are still being traced by the carbon dioxide and the exposure from droplets in the large range is not increasing as they have been deposited. The medium range now appears to be traced well by the carbon dioxide, though some particles are beginning to settle out. The same pattern can be seen for the contours of exposure at 300 s, the end of the simulation, in Figure 59**.**

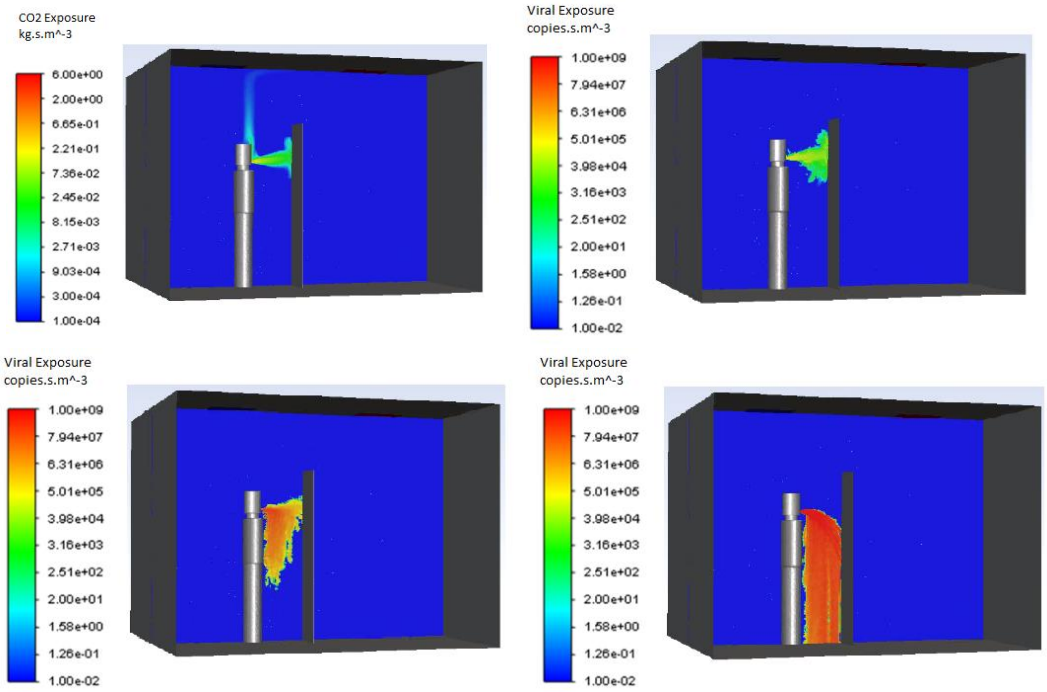

Figure 56 Comparison of carbon dioxide and viral exposure 4 s after exhalation, Top Left: carbon dioxide exposure. Viral exposure from droplets of initial size Top Right: $d_0 < 20$ µm, Bottom Left: 20 µm $< d_0 <$ 100 µm, Bottom right: 100 µm $< d_0$.

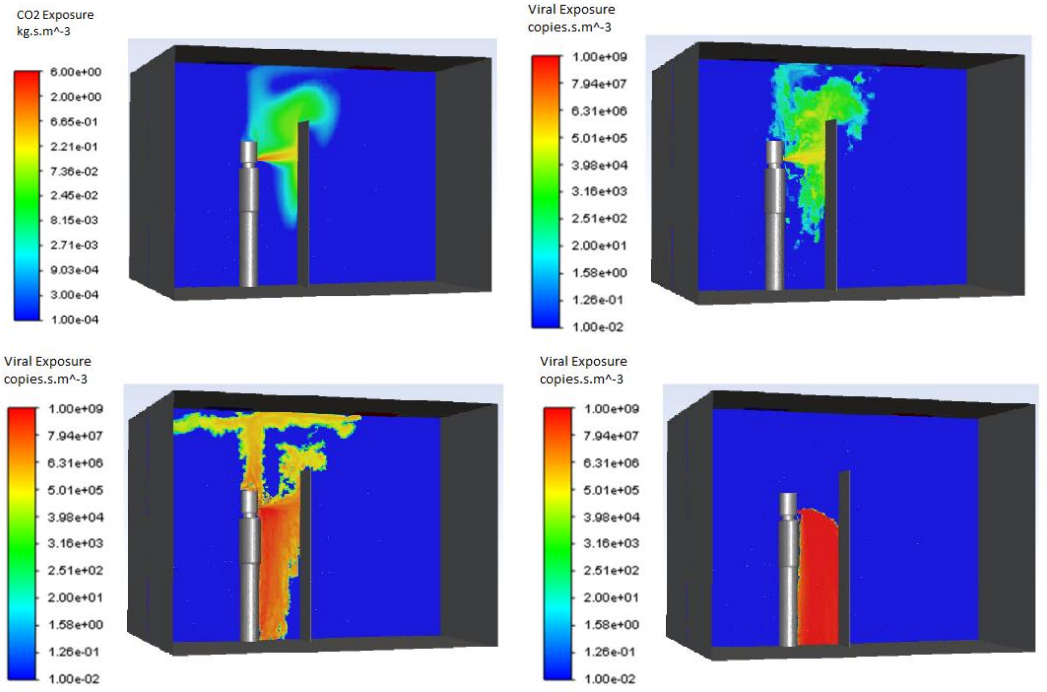

Figure 57 Comparison of carbon dioxide and viral exposure 25 s after exhalation,
Top Left: carbon dioxide exposure. Viral exposure from droplets of initial size Top Right: $d_0 < 20$ µm, Bottom Left: 20 µm $< d_0 <$ 100 µm, Bottom right: 100 µm $< d_0$.

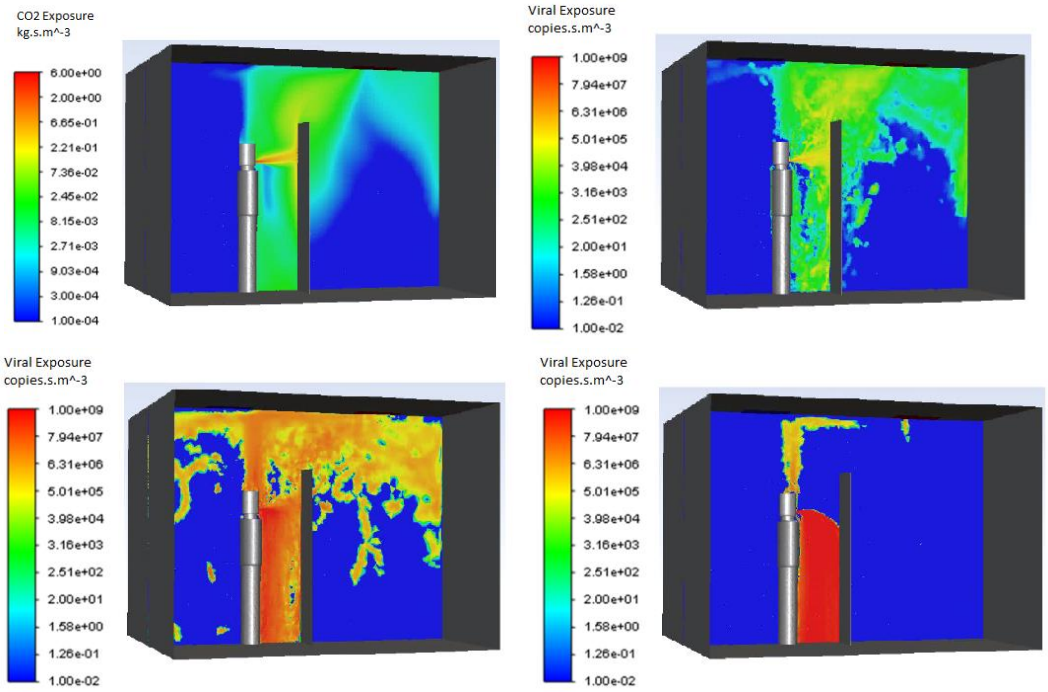

Figure 58 Comparison of carbon dioxide and viral exposure 150 s after exhalation, Top Left: carbon dioxide exposure. Viral exposure from droplets of initial size Top Right: $d_0 < 20$ µm, Bottom Left: 20 µm $< d_0 <$ 100 µm, Bottom right: 100 µm $< d_0$.

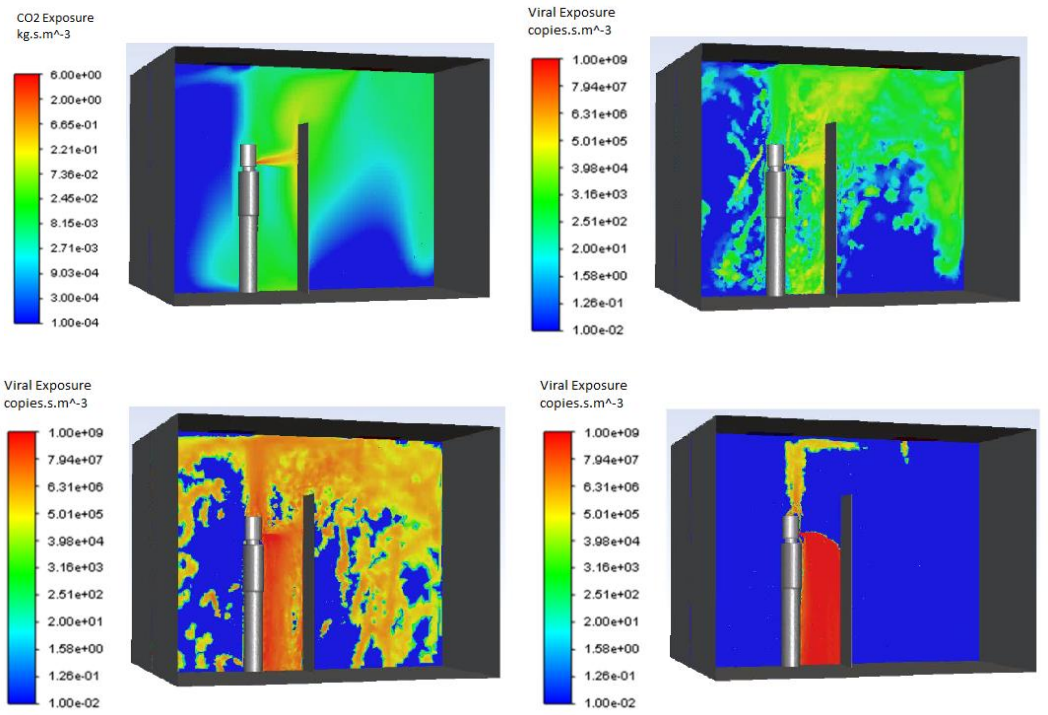

Figure 59 Comparison of carbon dioxide and viral exposure 300 s after exhalation, Top Left: carbon dioxide exposure. Viral exposure from droplets of initial size Top Right: $d_0 < 20$ µm, Bottom Left: 20 µm $< d_0 <$ 100 µm, Bottom right: 100 µm $< d_0$.

As discussed above, the exposure ratio compares viral exposure from droplets to carbon dioxide exposure. These are shown as contour plots for the small, medium and large size

ranges at times of 4 s, 25 s and 150 s and 300 s in Figure 60**.** The exposure ratios are calculated to eliminate any dependence on cell volume and also combine the carbon dioxide and viral exposure into one metric. For the small size range, Figure 60, the ratio appears consistent through time with little changes due to spatial variation. The carbon dioxide and viral exposure are showing the same variation, indicating that the carbon dioxide is a good tracer of viral exposure for this size range. For the large size range, shown in Figure 62, the ratio values on the emitter side are largest, indicating a high viral exposure relative to carbon dioxide exposure, during the exhalation time. As the carbon dioxide from the exhalation is transported through the domain this region of high exposure ratio decreases as the carbon dioxide exposure increases.

The mid-range exposure ratio, as seen in Figure 61, shows behaviours from both the other size ranges. Where the exhaled aerosols are traced by the carbon dioxide, the exposure ratio is of a similar order of magnitude to that of the small size range. For the particles which initially settle out of the carrier flow, there exists a region between the body and the screen where the exposure ratio is initially large and then decreases as the carbon dioxide exposure increases. For the droplets which evaporate down to a size able to be suspended by the thermal plume, the exposure ratio value is roughly midway between that seen at early times in the results for the small and large size ranges. The exposure ratio, Equation 32, is the ratio of viral exposure to carbon dioxide exposure. The viral exposure will be higher in the middle droplet size range, due to the assumption of uniform viral distribution by volume, while droplets in this size range do not always trace the path of the carbon dioxide, reducing the carbon dioxide exposure, the combination results in a range of exposure ratios.

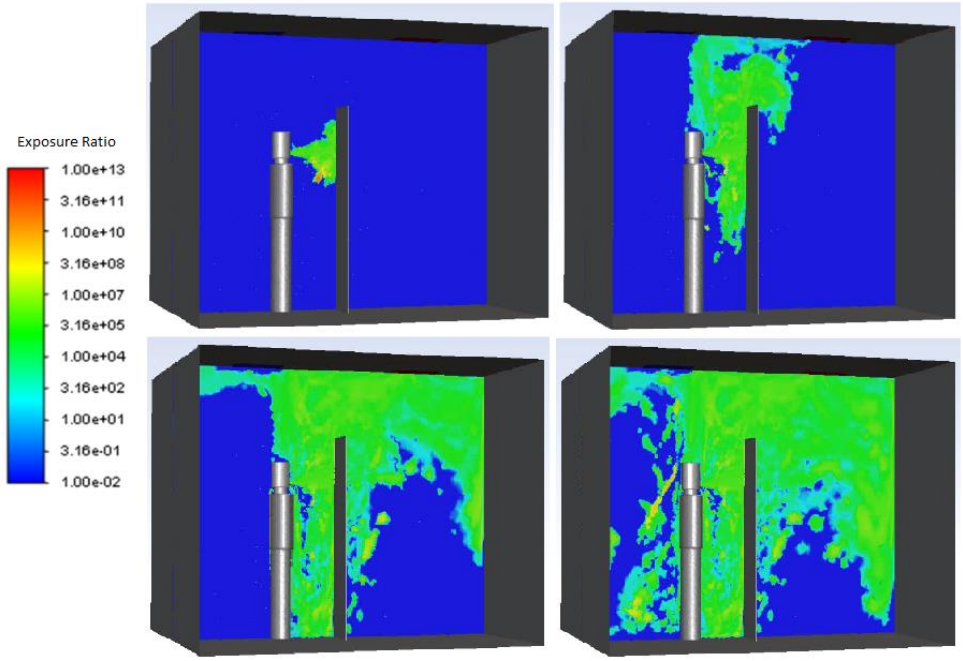

Figure 60 Exposure ratio of viral to carbon dioxide for droplets with initial size $d_0 < 20$ µm at, top to bottom, left to right: 5 s, 25 s, 150 s and 300 s.

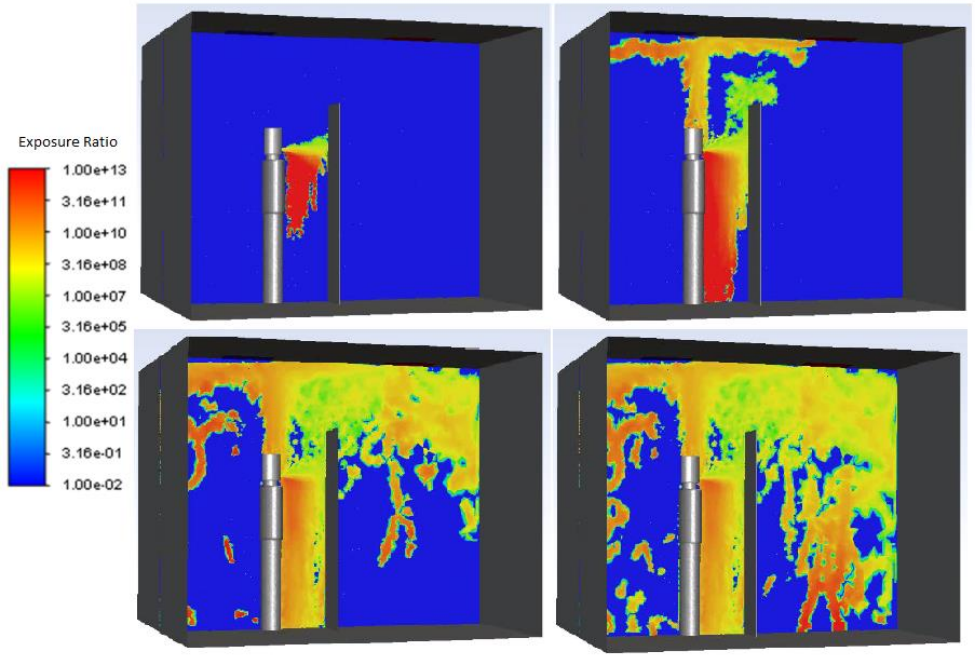

Figure 61 Exposure ratio of viral to carbon dioxide for droplets with initial size $20 < d_0 < 100$ µm at, top to bottom, left to right: 5 s, 25 s, 150 s and 300 s.

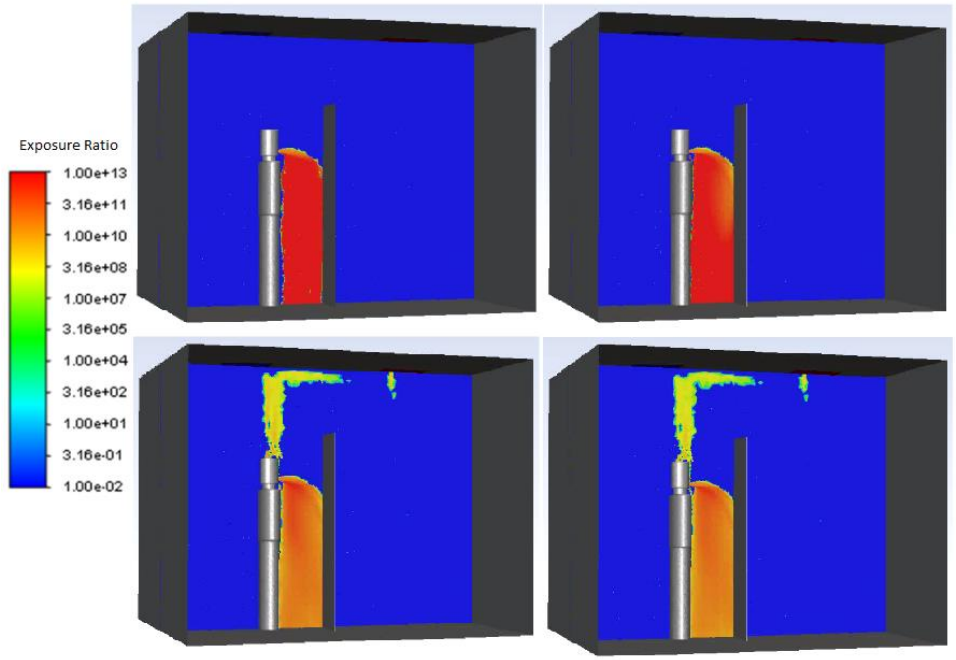

Figure 62 Exposure ratio of viral to carbon dioxide for droplets with initial size 100 µm$< d_0$ at, top to bottom, left to right: 5 s, 25 s, 150 s and 300 s.

6.3 Screen and ventilation discussion

6.3.1 Mitigation

Simulations have been performed to examine the effect of mitigations on exposure from exhalations. The base case simulations compare a person in the same position and orientation speaking for 25 seconds with and without a screen in front of them. After the exhalation has finished the simulations were continued for five minutes where the exhalation was mixed by the ventilation. An air change rate of 5 ACH was used throughout the simulations. The viral load in the droplets was assumed to be proportional to the droplet volume and once distributed the number of viral copies in a droplet remained the same throughout the simulation. Viral decay was not modelled, the simulations only considered changes in viral exposure due to the transport of droplets. The number of viral copies in a droplet does not change, but as the droplets evaporate, the concentration of the virus in the droplet (virus per unit volume) increases.

The simulations show that the screens block the large droplets that would otherwise travel into a sampling volume where a person could be standing. Screens modify the transport of airborne droplet nuclei into the sampling volume. Without a screen, the exhalation passes through the sampling volume and a person would be exposed to the exhalation flow with little mixing and dilution. When a screen is present, the exhalation flow impinges on the screen and is deflected, the exhalation cloud is carried to the top of the screen where it interacts with the ventilation flow. Exposure from airborne droplet nuclei is delayed by the presence of the screen, and the exhalation cloud is mixed before reaching the sampling volume. The interaction of coughing with a screen was also examined and compared to that from speaking. Overall, the behaviour for the exhalations is similar. The screen blocks large droplets and deflects smaller droplets at short times. Mixing in the room means that by the end of the simulation there is little difference in viral exposure on the non-emitter side with and without a screen. As modelled, the viral exposure from a single cough is only slightly less than that from 25 s of speaking. There are differences as more of the smaller droplets deposit on the screen from a cough because of the higher velocities when coughing. The cough is initially directed downward while speaking is level, this affects the time droplets move into the region of exposure from a cough compared to speaking but by the end of the simulation the exposures are similar.

At longer timescales, the effects of interactions between a person, their thermal plume, the screen and ventilation are complex. Additional simulations were performed to examine how exposure to virus was affected by these factors.

Three distances between the emitter and screen were examined, the base case used the middle distance, 0.5 m. The highest exposure on the non-emitter the screen was predicted for the middle distance. At the smallest distance, more droplets impinged on the screen. At the largest distance, fewer droplet nuclei were entrained into the thermal plume of the person, again reducing the amount of airborne droplet nuclei. Different factors were important in determining the level of exposure at the different separations between the emitter and the screen. These results highlighted the complexity of the flows and the sensitivity to relatively small changes in geometry.

The effect of different ventilation scenarios on exposure were also examined. The simulations performed balance available computing resources, the size of domain used and

the number of scenarios that could be examined. Some of the features of the flow were related to the size of room simulated in the base case. In a larger room than the base case, the exposure was reduced as there was more space for mixing to occur, reducing the viral concentration.

Examining the effect of different air change rates, the base case, which was at the highest air change rate simulated, of 5 ACH gave the greatest initial exposure and highest total exposure. This perhaps surprising result was due to the ventilation transporting droplets more quickly to the sampling volume. However, with time the reduction in viral concentration, was more rapid than at lower air change rates. The important factors in exposure also differed at different ventilation rates. At the lowest air change rate, 0.5 ACH, the dominant influence on mixing and concentration was the thermal plume from the emitter, while at the highest ventilation rate, the ventilation flow had the greatest effect. At the middle air change rate of 2.5 ACH, the behaviour was affected by both the thermal plume and the ventilation flow.

Even at the highest air change rate (5 ACH) the duration of five minutes used in the simulations corresponds to less than half an air change. At the end of the simulations, the airborne droplets from the exhalation are still not well-mixed, but the mixing and transport are being driven by ventilation flows not the original exhalation.

Screens have an immediate effect blocking large particles and modify exposure by redirecting the exhalation flow, but over longer times ventilation is more important in controlling exposure. The simulations performed only consider a single exhalation followed by mixing and transport. In actual scenarios other exhalations would occur during the period of mixing and transport. The simulations also focussed on a single, static emitter, in practice receptors (other people) would have to be present. The ventilation flow would be modified by multiple thermal plumes from people and their movement.

6.3.2 Droplet Size Effects

As well as examining different influences of screens as a mitigation strategy, the CFD simulations were also used to examine droplet behaviour. Droplets with initial diameters below 20 µm always evaporate to form droplet nuclei with diameters of 5 µm or less. These remain airborne, suspended by the flow in the room. At the other end of the droplet size distribution, droplets above 100 µm nearly always deposit before they have evaporated to droplet nuclei. Between these diameters the simulations predict that droplets may deposit before evaporating to a droplet nuclei or may form a droplet nuclei. The nuclei from droplets in this size range are larger than aerosol size, assumed to be 5 µm, but, under the influence of the flow field in the room, combining ventilation, exhalation and the thermal plume from the body of the emitter, may remain airborne and remain available for inhalation.

The droplet diameter range where both evaporation and deposition occur is also the range where the key differences in the droplet counts between the BLO model, Johnson et al. (2011), and the Pöhlker distribution, Pöhlker et al. (2021), are observed. Overall, more droplets are generated sampling from the Pöhlker distribution. Sampling from the BLO model results in few droplets with initial diameters in the range 20 µm to 100 µm. Both distributions are fitted to experimental data but using the Pöhlker distribution will give more information across the full range of droplet diameters and particularly about the possible behaviour of the droplets in the range 20 µm to 100 µm. As described, droplets in this size

range may deposit, but can remain airborne for the duration of the simulations. This has a large effect on the predicted viral exposure from droplets. Volume weighting the distribution of viral copies amongst droplets means that most of the airborne viral exposure comes from viral droplets in this medium size range, and more viral exposure is predicted using the Pöhlker distribution than using the BLO model.

The Pöhlker distribution is fitted to measured particle diameters for droplets in the bronchiolar and laryngeal modes, where the measurements would be expected to be of droplet nuclei, and initial droplet diameters for the oral modes, where measured diameters of stains from deposited droplets are converted to initial droplet diameters. The non-volatile fraction of droplets is specified in the CFD simulations, hence the initial diameter of droplets can be calculated from the diameter of droplet nuclei. Simulations were performed comparing the Pöhlker distribution for speaking with one where the bronchiolar and laryngeal modes were changed to represent initial droplet diameters. The distributions are compared in Figure 63, plotting the number concentration, $d\,Cn\,/d\,Log\,D$, the number of particles with diameters in the interval $d\,Log\,D$ per cm^3 of exhaled breath, against the droplet diameter, D (µm). Changing the bronchiolar and laryngeal modes to initial diameters moves the mode of the smallest distribution into the range of diameters sampled. The number of droplets with diameters less than 1 µm is significantly increased and the number of droplets with diameters up to 10 µm is increased. The time evolution of the particle counts of diameters after exhalation for the original and modified distributions are shown in Figure 64, the equivalent plots for the time evolution of viral exposure are shown in Figure 65. Figure 64 shows that the increase in the number of droplets towards the bottom end of the range of diameters in the initial droplet diameter distribution remains throughout the simulation. The effect on viral exposure, which is scaled by droplet volume, is that using the initial droplet diameter distribution widens the range of droplet diameters carrying higher viral exposure, Figure 65. The peak of viral exposure is similar with both distributions and occurs in the same range of droplet diameters.

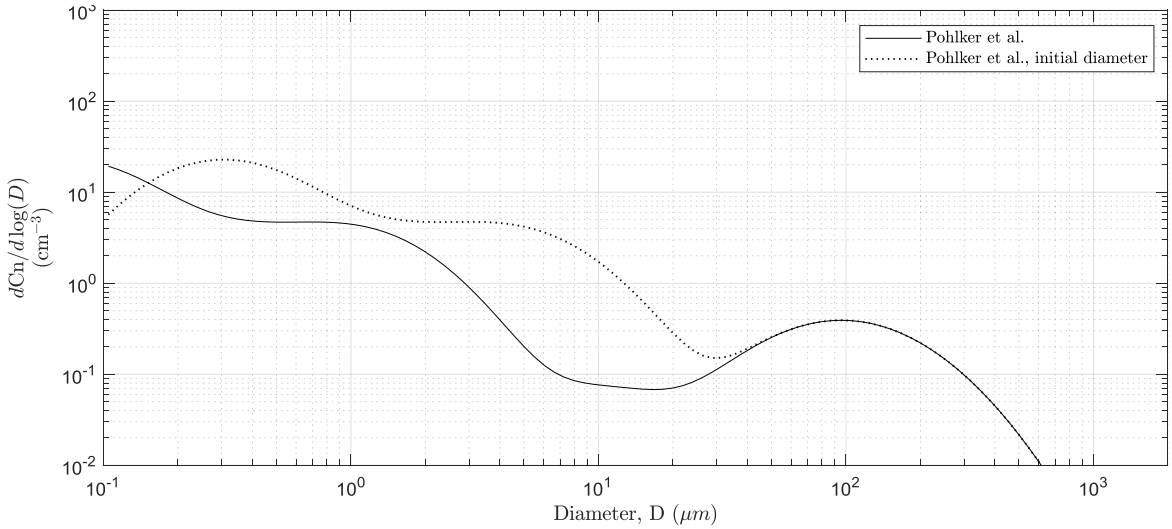

Figure 63 Pöhlker et al. droplet distribution for speaking, original and with bronchiolar and laryngeal modes modified to represent initial droplet diameters

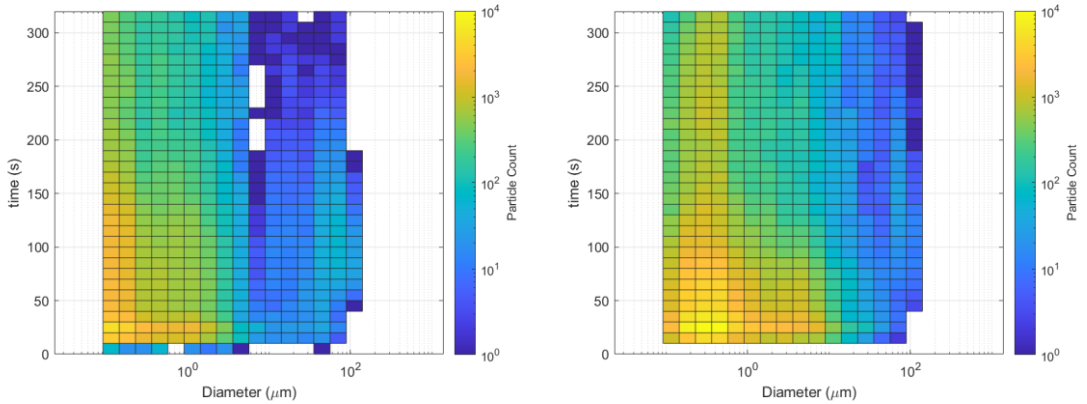

Figure 64 Particle count as a function of time and initial droplet diameter in the non-emitter side sample volume for speaking with a screen. Left: droplet distribution from Pöhlker paper, right: distribution modified for initial diameters

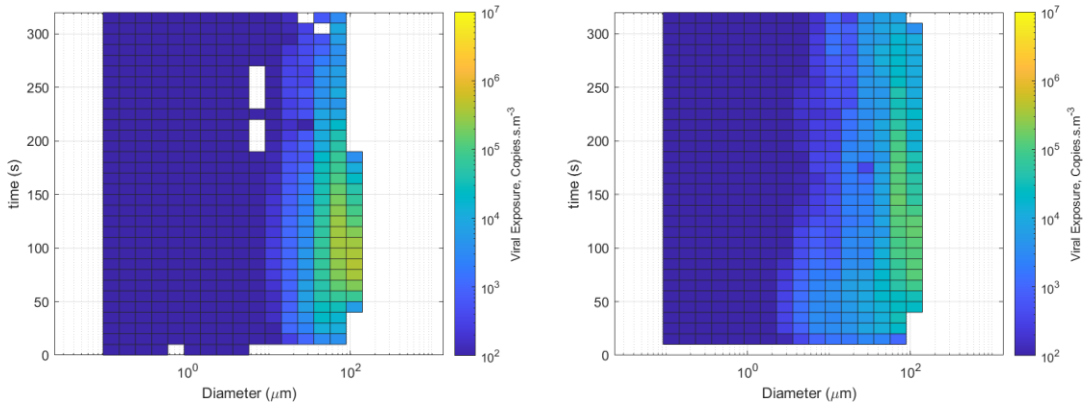

Figure 65 Viral exposure as a function of time and initial droplet diameter on the non-emitter side for speaking with a screen. Left: droplet distribution from Pöhlker paper, right: distribution modified for initial diameters

6.3.3 Distribution of viral copies

There is further uncertainty about how virus is distributed between droplets in exhalations. The simulations carried out in this report have assumed that the viral load is proportional to the droplet volume. Using this assumption means that most of the virus is in the large droplets, that deposit, but most of the airborne virus is in droplets in the medium diameter range. However, measurements in Coleman et al. (2021) suggest that most of the virus is in smaller droplets. While the droplet size distribution is specified in the simulations, the viral load, and resultant exposure, are post-processed and the effect of different distributions can be examined. An alternative approach to assuming viral load is proportional to droplet volume, is to assume that it is proportional to the droplet surface area. The distribution by surface area lies between those by count and volume and, if used, it would increase the number of viral copies in smaller droplets and reduce the number in large droplets. Figure 66 shows the Pöhlker et al. (2021) probability distribution by droplet count, droplet surface area and droplet volume. Figure 67 compares the viral exposure on the non-emitter side of a screen, with the virus distributed by surface area and by volume. The redistribution of viral copies, moving from distribution by volume to distribution by surface area, increases viral copies for airborne droplets of all diameters. The highest airborne viral exposure still comes from droplets with initial diameters in the range 20 µm to 100 µm. Viral load in droplets may

also depend on where the droplets originated from within the human airway and information to describe this is not available. However, if this information became available, it could be used to post-process the simulations using either the distributions of Pöhlker or BLO.

Uncertainty in the droplet size distribution from exhalations and in how the virus is distributed between droplets could have a significant effect on predictions of the amount of virus that could be inhaled and hence on transmission.

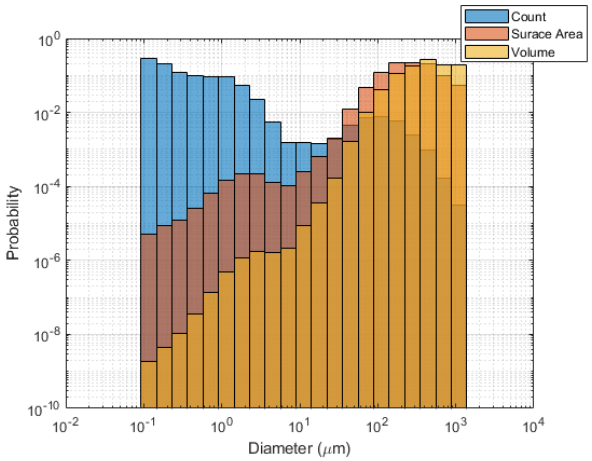

Figure 66 Probability distribution of droplet count, droplet surface area and droplet volume by initial droplet diameter for the Pöhlker distribution

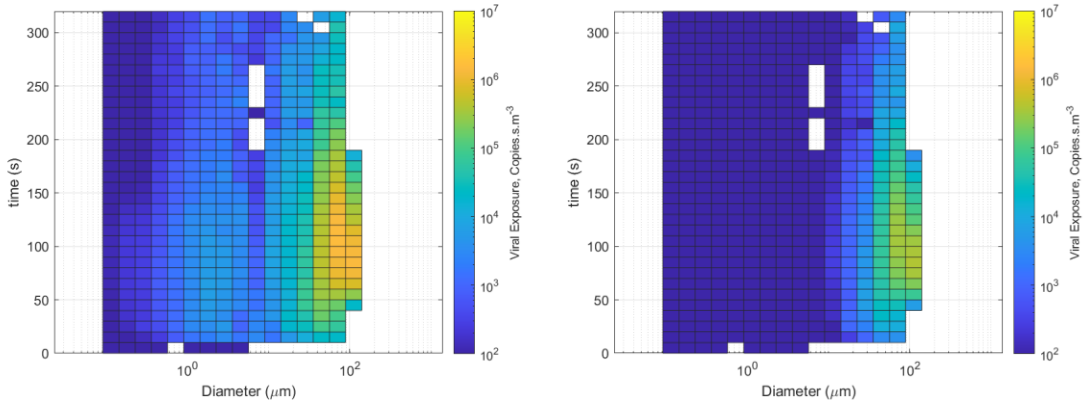

Figure 67 Viral exposure as a function of time and initial droplet diameter size on the non-emitter side for speaking with a screen. Left: Viral copies distributed by droplet surface area, right: Viral copies distributed by droplet volume

6.3.4 Comparing predicted carbon dioxide and viral exposures

Carbon dioxide concentration is frequently used as an indicator of ventilation efficiency and air quality. In models of transmission, carbon dioxide concentration from exhalations, or equivalently passive tracers from exhalations, has been used to predict the probability of infection, Rudnick and Milton (2003), Burridge et al. (2021). In this report, comparisons were made between the predicted carbon dioxide exposure from exhalations and viral exposure from exhaled droplets to examine this analogy between carbon dioxide and viral exposure.

Predictions of exposure from viral copies carried by droplets from exhalations, across the full range of droplet diameters, and carbon dioxide from exhalations were compared. Droplets

that were initially in the small diameter range, with initial diameters less than 20 µm, showed good agreement in the distribution of exposure from droplets compared to carbon dioxide throughout the simulation. There is no agreement between carbon dioxide exposure and exposure to large droplets, with initial diameters greater than 100 µm, because the large droplets deposit quickly and they do not contribute to long-term, long distance airborne exposure. For droplets in the medium diameter range, initial diameters 20 µm to 100 µm, some droplets deposit rapidly and do not contribute to long-term, long distance airborne exposure while others evaporate to droplet nuclei and remain airborne. At the end of the simulations, the viral exposure from the remaining airborne medium diameter range droplets does not compare as well to the carbon dioxide exposure as that from the small diameter droplets, but it does remains similar. The duration of these simulations is short compared to the modelled ventilation time scales, simulating less than half an air change at 5 ACH. If the medium diameter droplet nuclei continue to settle out the correlation may become worse. Additionally, uncertainty about the distribution of virus among droplets makes the comparison more difficult. The predicted carbon dioxide exposure captures small droplet behaviour, difficulties with the medium range droplets are related to the uncertainties already identified with the diameter and viral load distribution in this size range.

6.4 Scenarios with screen-like mitigations

When considering transmission within an open-plan office or meeting room, a number of obstacles may be present between people acting as an emitter and receptor, including desk dividers and PC monitors. However, unlike the screens considered in the previous sections of this report, dividers and monitors are not positioned to try to reduce airborne transmission. Despite this, it is anticipated that both will affect the background flow field, and may block droplets travelling from an emitter to a receptor.

To investigate airborne transmission in typical office environments, simulations of two people, an emitter and a receptor, sitting on opposite sides of a desk were performed using the computational model described in Section 3.

6.4.1 Geometry and mesh

A model meeting room was constructed using a rectangular desk placed in the centre of the room. In total, three cases were considered:

- Case 1: no desk divider, no monitors.
- Case 2: desk divider, no monitors.
- Case 3: no desk divider, two monitors.

Figure 68 shows a side view of the domain for the arrangement of Case 1. A refinement cone was superimposed in front of the emitter's mouth to capture the exhalation. The dimensions of the room were 7 m x 6 m x 3 m (L x W x H). The plan of the room is larger than the enclosure used in the screen simulations, 7 m x 6 m compared to 3.5 m x 3 m, and the room is also a more normal office height, 3 m compared to 2.5 m. The geometry origin $x = y = z = 0$ corresponds to the centre point of the floor.

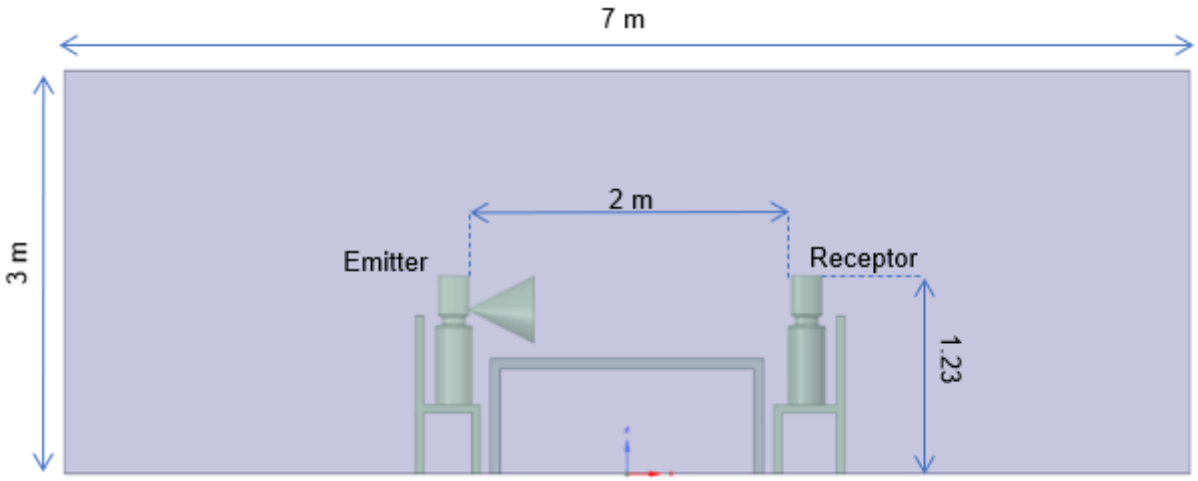

Figure 68 Geometry used for modelling an emitter and receptor sitting on opposite sides of a desk in a meeting room (side view).

Figure 69 presents another view of the geometry used in the CFD model. Both the desk divider and monitors are displayed at the same time in this figure. However, this geometry with both dividers and PC monitors was not simulated. The geometry was orientated such that the exhalation was in the positive x direction, and the monitors and dividers were orientated in the y-z plane. The divider was placed 0.949 m away from each person's mouth, at a height of 0.304 m. This resulted in the top surface of the divider being level with the person's mouth. Each monitor was placed 0.7 m away from the mouth, at a height of 0.554 m. The top surface of the monitor was approximately the same height as the heads of the people. The top surface of the desk was 2.4 m wide and 1.7 m in depth. The two individuals were separated by 2 m, taken to be the distance from the emitter to the receptor's mouth. Computational meshes were generated in Fluent Mesher 2019 R3 using the same methodology reported for the UKHSA experiments and the ventilated room described in Section 4.3.

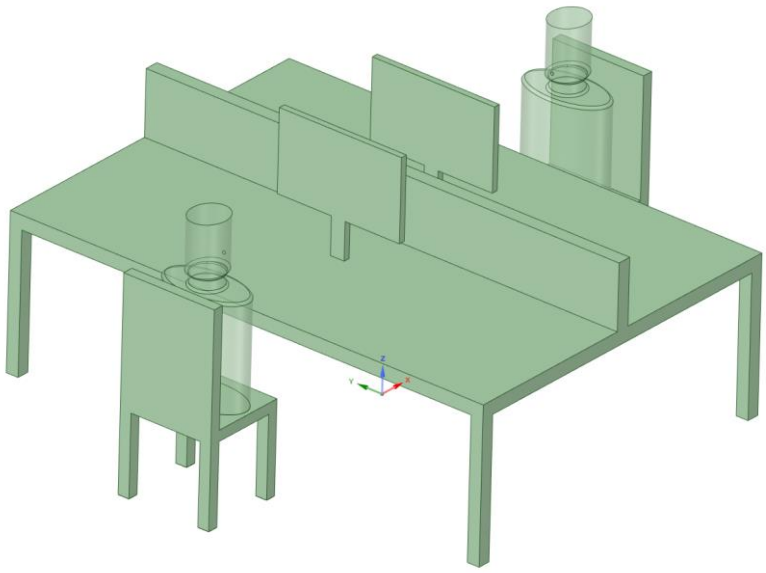

Figure 69 Full CAD geometry used in CFD simulations, with computer monitors and desk divider.

Two effects contributed to a background flow which had to be resolved before particles were injected into the system. They were: (i) mixing due to mechanical ventilation; (ii) buoyancy driven flow from each person's thermal plume. Before any particles were injected into the domain, 600 seconds were simulated in order to generate a suitable initial condition for the exhalation simulations. Particles were then injected from the emitter's mouth. The emitter was assumed to speak for a total of 25 seconds, after which a further 300 seconds was simulated to track particles as they are transported around the room.

A mixing ventilation arrangement compromises 4-way diffuser vents: two mass flow rate inlets, and two pressure outlets. Inlet and outlet vents have been labelled based on their positioning relative to the emitter in Figure 70. Each vent is a square two-dimensional plane on the ceiling. Flow at the vents is directed inwards or outwards, depending on the vent type, at an angle of $30°$ from the ceiling.The total flow was specified to give an air change rate of 5 ACH. Particles which come into contact with the outlet vents are removed from the simulation, i.e. assumed to exit the domain into the air conditioning system, and are therefore no longer a contributor to airborne transmission.

The exhalation boundary condition was prescribed following the speaking source given in Table 4. The particle sizes were defined using the distribution from Pöhlker et al. (2021) which is detailed in Section 3.3.7. A droplet has initial diameter d_0, which changes in time due to evaporation. Generally, the notation d is used below for particle diameter at an arbitrary time.

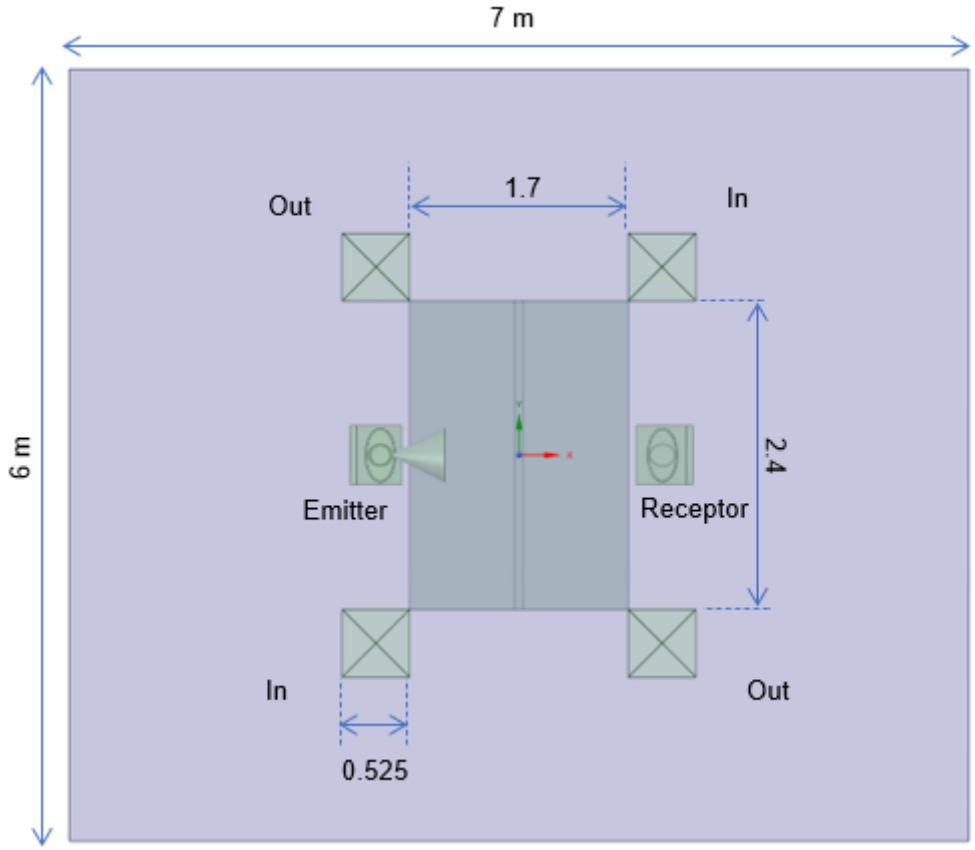

Figure 70 Top view of the meeting room and geometry for Case 2 (desk with divider). Each vent is split into 4 individual sections, allowing for a boundary condition to be prescribed on each triangular section.

6.5 Screen-like mitigation results

6.5.1 Jet dynamics

Figure 71 shows a visualisation of the exhalation jet and cloud dynamics at the end of the speaking period by plotting particle positions on a two-dimensional slice. Particles are coloured by their y coordinate to provide information on lateral position. Note that particles with $y_p < 0$ are somewhat obscured by particles with $y_p > 0$. The size of plot markers is constant and therefore does not correspond to a particle's diameter. Only the range -0.5 m $< y < 0.5$ m is considered because the majority of particles fit within this range, despite an increase in the spread of y_p being observed as the cloud moves downstream. The percentage of particles found outside of this range by each case is only: 0.25% (Case 1), 0.54% (Case 2), and 1.88% (Case 3). A dashed line is plotted to visualise cloud trajectory by calculating the median particle height at a range of downstream positions.

A number of behaviours can be seen in these results. Firstly, there are three main routes the particles can take upon exhalation: (i) carried away by the exhalation along with the bulk of the cloud; (ii) dropping to the floor or desk; (iii) carried upwards in the thermal plume of the emitter towards the ceiling. A considerable difference between the cases is observed for the particle cloud position and shape. The base case is characterised by a particle cloud which moves in the streamwise direction and towards the ceiling due to buoyancy. When a desk divider or pair of monitors are placed in between the two individuals, particles don't advance as far in the streamwise direction. This is a positive effect when it comes to airborne transmission because particles move above the receptor and then disperse around the room. Therefore, the receptor is exposed to a concentration that has been diluted compared to the initial cloud.

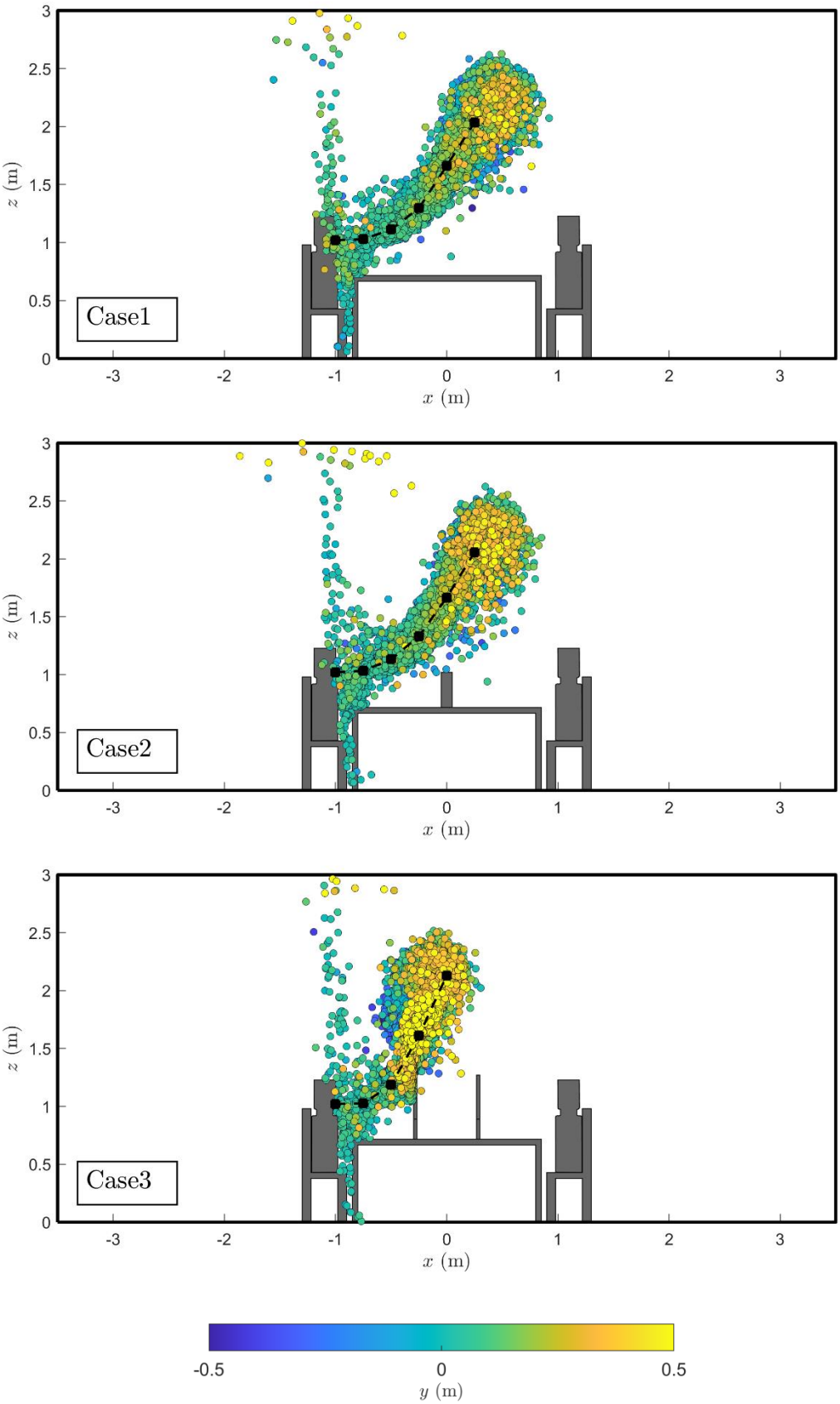

Figure 71 Particle cloud after 25 s, at the end of the speaking period. Particles coloured by their lateral position, y. A dashed line corresponds to the median particle height to show the trajectory of the particle cloud.

6.5.2 Deposition and extraction

The Pöhlker et al. (2021) particle distribution shown in Figure 72 is used to define the speaking boundary condition. As the droplets move through the domain they evaporate and some deposit on surfaces or are removed through the outlets. The size distributions of the airborne particles at 300 s are shown in Figure 72 in terms of the initial, d_0, and final, d, diameters of particles still suspended in the flow for Case 1. The difference between the initial Pöhlker distribution and the distribution of initial droplet diameters, d_0, at $t = 300$ s is due entirely to deposition and removal. The results show that all droplets with an initial diameter $d_0 > 100$ µm are deposited or removed. The differences between the profiles of d_0 and d are solely due to evaporation. The results confirm that a ratio of $d/d_0 = 0.2321$ holds for all particle sizes once all volatile components of the droplet have evaporated, see Section 3.2.2.

From the data presented in Figure 72, it is possible to calculate the percentage of particles which are deposited or removed as a function of particle diameter, which is presented in Figure 73 for all 3 cases. At the ends of the particle size distribution, $d_0 < 32$ µm and $d_0 \geq 100$ µm, deposition/removal is approximately constant. For $d_0 < 32$ µm, deposition and removal is in the range 20 – 40 %, depending on the case studied. Case 1 has the greatest amount of deposition/removal. In the middle size range, 32 µm $\leq d_0 < 100$ µm, there is a sharp transition in the amount deposited/removed, varying from $\sim 35\%$ to 100%, as the diameter increases.

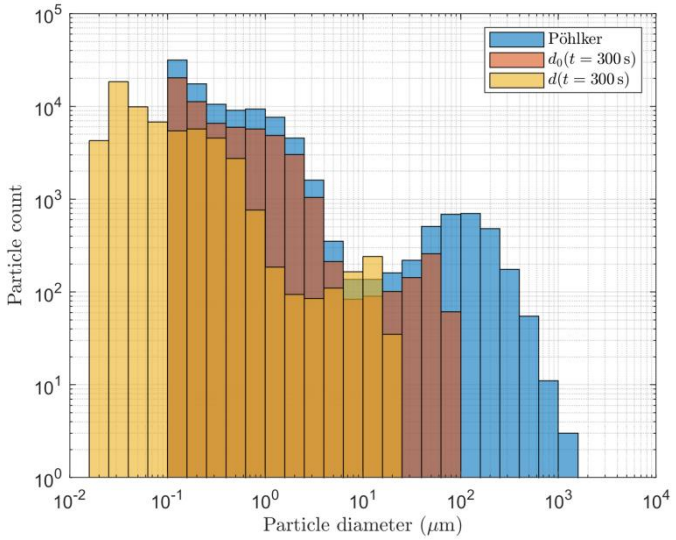

Figure 72 Initial Pöhlker et al., (2021) distribution and the resultant distributions, after deposition and evaporation, partitioned by their initial diameter (d_0) and by their evaporated diameter (d).

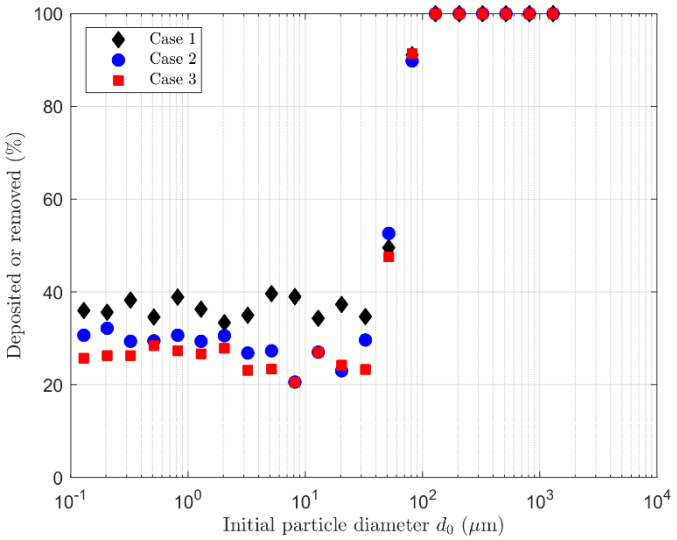

Figure 73 Percentage of particles deposited as a function of particle diameter after 300 s.

From Figure 73 it can be seen that deposition/removal is higher in Case 1 for smaller droplets than for the other cases. However, more information is required to understand why this is the case. Deposition/removal onto each surface/vent is presented in Table 14. For each surface/vent, the number of particles deposited or removed as a percentage of the total number of particles injected into the system is given. This is supplemented in Figure 74 with a pie chart for a smaller number of surfaces/vents. Initial and current particle diameters, taken as an average over all particles on the surface/vent, are listed as $\langle d_0 \rangle$ and $\langle d \rangle$, respectively. It is noted once again that a particle which fully evaporates yields $d/d_0 = 0.2321$. Two methods for calculating how far each particle travels before deposition/removal are used. The first method is the straight-line distance, measured directly from the mouth to the final position and is denoted $\overline{L}$. The total distance travelled by the particle along its path is denoted $\tilde{L}$. The ratio $\langle \tilde{L}/\overline{L} \rangle$ is also reported in Table 14. A particle which travels in a straight line and deposits onto a surface would therefore return $\tilde{L}/\overline{L} = 1$.

Over half of the particles injected into the domain are still suspended after 5 minutes: 58% in the base case, 64% in the divider case, and 68% in the monitor case. Out of the particles which are no longer suspended, a significant percentage are removed by the outlet vents, with Out (RHS) removing more particles than Out (LHS). Deposition onto the desk is similar between the cases with 2% of the particles depositing on the desk. These particles are large $\langle d_0 \rangle > 160$ µm and behave ballistically, depositing before they evaporate fully. A greater amount of deposition, around 4%, occurs on the ceiling. The average particle deposited onto the ceiling is < 1 µm. However, it's important to note that deposition on surfaces can be overestimated using the DRM model if the boundary layer is not resolved sufficiently. Deposition of small particles on the ceiling was not the main purpose of the work and this was not investigated further.

Negligible deposition is found on the bodies, chairs, and monitors. Some surfaces are clearly being deposited onto because of ballistic effects, i.e. desk and floor. This is evident from Table 14 in values of initial and final diameter. However, the ratio $\tilde{L}/\overline{L}$ also provides information on how particles travel to a surface. A ballistic projection will yield a value of $\tilde{L}/\overline{L}$ close to unity. A large $\tilde{L}/\overline{L}$ indicates the particle travelled around the domain before

depositing onto a surface and was probably suspended for a greater amount of time. Compared to other outlet or inlets, Out (RHS) returns the lowest values of $\tilde{L}/\overline{L}$. This indicates that particles have a more efficient route to this vent in these simulations, especially for Case 1.

Table 14 Deposition and removal recorded on boundary patches for the three cases, denoted C1-C3. Notation #p is used to denote # particles instead of a percentage when deposition <0.1%.

Surface	Deposited/ removed (%)			$\langle d_0 \rangle$ (μm)			$\langle d \rangle$ (μm)			$\langle \tilde{L}/\bar{L} \rangle$		
Case	C1	C2	C3	C1	C2	C3	C1	C2	C3	C1	C2	C3
Desk	2	2	2	167	161	161	150	142	142	2.2	2.6	2.4
Walls	0.2	0.3	0.5	0.6	0.8	0.7	0.1	0.2	0.2	3.6	3.5	2.8
Floor	0.2	0.2	0.2	102	109	107	46	53	50	2.5	2.1	2.1
Ceiling	3.7	3.7	4	0.6	0.6	0.6	0.1	0.1	0.1	3.9	3.6	3.1
In (RHS)	0	0.1	0.1	0	0.9	1.0	0	0.2	0.2	-	6.0	6.3
Out (LHS)	10	11	11	2	2	1.8	0.4	0.5	0.4	5.0	4.8	4.3
Out (RHS)	25	19	13	0.9	0.9	0.8	0.2	0.2	0.2	3.2	3.4	3.4
In (LHS)	0.1	0.2	0.1	0.3	0.4	0.5	0.1	0.1	0.1	5.7	4.5	5.3
Body1	0.2	0.1	0.1	63	49	48	15	12	12	7.0	13	11
Body2	6p	7p	2p	21	5	0.4	5	1	0.1	3.0	2.5	2.9
Chair1	35p	27p	35p	106	105	104	50	49	43	1.2	1.8	1.7
Chair2	2p	2p	3p	5	47	67	1	11	16	2.7	2.6	3.2
Divider	-	11p	-	-	64	-	-	15	-	-		-
Monitor1	-	-	0.6	-	-	8	-	-	2	-	-	1.4
Monitor2	-	-	1p	-	-	63	-	-	15	-	-	6.0

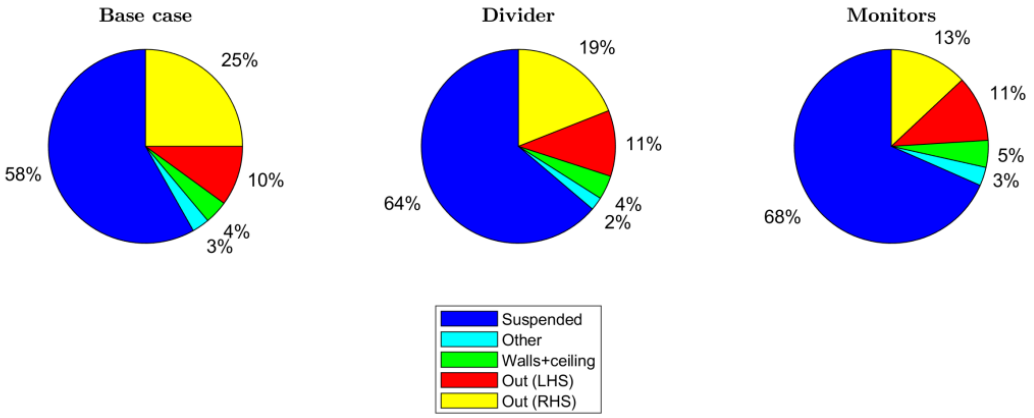

Figure 74 Deposition and removal at walls and through outlet vents.

6.5.3 The well-mixed assumption

After sufficient simulation time has passed, it would be reasonable to assume that particles become well-mixed throughout the room, i.e. uniformly distributed throughout the domain. However, although the flow induced by the exhalation decays over time, the ventilation and thermal plumes continue to drive the flow for the full duration of the simulation. At the ventilation rate of 5 ACH used in the simulation, less than half an air change occurs during the simulation and while mixing and transport will occur, a well-mixed environment would not be expected by the end of the simulation. In Figure 75, histograms of particle coordinates (x_p, y_p, z_p) at different times in the simulation are plotted to investigate particle spreading throughout the domain. A well-mixed situation would return top-hat profiles in the histogram, horizontally and vertically, for later times.

Profiles are shown at different times to capture the time-dependency of the particle positioning. Values on the vertical axis are given as a probability, i.e. particle count divided by the total number of particles in the system at that time step.

Generally, for all 3 cases, there is very little difference between the results at 5 s. During the exhalation period, profiles of x_p, y_p, and z_p are dominated by the source conditions. Spikes are present near the mouth at $(x, y, z) = (-1, 0, 1.02)$ m as particles are injected. At 5 s there is minimal spreading, apart from advection in the x-direction from the exhalation. At the end of the exhalation period, $t = 25$ s, profiles of x and y begin to resemble a Gaussian distribution as particles travel away from the emitter and spread laterally. However, z is closer to a top-hat profile as particles travel upwards towards the ceiling due to buoyancy effects. At 25 s there is little difference between Case 1 and Case 2. However, in Case 3 profiles of x_p and y_p are markedly different from the other two cases. This can be explained by reference to Figure 71. The PC monitor is a blockage to the exhalation jet, and particles travel upwards and to the side. There is enhanced spreading in the y direction, i.e. laterally. This corresponds to a flatter profile of y_p for Case 3, which persists throughout the simulation. The divider doesn't have the same effect because it is not in the jet region of the exhalation.

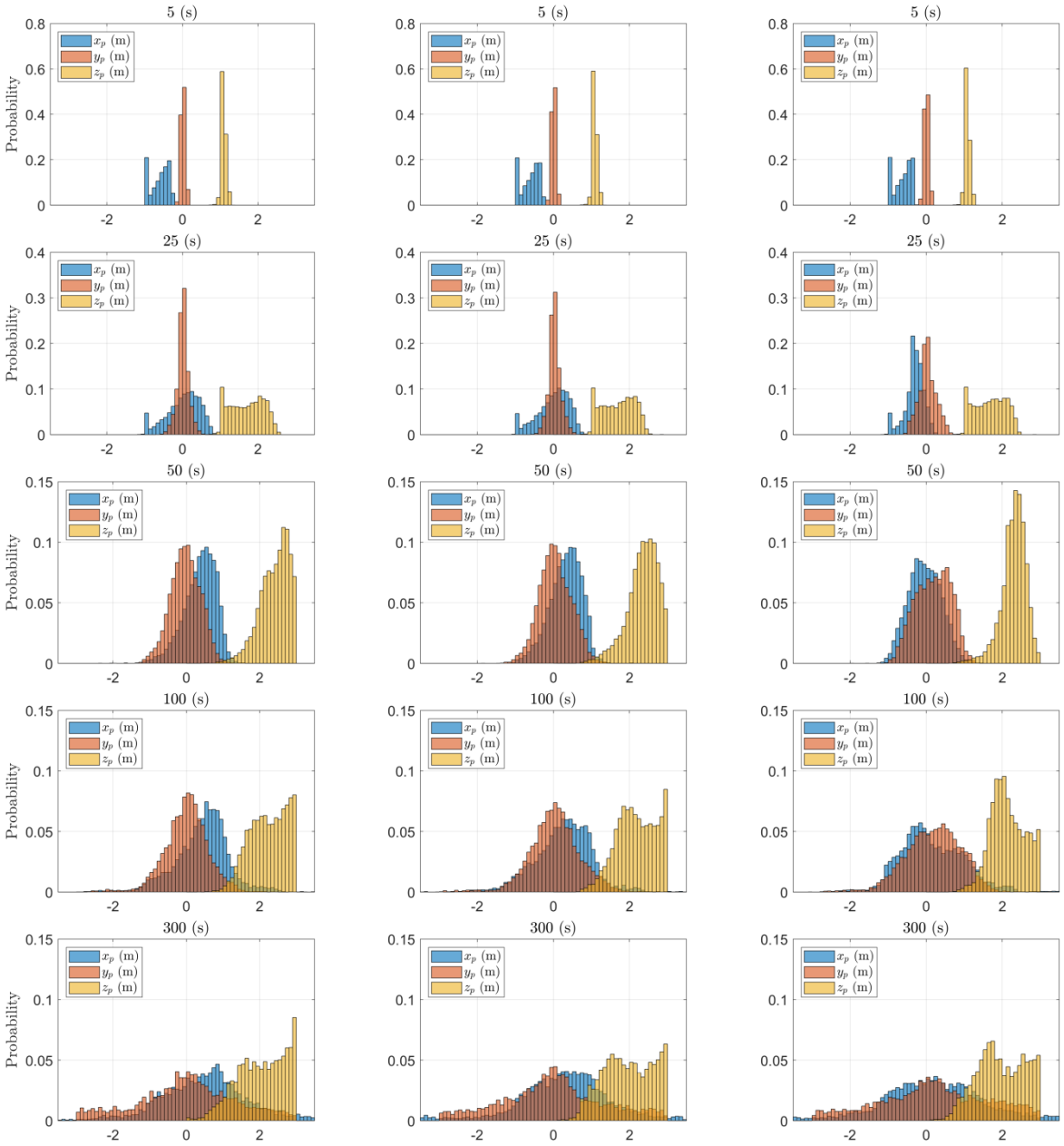

Figure 75 Histograms of particle positions at different times in the simulation. Left column: Case 1, centre: Case 2; right: Case 3. Note the change of y axis limits as time increases.

6.5.4 Buoyancy versus ventilation

Figure 76 shows how flow structures from the people, exhalation, and ventilation affect particle movement at different heights in the domain. The figure plots all particle data for the entire simulation at different heights in the domain. Particles are coloured by their velocity magnitude and are shown in 0.1 m 'slices' at z = 1.02 m, 2.0 m and 2.95 m. The mouths of both the receptor and emitter are positioned at z = 1.02 m, therefore particles at this height can be inhaled by the receptor. The 2 m height is just above head height for a person standing and 2.95 m is just below the ceiling. There are a number of competing effects which influence a particle's path, including (i) jet flow from the exhalation; (ii) interactions or modulation from the computer monitors and desk divider (iii) buoyancy effects from the thermal plume and exhalation; (iv) interaction with the ventilation flow and surrounding walls.

At $z = 1.02$ m, a strong jet from the mouth is observed across all cases. At this height, particles in Case 1 are unobstructed and can therefore travel freely towards the receptor. Adding a divider has little influence on the particle positioning, but computer monitors have a considerable effect. Particles have to travel around both monitors before making it to the receptor.

Differences between the cases at $z = 2.0$ m are subtle. The velocity magnitude is dominated by the vertical component of the thermal plume, which causes particle spreading in the vertical direction. For Case 1 and 2, a small region centred around $(x, y) = (0, 0)$ corresponds to the region in which the exhalation jet passes through the horizontal slice. This indicates that the vertical path of the exhalation jet has travelled above the height of a receptor's head. The computer monitors in Case 3 cause the exhalation jet to transition to a vertical buoyant plume over a shorter distance.

As the particles reach the ceiling, their movement becomes dominated by the ventilation flow. At $z = 2.95$ m particle trajectories are heavily influenced by the arrangement of the vents. There is very little difference between the cases near the ceiling because the flow is dominated by the ventilation. The ventilation is seen to "short circuit", i.e. flow directly from the inlets to the outlets. However, the streaks running parallel to the x axis are uninterrupted when compared to the streaks running parallel to the y axis. This could be an effect of the buoyancy driven thermal plume which acts to break up the strong ventilation flow. Large vortices are formed as the vent flow impinges onto the wall.

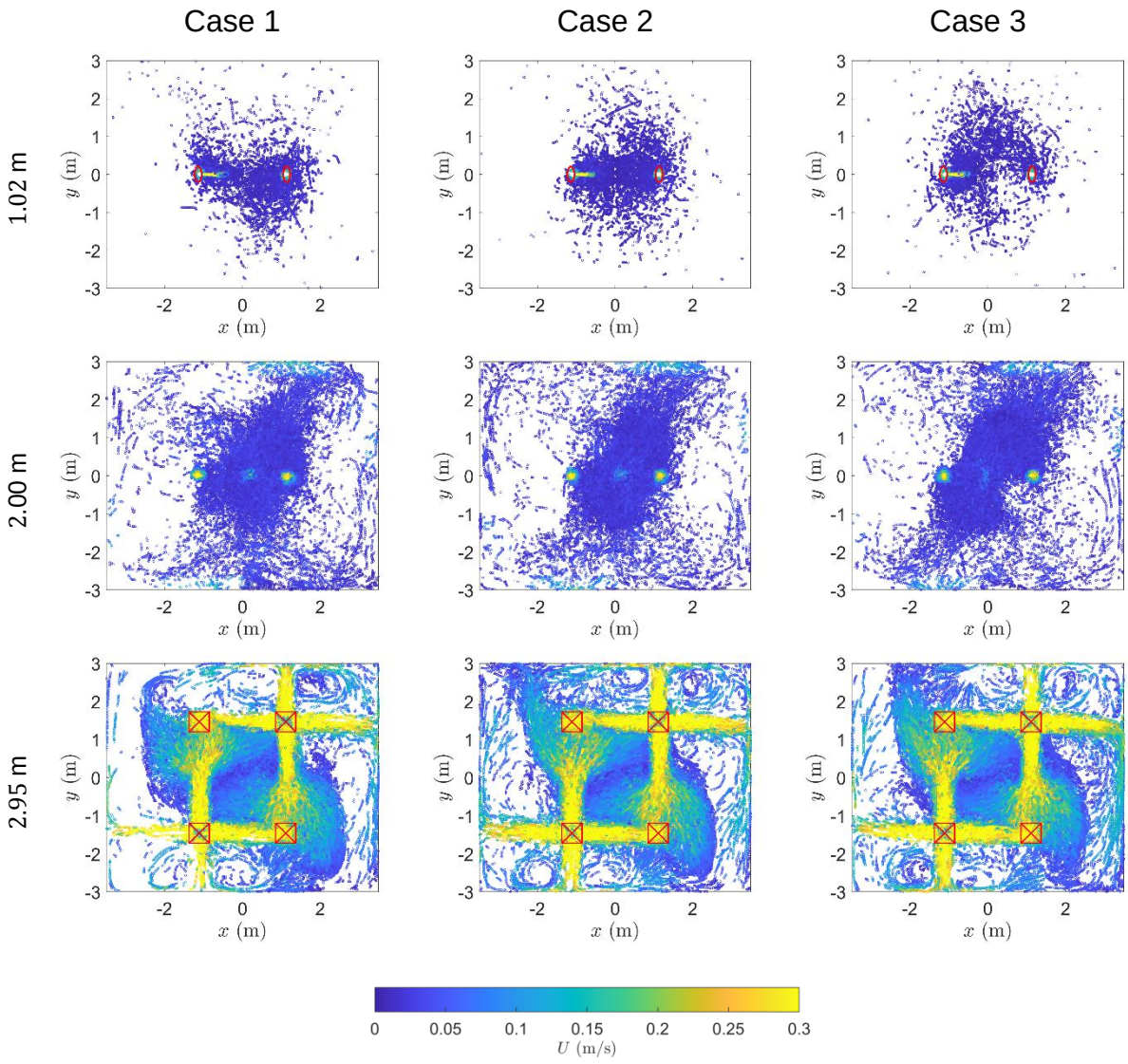

Figure 76 Particle tracks and velocities in 0.1 m slices around seated breathing height, 1.02 m, above head height, 2.00 m, and below the ceiling, 2.95 m. Each particle is coloured by its velocity magnitude.

Table 14 presented statistics on particles being deposited or removed and the distance travelled by particles along their path, $\tilde{L}$). The distance travelled by each particle is now considered for all particles, not just those which are deposited or removed. To understand how far particles travel as a function of their initial droplet diameter, a box plot of distance travelled, $\tilde{L}$, against initial diameter is presented in Figure 77. Particles have been partitioned into a number of ranges. The top and bottom edge of each box corresponds to the upper and lower quartile, respectively and the line through the box is the median. Whiskers around the box extend 1.5 times the interquartile range from the bottom or top of the box. Data outside of the whiskers are deemed to be outliers and are represented using circles.

Particle behaviour is similar for all three cases. For the three smallest size ranges, with initial droplet diameters up to 20 µm, the distance travelled has a fairly constant median value of $\tilde{L} \approx 10$ m, with outliers typically clustered just outside of the whiskers. In the range of initial droplet diameters 20 µm $< d_0 < 100$ µm, there are outliers present at $\tilde{L} \approx 25$ m and the

distribution is skewed. Droplets with an initial diameter greater than 20 µm can still travel a considerable distance once they evaporate. The distance travelled, by droplets with initial diameters in the medium range of 20 µm $< d_0 <$ 100 µm is shorter than smaller droplets, with a median distance of $\tilde{L} \approx 7$ m. At the largest end of the distribution, for initial droplet diameters, $d_0 > 100$ µm, the distribution is far tighter. Whiskers cover the range 0.37 m $< \tilde{L} <$ 0.62 m.

As an example of how particles in the largest size range can travel distances equal to the length of the room (> 5 m) the outlier in Case 1 for $d_0 > 100$ travels around 7 m. This droplet had an initial diameter of $d_0 = 100.25$ µm and once injected into the flow it begins to fall towards the ground. However, it evaporates to $d = 23.27$ µm within approximately 4 seconds and gets carried upwards by buoyancy from the thermal plume of the emitter. It travels up to the ceiling where it is picked up by the ventilation flow, and subsequently drops down and deposits onto the desk.

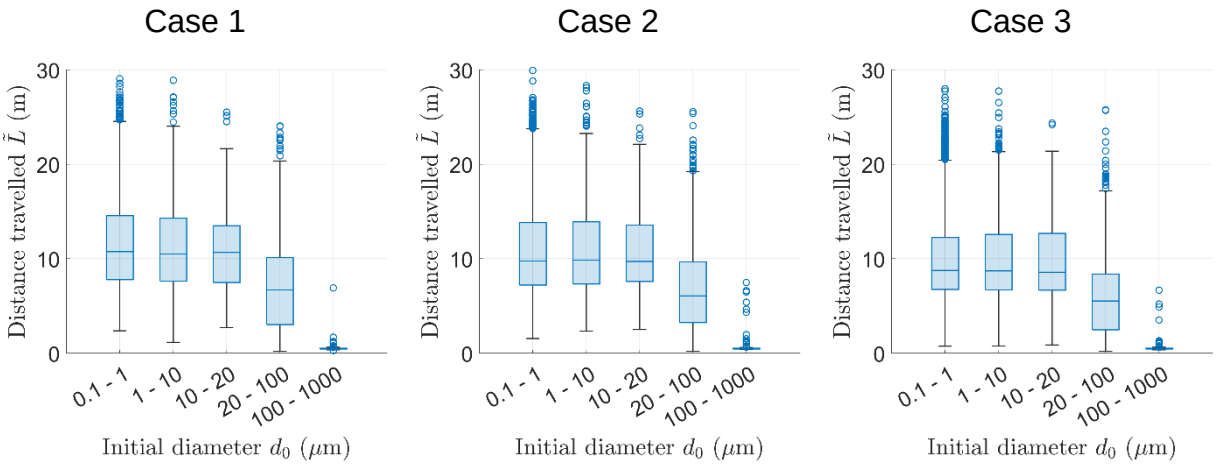

Figure 77 Distance travelled as a function of initial diameter for all three cases.

6.6 Screen-like mitigations discussion

In this section on screen-like mitigations, the computational model developed and discussed earlier in this report has been applied to three meeting room configurations of two people sitting at a desk, examining whether desk dividers and monitors can provide any mitigation by acting like screens.

Initially the bulk of the cloud from exhalations travels horizontally, due to the exhalation, and vertically upwards, due to buoyancy effects. In these simulations the effect would be to reduce airborne transmission as the cloud does not engulf the receptor, but instead travels up towards the ceiling. The monitors are seen to have a greater effect on the exhalation than the dividers or desk alone. The position and height of the monitors is such that they interrupt the exhalation jet/cloud and the plume rises more quickly. Once particles are directed towards the ceiling, the ventilation flow becomes dominant and either removes particles via the outlets or starts to disperse them through the room. The monitors do block or deflect all particles, but in all the cases the buoyant cloud from the exhalation rises above

head height before reaching the receptor. The receptor is not exposed to the concentration of the initial cloud from the exhalation. They would only be exposed after transport and mixing by the ventilation flow has occurred.

Less than half an air change is simulated, so particles would not be expected to be well-mixed at the end of the simulations. However, there is a transition from initial behaviour dominated by the exhalation towards mixing driven by ventilation. By the end of the simulations the distribution of particles shows approximately Gaussian distributions horizontally, and particles have spread to all the walls of the room. Vertically, the initial buoyancy lifts particles towards the ceiling, where they can be removed by flows through the outlet. The ventilation flows also mix particles down through the room. By the end of the simulation the particles have not reached the floor, but their distribution through the height is becoming more uniform

The distance travelled by particles is found to be dependent on the initial diameter. The smallest particles, with initial diameter $d_0 < 20$ µm, have a median distance travelled of between 8.5 m and 10.5 m. Some particles travel nearly 30 m which is more than four times the longest dimension of the room (7 m). In the mid-size range, $20\ \mu\text{m} < d_0 < 100\ \mu\text{m}$, the median travel length is lower, between 5.5 m and 6.5 m, but particles in this range can still travel up to 25 m. For the largest particles with initial diameters of $d_0 > 100$ µm, the droplets behave ballistically and the median distance travelled is 0.5 m, with much less variability in the distance travelled. While not well-mixed at the end of the simulations, both the distribution of particles and the distance travelled by the airborne particles, small and medium, show that significant transport and mixing has occurred.

6.7 Conclusions on application of CFD model

In this Section the results of applying the CFD model to a number of practical scenarios have been presented. This has provided some insight into the effects of screens on viral exposure and the use of exhaled carbon dioxide as a proxy for exposure risk. It has also helped to provide a better understanding of the physics of SARS-CoV-2 transmission.

Simulation findings

Screens have been used widely during the Covid-19 pandemic as a measure to control transmission. The simulations performed here show that large droplets are blocked by screens and that the exhalation cloud, containing droplet nuclei, is deflected by screens and rises due to buoyancy. Deflecting the exhalation cloud means that, compared to the same situation without a screen, transport and mixing would occur before the exhalation cloud reached the region where someone would be exposed to an exhalation. The effect of screen-like objects in offices, desk dividers and monitors, was also simulated. For the scenarios simulated these modified the flow but not to the same extent as screens used as intentional mitigations.

After the initial period of the exhalation, transport and mixing of the exhalation cloud and droplet nuclei is dominated by ventilation flows. Even with the simple geometries and scenarios simulated, the interaction between a person, their thermal plume, the ventilation flow and the screen were complex. In most of the simulations performed only a single person was present. In the simulations where two people were present, the additional thermal plume

modified the mixing behaviour. This emphasises that understanding ventilation and its operation is important where it is used as a control measure.

The momentum and buoyancy of exhalations only contribute to the transport of exhalations for a short period after which ventilation becomes the main driver of the transport and dispersion of the droplet nuclei. Screens can contribute to measures to control transmission, but ventilation is also required as part of the control.

Simulations were also performed to examine the analogy between carbon dioxide exposure and viral exposure from exhalations. There was a strong correlation between the predicted carbon dioxide and viral exposure for droplet nuclei in the aerosol size range, with diameters less than 5 μm, that behaved passively. The correlation between exposure from larger droplet nuclei that remained airborne and carbon dioxide exposure was less strong but could still provide useful information on where exposure could occur. Measurements of carbon dioxide concentration can provide useful information on viral exposure that people could receive, and be used as a way of assessing control measures against transmission.

Model conditions

The simulations of the application scenarios used the Pöhlker et al. (2021) droplet size distribution. This distribution does not show the same clear separation between the smaller droplets of the bronchiolar / laryngeal modes, and the larger droplets of the oral mode seen in the original BLO model, Johnson et al. (2011). Additionally, the Pöhlker distribution contains many more droplets than the BLO distribution, particularly at smaller droplet diameters. Analysis of surface and air samples showed that droplets with initial diameters in the range from 20 μm to 100 μm could either deposit or remain airborne. This is an important finding, as it indicates that particles whose initial diameter suggests they will fall out under gravity can instead evaporate to a droplet nuclei and remain suspended for relatively long periods. This range of diameters includes droplets that are relatively large and may carry more viral copies while remaining airborne. Due to the separation between the smaller and larger droplets in the BLO distribution the number of droplets predicted to be in this intermediate diameter range is low. Predictions of potential viral exposure, and the effectiveness of mitigations could be significantly affected by the droplet size distribution used in a simulation.

Calculation of the viral exposure from the droplets in exhalations requires the distribution of viral copies amongst droplets to be specified. A uniform distribution of viral copies by droplet volume was assumed for most of the analysis. The largest droplets contain the highest number of viral copies, but they rapidly deposit. The largest of the droplets that remain airborne then contain the highest number of viral copies. These droplets could have initial diameters up to 100 μm but remain airborne once they evaporate to droplet nuclei. There is little information about how viral copies are distributed amongst droplets of different diameter. Assuming that the distribution of virus is proportional to droplet surface area rather than volume increased the number of viral copies that remain airborne and increased the number of viral copies in smaller droplets. How viral copies are distributed amongst droplets affects the number of viral copies that could remain airborne and therefore affects transmission risk.

Experiments show large amounts of variability in the droplets exhaled between people and between exhalations from individuals. Differences between experiments also show uncertainty in these measurements, and there is uncertainty about how viral copies are distributed in droplets.

7 CONCLUSIONS

7.1 Summary of modelling options

Different approaches can be used for modelling exhalations (e.g., breathing, coughing) and room ventilation flows. The difference in scales and the processes that are important in exhalations and ventilation flows mean that modelling these flows separately can sometimes make more effective use of resources. CFD models can simulate both exhalations and ventilation flows within a single model, but often the computing resources required are significant. In contrast, integral and zone models are quicker to run and can therefore be used to examine a wide range of different scenarios, but they have some fundamental limitations (e.g., zone models typically assume full mixing within a room). Whichever approach is used it is important to understand the assumptions that are being made in the model and the implications when interpreting the model results.

A CFD modelling approach was used in the current study because it enabled relatively detailed description of the exhalation and ventilation flows. The use of the Eulerian-Lagrangian particle tracking approach also meant that the transport and deposition of different particle size distributions could be modelled. The model also took into account evaporation effects and the fraction of microbial material contained within respiratory particles. This model framework has been used in a number of previous CFD studies of aerosol transport in rooms.

A limitation of the CFD modelling approach is that in practice it can only be used to model a simple idealisation of real life and will often ignore factors that we know will have a significant effect on the flow within a room. The movement of people is a good example. However, acknowledging these assumptions, a CFD model is still a powerful tool in helping to provide a better understanding of the physics involved in exhalation flows, ventilation and therefore transmission of SARS-CoV-2.

7.2 Model validation

Models require data, both to set up the modelled boundary conditions and to validate the model. There is significant inter- and intra-person variability in quantities related to virus transmission including, for example, the numbers of droplets emitted by different people during different activities. These quantities are also difficult to measure and, as a result, there is uncertainty in the data. This should be considered both when specifying models and validating the results of model predictions.

Due to the challenge in validating complete exhalation models, the present work took the approach of validating key components of the model separately. Individual case studies were performed on the exhalation jet, the evaporation of droplets and indoor air flows. The aim was to demonstrate that the model was capable of adequately resolving the relevant flow physics in each of these cases, before putting all of the elements together to simulate virus transmission in a room. For the cases of droplet evaporation and the exhalation jet, the experimental data were relatively well defined. For the case of air flow in a ventilated room, there were a number of uncertain factors surrounding the thermal input conditions and these were found to significantly influence the results.

7.3 Particle material modelling

A number of different approaches were used to model the evaporation characteristics of the exhaled particles. It was found that the most detailed method, using an artificial saliva model, was too computationally expensive to enable it to be used for scenario modelling, where many model runs are required. A simpler approach was to model the particles as pure water having a non-volatile fraction and with no solution vapour pressure adjustment. This gave a reasonable approximation to the artificial saliva model for the value of non-volatile fraction used and at 50% relative humidity. It is recognised that the production of exhaled particles is a biological process and therefore subject to considerable uncertainly. The particle composition of salts and proteins used in the current study was based on a value derived from the literature and an area for further work would be to assess the sensitivity of the results to the composition.

7.4 UKHSA experiments

During the course of the PROTECT NCS project, data became available from UKHSA experiments on particle dispersion and deposition from human subjects. The experiments used bacteria as a surrogate for virus and were performed in an unventilated room. They were based on both airborne and surface samples and provided a relevant means to validate the complete CFD model of exhalation within a room.

There were a number of uncertainties involved in simulating these experiments. The room was nominally unventilated, but it was likely that there were small but finite ventilation flows which influenced particle dispersion. These ventilation flows will have been influenced by thermal effects from the surfaces and from the clothed subjects, but detailed temperature and heat flux measurements were not taken. Such measurements were not within the scope of the experiments which were designed instead to investigate the effects of face coverings. Finally, there was considerable variability within and between subjects in terms of the numbers and diameters of exhaled particles.

Despite these uncertainties, the CFD model predictions showed a similar pattern of behaviour to the experiments. The model correctly predicted that deposition was greater at 1 m than between 1 m and 2 m from the person. The model also predicted that fine particles would remain suspended in the air for longer in agreement with the measurements. This suggested that the CFD model could provide useful predictions of the spatial distribution of exhaled microbial particles. The validation of the CFD model against this dataset has been written up in the paper by Coldrick et al. (2022).

7.5 Practical applications of the CFD model

Following the validation of the CFD model, it was then applied to a number of practical scenarios. This has provided some insight into the effects of screens on viral exposure and the use of exhaled carbon dioxide as a proxy for exposure risk. The scenarios that have been modelled are based on relatively simple idealisations of real life including a person standing in front of a screen and two people sitting opposite each other in a work environment. These simple scenarios have allowed a better understanding to be developed of the physics involved in the transmission of the virus and the factors that contribute to variations in exposure.

Screens have been used widely during the Covid-19 pandemic as a measure to control transmission. The simulations performed show that large droplets are blocked by screens and that the exhalation cloud, containing droplet nuclei, is deflected by screens. Deflecting the exhalation cloud means that, compared to the same situation without a screen, transport, mixing and dilution would occur before the exhalation cloud reached the region where someone would be exposed to an exhalation. The effect of screen-like objects in offices, desk dividers and monitors, was also simulated. For the scenarios simulated these modified the flow but not to the same extent as the screens.

After the initial period of the exhalation, transport and mixing of the exhalation cloud and droplet nuclei is dominated by ventilation flows. Even with the simple geometries and scenarios simulated, the interaction between a person, their thermal plume, the ventilation flow and the screen were complex. In most of the simulations performed only a single person was present. In the simulations where two people were present, the additional thermal plume modified the mixing behaviour. This emphasises that understanding ventilation and its operation is important where it is used as a control measure, as well as people's thermal plumes and movement.

7.6 Describing exhalations

Exhalations vary between people and between individuals at different times. The approach taken in this work was to use representative descriptions of exhalations, based on Stettler et al. (2022). The representation of exhalations is simplified but based on the available data. Making measurements of exhalations, and exhalation related quantities, which are suitable to be used to describe source terms for CFD simulations is difficult as the available data is limited and there are uncertainties associated with the measurements.

7.6.1 Particle diameter distributions

The description of exhalations used in the CFD simulations were based on Stettler et al. (2022), alongside other information. Simulations of the UKHSA experiments were undertaken using three different particle diameter distributions. The first distribution used data from Duguid (1946), this was used in the sensitivity analysis of the CFD model, but the results were not analysed in depth. An improved method of introducing particles was developed, which enabled use of the BLO (Johnson et al., 2011) and Pöhlker et al. (2021) distributions. This latter approach was used in the practical application of the CFD model.

Results from the UKHSA experiments using the BLO model showed a distinct partitioning of particle diameters between the surface and air samples. This partitioning appeared to be, in part, due to the particle diameter distribution in the BLO model which has a pronounced dip in the initial diameter distribution, around 30 µm, between the small bronchiolar / laryngeal droplets, and larger oral droplets. Overall, the BLO model contained relatively few particles, meaning that an inflated particle count (oversampling) had to be used to improve the coverage of sampled particles. The small number of droplets overall, and the dip in the distribution, highlight that the use of this distribution would not necessarily capture the possible behaviour of intermediate sized particles.

The particle size distribution of Pöhlker et al. (2021) is a synthesis of the data available in the literature. Measurements of droplet diameter distribution show that there can be large differences between the number of droplets produced by individuals and between

exhalations from the same individual. Comparing the data available in the literature shows that there are also differences in the measurements between studies. Pöhlker et al. used available data to generate a representative droplet diameter distribution, using an approach based on the BLO model. The Pöhlker distribution did not have the same clear separation between the bronchiolar / laryngeal droplets and the oral droplets seen in the original BLO model. Sampling from the Pöhlker et al. (2021) distribution generated many more droplets than the BLO distribution, particularly for the smaller particle diameters. This meant that a reduced particle count, or under-sampling was necessary for practical computing run times.

Analysis of simulations that used the Pöhlker distribution showed that droplets with initial diameters in the range from 20 µm to 100 µm could either deposit or remain airborne. These initial droplet sizes suggest that deposition could occur, but they can remain airborne, because evaporation to droplet nuclei occurs before they deposit. The volume of droplets in this size range, compared to droplets with initial diameters less than 20 µm, could contain large numbers of viral copies compared to the smaller droplets. These diameters are in the range of diameters for which very few droplets are predicted using the BLO model. Therefore, very different predictions of airborne viral exposure could be obtained, depending on the droplet distribution used.

There is significant variability in the number of droplets in exhalations generated by different people and between exhalations from the same person. The resources required to run CFD simulations limit the ability to perform simulations to examine this variability, therefore, the droplet size distributions used in simulations will be representative. In addition to variability there is considerable uncertainty about droplet size distributions, shown by the difference in droplet counts for exhalations using the BLO model and Pöhlker distribution. The variability is irreducible, but, in principle, the uncertainty can be reduced. Reducing the uncertainty in droplet size distributions would improve confidence in the predictions of airborne exposure from exhalations.

7.6.2 Distribution of viral copies in droplets

To examine exposure to virus and the risk of transmission the droplet diameter distribution from an exhalation must be combined with the distribution of viral copies amongst the droplets.

The number of viral copies produced varies greatly between individuals, and between individuals at different stages of an infection. There is also uncertainty about how viral copies are distributed by initial droplet diameter. Most of the analyses presented here used an assumption that the amount of virus in droplets is proportional to the initial droplet volume. This weighted the distribution of viral copies towards the largest droplets, which always deposit, and so do not contribute to airborne transmission. Droplets with initial diameters from 20 µm to 100 µm can remain airborne. Using the Pöhlker distribution, droplets with initial diameters in this range that remained airborne contributed the most to the airborne volume of droplets and therefore most of the viral copies that were available for airborne transmission. The actual distribution of viral copies among droplets is not known. An assumption of virus distribution proportional to the droplet surface area was also considered. This moved proportionally more viral copies into smaller initial diameter droplets, but the viral exposure was still dominated by droplets with the biggest initial diameters that remained airborne. None of the simulations performed related viral copies per droplet to the source of

the droplets, i.e. bronchiolar, laryngeal or oral, as information was not available to allocate viral copies by source.

This work has shown that the distribution of viral copies across droplets plays an important role in determining exposure risk. However, more data is needed to feed into the models to further improve our understanding of the mechanisms of virus transmission.

7.7 The use of exhaled carbon dioxide as a proxy for exposure risk

Comparing predictions of carbon dioxide exposure and viral exposure from exhalations showed that for droplet nuclei small enough to behave passively, with diameters less than 5 µm, the ratio between predicted carbon dioxide and viral exposure did not change during the simulation. All the largest droplets deposited and did not contribute to airborne exposure. In between these, droplets of all sizes showed both behaviours, some depositing and some evaporating and remaining airborne. Where droplets in this size range remained airborne, they did not behave as passive tracers, unlike carbon dioxide and the small droplet nuclei. Carbon dioxide exposure was not as good an indicator of viral exposure, but could still provide useful information about levels of exposure and where they could occur.

Measuring carbon dioxide can provide a useful proxy for airborne exposure risk. The agreement decreases as the size of the droplets that remain airborne increases, but the carbon dioxide concentration measurements can still provide useful information about transport and dispersion. Reduced uncertainty in the droplet diameter distributions from exhalations and the distribution of viral copies within droplets would improve understanding of the risk of viral exposure and interpretation of measurements of carbon dioxide concentration.

8 REFERENCES

Abkarian, M., Mendez, S., Xue, N., Yang, F., Stone, H. A. (2020). Speech can produce jet-like transport relevant to asymptomatic spreading of virus. Proceedings of the National Academy of Sciences, 117 (41) 25237-25245; DOI: 10.1073/pnas.2012156117

Asadi, S., Wexler, A. S., Cappa, C. D., Barrreda, S., Bouvier, N. M. and Ristenpart, W. D. (2019). Aerosol emission and superemission during human speech increase with voice loudness. Scientific Reports 9:2348.

Alsved, M., Matamis, A., Bohlin, R., Richter, M., Bengtsson, P.-E., Fraenkel, C.-J. Medstrand, P. and Londahl, J. (2020). Exhaled Respiratory Particles During Singing and Talking. Aerosol Science and Technology 54, 1245-1248.

Altman, P. L. and Dittmer, D., S., ed. (1971). Respiration and Circulation, Federation of American Societies for Experimental Biology, Bethesda, Maryland.

Anand, S. and Mayya, Y. S. (2020). Size distribution of virus laden droplets from expiratory ejecta of infected subjects. Scientific reports, 10(1), pp.1-9.

ANSYS, (2019a) Fluent, release 19.0, theory guide. ANSYS Inc.

ANSYS, (2019b) Fluent, release 19.0, user's guide. ANSYS Inc.

Bhagat, R., Davies Wykes, M., Dalziel, S., and Linden, P. (2020). Effects of ventilation on the indoor spread of COVID-19. Journal of Fluid Mechanics, 903, F1. doi:10.1017/jfm.2020.720

Bourouiba, L. (2020). Turbulent gas clouds and respiratory pathogen emissions: potential implications for reducing transmission of COVID-19. Jama, 323, 1837-1838.

Bourouiba, L. (2021). The Fluid Dynamics of Disease Transmission. Annual Review of Fluid Mechanics 53, 473-508.

Bourouiba, L., Dehandschoewercker, E., & Bush, J. (2014). Violent expiratory events: On coughing and sneezing. Journal of Fluid Mechanics, 745, 537-563. doi:10.1017/jfm.2014.88

Burridge, H. C., Fan, S., Jones, R. L., Noakes, C. J. and Linden, P. F. (2021). Predictive and retrospective modelling of airborne exposure risk using monitored carbon dioxide, submitted. arXiv:2009.02999v2 [physics.soc-ph]

Busco, G., Yang, S.R., Seo, J. and Hassan, Y.A. (2020). Sneezing and asymptomatic virus transmission. Physics of Fluids, 32(7), p.073309.

Chao, C. Y., and Wan, M. P. (2006). A study of the dispersion of expiratory aerosols in unidirectional downward and ceiling-return type airflows using a multiphase approach. Indoor air, 16(4), 296-312.

Chen, C. and Zhao, B. (2010). Some questions on dispersion of human exhaled droplets in ventilation room: answers from numerical investigation. Indoor Air, 20(2), pp.95-111.

Chao, C. Y. H., Wan, M. P., Morawska, L., Johnson, G. R. Ristovski, Z. D., Hargreaves, M., Mengersen, K., Corbett, S., Li, Y., Xie, X., and Katoshevski, D. (2009). Interferometric Mie imaging, PIV, coughing, droplet counts, droplet volumes, expiratory droplets, speaking. Journal of Aerosol Science 40, 122-133.

Chen, P. Z., Bobrovitz, N., Premji, Z., Koopmans, M., Fisman, D. N., Gu, F. X. (2021). Heterogeneity in transmissibility and shedding SARS-CoV-2 via droplets and aerosols. eLife;10:e65774.

Chong, K. L., Ng, C. S. Hori, N., Yang, R., and Verzicco, R. (2020). Extended lifetime of respiratory droplets in a turbulent vapor puff and its implications on airborne disease transmission. Physical Review Letters 126, 034502.

Coldrick, S., Kelsey, A., Ivings, M. J., Foat, T. G., Parker, S. T., Noakes, C. J., Bennett, A., Rickard, H. and Moore, G. (2022). Modeling and experimental study of dispersion and deposition of respiratory emissions with implications for disease transmission. Indoor air, 32(2), p.e13000.

Coleman, K. K., Tay, D. J. W., Tan, K. S., Ong, S. W. X., Koh, M. H., Chin, Y. Q., Nasir, H., Mak, T. M., Chu, J. J. H., Milton, D. K. and Chow, V. T. (2021). Viral load of severe acute respiratory syndrome Coronavirus 2 (SARS-CoV-2) in respiratory aerosols emitted by patients with coronavirus disease 2019 (COVID-19) while breathing, talking, and singing. Clinical Infectious Diseases, 2021, ciab691, https://doi.org/10.1093/cid/ciab691

Dada, A. C., & Gyawali, P. (2021). Quantitative microbial risk assessment (QMRA) of occupational exposure to SARS-CoV-2 in wastewater treatment plants. The Science of the total environment, 763, 142989. https://doi.org/10.1016/j.scitotenv.2020.142989

Dargaville, S., Salinas, P., Aniket, J., Mottet, L. and Pain, C. (2021). Progress report on modelling spatially and temporally inhomogeneous spaces and the role of CO2 as a proxy for virus exposure. National Core Study – PROTECT Work Package 2.2.2. Imperial College London.

Dbouk, T., and Drikakis, D. (2020). On coughing and airborne droplet transmission to humans. Physics of Fluids 32, 053310 (2020); https://doi.org/10.1063/5.0011960

Deevy, M. and Gobeau, N. (2006). CFD modelling of benchmark test cases for a flow around a computer simulated person. HSL/2006/51.

de Oliveira, P. M., Mesquita, L. C., Gkantonas, S., Giusti, A. and Mastorakos, E. (2021). Evolution of spray and aerosol from respiratory releases: theoretical estimates for insight on viral transmission. Proceedings of the Royal Society A, 477:20200584, https://doi.org/10.1098/rspa.2020.0584

Duguid, J.P. (1946). The size and the duration of air-carriage of respiratory droplets and droplet-nuclei. Epidemiology & Infection, 44(6), 471-479.

Faulkner, C. A., Castellini, Jr. J. R., Zuo, W., Lorenzetti, D. M. and Sohn, M. D. (2021). Investigation of HVAC Operation Strategies for Office Buildings During COVID-19 Pandemic. engrXiv. August 13. doi:10.31224/osf.io/hx2ct

Feng, Y., Marchal, T., Sperry, T. and Yi, H. (2020). Influence of wind and relative humidity on the social distancing effectiveness to prevent COVID-19 airborne transmission: A numerical study. Journal of aerosol science, 147, p.105585.

Fernandez, M. O., Thomas, R. J., Garton, N. J., Hudson, A., Haddrell, A. and Reid, J. P. (2019). Assessing the airborne survival of bacteria in populations of aerosol droplets with a novel technology. Journal of the Royal Society Interface, 16:20180779, http://dx.doi.org/10.1098/rsif.2018.0779

Foat, T.G., Nally, J. and Parker, S.T. (2017). Investigating a selection of mixing times for transient pollutants in mechanically ventilated, isothermal rooms using automated computational fluid dynamics analysis. Building and Environment 118, 313-322.

Foat, T., Higgins, B., Abbs, S., Maishman T. and Parker, S. (2022). The effect of temperature and relative humidity on exposure to SARS-CoV-2 in a mechanically ventilated room. Dstl report TR138149.

Foat, T. G., Higgins, B., Abbs, C. Maishman, T., Coldrick, S., Kelsey, A., Ivings, M. J., Parker, S. T. and Noakes, C. J. (2022). Modelling the effect of temperature and relative humidity on exposure to SARS-CoV-2 in a mechanically ventilated room. Indoor Air 32, e13146.

Gosman, A. D. and Ioannides, E. (1983). Aspects of computer simulation of liquid-fuelled combustors. J. Energy. 7(6). 482–490.

Graham, D. I. and Moyeed, R. A. (2002). How many particles for my Lagrangian simulations?. Powder technology, 125(2-3), pp.179-186.

Gregson, F. K. A., Watson, N. A., Orton, C. M., Haddrell, A. E., McCarthy, L. P., Finnie, T. J. R., Gent, N., Donaldson, G. C., Shah, P. L., Calder, J. D., Bzdek, B. R., Costello, D. and Reid, J. P. (2020). Comparing the respirable aerosol concentrations and particle size distributions generated by singing, speaking and breathing. ChemRxiv Preprint. https://doi.org/10.26434/chemrxiv.12789221.v1

Gupta, J. K., Lin, C. H. and Chen, Q. (2009). Flow dynamics and characterization of a cough. Indoor air, 19(6), pp.517-525.

Gupta, J. K., Lin, C. H. and Chen, Q. (2010). Characterizing exhaled airflow from breathing and talking. Indoor air, 20(1), pp.31-39.

Hamey, P. Y. (1982). The evaporation of airborne droplets, MSc Thesis, Cranfield University, Bedfordshire, UK, 48–58.

Han Z. Y., Weng W. G., Huang Q, Y. (2013). Characterizations of particle size distribution of the droplets exhaled by sneeze. J R Soc Interface 10: 20130560.

Hanna, S. (2022). Transport and dispersion of tracers simulating COVID-19 aerosols in passenger aircraft. Indoor Air; 32:e12974. doi:10.1111/ina.12974

Hartmann, A., Lange, J., Rotheudt, H. and Kriegel, M. (2020). Emission rate and particle size of bioaerosols during breathing, speaking and coughing. Hermann Reitschel Institute, TU Berlin, http://dx.doi.org/10.14279/depositonce-10331

He, Q., Niu, J., Gao, N., Zhu, T. and Wu, J. (2011). CFD study of exhaled droplet transmission between occupants under different ventilation strategies in a typical office room. Building and Environment 46, 397-408.

Hinds, W. C. (1999). Aerosol technology: properties, behavior, and measurement of airborne particles. Second Edition, John Wiley & Sons.

Ho, C. K. (2021). Modeling airborne pathogen transport and transmission risks of SARS-CoV-2. Applied mathematical modelling, 95, 297-319.

Hussein, H.J., Capp, S.P. and George, W.K. (1994). Velocity measurements in a high-Reynolds-number, momentum-conserving, axisymmetric, turbulent jet. Journal of Fluid Mechanics, 258, 31-75.

Johnson, G. R. and Morawska, L. (2009). The mechanism of breath aerosol formation. Journal of Aerosol Medicine and Pulmonary Drug Delivery, 22, 229-237.

Johnson, G. R., Morawska, L., Ristovski, Z. D., Hargreaves, M., Mengersen, K., Chao, C. Y. H., Wan, M. P., Li, Y., Xie, X., Katoshevski, D. and Corbett, S. (2011). Modality of human expired aerosol size distributions. Journal of Aerosol Science 42, 839-851.

Jones, B., Sharpe, P., Iddon, C., Hathway, E.A., Noakes, C.J. and Fitzgerald, S. (2021). Modelling uncertainty in the relative risk of exposure to the SARS-CoV-2 virus by airborne aerosol transmission in well mixed indoor air. Building and environment, 191, p.107617.

Launder, B. E. and Spalding D. B. (1972). Lectures in Mathematical Models of Turbulence. Academic Press, London.

Lai, K.-M., C. Bottomley, and R. McNerney (2011). Propagation of Respiratory Aerosols by the Vuvuzela. PLoS ONE 6: e20086. https://doi.org/10.1371/journal.pone.0020086

Lee, J., Yoo, D., Ryu, S., Ham, S., Lee, K., Yeo, M., Min, K. and Yoon, C. (2019). Quantity, Size Distribution, and Characteristics of Cough-Generated Aerosol Produced By Patients With an Upper Respiratory Tract Infection. Aerosol and Air Quality Research 19, 840-853.

Li, H., Leong, F. Y., Xu, G., Ge, Z., Kang, C. W. and Lim, K. H. (2020). Dispersion of evaporating cough droplets in tropical outdoor environment. Physics of Fluids, 32(11), p.113301.

Lindsley, W. G., Pearce, T. A. , Hudnall, J. B. , Davis, K. A., Davis, S. M., Fisher, M. A. , Khakoo, R., Palmer, J. E. , Clark, K. E., Celik, I., Coffey, C. C., Blachere, F. M. and Beezhold, D. H. (2012). Quantity and Size Distribution of Cough-Generated Aerosol Particles Produced by Influenza Patient During and After Illness. Journal of Occupational and Environmental Hygiene 9, 443-449.

Liu, L., Li, Y., Nielsen, P. V., Wei, J. and Jensen, R. L. (2017a). Short-range airborne transmission of expiratory droplets between two people. Indoor Air 27, 452-462. doi: 10.1111/ina.12314.

Liu, L., Wei, J., Li, Y. and Ooi, A. (2017b). Evaporation and dispersion of respiratory droplets from coughing. Indoor Air, 27: 179-190. doi: 10.1111/ina.12297.

Liu, F., Zhang, C., Qian, H, Zheng, X. and Nielsen, P. V. (2019). Direct or indirect exposure of exhaled contaminants in stratified environments using an integral model of an expiratory jet. Indoor Air 29, 591-603. doi: 10.1111/ina.12563

Loudon, R. G. and Roberts, R. M. (1967a). Droplet expulsion from the respiratory tract. American Review of Respiratory Disease 95(3):435-42. doi: 10.1164/arrd.1967.95.3.435.

Loudon, R. and Roberts, R. (1967b). Relation between the Airborne Diameters of Respiratory Droplets and the Diameter of the Stains left after Recovery. *Nature* **213**, 95–96. https://doi.org/10.1038/213095a0

Loudon, R. G. and Roberts, R. M. (1968). Singing and the dissemination of tuberculosis. American Review of Respiratory Disease 98(2):297-300. doi: 10.1164/arrd.1968.98.2.297.

Mentor, F. (1994). Two-equation eddy-viscosity turbulence models for engineering applications, AIAA J. 32 1598-1605.

Mikhailov, E., Vlasenko, S., Niessner, R. and Pöschl, U. (2003). Interaction of aerosol particles composed of protein and salts with water vapor: hygroscopic growth and microstructural rearrangement. Atmospheric Chemistry and Physics Discussions, 3(5), 4755-4832.

Miller, S.L., Nazaroff, W.W., Jimenez, J.L., Boerstra, A., Buonanno, G., Dancer, S.J., Kurnitski, J., Marr, L.C., Morawska, L. and Noakes, C. (2021). Transmission of SARS-CoV-2 by inhalation of respiratory aerosol in the Skagit Valley Chorale superspreading event. Indoor air 31, 314-323.

Morawska, L., Johnson, G. R., Ristovski, Z. D., Hargreaves, M., Mengersen, K., Corbett, S., Chao, C. Y. H., Li, Y. and Katoshevski, D. (2009). Size distribution and sites of origin of droplets expelled from the human respiratory tract during expiratory activities. Journal of Aerosol Science 40, pp.256-269.

NASA (1995). Man-Systems Integration Standards Revision B, Volume I, Section 3 Anthropometry and Biomechanics, (https://msis.jsc.nasa.gov/sections/section03.htm, accessed 01-03-2022).

Nielsen, P.V., Murakami, S., Kato, S., Topp, C. and Yang, J.H. (2003). Benchmark tests for a computer simulated person. Aalborg University, Indoor Environmental Engineering.

Orszag, S. A., Yakhot, V., Flannery, W. S., Boysan, F., Choudhury, D., Maruzewski, J. and Patel., B. (1993). Renormalization Group Modeling and Turbulence Simulations. In International Conference on Near-Wall Turbulent Flows, Tempe, Arizona.

Ounis, H., Ahmadi, G. and McLaughlin, J.B. (1991). Brownian diffusion of submicrometer particles in the viscous sublayer. Journal of Colloid and Interface Science, 143(1), pp.266-277.

Parker, S., Foat, T. and Preston, S. (2008). Towards quantitative prediction of aerosol deposition from turbulent flows. Journal of Aerosol Science, 39(2), pp.99-112.

Pease, L.F., Wang, N., Salsbury, T.I., Underhill, R.M., Flaherty, J.E., Vlachokostas, A., Kulkarni, G. and James, D.P. (2021). Investigation of potential aerosol transmission and infectivity of SARS-CoV-2 through central ventilation systems. Building and Environment 197, p.107633.

Pöhlker, M. L., Krüger, O. O., Förster, J. D., Elbert, W., Fröhlich-Nowoisky, J., Pöschl, U., Pöhlker, C., Bagheri, G., Bodenschatz, E., Huffman, J. A. and Scheithauer, S. (2021). Respiratory aerosols and droplets in the transmission of infectious diseases. arXiv preprint arXiv:2103.01188.

Redrow, J., Mao, S., Celik, I., Posada, J. A. and Feng, Z. G. (2011). Modeling the evaporation and dispersion of airborne sputum droplets expelled from a human cough. Building and Environment, 46(10), pp.2042-2051.

Riley, E.C., Murphy, G. and Riley, R.L. (1978). Airborne spread of measles in a suburban elementary school. American journal of epidemiology, 107(5), pp.421-432.

Rudnick, S.N. and Milton, D.K. (2003). Risk of indoor airborne infection transmission estimated from carbon dioxide concentration. Indoor air 13, 237-245.

SAGE (2020). SARS-CoV-2: Transmission routes and environments, 22 October 2020, Government Office for Science, SARS-COV-2: Transmission Routes and Environments, 22 October 2020 - GOV.UK (www.gov.uk), accessed 16/03/2021.

Seinfeld, J. H. and Pandis, S. N. (2016). Atmospheric chemistry and physics: from air pollution to climate change. John Wiley & Sons.

Singanayagam A, et al. (2022). Community transmission and viral load kinetics of the SARS-CoV-2 delta (B. 1.617. 2) variant in vaccinated and unvaccinated individuals in the UK: a prospective, longitudinal, cohort study. The Lancet Infectious Diseases 2022, 183-195.

Srebric, J., Vukovic, V., He, G. and Yang, X. (2008). CFD boundary conditions for contaminant dispersion, heat transfer and airflow simulations around human occupants in indoor environments. Building and Environment, 43(3), pp.294-303.

Stettler, M. E. J., Nishida, R. T., de Oliveira, P. M. et al. (2022). Source terms for benchmarking models of SARS-CoV-2 transmission via aerosols and droplets. medRxiv 2022.02.11.22270844; doi: https://doi.org/10.1101/2022.02.11.22270844

Vuorinen, V., Aarnio, M., Alava, M., Alopaeus, V., Atanasova, N., Auvinen, M., Balasubramanian, N., Bordbar, H., Erästö, P., Grande, R., Hayward, N., Hellsten, A., Hostikka, S., Hokkanen, L., Kaario, O., Karvinen, A., Kivistö, I., Korhonen, M., Kosonen, R., Kuusela, J., Lestinen, S., Laurila, E., Nieminen, H. J., Peltonen, P., Pokki, J., Puisto, A., Råback, P., Salmenjoki, H., Sironen, T. and Österberg, M. (2020). Modelling aerosol transport and virus exposure with numerical simulations in relation to SARS-CoV-2 transmission by inhalation indoors. Safety Science 130, 104866, doi: 10.1016/j.ssci.2020.104866.

Walker, J. S., Archer, J., Gregson, F. K., Michel, S. E., Bzdek, B. R. and Reid, J. P. (2021). Accurate Representations of the Microphysical Processes Occurring during the Transport of Exhaled Aerosols and Droplets. ACS central science, 7(1), pp.200-209.

Wan, M. P., Sze To, G. N., Chao, C. Y. H., Fang, L. and Melikov, A. (2009). Modeling the Fate of Expiratory Aerosols and the Associated Exposure risk in an Aircraft Cabin Environment, Aerosol Science and Technology, 43:4, 322-343, DOI: 10.1080/02786820802641461.

Wang, B., Wu, H. and Wan, X.F. (2020). Transport and fate of human expiratory droplets—A modeling approach. Physics of Fluids 32, 083307.

Wells, W.F. (1934). On air-borne infection. Study II. Droplets and droplet nuclei. American Journal of Hygiene 20, 611-18.

Xie, X., Li, Y., Chwang, A. T. Y., Ho, P. L. and Seto, W. H. (2007). How far droplets can move in indoor environments-revisiting the Wells evaporation-falling curve. Indoor air, 17, pp. 211-225.

Xie, X., Li, Y., Sun, H. and Liu, L. (2009). Exhaled droplets due to talking and coughing. Journal of the Royal Society Interface 6, S703-S714.

Zhu, S., Kato, S. and Yang, J. H. (2006). Study on transport characteristics of saliva droplets produced by coughing in a calm indoor environment. Building and environment, 41(12), pp.1691-1702.

APPENDIX A

A.1 Model structure

The simulations were carried out using the ANSYS Fluent software (ANSYS, 2019b), making use where possible of the in-built models. Some aspects of the simulations required functionality or models beyond the scope of the standard Fluent installation. These were incorporated through User Defined Functions (UDFs) or through additional Matlab code. The interactions between the Fluent software, the UDFs and the Matlab code are shown in Figure 78.

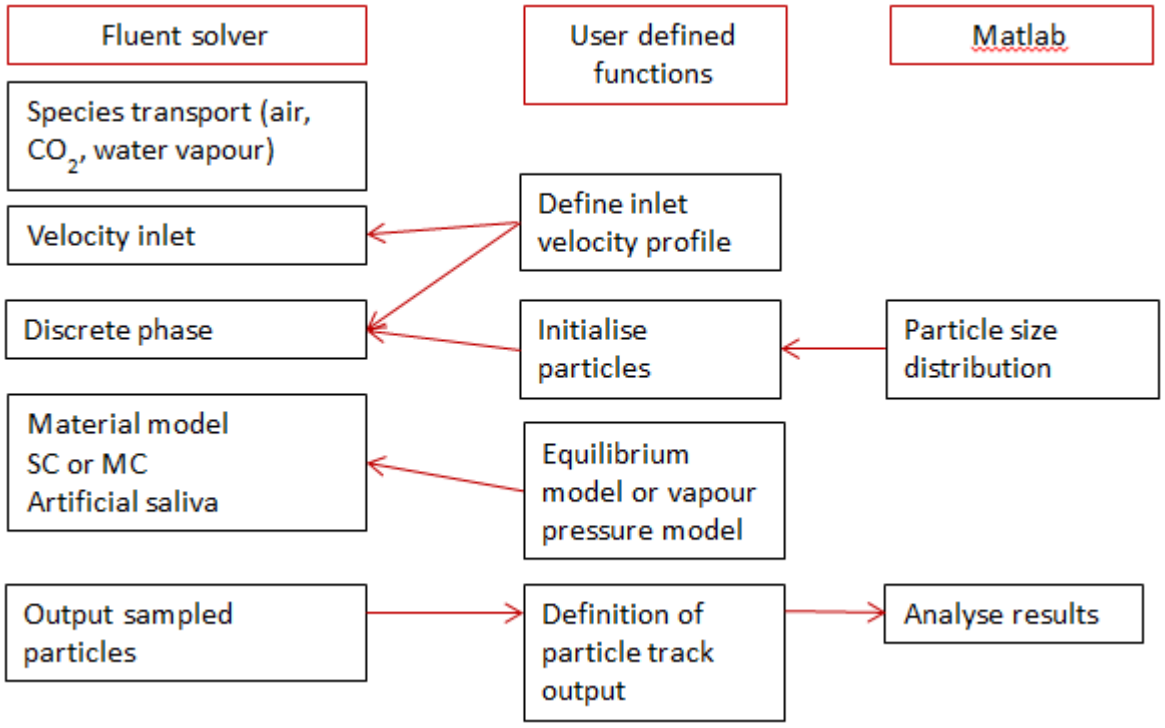

Figure 78 Schematic of the interactions of the Fluent software with additional User Defined Functions

A.2 Particle track output modification

The standard sample output particle track data were modified to provide additional information. The complete set of output information for each sample file is shown in Table 15. The parcel ID number was used in several post-processing tasks and was also used to check that each individual parcel injected into the domain was sampled, i.e. that parcels were not being lost or deleted.

Table 15 Particle sample output file contents

Variable	Description	Units
ID	Parcel ID	-
x	x-position	m
y	y-position	m
z	z-position	m
x_0	Initial x-position	m
y_0	Initial y-position	m
z_0	Initial z-position	m
u	Velocity component u	m/s
v	Velocity component v	m/s
w	Velocity component w	m/s
p_diam	Current particle diameter	m
p_diam_0	Initial particle diameter	m
n_in_parcel	Number in parcel	-
p_temp	Temperature	K
p_mass	Particle mass	kg
p_mass_0	Initial particle mass	kg
flow_rate	Flow rate	kg/s
time	Current particle time	s
time_0	Particle injection time	s
mass_frac_a	Mass fraction water	-
mass_frac_b	Mass fraction solids	-

A.3 Evaporation of a falling droplet - sensitivity analysis

The simulations of falling droplets described in Section 4.2 were run on three different meshes and for two timesteps. The meshes had cell sizes of 5 mm, 10 mm and 20 mm, giving node counts of 890,000 nodes, 430,000 nodes and 116,000 nodes respectively. Timesteps of 0.01 s and 0.1 s were run. The results are shown in Figure 79. The CFD model results are overlaid as this model was relatively insensitive to the mesh and timestep.

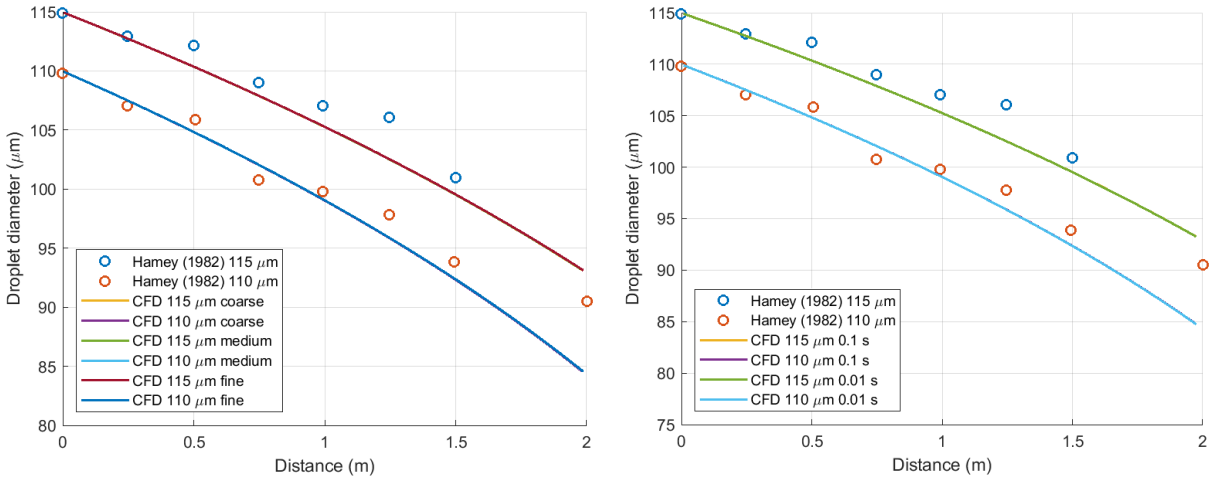

a b

Figure 79 Sensitivity analysis of the falling droplet model. a) mesh sensitivity, b) timestep sensitivity

A.4 Particle material model

The data of Hamey (1982) are for pure water droplets. Therefore, it was not possible to check the evaporation characteristics of the artificial saliva model described in Section 3.2.5 directly against it. However, it was used to provide a check that the modifications to the particle evaporation model were implemented correctly in Fluent. Figure 80 (a) compares the default in-built diffusion controlled evaporation model with the user coded single component (SC) evaporation model. This is the model given in Equation 9, when the activity, α_w, is set to one, i.e. using the normal particle vapour pressure and both model curves are overlaid. Figure 80 (b) is a comparison of the single component (SC) and multicomponent (MC) model when the activity, α_w, is a function of the non-volatile fraction. Since the non-volatile fraction is small in each case, the model curves are overlaid.

Walker et al. (2021) show activity curves for artificial saliva, deep lung fluid and NaCl. For comparison of these materials against pure water, a simulation was run in which droplets between 10 µm and 100 µm were introduced at the top of a 4 m high cylinder in a moist atmosphere of 50% RH. As noted in Section 3.2.5, a single parameterisation was used for artificial saliva and deep lung fluid due to their similarity. The model for water used the same multicomponent model, but with no solution vapour pressure adjustment. Since the settling velocity is substantially different across the size range, a slow co-flow was introduced at the top of the cylinder. The results are shown in Figure 81. It can be seen that, at the level of humidity considered, the evaporation timescales are similar across all materials. The main effect of the different material models is therefore on the final evaporated diameter.

A comparison was also made between the multicomponent artificial saliva model and the single component model using water with no solution vapour pressure adjustment. The results are shown in Figure 82 for an ambient humidity of 50% RH. Under these conditions, the evaporation timescales and final diameters are similar. This is because, for a given initial non-volatile mass fraction, the pure water droplets have a less dense non-volatile core than the multicomponent droplets. The lower density core (980 kg/m^3 for water versus 1830 kg/m^3 for the mixture of salts, protein and surfactant) results in a larger final diameter. However, the

pure water droplets evaporate to their core non-volatile diameter, whereas the multicomponent droplets retain some moisture, due to their modified vapour pressure.

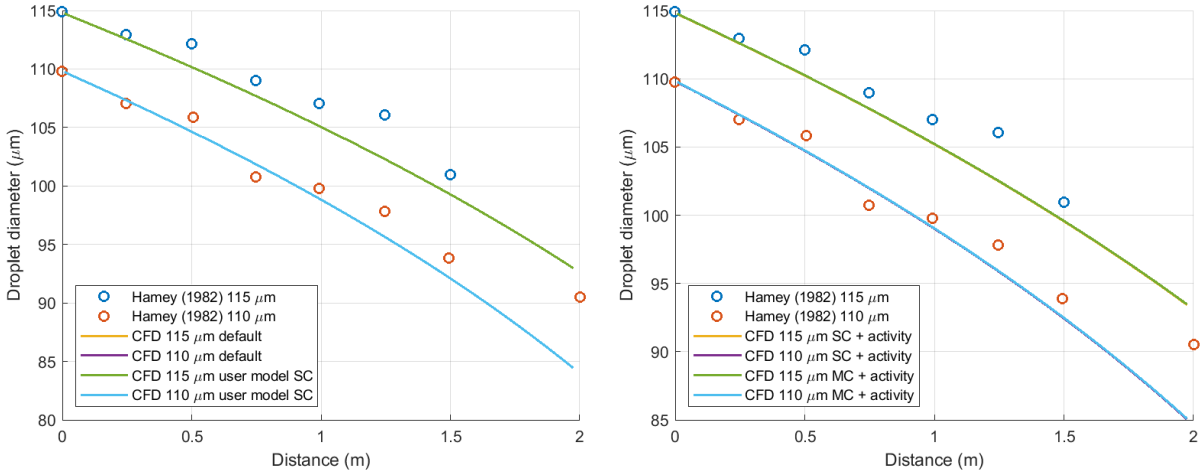

a b

Figure 80 a) comparison of the default single component evaporation model with the user-coded single component model and the data of Hamey (1982), b) comparison of single component and multicomponent models, with solution vapour pressure adjustment according to the model of Walker et al. (2021)

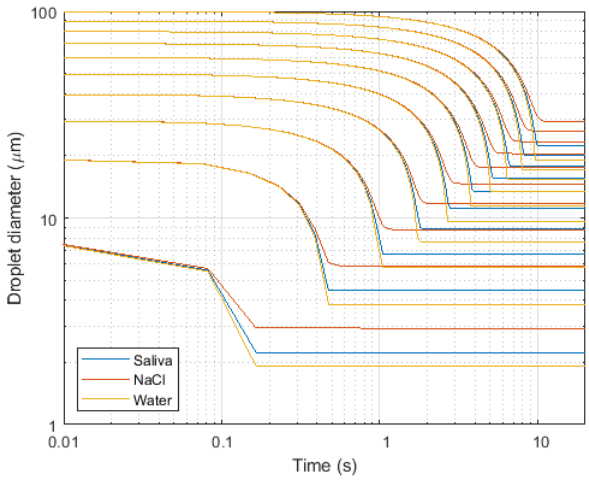

Figure 81 Comparison of evaporation timescales for artificial saliva, NaCl and pure water

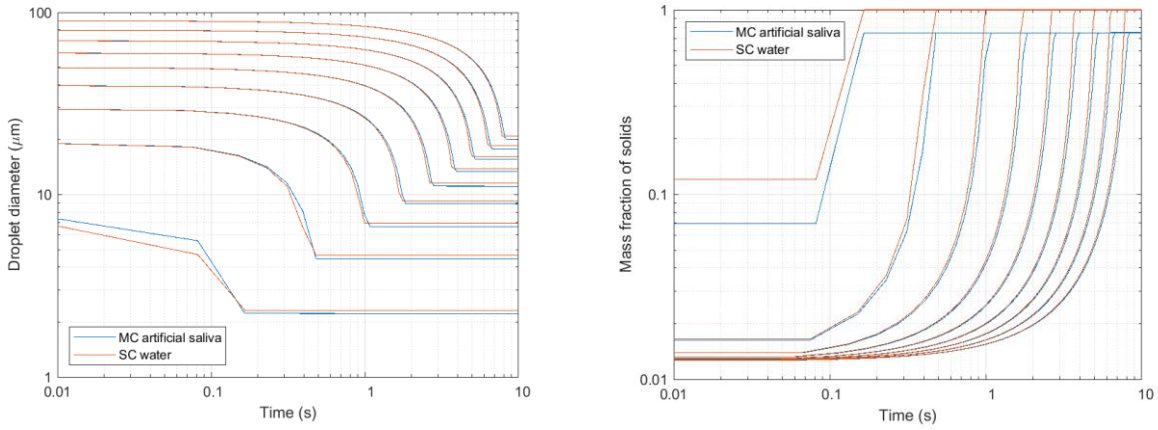

a b

Figure 82 Comparison between the multicomponent artificial saliva model and the single component model using water with no solution vapour pressure adjustment. In each case the composition is 98.75% by mass water and 1.25% by mass solids. The results are shown for an ambient humidity of 50% RH. a) shows the evolution of diameter with time and b) shows the evolution of solids mass fraction with time

A.5 UKHSA experiments - sensitivity analysis

A.5.1 Simulations using the Rosin-Rammler distribution

Four meshes were created, being composed of tetrahedral cells with prismatic inflation layers adjacent to the solid surfaces and having a volumetric refinement region in the vicinity of the mouth to capture the jet. The sizes of the meshes were guided by the results obtained in Section 4. The sensitivity of the particle parcel samples on the centreline plates and the air samplers is shown in Figure 83. The results across all the meshes were similar, other than for the off-axis plates to the right of the person. These plates captured relatively few particle parcels and the deposition does not follow an obvious pattern across the different meshes. In view of the relative computational overhead, the coarser mesh was used for subsequent simulations.

Table 16 Mesh node counts

Mesh	Node count
Mesh1	648316
Mesh2	889746
Mesh3	1633306
Mesh4	2283454

Sensitivity of the deposition result to the timestep and time discretisation scheme are shown in Figure 84 and Figure 85. Overall deposition results appeared to be relatively insensitive to these parameters.

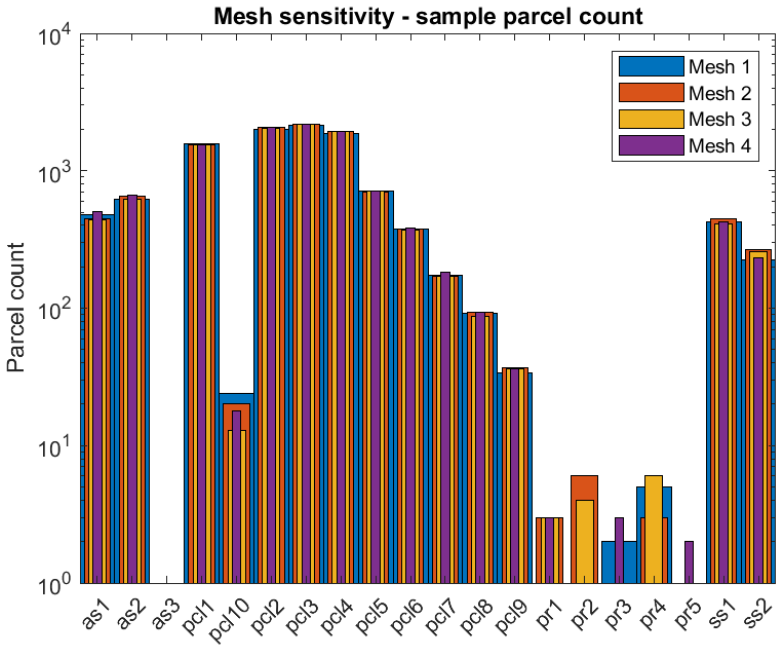

Figure 83 Sensitivity of deposited parcel count to mesh density (one cough)

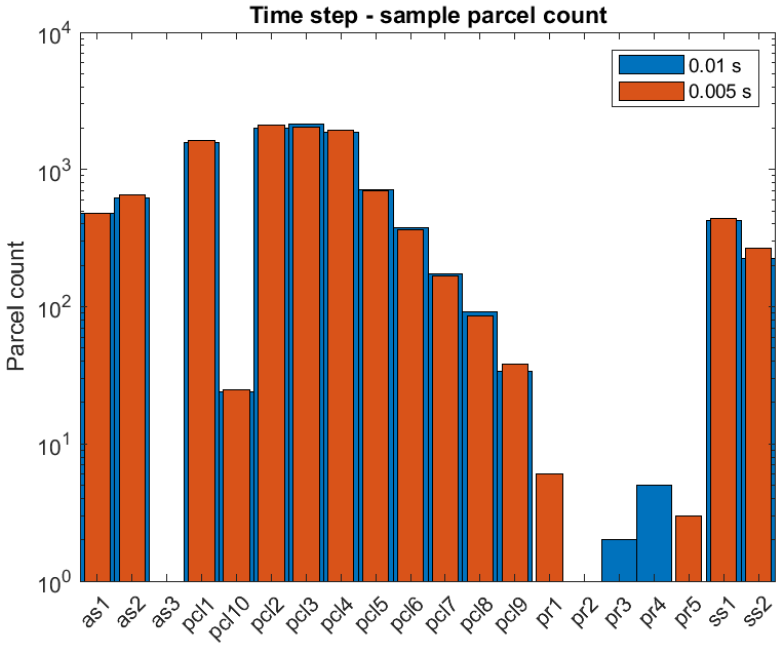

Figure 84 Sensitivity of deposited parcel count to simulation timestep during the injection period (one cough)

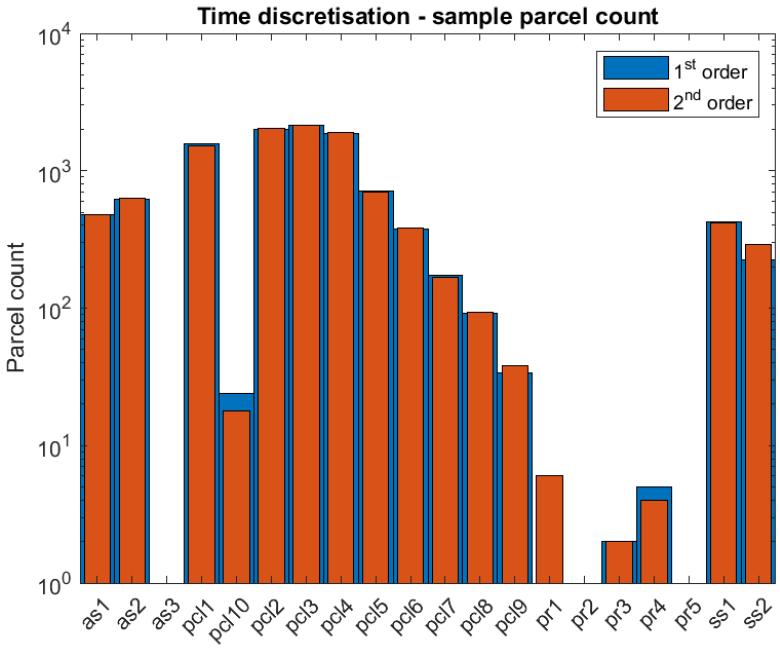

Figure 85 Sensitivity of deposited parcel count to the time discretisation scheme (one cough)

A.5.2 Simulations using the BLO model

Simulations using the BLO model for one cough were run with different levels of oversampling. Deposition results for the deposited parcel count and normalised parcel count are shown in Figure 86 and Figure 87. These simulations were run with pure water particles having a non-volatile fraction (Appendix A.4). The simulation with 1× oversample resulted in insufficient coverage as samples were not obtained at all locations. The simulations with 10× and 100× oversample resulted in similar deposition patterns. Although it would have been preferable to use the increased particle count given by the 100× oversample, the amount of particles involved meant that the simulation became intractable in terms of the time required to solve the particle tracks.

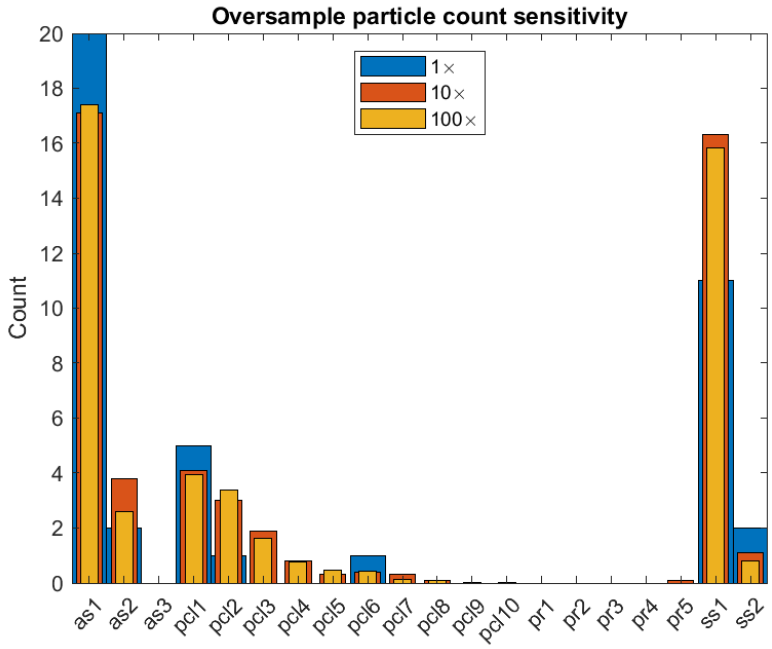

Figure 86 Simulation particle count sensitivity for the BLO model (one cough, actual particle count)

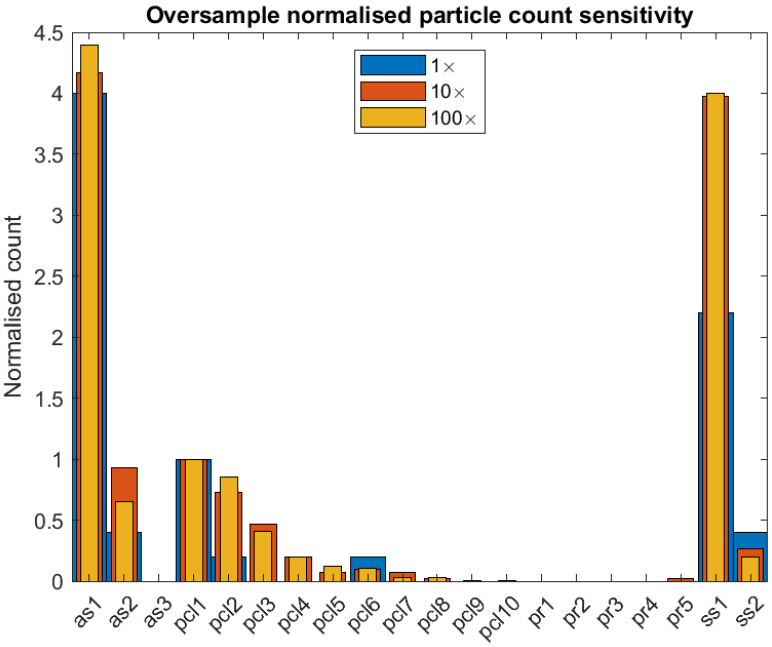

Figure 87 Simulation particle count sensitivity for the BLO model (one cough, normalised particle count)

APPENDIX B OUTPUTS

B.1 Presentations

The work was presented at several PROTECT Theme 2 meetings. A summary presentation was given at the PROTECT conference in Manchester on the 17th and 18th November 2021.

B.2 Research papers

A collaborative paper describing the modelling of the UKHSA experiments has been published in Indoor Air:

Coldrick, S, Kelsey, A, Ivings, M J, et al., 2022. Modeling and experimental study of dispersion and deposition of respiratory emissions with implications for disease transmission. Indoor Air; 32:e13000. doi:10.1111/ina.13000

A collaborative paper with DSTL describing the effects of temperature and relative humidity on exposure:

Foat, T.G., Higgins, B., Abbs, C., Maishman, T., Coldrick, S., Kelsey, A., Ivings, M.J., Parker, S.T. and Noakes, C.J., 2022. Modeling the effect of temperature and relative humidity on exposure to SARS-CoV-2 in a mechanically ventilated room. Indoor air, 32(11), p.e13146.

The PROTECT COVID-19 National Core Study on transmission and environment is a UK-wide research programme improving our understanding of how SARS-CoV-2 (the virus that causes COVID-19) is transmitted from person to person, and how this varies in different settings and environments. This improved understanding is enabling more effective measures to reduce transmission – saving lives and getting society back towards 'normal'.

Published by the PROTECT COVID-19 National Core Study 04/2023